ABSTRACT

Title of Dissertation: NON-CATALYTIC THERMAL
                              REFORMING OF JP-8 IN A DISTRIBUTED
                              REACTOR

                              Richard Michael Scenna, Ph.D, 2017

Dissertation directed by: Dr. Ashwani K. Gupta
                              Distinguished University Professor
                              Department of Mechanical Engineering

This investigation focuses on developing a fundamental understanding of the

thermochemical behavior of the application of the advanced combustion technique of

Colorless Distributed Combustion to the thermal partial oxidation of a hydrocarbon

fuel. Distributed Reaction Regime is achieved through internal entrainment and

dilution to enlarge the "reaction zone" to encompass the entire reactor. The expanded

reaction zone results in a uniform thermal field and product distribution. This in turn

increases the local availability of water and carbon dioxide, which promotes steam

and dry reforming reactions to a lesser extent, enhancing syngas yields. It was

observed that the more distributed conditions (greater entrainment) yielded higher

reformate quality. In the high temperature reactor, this resulted in higher hydrogen

yields. In lower temperature reactor, the more distributed conditions shifted the

hydrocarbon carbon distribution to favor ethylene and methane over acetylene.

Middle distillate fuels are very challenging to reform. The high sulfur, aromatic, and carbon content inherent in these fuels will often deactivate conventional reforming catalysts. To compensate for the lack of catalyst, non-catalytic reformers employ high reactor temperatures, but this promotes soot formation and reduces reforming efficiency. Reforming under Distributed Reaction Regime avoids the issues associated with catalysts, while avoiding the issues associated with operating at higher reactor temperatures. The middle distillate fuel, Jet Propellant 8 (JP-8) is of particular interest to the military for small fuel cell applications and was determined to be a good representative for middle distillate fuels.

This novel approach to reforming is undocumented in literature for a non-catalytic approach. This investigation studies the thermochemical behavior of a middle distillate fuel under reforming conditions. Chemical time and length scales are controlled through variations in injection temperature, oxidizer concentration, and steam addition. Two reactors were developed to study two different temperature ranges (700-800°C and 900-1100°C). These reactors will allow systematic means to enhance favorable hydrogen and carbon monoxide yields.

Through the course of investigation it was observed that conditions that promoted a more distributed reactor were found to yield higher quality reformate. On multiple instances, the improvement to reforming efficiencies was greater than could be accounted for by varying the reactants alone. Reforming efficiency was demonstrated as high as 80%, rivaling that of catalytic reforming (85%)[1]. The Distributed Reaction Regime suppressed soot formation from occurring within

reactor. No soot formation within the reactor was observed while operating within the Distributed Reaction Regime.

NON-CATALYTIC THERMAL REFORMING OF JP-8 IN A DISTRIBUTED
REACTOR

by

Richard Michael Scenna

Dissertation submitted to the Faculty of the Graduate School of the
University of Maryland, College Park, in partial fulfillment
of the requirements for the degree of
Doctor of Philosophy
2017

Advisory Committee:
 Professor Dr. Ashwani K. Gupta, Chair
 Dr. Gary Pertmer
 Dr. Bao Yang
 Dr. Kenneth H. Yu
 Dr. Nam Wang

Dedication

I dedicate this dissertation to my parents Richard Scenna and Marilynn

Scenna for their love and support.

Acknowledgements

Table of Contents

List of Tables

List of Figures

Glossary

Da	Damkohler number
l_k	Kolmogorov length Scale
l_o	Integral length Scale
k	Turbulent kinetic energy
$PEMFC$	Polymer Electrolyte Membrane Fuel Cell
Re	Reynolds number
Re_o	Turbulent Reynolds number
O/C	Molar oxygen to carbon ratio
S_l	Laminar flame speed
S/C	Molar steam to carbon ratio
$SOFC$	Solid Oxide Fuel Cell
τ_{chem}	Characteristic chemical time scale
τ_m	Characteristic turbulent time scale
u'	Turbulent velocity fluctuations
α	Thermal diffusivity
ε	Turbulent energy dissipation
μ	Dynamic viscosity
δ	Laminar flame thickness

Chapter 1: Introduction

1.1 Background

Reforming is the chemical decomposition of a hydrocarbon fuel into hydrogen rich gas, known as syngas. Fuel rich reforming conditions (O/C=1.0) yield an adiabatic flame temperatures on the order of 800-900°C, which reduces the flame stability. To compensate, catalysts are often employed to reduce the activation energy, allowing the reactions to propagate at lower temperatures. Alternatively, non-catalytic reformers preheat the reactants through filtration combustion or heat exchanges. These techniques yield temperatures greater than the adiabatic flame temperatures, on order of 1200-1400°C. Higher reactor temperatures compensate for the lack of catalysts, by fostering a more rapid and stable flame front, which promotes higher conversion. Both catalytic and non-catalytic reformers operate under the Laminar Flame Regime[2].

The steam reforming of natural gas and methane is a well understood technology and has been in use since the 1930's[3]. Reformers are the primary approach for producing hydrogen for large-scale industrial applications. Together, oil refineries (2.7 million tons per year) and ammonia industries (2.3 million tons per year) account for 46% of hydrogen produced in the United States[4]. Currently, 95% of all hydrogen is produced through catalytic steam reforming of natural gas[5]. Natural gas's (methane) low cost and availability make it an ideal feedstock for industrial applications. From 2005 to 2015 natural gas prices for commercial consumers ranged between 7.22 to 15.64 dollars per thousand cubic foot[6]. As methane lacks C-C bonds, it is less likely to form soot than more complicated

1

hydrocarbon species (acetylene, ethylene, and ethane). Methane has a molar hydrogen to carbon ratio of four, which generates high hydrogen yields that minimize the post processing of carbon monoxide and carbon dioxide.

Nickel catalysts are often employed in the steam reforming of methane due to their low cost and high catalytic activity[2]. This generates high purity hydrogen without nitrogen dilution, which further reduces post processing. Sulfur compounds found within natural gases (hydrogen sulfide and sulfur oxides) are removed through the Amine Claus Process, which is suitable for large-scale stationary applications.

A secondary use has emerged, wherein reformers allow a fuel cell to operate with a wider range of logistically available fuels. The pairing of a reformer with a fuel cell offers unique advantages over conventional internal combustion technology: including superior efficiency, quiet operation, and enhanced reliability. For mobile fuel cell applications, it is more desirable to reform logistically available fuels, generally middle distillates, than employ the less commonly available liquid or compressed hydrogen. In addition to being logistically simpler, liquid hydrocarbon fuels yield a higher volumetric energy density than either liquid or compressed hydrogen, as shown Table. 1-1. Middle distillate fuels of interest are diesels and kerosene; both are abundant in commercial sectors and defense applications require the kerosene (JP-8) due to convenience and logistics.

Fuel	Mole H_2/L
JP-8	53.99
Methane (298 K & 246 atm.)	23.43
Liquid Hydrogen (20 K & 1 atm.)	35.36
DOE target for Metal Hydride	19.80

Table 1-1. Hydrogen density of select fuels

Reformation of middle distillate fuels is a developing technology and is less mature than the reformation of methane or natural gas. Catalytic partial oxidation and autothermal reforming employing noble metal catalysts, are the leading approaches to reforming middle distillate fuels[7].

However, current catalytic reformers are not yet compatible with middle distillate fuels[7,8]. Middle distillate fuels contain multiple C-C bonds and aromatics/olefins compounds, which promote the formation of carbon deposits and unconverted hydrocarbons, which block active catalyst sites. In addition, these fuels can have high sulfur concentrations (up to 3000 ppm_w), and prolonged exposure to sulfur compounds will deactivate most catalysts. Active research has focused on removing the sulfur compounds and improving the catalyst's tolerance to sulfur and carbon[7]. Non-catalytic reactors avoid issues associated with catalyst deactivation and have yielded positive results. However, each approach has its own prospective drawbacks. Filtration combustion requires a porous media, which reduces residence time and reactor capacity. Additionally, multiple authors have cited reformer damage as a direct result of achieving temperatures exceeding the adiabatic flame temperature [9–11]. In addition, Chen et al.[12] found that material properties in designs that used heat exchangers limited the reactor to less favorable conditions. Non-catalytic designs often demonstrate lower reforming efficiencies.

This work explores an alternative form of non-catalytic reforming which does not operate at excessive temperatures of 1200-1400°C. Instead, the advanced combustion technique of Colorless Distributed Combustion will be applied to reforming to enhance conversion and reformate quality. Distributed Reaction Regime

offers the ability to achieve stable reactions without the need for ceramic foam or a heat exchanger, as internal entrainment stabilizes the flame. This results in longer residence times and removes the limitation imposed by heat exchanger based designs. It is also believed the Distributed Reaction Regime will promote steam and dry reforming reactions.

The characteristic chemical time and length scales were altered through preheats, reactant concentrations, and steam addition in order to observe the thermochemical behavior under the Distributed Reaction Regime. The kerosene based Jet Propellant Eight (JP-8) was chosen, as it is strong representative of middle distillate fuels. JP-8 is considered challenging to reform, as it is extremely susceptible to soot formation and its high sulfur content renders most common reformer catalysts inert. Conversely, a simpler hydrocarbon such as methane would not be a good candidate, as it would not demonstrate the potential for soot reductions. Reformer design was based on Colorless Distributed Combustor literature. The following sections provide an introduction to reforming, fuel cells, and the Distributed Reaction Regime.

1.2 Reforming

An ideal reformer minimizes the energy converted to sensible heat and maximizes chemical potential contained within the hydrogen and carbon monoxide yields, while avoiding the formation of hydrocarbons. Reformers typically operate with one-fifth the air typically used in combustors, which results in lower volumetric flow rates, temperatures, and residence times.

Reforming occurs in three phases: (1) Chemical Decomposition, (2) Oxidation, and (3) Steam Reformation. Figure 1-1 shows all three phases for an n-heptane fuel (C_7H_{14}) at a molar O/C ratio of one. Initially, a hydrocarbon fuel decomposes into simpler hydrocarbons (CH_4, C_2H_2, and C_2H_4). Decomposition occurs primarily at the front of the reactor, but can occur to a lesser extent in the following stages. This is followed by a highly exothermic oxidative region, where hydrocarbons generated in the first phase rapidly react with the available oxygen. This presents as a rapid increase in reactor temperatures, hydrogen, steam, and other combustion products. After the oxygen is consumed, the steam, generated as a byproduct of the oxidative phase, promotes the endothermic steam reforming of the remaining unconverted hydrocarbons. These reactions are slower and occur near the rear of the reactor. This last phase is denoted by decreasing concentrations of steam and reactor temperatures.
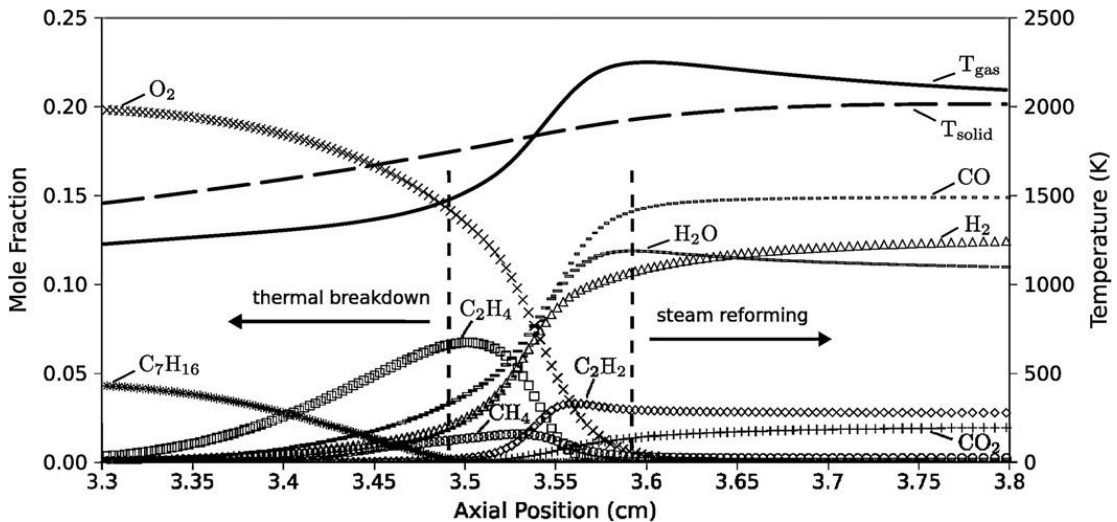
Figure 1-1. Three phases of reformation[13]

There are three major approaches to thermal based reforming: partial oxidation, steam reforming, and autothermal reforming, shown in Figure 1-2. Each approach yields different reformate compositions and combustion characteristics.
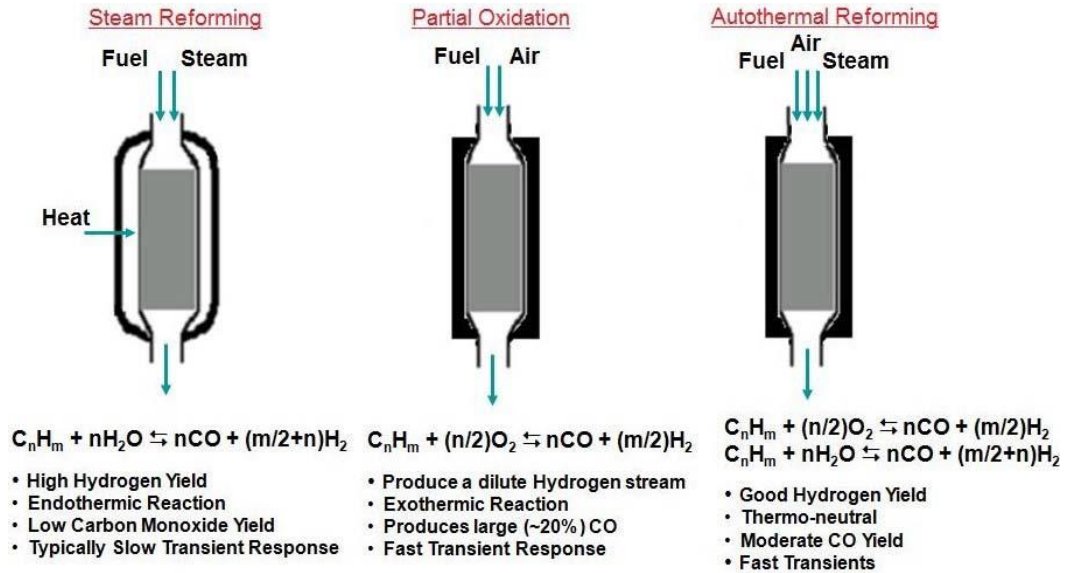
Figure 1-2. Reformer configurations[8]

In partial oxidation, fuel and air undergo a highly exothermic reaction to produce a hydrogen (20-26%) and carbon monoxide (20-24%) rich gas. This approach yields high concentrations of carbon monoxide, but is the least efficient of the reforming approaches. Under ideal reforming conditions (O/C=1.0), non-catalytic reformers typically yield reforming efficiencies ranging between 40-70%[14,15]. A catalytic reactor presents higher reforming efficiencies ranging between 75-90%[7,8]. These reactors tend to be very small and responsive to changes in load. As air is the sole oxidizer, nitrogen will reduce syngas concentrations. Due to high concentrations of carbon monoxide, non-catalytic reformers are often coupled with a solid oxide fuel cell.

A variation, known as wet partial oxidation, adds trace amounts of steam (S/C<1.0) to enhance conversion and reforming efficiency of the partial oxidation process. The steam acts as an oxidizer and promotes the water gas shift and steam reforming reactions, enhancing conversion. The steam moderates the reactor temperature and reduces local hot spots, which in turn protects both the catalyst and reactor. This also reduces the formation of carbon deposits occurring with the reactor and downstream component.

Alternatively, in an approach known as steam reforming, steam can be used as the primary oxidizer. Steam reforming is the endothermic decomposition of a fuel-steam mixture, generates a syngas consisting of 60-70% hydrogen and 8-12% carbon monoxide. Fuel and steam are typically premixed and injected over a heated catalyst bed. The bed is heated through an external burner. Reforming efficiency have been demonstrated exceeding 90%[8]. Steam content varies with reformer design, but reformers typically operate at a steam to carbon ratio of 2-3.

Steam reformers have been used by commercial industry to produce hydrogen for commercial applications since the 1930's[3]. As these reformers activate endothermic steam reforming reactions, an external heat source (burner) heats the catalyst bed, allowing reactions to propagate. As steam reformers are considered heat transfer limited, this results in slow transient response to changes in load. Steam reformers are further limited by their need for large volumes of water, requiring proximity to a water supply. These reformers are larger stationary systems due to their need of heat exchangers, external burners, and water requirements. Water recovery from a fuel cell can allow for enhanced mobility, but increases system size

and weight. These are minor issues for industrial applications, but make steam reforming ill-suited for fluctuating loads as seen in fuel cells and mobile power applications.

A variation on steam reforming, known as oxidative steam reforming, adds trace amounts of oxygen to steam reforming to improve transition in thermal loads or the conversion of challenging fuels. The oxygen helps break up more stable compounds (poly-aromatic hydrocarbons). This is less common, as steam reforming is used most often in industrial applications primarily employing low cost feedstock. Steam reforming or oxidative steam reforming of a middle distillate feedstock would be cost prohibitive.

Autothermal reforming is the combination of partial oxidation and steam reforming in a thermal neutral reaction. Reactants are injected at a molar steam to carbon ratio of 1.5 to 2.0 and oxygen to carbon ratio of 0.7 to 1.0[2]. Air and steam oxidize the fuel to produce moderate hydrogen (30-40%) and carbon monoxide (10-15%) concentrations. This process is characterized by good reforming efficiency ($\eta_{H_2,CO}$=80-90%) and fast transient responses. Typically, under these conditions, steam is added at a molar steam to carbon ratio between one and two. This has also been described as internal heated steam reforming. Nitrogen dilution still occurs, but it is less pronounced than in pure partial oxidation. In an autothermal reformer, no external burner is employed.

1.2.1 Catalytic Reforming

Common fuel rich conditions in reforming generate reactor temperatures on the order of 800-900°C. Catalysts are often employed to reduce the activation energy

8

of the reactions, allowing reactions to propagate under the low temperature

conditions. Conventional catalytic reforming yields efficiency ($\eta_{H_2,CO}$) ranging

between 75-90%[8]. Steam reformers typically employ nickel catalysts, supported on

packed beds or monoliths, for their low cost and ability to activate steam reforming

reactions. Partial oxidation and autothermal reformers, however, more commonly

employ noble metal catalysts such as platinum, rhodium, and palladium, which are all

supported in a powder, monolith, mesh, or packed bad configuration. Catalysts

supported on powders are commonly used for catalyst evaluation and research, but

are less conducive for industrial applications. Conversely, monolith and packed bed

reactors are more typical in industrial applications.

Catalysts are highly reactive to sulfur compounds, which if left untreated, will

bind with the active catalyst sites rendering them inert. In large-scale commercial

hydrogen production, the Amine Claus Process is used to remove sulfur (hydrogen

sulfide & sulfur oxides) from natural gas. This is currently used in the natural gas

industry and is a well-understood technology.

Reformation of logistically available fuels, generally middle distillates, for

mobile power applications are more challenging and less understood. Middle

distillate fuels are commonly available in existing supply chains, such as diesels or jet

fuels. These fuels contain high concentrations of sulfur up to 3000 ppm$_w$. As sulfur is

contained within aromatic hydrocarbons, often within multiple benzene rings, sulfur

is difficult to remove. In addition, middle distillate fuels have a high carbon and

aromatic content, which promotes the fouling of the catalysts and downstream

components. Fouling and poisoning are active areas of research for catalytic

reforming, but a viable solution has not been achieved. High temperature conditions can damage the catalyst through sintering. More information on these issues is provided in Section 1.3.

1.2.2 Non-Catalytic Reforming

Reforming without a catalyst eliminates issues related to catalyst degradation, from sinter, fouling, and sulfur poisoning, while also reducing reformer costs. However, flame temperatures of 800-900°C (O/C=1.0) result in an unstable flame front, forcing non-catalytic reactors to operate at higher temperatures and O/C ratios. To compensate for the lack of catalysts, non-catalytic reformers enhance the activity of reforming reactions by operating at elevated reactor temperatures, often exceeding the adiabatic flame temperatures (800-900°C). In literature, this condition is referred to as a "super adiabatic" and is achieved by internal preheating of reactants through heat exchanger or combusting within a porous media. The removal of catalysts reduces reactor cost and has the potential to increase reactor reliability. More information is provided in the literature review presented in Chapter 2. Most non-catalytic reformers are designed to operate under partial oxidation conditions, as elevated temperatures are used to compensate for the lack of catalyst. Limited literature is available studying either non-catalytic steam reforming or non-catalytic autothermal reforming[16].

Aromatic sulfur compounds present in the liquid fuel will be converted to hydrogen sulfur and sulfur oxides. A non-catalytic reformer/fuel cell system would still require a desulfurizer bed to protect the fuel stack and downstream components. However, the desulfurization of hydrogen sulfide and sulfur oxides through absorbent

beds (lanthanum or zinc oxides) are a better-understood technology than liquid phase desulfurization. Additional information on the effects of sulfur is presented in Section 1.3.2.

Literature on non-catalytic reformers has reported reforming efficiencies ranging between 40-70%[14,15]. Higher reactor temperatures (1200-1400°C) promote the cracking of hydrocarbons, leading to both soot formation and thermal damage[17]. Smith[17] determined through a molar carbon balance that as much as 40% of the carbon in the fuel formed as soot on the reactor walls. Middle distillates (diesel and jet fuels) have a stronger tendency to promote carbon deposits, when compared to that of a natural gases[18].

However, super-adiabatic conditions can also damage the reactor and increase wear on components. Damage to the reactor has been reported in multiple instances [9–11] while operating under super-adiabatic conditions. Additionally, reactor temperatures of 1000-1400°C promote cracking reactions; which further promotes soot formation, either in the reactor or in downstream components[19].

1.3 Reformer Degradation

Both catalytic and non-catalytic reformers are prone to multiple forms of degradation. In particular, catalytic reformers are prone to develop carbon formation, sulfur poisoning, and catalyst sintering. Non-catalytic reformers are prone to thermal damage from the elevated reactor temperatures and temperature fluctuations.

1.3.1 Catalyst Poisoning

Catalyst poisoning is defined as the strong chemical absorption of a species on the surface of the catalyst, which renders an active catalyst site inert. In the context of reforming, this typically refers to the sulfur compounds inherent in the fuel binding to the reforming catalyst. Sulfur species have a strong affinity for commonly used reforming and fuel cell catalysts (nickel, rhodium, and platinum). Sulfur compounds deactivate the reactions associated with steam reforming, while promoting the methanation of carbon monoxide to hydrogen poor products[18]. In addition, sulfur compounds catalytically promote the formation of a carbon film from the absorbed carbonous compounds[18]. Carbon film and Coke species block access to activate catalyst sites. More information is presented in Section 1.3.2.

Sulfur compounds within gaseous fuels (natural gas / propane) most commonly occur in the form of hydrogen sulfide and sulfur oxides. In middle distillate fuels (kerosene and diesel), sulfur-bearing species occur in the form of aromatic hydrocarbons. Prominent sulfur compounds in diesel fuels consist of alkylated benzothiophene, dibenzothiophene, and alkylated derivatives[20]. In jet fuels, sulfur is primarily contained within alkylated benzothiophenes[21]. Current approaches for removing sulfur vary by application and feedstock.

When sulfur is contained within hydrogen sulfide, the Amine Claus Process can be employed to purify the feedstock. Natural gas containing high concentrations of hydrogen sulfide is referred to as sour gas. The natural gas industry uses this approach to sweeten natural gas (reduce sulfur compounds). This two-step process separates the hydrogen sulfide from the natural gas with an alkylamines solution, and

converts the hydrogen sulfide into pure sulfur and steam, see Figure 1-3. An

alkylamines solution, also known as amine, selectively absorbs the hydrogen sulfide

in the sour gas[22–24]. The purification of the hydrogen sulfide occurs in two phases

(absorption and regeneration).

In the absorption phase, hydrogen sulfide lean amine is injected into the

upward flowing sour gas, where the amine solution absorbs the hydrogen sulfide and

carbon dioxide compounds. The purified sour gas, now called sweet gas, is collected

at the top of the absorber and is ready to be processed by a reformer. The hydrogen

sulfide rich amine pooling at the bottom of the reactor is then transferred to the

regenerator for purification.

Within the regeneration phase, the hydrogen sulfide rich amine is heated in

the presence of steam, releasing the hydrogen sulfide and carbon dioxide compounds.

Hydrogen sulfide compounds leave through the top of the column, while the

hydrogen sulfide lean amine is collected at the bottom to be reused in the absorber.
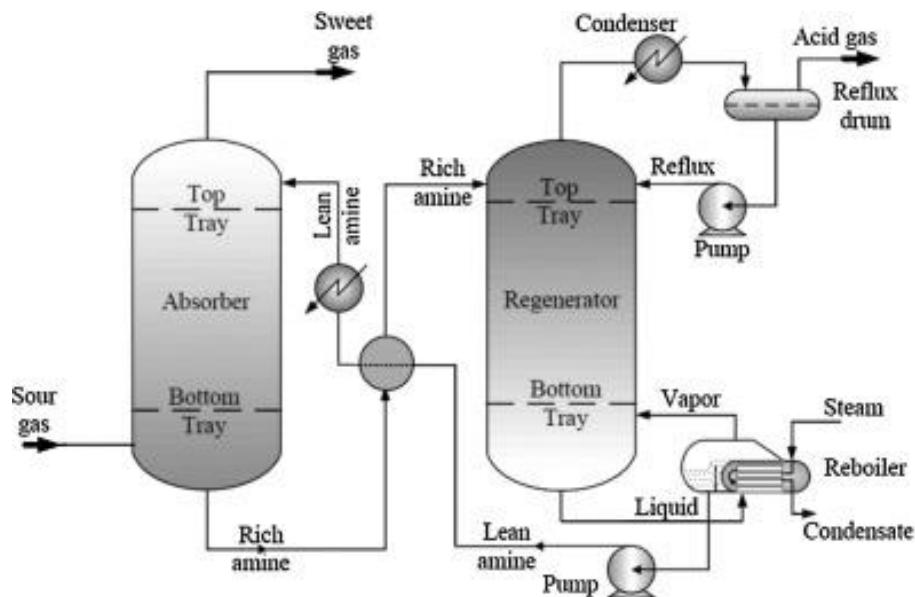
Figure 1-3. Amine separation of hydrogen sulfide[25].

13

As hydrogen sulfide is a toxic pollutant and cannot be directly released into atmosphere, the hydrogen sulfide must be neutralized. The Claus Process selectively oxidizes the hydrogen sulfide into sulfur and water through a two-step process, R. 1-1 and R. 1-2. This process is also used in the petroleum industry for treating hydrogen sulfide.

$$2H_2S + 3O_2 \rightarrow 2SO_2 + 2H_2O \qquad\qquad \text{R. 1-1}$$
$$2H_2S + SO_2 \rightarrow S + 2H_2O \qquad\qquad \text{R. 1-2}$$

The Amine Claus Process is best suited for stationary applications. For mobile applications employing logistics fuels (diesel and jet fuels), the removal of sulfur compounds is best accomplished through an absorbent bed or employing sulfur resistant catalysts.

Absorbents selectively absorb the desired chemical compounds, reducing sulfur concentrations to less than 1 ppm$_w$, while leaving the remaining fuel unaffected. Absorption can occur as physical absorption (van der Waals and electrostatic forces) or chemical absorption. Absorbents are characterized by the amount of sulfur that can be absorbed before saturation and breakthrough occurs[20]. Absorbents have a finite capacity. After saturation, they must be replaced or regenerated. Regeneration of an absorbent bed can occur under inert (nitrogen), oxidative (air), or reducing (hydrogen) environments.

In liquid phase desulfurization, the sulfur absorption is governed by the electron structure of the organic compounds. Lee[26] evaluated JP-8 from multiple sources over a four year period and determined that both 2,3-dimethylbenzothiophene and 2,3,7-trimethylbenzothiophene were the primary sulfur

14

bearing species. Thiophene has high electrostatic potential[20] and the addition of either aromatic and methyl groups increase it[20]. This aspect is used in absorbents to separate sulfur bearing species from the desired hydrocarbons.

Multiple absorbent compounds have been evaluated in literature[20]. Metal oxides and mixed-metal oxides such as zinc oxides, lanthanum oxides, and titanium-cerium commonly are used to remove both gaseous and liquid sulfur compounds. These absorbents can be regenerated with air, making them strong candidates for fuel cell systems. Alternatively, activated carbon is abundant and has shown a high capacity for absorbing sulfur compounds found in both gasoline and jet fuel. However, regeneration requires washing with a polar solvent, which is not practical for mobile fuel cell applications. This absorbent can be used best as a replaceable filter. Nickel based absorbents have been found to have a high sulfur capacity[20], but require hydrogen for regeneration. Zeolite based absorbents have a more limited capacity to absorb sulfur compounds[20]. In addition, olefins and aromatic hydrocarbons decrease the effectiveness in removing thiophene compounds[20]. As JP-8 contains a high olefinic and aromatic content, zeolite absorbents are the least compatible.

Alternatively, there are ongoing efforts to develop a catalyst compatible with the high sulfur concentrations found in JP-8. A catalyst's resistance to sulfur varies with material[7,18,27]. Nickel is one of the most commonly used reforming catalyst, but is highly susceptible to sulfur compounds[28]. The addition of molybdenum or boron to nickel catalysts have been reported to improve the catalyst's resistance to sulfur compounds[29]. Noble metals such as rhodium and platinum have shown

higher resistance to sulfur poisoning[18]. Hydrogen sulfide has a strong affinity for nickel and is highly selective towards active nickel sites. To further protect noble metals, nickel can been added as a sacrificial catalyst. Sulfur compounds selectively bond to the active nickel sites, protecting the noble metal catalyst sites[18].

However, even if sulfur tolerant catalysts are employed, an absorbent bed would be required to the protect catalyst within the fuel cell[7]. After the reforming process, sulfur would be converted to hydrogen sulfide and sulfur oxides.

1.3.2 Fouling of the Reformer

Primarily, fouling in reforming occurs due to the deposition of carbonous species on to the catalyst's surface or downstream components. Carbon deposition occurs in two forms: Carbon and Coke[18]. The term Carbon refers to when graphitic carbon is formed through the carbon monoxide disproportionation reaction. Coke refers to the chemical decomposition or polymerization of hydrocarbons. Carbon deposition can vary in severity. In its mild and reversible form, it can coat and block the active catalyst sites. In its most severe form, it can physically damage and delaminate the catalyst. In literature, carbon deposition has been classified into five forms[18,29,30].

- Carbon species can block access to catalyst sites through chemisorption in monolayer or physical absorption in multilayer.
- Encapsulating film is the slow polymerization of unsaturated hydrocarbons, encasing the metal partials blocking active sites. This condition occurs below 500°C.

16

- Pyrolytic carbon is deposition of carbon precursors on catalyst surface, blocking catalyst pores and increasing pressure drop. Temperatures greater than 600°C promote this form of carbon deposits.

- Carbon whisker is the diffusion of carbon through the catalyst crystallite. In extreme cases, this results in the catalyst detaching from the support. This form of carbon typically forms at temperatures greater than 450°C.

- Soot is the homogeneous nucleation and growth of carbon particles.

Carbon formation is influenced by reactor conditions and feedstock. Low oxidizer concentrations (S/C or O/C ratios) promote the formation of carbon deposition. Feedstock has a strong impact on the emergence of carbon formation. It is generally agreed upon that carbon formation increases in order of poly-aromatic > mono-aromatic > olefin > branched alkanes > normal alkanes[18]. Therefore, fuels such as methane are more resistant to carbon formation than middle distillate fuels, which contain both mono-aromatic and poly-aromatic hydrocarbons. Aromatic and olefins promote the formation of carbon deposition in the form of whisker and encapsulating films[18]. High pressure and acidic catalysts promote the formation of pyrolytic carbon[18].

In non-catalytic reforming only two forms of carbon have been observed: Film/Gum and Soot. Film/Gum can occur downstream of the reactor, under regimes of low conversion and temperature (less than 500°C). Bartholomew[29] observed that operating at low temperatures induced gum formation for diesel fuels, but not for jet fuels.

Within the work outlined within this dissertation, gum formation was observed during the startup of the low temperatures reactor. At higher temperatures, visible soot formation was observed in exhaust line. While catalyst deactivation from carbon is a concern, downstream components are inadvertently affected by soot generated in the reformer.

Current catalytic efforts focus on developing catalysts that suppress the formation of Coke and Carbon[7,31]. Nickel based catalysts have a tendency to promote carbon formation[32]. Carbon formation can be reduced by doping nickel catalysts with Ag, Sn, Cu, Co, Fe, Gd, and Bi[33–35]. Nikolla showed that the addition of Sn in amounts of $1\%_{wt}$ to nickel, suppressed the formation of C-C bond, preventing carbon deposition[34,35]. Doping non-catalytic the catalyst with silver and gold has also been shown to enhance the reactivity of the partial oxidation reaction, while suppressing carbon formation[36–38]. Alternatively, a reduction in the ensemble size of the catalyst by selective sulfur passivation reduces the polymerization of monatomic carbon on the catalyst surface[7]. Lee et al.[7] cited carbon formation could be prevented if a H_2S-to-H_2 ratio greater than 7.5×10^{-7} was applied. Noble metals of platinum or rhodium are less susceptible to formation of carbon[39].

1.3.3 Thermal Damage

High reactor temperatures or rapid changes in temperature can damage both non-catalytic and catalytic reformers. In non-catalytic reformers, excessive temperatures (1200-1400°C) are often employed to compensate for the lack of catalyst. Over time, prolonged exposure to this environment induces thermal stress

and fatigue, resulting in damage to the ceramic components. In catalytic reformers, higher operating temperatures are not required, but are generated unintentionally. Poor mixing results in the uneven distribution of oxidizer throughout the reactor. Regions that are fuel lean will promote full combustion over reforming reactions, which results in localized regions of elevated temperatures, likewise resulting in damage. Thermal damage to the reactor can appear in two forms: catalyst sintering and thermal shock.

Sintering, which applies only to catalytic reforming, is the migration of multiple small metallic particles into a single larger particle, which causes a reduction in the effective surface area of the catalyst. The Tamman temperature of the catalyst is defined as half the melting temperature of the catalyst material. Operating the reactor above this temperature promotes sintering of the catalyst, while temperatures below are believed to be too low for diffusion of metal particles too occur[18].

Two mechanisms for sintering have been proposed: atom migration and particle migration. In atom migration, metal atoms are emitted from one particle and transferred to a second. In particle migration, particles move across the support to form a larger particle. Figure 1-4 shows a graphical representation of the two forms of sintering.
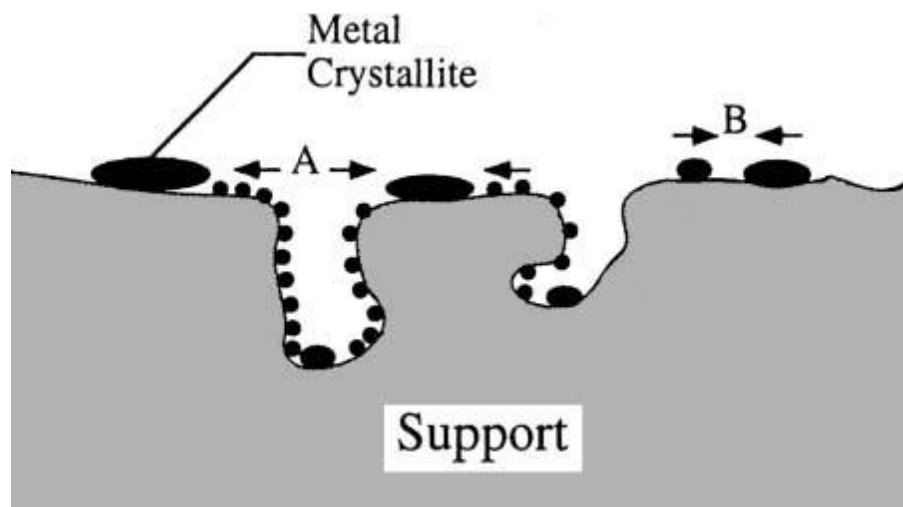
Figure 1-4. Catalyst sintering: (A) Atomic migration, (B) Particle migrations[29]

Thermal shock is the thermal degradation induced by the thermal stresses on the reactor. Thermal shock is a common issue in non-catalytic reformers, but can also damage catalytic reactors. Reforming is considered a reducing environment (hydrogen and carbon monoxide), which limits the selection of insulation to more brittle insulation. Alumina is resistant to the reduction, but is prone to thermal shock. Insulations containing a high silica content are resistant to thermal shock, but prone to reduction by syngas. Literature[40] has shown up to 28% weight loss within 30 hours of exposure to hydrogen at temperatures of 1400°C.

Thermal shock can be mitigated by careful control of the reactor conditions. Steam injection can mitigate reactor temperature fluctuations, by acting as a thermal dilutant and promoter of endothermic reactions. Stress relief can be incorporated into the insulation, minimizing fatigue. Within this work, the cylindrical insulation was divided into four segments to reduce thermal stress induced during ignition and shutdown. Using a well-mixed injection avoids local hot spots. Thermal stress can also be reduced by operating at reduced temperatures.

1.4 Turbulent Flame Regime

Turbulent Flamelet Theory approximates the bulk turbulent flame as a
compilation of multiple laminar flamelets[41]. This permits the independent
calculation of the properties relating to turbulent flow and chemistry. In Figure 1-5
and Figure 1-6 the relevant Premixed Turbulent Flame Regimes are defined.
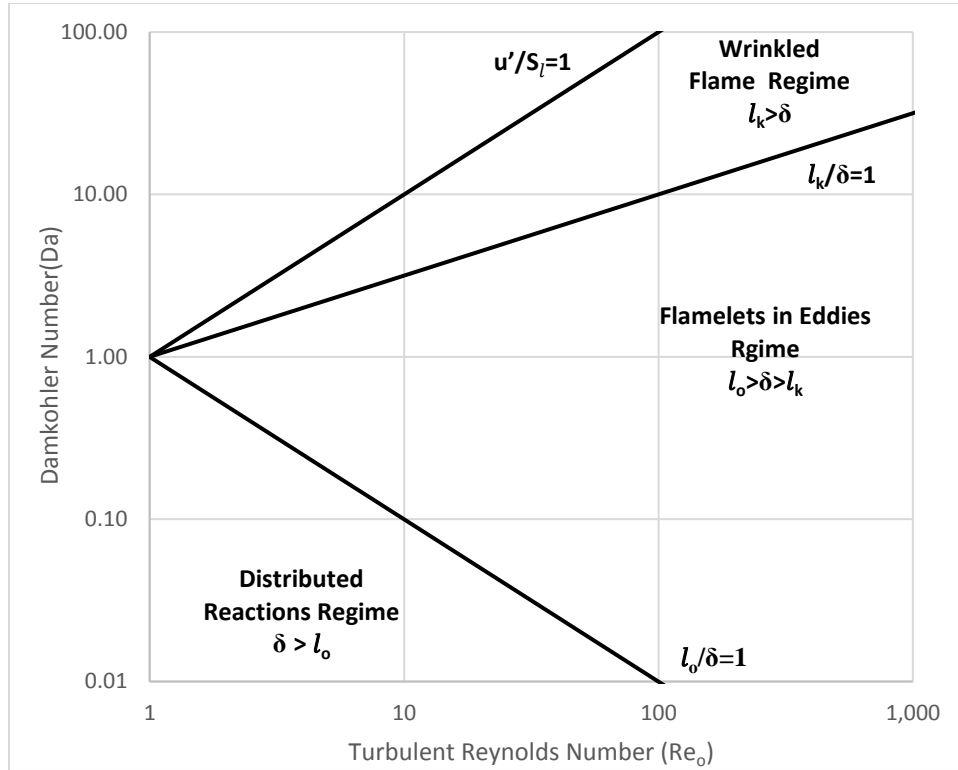
Figure 1-5. Premixed turbulent flame regimes

Turbulent premixed combustion flame regimes are classified by the ratios of
the characteristic lengths and time scales relating to turbulence (transport) and
chemistry. Relevant properties for species transport are based on turbulent flow, as
transport is primarily achieved through turbulence transport, not diffusion[42]. The
ratio of the turbulent time scale to chemical time scale, known as the Damkohler
number (Da), indicates whether the flame is limited by transport or chemistry.

21

Turbulent Reynolds (Re_o) is the ratio of vicious dissipation to turbulent transport. It provides a measurement of turbulence relative to the integral length scale. Turbulent velocity fluctuations (u') represent the root mean squared of velocity fluctuations within the flow. The Integral (l_o) and Kolmogorov (l_k) length scales represent the mean diameter of largest and smallest eddies in the flow.

Properties pertaining to the chemistry are based on laminar flame conditions. Laminar flame thickness (δ) represents the characteristic length for the reactions to occur, while laminar flame speed (S_l) represents the rate of propagation of a laminar flame.

Flame regimes associated with conventional combustion are the Wrinkled Flame Regime and Flamelets in Eddie Regime. The Wrinkled Flame Regime occurs at Da greater than one and when δ is less than l_k. Under this regime, the reaction front (δ) resides within the smallest eddies in the flow (l_k). This results in the flame appearing as a thin sheet. The Flamelets in Eddies Regime occurs when δ is greater than l_k, but less than l_o. The reaction front is sufficiently small enough to reside in-between the largest (l_o) and smallest (l_k) eddies in the flow, and presents as an elongated flame with visible emissions. In this intermediate regime, the flame can be limited by either transport or chemistry as the Da can be greater or less than one. The boundary between the Flamelets in Eddies and Wrinkled Flame Regimes is called Klimov-Williams Criterion, which occurs when δ equals l_k.

Distributed Reaction Regime occurs at Da less than one and when δ exceeds the l_o [43]. Under this condition, the flame front (δ) is too wide to completely reside within the largest eddies in the flow (l_o), and is considered chemistry limited. As

transport is sufficiently faster than the chemistry, reactions occur over a large volume. The Distributed Reaction Regime is associated with conditions causing volumetric distributed combustion. The upper limit of the Distributed Reaction Regime, known as Damkohler criterion, occurs when δ equals l_o. The Distributed Reaction Regime presents as low visible emissions. Under these conditions, the reaction front envelopes the reactor, presenting a colorless image. In some literature[44,45], the term flameless has been used to describe the transparent nature of the reaction zone.
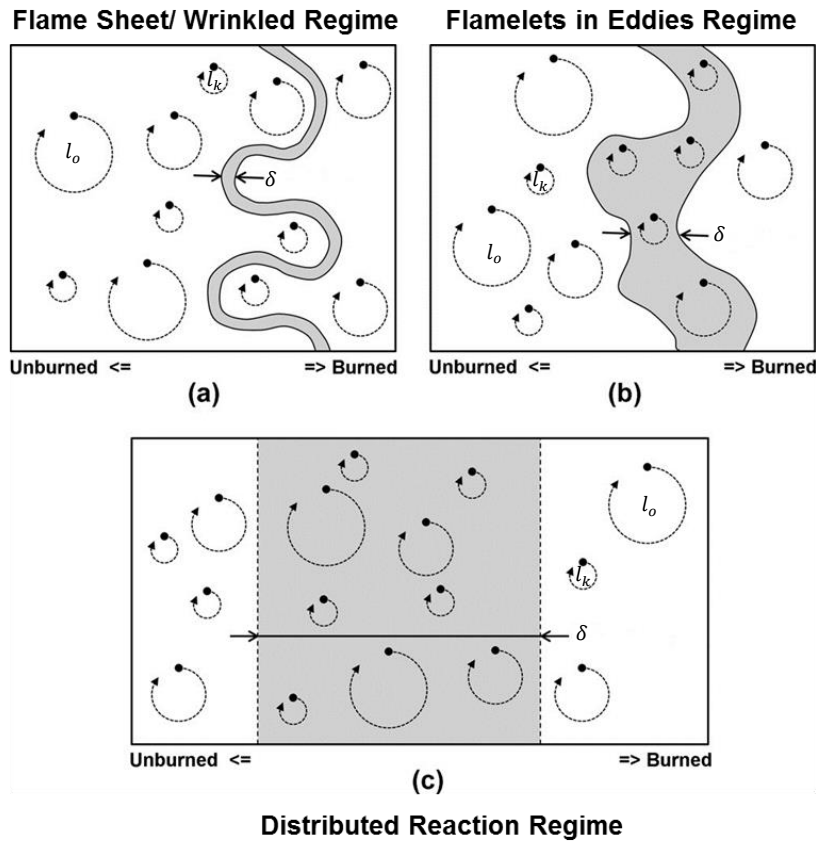
Figure 1-6. Graphical representation of the premixed turbulent flame regimes[46]

For the Distributed Reaction Regime to develop, the air fuel mixture is injected through a high velocity jet, entraining the exhaust products into the mixture before ignition can occur. The entrainment of exhaust products reduces local oxygen

23

concentrations. When ignition occurs, this elongates the chemical time and length scales. The high velocity jet promotes a more rapid mixing, which reduces the turbulent time and length scales. This results in the characteristic chemical length scales exceeding the characteristic turbulent length scales, generating a volumetric distributed flame.

Entraining the hot effluent into the fuel-air mixture causes thermal dilution, which reduces peak reactor temperature, but raises the average reactor temperature. This in turn induces a uniform thermal field. Operating at reduced oxygen concentrations (less than 12%), without preheating the air and fuel, will destabilize the reaction zone. Preheating the reactant to temperature of 1000 K extends the lower flammability limit beyond conventional combustion conditions, allowing a stable flame to emerge at reduced oxygen concentrations, see Figure 1-7.
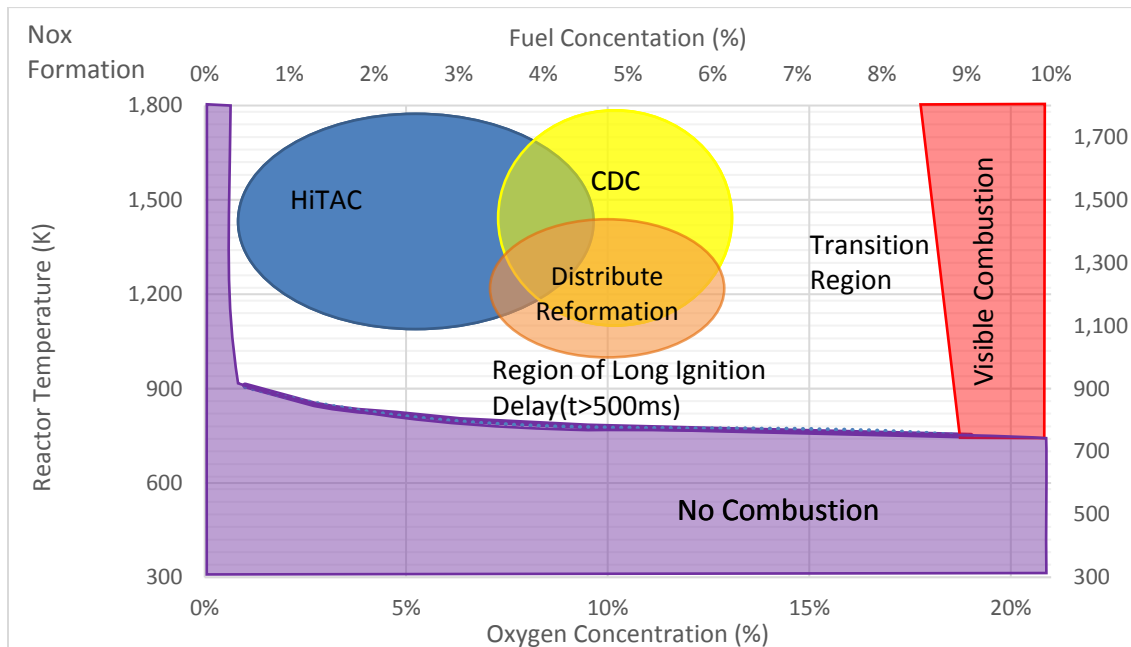
Figure 1-7. Regions of flame stability under reduced oxygen and fuel concentrations. Methane O/C=3.0

Figure 1-8 shows a methane diffusion flame with and without dilution (nitrogen) and corresponding numerical simulations. The addition of nitrogen to the mixture reduced the oxygen concentrations, which drastically thickened the flame. Flame thickness is shown in red. In the non-diluted case, there is a defined interface between the regions of fuel and air. However, in the diluted-distributed case the interface is not well defined, as a gradual transition exists between the two regions. Dilution reduced both peak temperature and the temperature gradient, but resulted in a higher average reactor temperature.
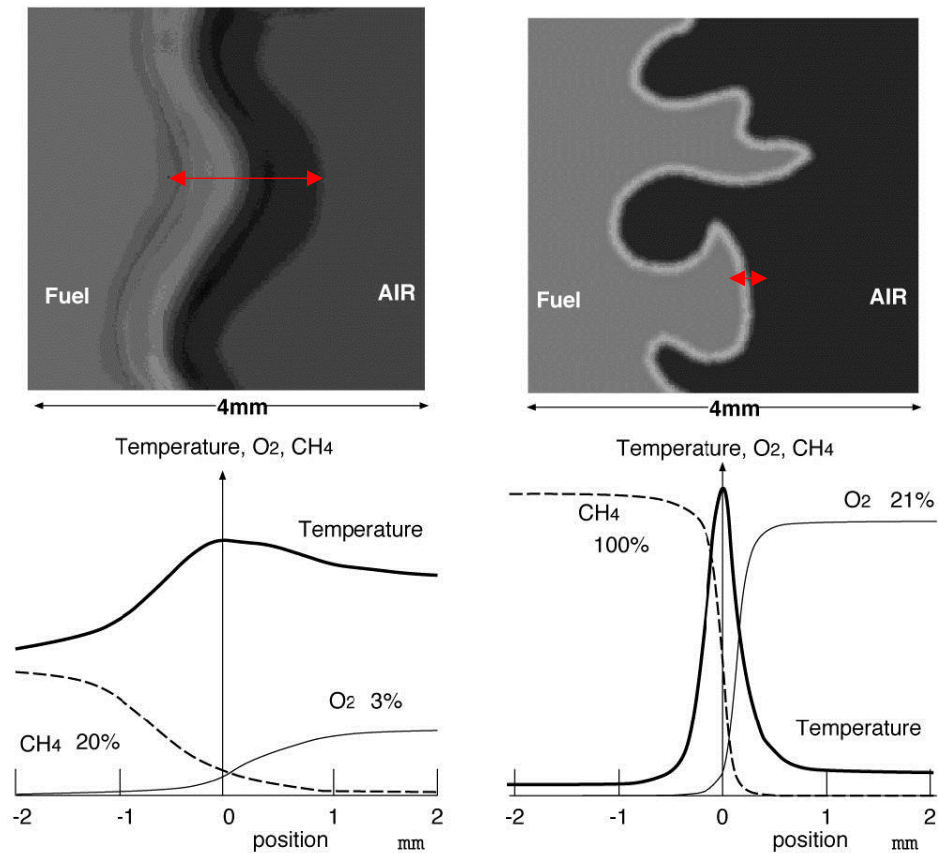
Figure 1-8. Experimental and numerical methane flame with and without dilution[47]

High Temperature Air Combustion (HiTAC) and Colorless Distributed Combustion (CDC) are two leading approaches to achieve this condition and reduced

NO$_x$ emissions. Both HiTAC and CDC use the entrainment of exhaust products to reduce oxygen concentrations and develop a uniform thermal field. However, each application imposes unique requirements. Figure 1-9 shows the approximate location of CDC and HiTAC within the Distributed Reaction Regime.
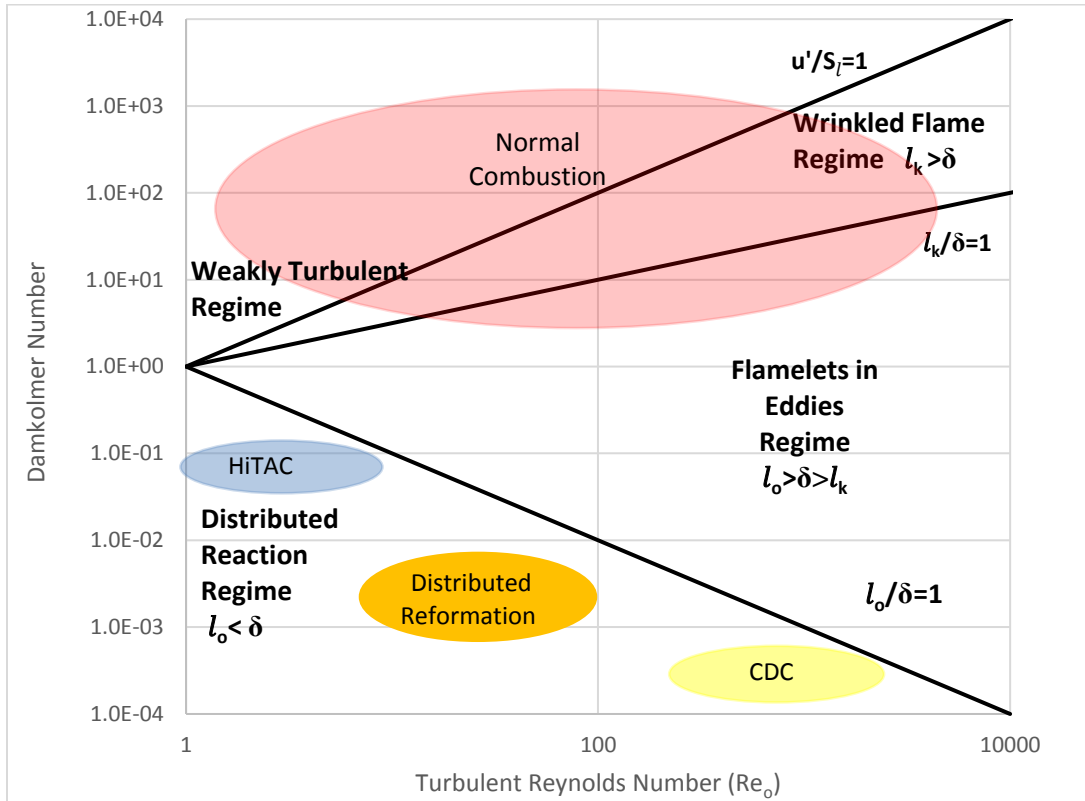
Figure 1-9. Borghi diagram showing the combustion regimes

1.4.1 High Temperature Air Combustion

High Temperature Air Combustion (HiTAC) is intended for furnace applications, operating at low thermal intensities, generally less than 1MW/m^3-atm [47,48]. Injection velocities range between 29-40m/s, while reactor oxygen concentrations typically range between 2-8%[47]. This results in lower Turbulent

Reynolds numbers, but longer characteristic chemical time scales than equivalent

Colorless Distributed Combustion.

To ensure stable operation, the air must be preheated to or above the auto

ignition temperature of fuel, on the order of 1000-1400°C. This eliminates the need

for stabilizing media, such as bluff body. The removal of stabilizing media reduces

the pressure drop across the reactor, while increasing the average residence. Higher

preheats result in HiTAC operating only under the non-premixed combustion mode.

Fuel and air are injected at discreet locations, relying on turbulent transport to

propagate the reaction. Under HiTAC conditions, peak reactor temperatures are

usually no more than 50-100°C greater than preheated air temperature[49].

1.4.2 Colorless Distributed Combustion

It was later determined that high temperature air was not a requirement to

achieve low emissions and the characteristic colorless reaction zone[48]. In Colorless

Distributed Combustion (CDC), fuel and air are injected at temperatures below the

fuel auto-ignition temperature. Instead, CDC relies on the entrainment of hot exhaust

gases to elevate the mixture's temperature to conditions exceeding the auto-ignition

temperature, allowing a stable combustion. Lower injection temperatures allowed the

combustor to be able to operate in either premixed or non-premixed modes.

Colorless Distributed Combustion is intended to provide low NOx emissions

with high thermal intensity for turbine applications. Typically, these combustors

operate at high thermal intensity of 20 to 400MW/m^3-atm[48]. Injection velocities

typically range between 100-200m/s, which results in a smaller character turbulent

time scales and higher Turbulent Reynolds numbers (still restricting $D_a < 1$) when

compared to an equivalent HiTAC combustor. Turbine applications require operation with excess air (Φ=0.6). This results in the entraining of combustion products with high concentrations of oxygen, which limits the recirculation ability to reduce oxygen concentrations. This limits CDC conditions of oxygen concentrations ranging between 8-12%.

1.4.3 Distributed Reformation

The application of the Distributed Reaction Regime to fuel reformation is called Distributed Reforming. This approach draws on aspects of both HiTAC and Colorless Distributed Combustion to overcome some of the key issues of reforming middle distillate fuels. While this approach was originally pioneered for NO_x reduction for furnace and turbine applications, this is not the main concern under reforming. Reformers operate at temperatures (1200-1400°C) too low for NO_x formation to occur. As reforming occurs within the soot formation regime, soot produced in conventional reforming can damage downstream components. To compensate, reformers are operated at less than ideal conditions (O/C>1.0) to avoid soot formation. The Distributed Reaction Regime has been shown in both combustion and reforming (within this work) to suppress soot formation [47,48,50], thus allowing operation under more ideal conditions without soot formation.

Reforming typically occurs at temperatures of 800-900°C, which results in an unstable flame with poor yields. Typically, non-catalytic reformers compensate by operating at elevated temperatures (1200-1400°C), which promote sooting and damage to the reactor. The Distributed Reaction Regime presented enhanced conversion and stability over conventional flames.

28

In the Distributed Reaction Regime, the characteristic chemical time and length scales exceed characteristic time and length scales associated with turbulent transport. To initiate this, the fuel-air mixture was injected through a high velocity jet into the reactor. This jet entrained exhaust products into the mixture, which diluted the local oxygen concentrations. This reduced the activity of the oxidative reactions[48,51], elongating the chemical time and length scales. As partial oxidation is a rapid reaction, a small reduction in activity will not affect the overall conversion. The high velocity jet also enhanced mixing, which reduced characteristic time and length scales associated with turbulent transport. This delay allows the exhaust products to entrain into the flow, which alters the chemistry when ignition does occur. More distributed conditions promote a greater entrainment of exhaust products into the fuel-air mixture. Without the enhanced mixing and dilution, a conventional flame would have emerged, as reactions would have proceeded at conventional time and length scales. As recirculation increased, the local fuel and oxygen concentrations diminished, while local concentrations of hydrogen, steam, carbon monoxide, and carbon dioxide increased.

The entrainment of hot exhaust products influenced the temperature distribution within the reactor. The entrainment of hot exhaust gases into the reaction zone raised the average reactor temperature, while the entrained exhaust gases reduced peak temperatures through thermal dilution. Elevating the average reactor temperature enhanced the activity of the reforming reactions, while reducing the peak reactor temperature reduced both the cracking of the fuel and wear on the reactor.

Higher average temperatures also served to stabilize the reactions under oxygen-depleted conditions.

The benefits from the Distributed Reaction Regime are derived from the entrainment of the hot exhaust products. In reforming, soot is primarily formed through hydrogen abstraction carbon addition (HACA) mechanism[52] (R. 1-3 to R. 1-4), while acetylene forms through dehydrogenation reactions[53] (R. 1-5 to R. 1.6). In particular, steam and carbon dioxide have been shown in combustion literature to suppress acetylene and soot formation[16,54–56]. Soot abatement is induced through dilution and chemical interactions of the carbon dioxide and steam. Steam and carbon dioxide promote hydroxyl radical formation, which interferes with acetylene formation through hydrogen abstraction and soot formation through the hydrogen abstraction carbon addition mechanism[16,54–56], shown in R. 1-7 to R. 1-10. Conditions occurring within the Flamelet in Eddies Regime caused the partial oxidation reactions to propagate faster, limiting entrainment. The more distributed condition should limit activity of dehydrogenation reaction, which should cause the more distributed conditions to favor reformate products hydrocarbon with a higher H/C ratio.

Hydrogen Abstraction Carbon Addition

$$C_xH_y + H \Rightarrow C_xH_{y-1} + H_2 \hspace{4cm} \text{R. 1-3}$$
$$C_xH_{y-1} + C_2H_2 \Rightarrow PAH \hspace{4cm} \text{R. 1-4}$$

Acetylene Formation

$$C_2H_4 + H \rightarrow C_2H_3 + H_2 \hspace{4cm} \text{R. 1-5}$$
$$C_2H_3 + H \rightarrow C_2H_2 + H_2 \hspace{4cm} \text{R. 1-6}$$

Soot Oxidation

$$CO_2 + H \Rightarrow OH + CO \hspace{6cm} \text{R. 1-7}$$
$$H_2O + H \Rightarrow OH + H_2 \hspace{5.8cm} \text{R. 1-8}$$
$$H_2O + O \Rightarrow 2OH + H_2 \hspace{5.6cm} \text{R. 1-9}$$
$$OH + Products \Rightarrow CO + H_2O \hspace{5cm} \text{R. 1-10}$$
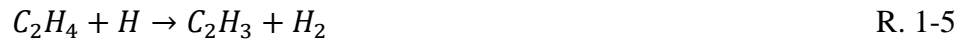
Higher reactor temperatures of 800-1100°C will cause the entrained exhaust

products (steam and carbon dioxide) to promote steam and dry reforming reactions,

enhancing reformate yield. Adding additional steam (wet partial oxidation) will only

increase this effect. As mentioned previously, the more distributed condition

promoted greater entrainment; this corresponds to increased potential for steam and

dry reforming reactions. However, as the Distributed Reaction Regime promotes a

well-mixed condition (minimizing carbon dioxide formation) and as the steam

reforming reactions are considered up to three times faster[57], it is thought that the

Distributed Reaction Regime will primarily be influenced by steam reforming

reactions. Dry reforming reaction are still thought to occur, but are not as active. In

conventional partial oxidation, steam reforming reactions only occur toward the rear

of the reactor, where in distributed reforming they occur throughout the reactor.

Limited research has been conducted in non-catalytic steam and dry reforming of

hydrocarbons fuels. Most information was derived from the experimental results from

blank reactors used in catalyst evaluations and the gasification of biomass and waste.

It was generally observed that reactor temperatures of 800-1000°C are

required to activate steam reforming reactions in non-catalytic reformers[16,58–63].

Steam reforming reactions are slower, generally requiring residence times greater

than 400-500 ms. Best results appeared when the reactor residence time was on the

order of 1000 ms or operating at higher operating temperatures 1300°C. Studies

31

[64,65] using residence times of 50-200 ms, more typical of catalytic reformers, indicated that steam reforming reactions were inactive at these temperatures and time scales. Catalysts enhance the activity of the steam reforming reactions, allowing full conversion within shorter time scales of 50-200 ms. This results in the steam reforming reactions often being cited as inactive without catalysts[64,65].

Woodruff[58] evaluated the steam gasification of char at temperatures of 1000-1050°C and residence time of 1000 ms. Molintas[59] showed steam reforming of tar at temperatures of 800-900°C could occur within short residence times of 5-10 ms. Sharma et al.[60] evaluated the steam reforming of propane and determined reactor temperatures of 800-1000°C and residence time of 1300 ms were necessary to promote steam reforming reactions. Bartekova[61] investigated the steam cracking (S/C=4.5) of hexadecane at time scales of 50-300 ms and reactor temperatures of 700-760°C. Under these conditions, the formation of carbon monoxide and carbon dioxide were observed, which is indicative of steam reforming reactions. Parmar[62] evaluated diesel at O/C ratios of 0.4-1.0, and reactor temperatures of 700-850°C. The reactor was operated at an S/C ratio of 1.5 and a residence time of 2830 ms. From the data (850°C and O/C=0.4), 25% more oxygen was detected in molar flow rate of carbon monoxide and carbon dioxide than was available in the air. This extra oxygen is indicative of steam reforming reactions. Roth[16] operated the reactor at residence times of 400 ms and temperature of 1300°C. He showed increasing the steam to carbon ratio promoted increasing carbon monoxide and hydrogen concentrations, indicative of steam reforming reactions. The work detailed in Section 7.3 showed active steam reforming reactions using JP-8 occurring at time scales of 750-850 ms

32

and temperatures of 800-1000°C. The addition of steam (S/C=0-0.10) reduced reactor temperatures from 1000°C to 755°C, while increase conversion from 90% to 97%. An additional increase in steam content beyond S/C=0.1 did not improve conversion.

Dry reforming is the interaction of carbon dioxide with a hydrocarbon fuel and is considered a slow reaction. Dry reforming reactions are up to three times slower than steam reforming[57]. Dry reforming literature often evaluated sample over a period of 15-20 minutes, until the sample was completely converted[66]. However, the initial reactions occurred over a shorter period. Dry reforming literature was very limited, focusing primarily on waste and biomass feedstocks. The following articles were relevant to this work.

These reactions require temperatures of 800-1000°C to activate, and time scales of at least 1000 ms[67–71]. Zhang[67] observed meaningful conversion (10-80%) of methane through dry reforming reactions at temperatures of 1000-1200°C. Residence time was on order of 2000 ms. The dry reformation of char from various biomass sources have been examined by multiple authors[68–70]. Reactor temperatures of 800-1000°C were required to activate the dry reforming reactions. Barkia[71] found that reactor temperatures of 900°C were required to dry reform shale oil, but no information was shown of reformate composition over time.

The Distributed Reaction Regime offers the ability to achieve stable reactions without the need for ceramic foam or heat exchanger. Reactor construction is simpler, as internal entrainment stabilizes the flame. This approach allows high temperature insulation to cover a simple pressure vessel, constructed of stainless steel, for enhanced durability and robustness. The Distributed Reaction Regime's uniform

thermal field reduces the thermal stress on insulation over that of a conventional non-catalytic reactor.

Distributed reformer design was modeled after Colorless Distributed Combustor design. However, a key difference should be noted. In Colorless Distributed Combustion, the hot exhaust gases are relatively inert (CO_2, N_2, and H_2O), but within Distributed Reformation the exhaust gases are composed of more active species (H_2, H_2O, CO, CO_2, CH_4, C_2H_2). This in turn will change the effective chemistry. Mi et al.[72] and Khalil and Gupta[73] observed the cofiring of methane with hydrogen altered the combustion characteristics of the CDC reactors. The flame front occurred sooner and higher entrainment was needed to maintain the Distributed Reaction Regime. Reforming under the Distributed Reaction Regime is thought to be similar.

1.5 Fuel Cell System

The fuel cell system is composed of a reformer, a fuel cell stack, and syngas conditioning. Fuel cell stacks impose certain unique requirements on the reformate composition, while each reforming approach yields syngas of varying quality. Further syngas conditioning is determined by the fuel cell stack requirements, as well as the reformer syngas composition. For example, the steam reforming of natural gas generates a relatively pure stream of hydrogen; only requiring minor syngas gas conditioning for use with a high temperature PEMFC. However, the partial oxidation of natural gas generates high concentrations of carbon monoxide, which requires significant syngas conditioning for operation with a low temperature PEMFC. The following section describes the requirements of the PEMFC and SOFC system.

34

1.5.1 Fuel Cell Stack

A fuel cell is an electrochemical device, consisting of a cathode, anode, and electrolyte. Each fuel cell stack has unique syngas requirements vary with fuel cell designs. The most common fuel cell configurations are the solid oxide and the proton exchange membrane fuel cells. Other designs exist, such as solid acid, phosphoric acid, molten carbide, and alkaline fuel cells, but are not as prevalent or thoroughly researched[74].

1.5.1.1 Solid Oxide Fuel Cells

Solid oxide fuel cells (SOFC) are ceramic-based fuel cells capable of accepting a wide range of reformate quality, see Figure 1-10. In a SOFC, oxygen ions act as the charge carrier. Oxygen dissociates at the cathode catalyst and migrates across a ceramic electrolyte to react with the syngas (hydrogen, carbon monoxide, and methane) at the anode surface. The ceramic electrolyte blocks electron transport, forcing electrons through an external electrical load.

Anode Reactions

$$H_2 + O^{2-} \rightarrow H_2O + 2e^-$$ R. 1-11
$$CO + O^{2-} \rightarrow CO_2 + 2e^-$$ R. 1-12
$$CH_4 + 4O^{2-} \rightarrow 4H_2O + CO_2 + 8e^-$$ R. 1-13

Cathode Reactions

$$\frac{1}{2}O_2 + 2e^- \rightarrow H_2O + O^{2-}$$ R. 1-14
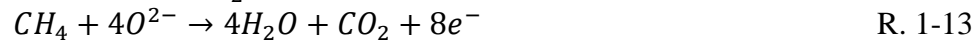
The higher operating temperatures allow the SOFC to reform simpler hydrocarbons, such as methane, at the anode. As oxygen ions are the charge carriers, SOFC is able accept a wide range of fuel feeds (hydrogen, carbon monoxide, and methane) for processing.

Typically, a solid ceramic yittria-stabilized zirconia acts as the electrolyte[74]. Originally, noble metals were used in anode and cathode construction, but lower cost alternatives have been developed[74]. Currently, a cermet of nickel and yittria-stabilized zirconia are common anode materials, while doped lanthanum manganites are used to construct the cathodes[74]. Compared to other fuel cells, SOFC operate at higher temperatures, typically between 600-1000°C[74]. However, high operating temperatures increase material and fabrication costs, while also lengthening startup.
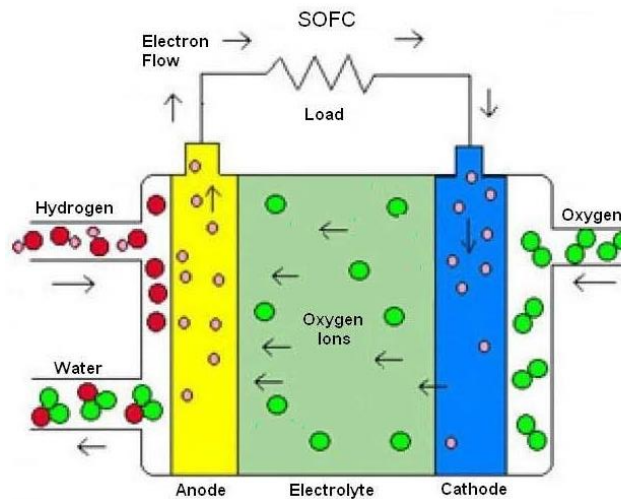
Figure 1-10. Schematic of a solid oxide fuel cell[8]

SOFC occur in either planar or tubular configurations. Baur and Preis[75] developed the first solid electrolytes (zirconium, yttrium, cerium, lanthanum, and tungsten oxide) and planar ceramic fuel cell in the 1930s. Variances in thermal expansion between the ceramic and support structures can induce thermal strain and structural damage. Thermal cycling is an ongoing issue with planar SOFC. The tubular configuration was developed in late 1950s by Westinghouse as an alternative to geometry, to alleviate issues with thermal cycling[75].

A tubular form allows the supported structure to be isolated from the high temperature region, resulting in greater thermal cycling. However, the tubular configurations have lower volumetric power density[74].

Higher operating temperatures enhance the anode catalyst's tolerance to hydrogen sulfide[74]. Stack temperatures of 750°C allow a tolerance of 50 ppb, while stack temperatures of 1000°C increase the anode catalysts tolerance to 1 ppm[74].

Solid oxide fuel cells are considered the best match for reformate regenerated through a non-catalytic process. Typically, the syngas is at temperatures of 600-1000°C and contains high concentrations of carbon monoxide (16-19%). Other fuel cells would require cooling and significant conditioning to reduce carbon monoxide into a tolerable range. Solid oxide fuel cells can directly process reformate, and require little or no conditioning.

1.5.1.2 Proton Exchange Membrane Fuel Cells

A proton exchange membrane fuel cell (PEMFC), also known as polymer electrolyte membrane, is one of the leading fuel cells for the transportation industry. PEMFC exists in a low temperature (0-120°C) and high temperature (120-160°C) variant. Both approaches operate at lower temperatures than other leading fuel cell technologies (600-1000°C), which simplifies construction (seals, materials), reduces costs, and allows quick start-ups. Originally developed by William T. Grubb in 1959, this fuel cell has replaced alkaline fuel cells as the leading low temperature fuel cell[74]. Current densities as high as 4 amp/cm^2 have been recorded[2,74]. Both the anode and cathode employ platinum catalysts. The membrane consists of a solid phase polymer (either perfluorosulfonic acid or polybenzimidizole)[2,74].

Membranes used in low temperature PEMFC (0-120°C) consist of a perfluorosulfonic acid polymer (Nafion). Humidification is required to enhance proton conduction, but dehydration occurs at temperatures exceeding 120°C, limiting operating temperatures.

To achieve higher operating temperatures of 120-160°C and avoid dehydration issues, a polybenzimidizole polymer impregnated with phosphoric acid is typically used. Higher temperatures are more desirable as heat enhances the stacks tolerance to carbon monoxide. This approach does not require liquid water humidification for proton transport, and is resistant of carbon monoxide poisoning.

Anode Reactions

$$H_2 \rightarrow 2H^+ + 2e^-$$
R. 1-15

Cathode Reactions

$$\frac{1}{2}O_2 + 2H^+ + 2e^- \rightarrow H_2O$$
R. 1-16
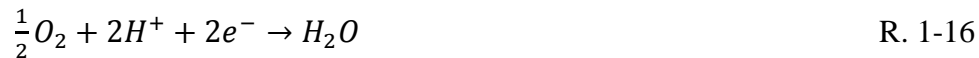
Figure 1-11 shows a schematic for the PEMFC. Fuel (hydrogen & syngas) enters at the anode, while air enters at the cathode. Diatomic hydrogen present in the syngas absorbs onto the anode catalyst surface and dissociates. Protons are conducted through the membrane, toward the cathode, where they react with oxygen to form water at the cathode. Electrons are conducted away from the membrane, toward the cathode, through an electrical load. Inert compounds, such as nitrogen and carbon dioxide, must periodically be purged from the anode.
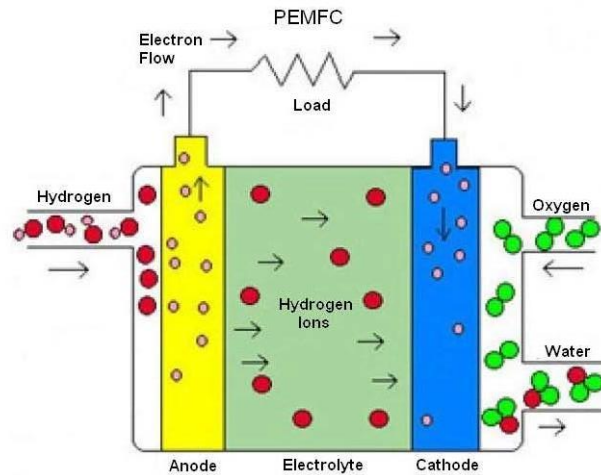
Figure 1-11. Proton exchange membrane fuel cell[8]

Proton exchange membrane fuel cells require a hydrogen rich feed stream. The most common hydrogen sources are compressed hydrogen or a metal hydride. However, a reformer allows widest compatibility with existing infrastructure, but depending on the reformer, the syngas can consist of 5-23% carbon monoxide. Carbon monoxide concentrations as low as 10 ppm can damage the platinum catalyst in the anode of the low temperature PEMFC[74]. Platinum-rhodium catalysts show greater tolerance to carbon monoxide, as damage occurs at concentrations of 200 ppm[74]. Operating at temperatures of 120-160°C increases carbon monoxide tolerance to 3.0%, before irreparable damage occurs[76].

A steam reformer's syngas consists of 60-70% hydrogen and no more than 5-6% carbon monoxide, making it one of the most compatible with PEMFC. Syngas generated through a non-catalytic reformer is less compatible with PEMFC, as it consists of carbon monoxide concentrations on the order of 19-24% and hydrogen concentrations of 13%. Significant syngas conditioning (water gas shift and preferential oxidation reactor) would be required to operate with a low temperature

PEMFC. The parasitic losses from reformate conditioning would significantly degrade system level efficiency. A non-catalytic reactor is better paired with a high temperature PEMFC, as it would only require a water gas shift rector to enhance the usability of syngas. Operating temperatures of 160°C are too low for internal reformation of unconverted hydrocarbons, which reduces the compatibility with syngas from a reformer.

1.5.2 Syngas Conditioning

Syngas taken directly from the reformer may not be of sufficient quality for direct usage in a fuel cell. Depending on reformate requirements imposed by the fuel cell, the product distribution can be altered through a series of secondary reactors and membranes to achieve the desired composition.

1.5.2.1 Water Gas Shift Reactor

Water Gas Shift reactors (WGS) are employed to enhance hydrogen yields, while minimizing carbon monoxide concentrations. When a reformer is paired with a PEMFC, the WGS enhances the recoverable energy, while avoiding carbon monoxide poisoning of the fuel cell's catalysts. Within this reactor, the water gas shift reaction converts carbon monoxide and water into carbon dioxide and hydrogen through a mildly exothermic reaction (R. 1-17).

$$CO + H_2O \rightarrow H_2 + CO_2 \qquad\qquad \Delta H_R = -41\frac{kJ}{mol} \qquad\qquad \text{R. 1-17}$$

Water Gas Shifts Reactors are often employed in stages. The first stage, called a "High Temperature Water Shift", operates at temperatures of 260-500°C and

reduces carbon monoxide concentrations to 2-5%[77]. These reactors use chromium, copper, and iron based catalysts. The second stage, called the "Low Temperature Water Gas Shift", operates at temperatures of 200-260°C and reduces carbon monoxide concentrations to less than 1%[77]. Copper, zinc, and aluminum based catalysts are typically used under low temperature conditions. Both stages are sensitive to sulfur poisoning.

1.5.2.2 Preferential Oxidation Reactor

Preferential Oxidation Reactors (PROX) are used in applications which have a high susceptibility to carbon monoxide poisoning (PEMFC). In this process, carbon monoxide is selectively oxidized through platinum or platinum-rhodium catalysts, reducing carbon monoxide concentrations from 0.5-1% to less than 10 ppm. A byproduct of this process is the unintended oxidation of hydrogen, generally on the order of 0.1 to 2.0%[74]. This reactor is placed after the Water Gas Shift reactor to minimize the amount of carbon monoxide and hydrogen consumed. Reactor temperatures of 100 to 180°C yield optimum conditions[74]. Higher reactor temperatures decrease the carbon monoxide selectivity, while promoting the reverse water gas shift reaction. In order to minimize oxidation of hydrogen, strict temperature control must be maintained. To maintain a constant temperature, PROX reactors are divided into multiple stages with intercooling[74].

1.5.2.3 Membranes

In an alternative approach, membranes can be used to change the chemical composition by filtering out the undesirable species, which results in a high purity hydrogen stream without the toxic (CO) or neutral gases (CO_2 & N_2). The membranes

separate the two regions, allowing only hydrogen to diffuse across the membrane. The remainder of the syngas (N_2 CO, CO_2) on the high-pressure side is exhausted. This increases residence times and partial pressure of hydrogen within the fuel cell, which results in a higher utilization of the syngas. To achieve the highest hydrogen yields, membranes are placed after the water gas shift. Membranes are employed when trace amounts of carbon monoxide can damage downstream components, such as a Low Temperature PEMFC. Commercial grade palladium membranes have achieved purities as high as 99.9999999%[78].

A simple representation of a membrane is shown in Figure 1-12. The high-pressure side contains the unfiltered reformate, which typically consists of a mixture of a nitrogen, hydrogen, water, oxygen, carbon monoxide, and carbon dioxide. The diatomic hydrogen is absorbed onto the membrane surface, and then undergoes dissociations and ionization. Then, the protons diffuse through the membrane. On the surface of the low-pressure side, protons recombine into hydrogen and desorb. This generates a high purity hydrogen stream.
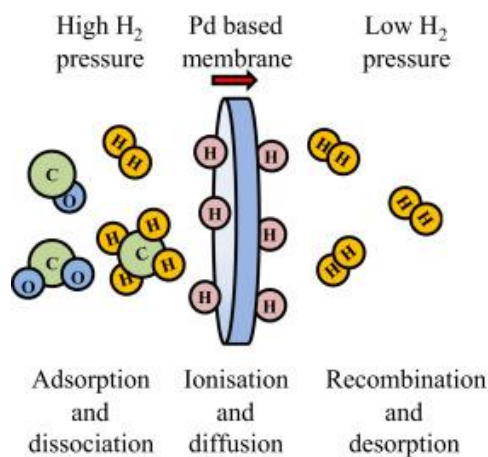
Figure 1-12. Schematic representation of a palladium membrane and hydrogen transport[79]

A wide variety of hydrogen-separating membranes exist, ranging from dense metallic, dense ceramic, porous carbon, porous ceramic, and dense polymer[80,81]. The dense metallic membrane's high selectivity, operating temperature, and hydrogen flux[80] make it an ideal selection for fuel cell applications. These membranes often consist of a palladium and palladium alloys of Pd-Ag, Pd-Cu[7,80,81].

Palladium membranes operate most efficiently at temperatures of 390-410°C. Exposure of a pure palladium membrane to hydrogen at temperatures below 300°C and pressures under 2MPa will induce a phase change. The α-phase transitions to β-hybrid, causing strain on the lattice, which presents as embrittlement of the membrane[82]. Carbon species will deactivate a pure palladium membrane at temperatures exceeding 450°C[82]. Carbon monoxide and water at temperatures below 150°C can block the absorption of hydrogen species on to the membrane surface. Membranes are often placed after the water gas shift reactor to maximize hydrogen yields, and reduce carbon monoxide and steam concentrations. Palladium membranes are also prone to sulfur poisoning. Exposure to hydrogen sulfide or sulfur oxides will form palladium sulfide.

Alloying the palladium reduces cost and enhances the chemical and dimensional stability. Basile[82] explained this effect by noting the similarity between the hydrogen and silver electron donating behavior, causing a competition between the silver and hydrogen atom for filling the electron holes. Palladium copper alloys have shown a higher tolerance to sulfur poisoning[81].

43

Thinner membranes reduce pressure drop, but increase the chance of introducing a micro-defect to the membrane structure, reducing the purity of the stream.

1.6 Middle Distillate Fuels

For mobile power applications, there is a desire to reform logistically available fuels, predominately middle distillates of kerosenes and diesels. Both fuels are abundant in the commercial and transportation sectors, and defense applications require kerosene, specifically JP-8, due to convenience and logistics. Diesels have a higher poly-aromatic content, which makes conversion more challenging[83]. Jet fuels (3000 ppm_w) have a higher allowed sulfur content than diesels (15 ppm_w), which makes it more compatible for a non-catalytic approach. Pastor[11] observed comparable behavior and yields in the non-catalytic reformation of jet and diesel fuels. The higher operating temperatures in non-catalytic reforming may help compensate for the poly-aromatic content.

The kerosene based fuel Jet Propellant Eight (JP-8) was chosen to represent of middle distillate fuels because it is challenging to reforming, has a high sulfur content (3000 ppm_w), and is susceptible to soot formation. The United States Military's One Fuel Forward Policy requires the use of JP-8 in all fueled applications[84]. Jet fuels of JP-8, Jet-A, and Jet-A1 are chemically similar. Moreover, JP-8 is chemically identical to Jet-A1, except for the additional additives of a corrosion inhibitor and lubricity promoter, icing inhibitor, and a static dissipater[85–87]. These additives have little effect on the reforming processes[88]. The Army Quarter Master[85]

conducted a long term study of both Jet-A1 and JP-8 and concluded there was little difference in performance. Jet-A and Jet-A1 have identical specifications[89], only differing in freezing point (-40°C Jet-A vs -47°C Jet-A1).
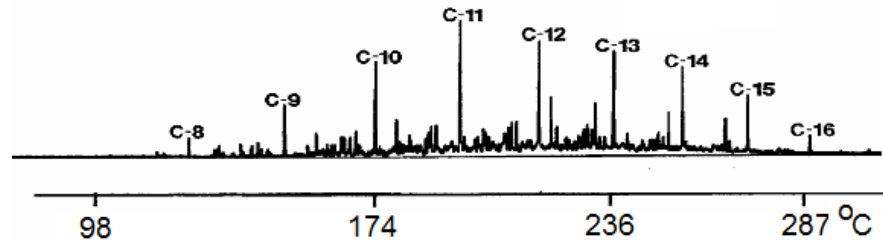
Figure 1-13. Hydrocarbon peaks of JP-8 in liquid phase chromatography[8]

JP-8 is a kerosene based middle distillate fuel composed of hundreds of hydrocarbons ranging from hexane to hexadecane. Figure 1-13 shows liquid chromatograph signal of a JP-8 sample. Each individual peak corresponds to an individual hydrocarbon. The average chemical composition of JP-8 on a volumetric basis consists of 50-65% iso and normal alkanes, 10-20% cyclo-alkanes, 15-20% mono-aromatics, and 1-3% poly-aromatics. As a point of comparison, diesel No. 1 & No. 2 have a general hydrocarbon distribution on a volumetric basis consisting of 25-50% iso and normal alkanes, 20-40% cyclo-alkanes, 15-35% mono-aromatics, and 5% poly-aromatics[90].

JP-8 has an average molar hydrogen to carbon ratio (H/C) of ~1.9 and an average molecular formula of $C_{11}H_{21}$. Dagaut[91] completed a comprehensive survey of JP-8, and determined the average molecular formula of JP-8 varies between $C_{10.9}H_{20.9}$ to $C_{12}H_{23}$. The average molecular weight of JP-8 was reported to be 151.98-167.31 g/mol, and a lower heating value ranging between 42.48-43.22 MJ/kg. In

comparison, diesel fuels are slightly heavier distillates. The average molecular formula range from $C_{10}H_{20}$ to $C_{15}H_{28}$, with corresponding molecular weight of 140.27 to 208.38 g/mol[92].

	JP-8	Diesel
MW(g/mol)	151.98-167.31	140.27 to 208.38
Density (kg/L) @15°C	0.775-0.840	0.820-0.835
Molecular Formula	$C_{10.9}H_{20.9}$ - $C_{12}H_{23}$	$C_{10}H_{20}$ to $C_{15}H_{28}$
LHV(MJ/kg)	42.48-43.22	43.0
Flash Point (°C)	38	60-80
Auto Ignition(°C)	210	315

Table 1-2. Thermal Properties of Jet Propellant 8 and Diesel Fuels[11,91,92]

JP-8 specification allows for a maximum sulfur content of 3000 ppm$_w$, which can render most conventional catalysts in reformers inert[7]. A broad specification allows easier acquisition from various markets within the continental United States and overseas, but requires the fuel cell/reformer system to tolerate a wide range of contaminates. Sulfur concentration of JP-8 found in the United States typically range between 500-700 ppm$_w$[26]. Sulfur compounds within jet fuel are primarily alkylated benzothiophenes[20]. In a four year study conducted by Lee[26], showed the prominent sulfur bearing species to be 2,3-dimethylbenzothiophene and 2,3,7-trimethylbenzothiophene, but up to 16 distinct organic sulfur peaks were identified. Prominent sulfur compounds in diesel fuels consist of alkylated benzothiophene, dibenzothiophene, and alkylated derivatives[20]. However, in natural gas, sulfur primarily occurs in the form of hydrogen sulfide, which can be easily removed through the Amine Claus Process. This approach is well suited for large-scale commercial applications, but not for mobile power applications.

Unlike natural gas, JP-8 has greater potential to undergo soot deposition. It is generally agreed upon that sooting propensity increases in order of poly-aromatic> mono-aromatic> olefin> branched alkanes > normal alkanes[18]. The roles of individual aromatic hydrocarbons in reforming are not well understood[88]. An initial investigation done by DuBois[88], observed nonlinear effects on reformate product distribution with the addition of aromatic hydrocarbons. JP-8 general composition varies, but the aromatic composition on a liquid volumetric basis consists of 15-20% mono-aromatics and 1-3% poly-aromatic hydrocarbons[8]. Aromatic hydrocarbons are known promoters of Coke and soot on the catalyst surface and downstream components. Coke formation can either physically blocks access to the catalyst sites, reducing the activity of the catalyst, or through the chemical absorption, migrate through the catalyst causing delamination from the support. The slight acidic nature of sulfur can act as a catalyst for carbon formation.

1.7 Calculations

The following section lists the terms and calculations common to reforming.

Oxygen to Carbon Ratio (O/C): The molar ratio of oxygen in air to molar carbon content in the fuel. It acts as a measure of the potential for oxidative reactions. An O/C ratio of 1.0 is equivalent to stoichiometric amount of oxygen needed for full partial oxidation as defined by Eq. 1-1. For dodecane, an O/C ratio of 1.0 corresponds to an equivalence ratio of 3.08.

$$O/C = \frac{Molar\ oxygen\ content\ of\ air}{Molar\ carbon\ content\ of\ fuel} \qquad\qquad \text{Eq. 1-1}$$

Equivalence ratio (Φ): The actual fuel-air ratio to the molar stoichiometric fuel-air ratio. It is a common reporting metric in non-catalytic work and combustion literature.

$$\Phi = \frac{\left(\frac{F}{A}\right)_{act}}{\left(\frac{F}{A}\right)_{stoic}}$$

Eq. 1-2

Steam to Carbon Ratio (S/C): Steam to carbon ratio is defined as the molar ratio of steam to the carbon content in the fuel. It is measure of the potential for steam reforming reactions.

$$S/C = \frac{Molar\ steam}{Molar\ carbon\ content\ of\ fuel}$$

Eq. 1-3

Reforming Efficiency: The measure of energy retained in the syngas after the reforming process. It is the best metric to compare reformers as fuel composition can vary over time and by batch. Reforming efficiency is defined as the ratio of the lower heating value of the syngas to the lower heating value of the fuel.

Within this work, reforming efficiency is presented for both High Temperature Proton Exchange Membrane fuel cell (PEMFC) and Solid Oxide fuel cell (SOFC). The high temperature PEMFC is the more mature technology, but is also more restrictive on syngas tolerance. Generally, a water gas shift will be used in conjunction with PEMFC. Reforming efficiency ($\eta_{H_2,CO}$) for the high temperature PEMFC is defined as the lower heating value of hydrogen and carbon monoxide to

the lower heating value in the fuel. Carbon monoxide is included, as it is assumed to

be shifted through a water gas shift reactor, promoting additional hydrogen formation.

$$\eta_{H_2,CO} = \frac{\dot{N}_{H_2}*LHV_{H_2} + \dot{N}_{CO}*LHV_{CO}}{\dot{N}_{C_xH_y}*LHV_{C_xH_y}} \qquad \text{Eq. 1-4}$$

However, the SOFC fuel cell operates at system level efficiency of 45-60%[75] and accepts a wider range of syngas composition, but is a less mature technology[28,74]. Hydrogen and carbon monoxide are both potential fuel sources for a solid oxide fuel cell. In addition, the higher operating temperatures (600-1000°C) allow for internal reforming of simple hydrocarbons, such as methane. Therefore, the reforming efficiency for SOFC is defined as the combined sum of the lower heating value of hydrogen, carbon monoxide, and methane to the lower heating value in the fuel.

$$\eta_{H_2,CO,CH_4} = \frac{\dot{N}_{H_2}*LHV_{H_2} + \dot{N}_{CO}*LHV_{CO} + \dot{N}_{CH4}*LHV_{CH4}}{\dot{N}_{C_xH_y}*LHV_{C_xH_y}} \qquad \text{Eq. 1-5}$$

Conversion: Conversion is a measure of the oxidation of the carbon content of the fuel. It is defined as the molar ratio of carbon monoxide and carbon dioxide generated within the process to the original carbon content of the fuel.

$$\eta_{Conv} = \frac{\dot{N}_{CO} + \dot{N}_{CO_2}}{\dot{N}_{C_xH_y}(x)} \qquad \text{Eq. 1-6}$$

Recirculation: The ratios of entrained mass ($\dot{M}_{Rec}$) to the mass injected ($\dot{M}_{Jet}$).

$$R = \frac{\dot{M}_{Rec}}{\dot{M}_{Jet}} \qquad \text{Eq. 1-7}$$

Yield: The molar ratio of the species to that found in fuel. It gives a measure of the level of extractions.

$$Hydrogen\ Yield = \frac{H_2\ in\ syngas}{(H\ in\ Fuel/2)} \qquad Carbon\ monoxide\ Yield = \frac{CO}{(C\ in\ Fuel)} \quad Eq.\ 1\text{-}8$$

1.8 Objective

The objective of this work is to characterize the thermochemical behavior of the reformation of a middle distillate fuel within the Distributed Reaction Regime. The characteristic chemical time and length scales will be altered through variations in preheats, reactant concentrations, and steam addition. Reformer performance will be evaluated based on reformate quality and product distribution. The major investigations are listed as follows.

- Numerical investigations to assist in the development of the reformer.

- Experimental investigation of a low temperature reactor: visual flame characteristics, oxygen concentrations, and air preheats.

- Experimental investigation of a high temperature reactor: oxygen concentrations, air preheats, and steam addition.

Chapter 2: Literature Review

The literature review focuses on the knowledge necessary for the development of a reformer that can operate within the Distributed Reaction Regime. Multiple non-catalytic reformer designs were reviewed for construction suggestions, operating regime conditions, and overall performance. Distributed combustor literature was reviewed to determine a design that would be compatible with conventional reformer limitations, while achieving the necessary conditions to allow for operation within the Distributed Reaction Regime.

2.1 Review of Non-Catalytic Reformers

Reforming without catalysts avoids issues associated catalyst deactivation through sintering and poisoning. However, operating at fuel rich conditions without catalysts provides unique challenges to overcome. Fuel rich conditions yield adiabatic flame temperatures of 800-900°C. In catalytic reformers, catalysts reduce the activation energies, allowing reactions to propagate under these conditions. Without catalysts, operating at lower temperatures (800-900°C) reduces the activity of the reactions, which in turn reduces stability, conversion, and reforming efficiency.

To compensate for the lack of catalysts, non-catalytic reformers enhance the activity of reactions by operating at elevated temperatures of 1200-1400°C, exceeding the adiabatic flame temperature (800-900°C). In literature, this condition is referred to as a "super adiabatic condition" and is achieved by internal preheating of reactants through heat exchangers or combusting within a porous media. Higher operating temperatures promote the cracking of hydrocarbons, soot formation, and thermal

damage[17]. For comparable conditions, non-catalytic reformers typically operate at lower reforming efficiencies (40-70%) than catalytic reformer (75-90%)[7,8,14,17].

Non-catalytic literature often reports oxygen concentrations in equivalence ratios, while catalytic reforming often reports in molar oxygen to carbon ratios. The equivalence ratio is the measure of oxygen needed to fully oxidize all carbon and hydrogen in the fuel. The molar oxygen to carbon ratio is a measure of the oxygen content of air relative to the carbon content of fuel. Due to variations in the hydrogen and carbon contents of fuels, ideal reforming conditions (O/C=1.0) will occur at different equivalence ratios. For example, ideal reforming conditions (O/C=1.0) occurs at an equivalence ratio of 4.0 for methane, but at an equivalence ratio of 3.08 for dodecane. Results within this work are reported in molar oxygen to carbon ratios (O/C) for easier comparison across fuels. Diesel and jet fuels were assumed to have a molecular formula of $C_{14.4}H_{24.9}$ and $C_{11.45}H_{21.95}$, respectively.

2.1.1 Porous Media

Reforming within a porous media is the most prevalent design in non-catalytic literature. The porous media consists of either a ceramic foam or a packed bed. These reactors achieve super-adiabatic conditions by preheating reactants through radiation and conduction. The porous media also promotes internal mixing. Silicon oxide, zirconia oxide, and alumina are commonly used as materials because they can withstand both the reducing environment as well as the high reactor temperatures.

These reactors operate in two possible modes. In the first mode, the the flame front is anchored within the porous media. In second mode, flame front propagates through the porous media, preheating the reactants. The Peclet number can be used as

a measure to estimate whether the flame front will anchor or propagate. The Peclet

number (Pe), as defined in Eq. 2-1, represents the ratio between convective and

diffusive transport. Where S_L is the laminar flame speed, d_m is the equivalent pore

diameter, and α is the thermal diffusivity of the gas. The critical Peclet number (Pe$_{crit}$)

is defined as the point when the flame begins to propagate, but will vary with

material. Values lower than Pe$_{crit}$ promote quenching[93], while higher values allow

the propagation of the flame.

$$Pe = \frac{S_L * d_m}{\alpha} \qquad\qquad \text{Eq. 2-1}$$

Employing porous media can be disadvantageous to reforming. The sooting

nature of the flame can induce blockages in the porous media and increase reactor

pressure. Packing a reactor with porous media also reduces reactor volume and

residence times, reducing reactor capacity. The porosity for ceramic foams is on the

order of 75-95%[10,14], while the porosity of pack beds used in literature has been on

the order of 40-60%[14,19,94].

2.1.1.1 Stationary Flame

When the flame front is stationary, the flame is anchored to a section of the

porous media that acts as a flame holder. There is conflicting information in the

literature[11,94] as to whether pack bed or ceramic foam is better. The porous media

is commonly a packed bed or a ceramic foam. The flame holder is generally

constructed from a porous media, with pore diameter smaller than the quenching

distance of the flame. The diffuser section has a larger porosity, with a pore diameter

greater than the quenching distance. Figure 2-1 shows porous media reformer with

stationary flame.
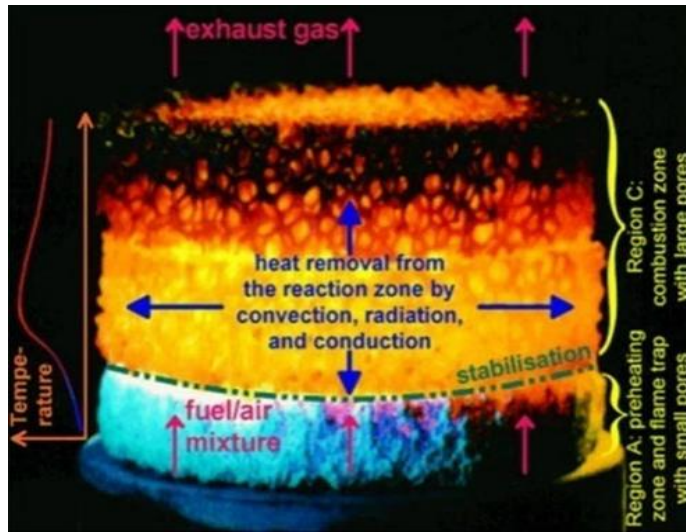
Figure 2-1. Porous media with flame holder[93]

Pedersen-Mjaanes and Mastorakos's[10] reformer consisted of two regions of varying porosity, see Figure 2-2. The low porosity region acted as a flame holder and arrestor, while the high porosity region acted as a diffuser. Four fuels were evaluated: methane, methanol, gasoline, and octane. Three porous media were also evaluated: cordierite foam, alumina foam, and alumina beads. The cordierite foam experienced significant damage, which was attributed to melting. No results were reported for the cordate foam. No melting was observed in the alumina foam, but after 20 hours of operation, the foam deteriorated. This was attributed to thermal stresses. No degradation was observed within the alumina beads in a 100-hour period of testing. Pedersen concluded that the lack of a ridged structure within the alumina beads relieved thermal stress induced by thermal cycling.

Methanol was reformed in two reactors: one consisting of alumina beads (porosity 75%), and another consisting of alumina foam (porosity 84-86%). A porous media consisting of alumina beads yielded a reforming efficiency of 66%, at O/C ratio of 0.79, with hydrogen concentrations as high as 42%. Reforming methanol

within a porous foam yielded reforming efficiencies of 56%, at O/C ratio of 0.67. Hydrogen concentrations under this condition were as high as 28%.

Methanol, methane, and gasoline were also compared in a reactor using an alumina foam. The liquid fuels were vaporized in a commercial vaporizer and injected into heated air before entering the reactor. No mixer was mentioned in the paper. Soot formation was observed for methanol at O/C ratio less than 2.0. While it was observed for methane and gasoline at O/C ratios less than of 1.5. Conversion for methane and gasoline was relatively low. Reforming of methanol generated reforming efficiencies up to 56% at O/C ratio of 0.67, with syngas composition consisting of 28% hydrogen. Syngas from methane consisted of 13% hydrogen, which yielded a reforming efficiency of 45%. Reforming of octane showed lower performance, only generating efficiencies up to 36% at O/C ratio of 2.08, consisting of only 11% hydrogen.
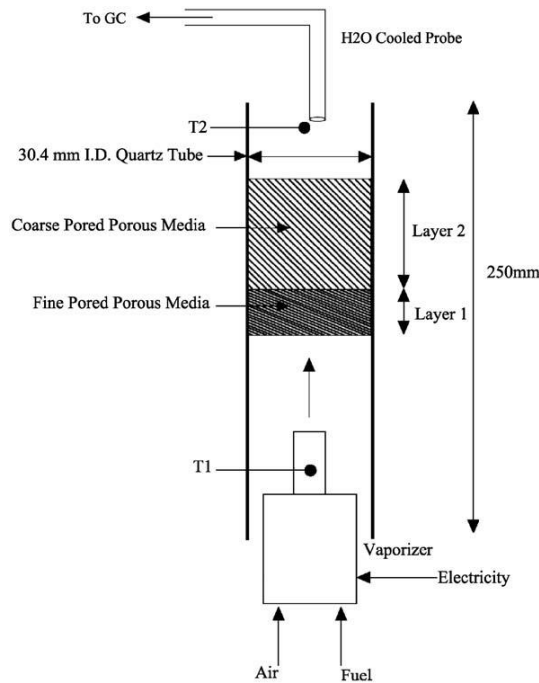
Figure 2-2. Pedersen-Mjaanes ceramic foam reformer[10]

Al Hamamre[95] investigated the uses of high temperature inlet air temperature (400-700°C) on vaporized fuel. The reactor consisted of zirconia oxide foam. He determined that careful control of residence times of the mixer and vaporizer could permit injection temperatures as high as 700°C without pre-ignition. Syngas consisted of 16% hydrogen and 18% carbon monoxide. The highest hydrogen concentrations occurred at O/C ratio of 1.3. Al Hamamre compared this reformer to a free flame reformer described in Section 2.1.3.

Pastore[11] evaluated the effects of porosity, material properties, configuration, and diffuser length on reformate quality and product distribution. Pastore used two sections of porous media with different porosity. The first section generally was composed of 3 mm alumina beads, which acted as a flame holder. The second section was comprised of a larger porosity foam 10 ppi, which acted as a diffuser. Fuel was first atomized and then injected into preheated air (300°C) for vaporization. The sautermean diameter of the droplets was 50 μm. The premixed air fuel mixture then flowed into the flame holder.

Pastore compared n-heptane, a common diesel combustion surrogate, to commercial diesel at O/C ratios of 1.3-1.6. The reformation of the commercial diesel achieved efficiencies as high as 77.6%, with a syngas composition consisting of 15.2% hydrogen and 19.1% carbon monoxide. Under similar test conditions, n-heptane only yielded a reforming efficiency up to 54.1%, with a syngas composition consisting of 12.2% hydrogen and 15.0% carbon monoxide. The maximum flame temperature measured was 1390°C for n-heptane and 1436°C for the diesel. Pastore concluded n-heptane was a poor representation for diesel under reforming conditions.

56

In a second set of experiments, diffuser configuration and materials[14] were altered to understand its effects on reformate quality and product distribution. A zirconia foam (porosity 30 ppi) was compared to a packed bed of 6 mm diameter alumina beads (porosity 40%). N-heptane was reformed at an O/C ratio of 1.26. The alumina beads yielded higher reforming efficiencies of 75%, with syngas composition consisting of 19.3% hydrogen, 19.9% carbon monoxide, and 2.3% carbon dioxide. The zirconia foam yielded a reforming efficiency of 56.7%, with syngas composition consisting of 15.1% hydrogen, 15.2% carbon monoxide, and 3.1% carbon dioxide. Pastore attributed the better performance of the alumina beads to the higher thermal conductivity of the alumina (28.9 w/m-k vs 2.0 w/m-k) enhancing the super-adiabatic effect, generating higher reactor temperatures.

Ceramic porosity was determined to have a limited effect on reformate composition. Two zirconia foams with varying porosity were compared (30 ppi and 10 ppi) using diesel. The smaller porosity foam (10 ppi) showed a small improvement in reformate quality. At an O/C ratio of 1.29, the foam with a porosity of 10 ppi yielded a reforming efficiency of 56.7%, while the higher porosity foam (30 ppi) yielded a reforming efficiency of 54.7%.

Pastore also studied the effect of diffuser length on reformate composition. The diffuser was a cylindrical zirconia foam (porosity 30 ppi); with a diameter of 70 mm. Diffuser length was alternated between 25 mm and 50 mm. The 50 mm length showed a marginal increase in reformat quality, which was attributed to higher heat recirculation in the thicker matrix and longer residence times.

Pastore also augmented the non-catalytic reformer with both a steam reforming and water gas shift catalysts. The steam reforming catalyst was a G90-EW (Süd-chemie), a nickel catalyst supported on an aluminum oxide / calcium aluminate support. The water gas shift catalyst was a commercial grade (NextCatA), which consisted of Pt–Ce (2% Pt). Using a sulfur free n-heptane, the reformer was operated at an O/C ratio of 1.26. The reformate consisted of 27.1% hydrogen, 8.7% carbon monoxide, and 11.8% carbon dioxide. Methane was detected at concentrations up to 0.98%. Trace amounts of acetylene (0.02%), ethylene (40 ppm), and ethane (16 ppm) were detected.

Pastore[11] also investigated variation in reformate quality of multiple middle distillate fuels (diesel, bio diesel, and Jet-A1). Syngas composition for the diesel (H_2=12.0% & CO=16.6%, $\eta_{H_2,CO}$=62.7%), bio-diesel (H_2=14.0%, CO=19.1%, $\eta_{H_2,CO}$=64.9%), and Jet-A1 (H_2=13.8%, CO=18.9%, $\eta_{H_2,CO}$=69.6%) were fairly comparable. Peak reforming efficiencies occurred at comparable conditions for diesel (O/C=1.43) and Jet-A1 (O/C = 1.41). Peak reforming efficiencies for bio-diesel occurred at a lower O/C ratio of 1.30.

2.1.1.2 Propagating Flame

In the filtration method, the flame front propagates through porous media, instead of remaining stationary within. This effect occurs when the Pe number exceeds the critical Pe for the porous material. For the flame to propagate down the reactor, interstitial velocity must be higher than the flame speed. Reaction fronts typically propagate at speeds of 0.1-10 mm/sec, but up to 770 mm/sec have been demonstrated[96,97].

Figure 2-3 shows six images of the flame front propagating down the reactor. Initially at τ_o, the reaction is ignited at the front of the reactor and heat is absorbed into the surrounding porous media. As the reaction propagates downstream, at τ_3 the heated porous media preheats the incoming reactants, allowing conditions to exceed the adiabatic flame temperature. Eventually, the reaction will propagate out of the reactor at τ_5. This approach yields higher reactor temperatures than a stationary flame front.
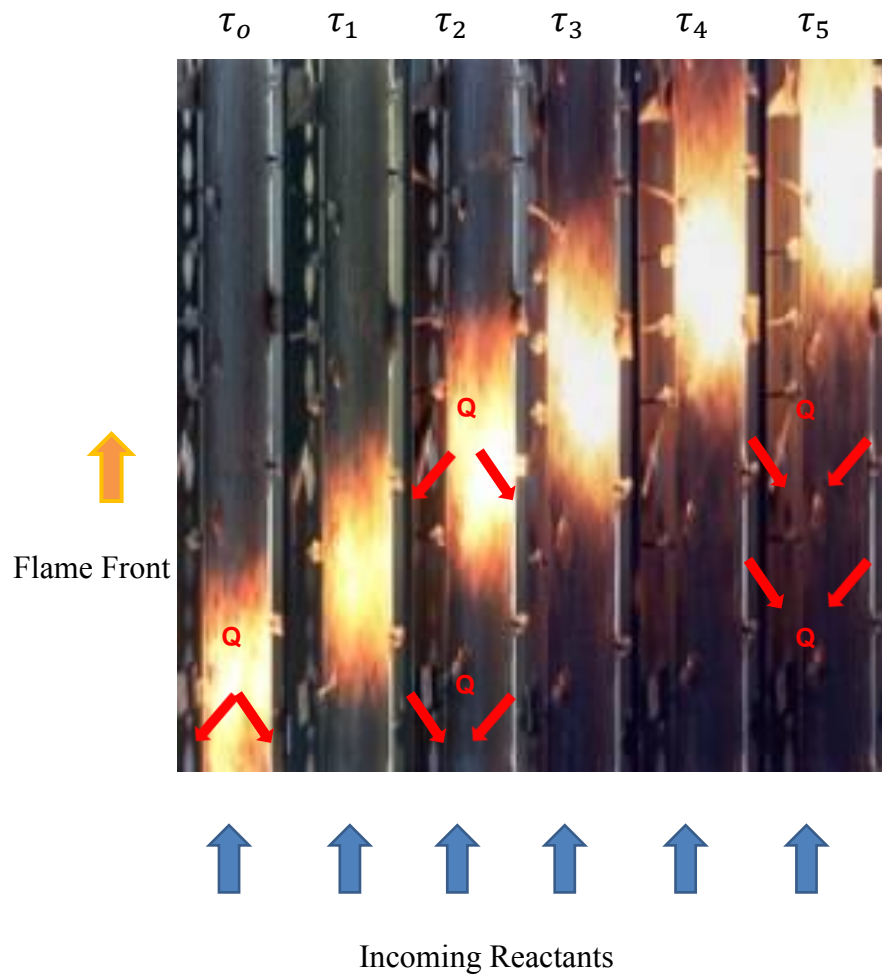
Figure 2-3. Flame propagating through a porous media [98]

Dhamrat[96] investigated methane under filtration wave conditions in an YZA foam, see Figure 2-4. Syngas composition consisted of hydrogen up to 25%. Carbon monoxide concentrations were not given. Reactants were injected at 300°C, while O/C ratios were varied between 0.8-2.67. Peak temperatures were recorded at 1799°C. Propagation wave speeds were between 0.14-11.8 mm/sec. Drahmat stated that there was no observed damage, but noted it was a brief test.

Drayton developed a packed bed reformer that operated under a reciprocating flame front[97]. A system of valves alternated the direction of the flow. As the flame would not propagate out of the reactor, the process was more continuous, which allowed propagation speeds as high as 700-900 mm/sec.
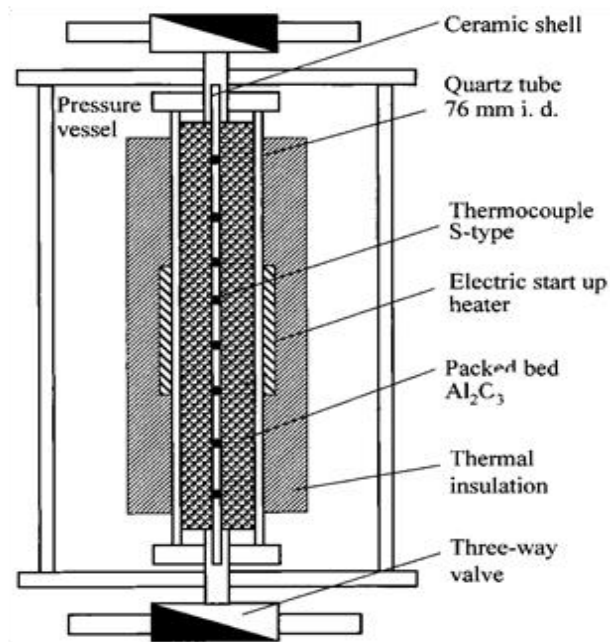
Figure 2-4. Oscillating filtration wave reformer[97]

The system evaluated methane at O/C ratios of 0.5-2.0. Drayton only referred to reformate products in yields. At atmospheric conditions, hydrogen and carbon

monoxide yields were between 70-76% and 57-65%, respectively. There were significant yields of unconverted hydrocarbons (5.9% acetylene and 8.1% ethylene). Reactor temperatures as high as 1180°C were reported. Drayton found that operating at higher pressures (5 atm) positively influenced reforming results, increasing both hydrogen (24-32%) and carbon monoxide (48-63%) yields. Peak temperatures were demonstrated up to 1380°C at 5 atm.

Faye[94] compared the effects of porous media using the partial oxidation of methane. Two beds were compared, a YZA reticulated foam (porosity 83.5%) and 3 mm aluminum oxide spheres in packed bed (porosity 40%). The reactor was heated to 1527°C to initiate reaction and O/C ratios were varied between 0.8-2.0. Peak conversion occurred at O/C a ratio of 1.6. Fay noted that the propagation velocity of the transient flame in the ceramic foam was 10-20 times faster than that of the packed bed. The reticulated foam demonstrated higher hydrogen yields (~75%) than the packed bed (~60%). Fay attributed the higher performance to the lower volumetric heat transfer coefficient for the reticulated foam. The packed bed configuration reached a peak temperature 1817°C, and the reticulated ceramic reactor reached temperatures up to 1907°C. Carbon deposits were not detected.

Zhdanok[19] evaluated the influence of pellet shape, material, and size on the products distribution of packed bed reactor. Methane was injected at an O/C ratio of 1.0, with an inlet temperature of 220-240°C. The following pellets were evaluated: zirconium oxide grains (D=2-3 mm), alumina spheres (3 mm & 6 mm), alumina cylinders (D=5 mm, L=10 mm), and silicon-oxide chips (~3 mm, by 6 mm, by 15 mm). Flow rate was varied between 0.967-5.71 m^3/hr.

It was observed that a packed bed with a lower porosity produced higher

conversion and concentrations of hydrogen. Table 2-1 shows reformate composition

for emptied peak hydrogen concentrations. Porosity had little discernable impact on

reactor temperatures. Zhdanok observed carbon deposits forming on the silicon oxide

chips. No carbon formation was noted on alumina or zirconia pellets. He believed that

the silicon oxide chips promoted cracking reactions. This is supported by a reduction

in both reactor temperature and carbon monoxide; with a corresponding increase in

hydrogen concentrations.

	Porosity	H_2%	CO%	CH_4%	Methane Conversion	Temperature($°C$)
Zirconium Oxide Grains	68%	21.6%	10.4%	14.2%	51%	1353
3 mm Alumina Spheres	67%	22.1%	11.7%	13.2%	54%	1390
6 mm Alumina Spheres	66%	26.0%	10.9%	10.2%	64%	1421
Alumina Cylinders	49%	27.2%	15.6%	9.6%	67%	1365
Silicon-Oxide Chips	46%	29.5%	8.6%	4.9%	84%	1380

Table 2-1. Peak hydrogen concentration and corresponding methane and reactor
temperature for various pack bed configurations[19]

Zhdanok also evaluated a kerosene surrogate. The surrogate consisted of a

mixture of 16.7% ethylbenzene and 83.3% undecane. Fuel and air were independently

heated to 220-240°C, and then mixed within a swirling jet mixer. The packed bed

reactor was filled with alumina spheres with a diameter of 5-6 mm. The reformer

demonstrated hydrogen yields as high as 93% between an O/C ratios of 0.99 to 1.06.

Reformate concentrations consisted of up to 24% hydrogen, 22% carbon monoxide,

3% carbon dioxide, and 3% methane. Hydrocarbons (C_2H_2 and C_2H_4) were reported

62

not to exceed 1%. Under these conditions, the reactor temperatures were between 1070-1125°C.

Bingue[99] studies the effect of oxygen enrichment on thermal partial oxidation of methane. Oxygen concentrations between 10-35% were evaluated. Oxygen enrichment improved both hydrogen and carbon monoxide concentrations. This increase is a result of the removal of the dilutant nitrogen and the increase in residence time. At an O/C ratio of 1.45 and an oxygen enrichment of 35%, the syngas consisted of up to 25% hydrogen and 18% carbon monoxide. Significant concentrations of methane (7-14%) were detected in the reformate. One point of interest at atmospheric oxygen concentrations (O_2=21%), methane was detected up to 7%. However, under an oxygen enriched state (O_2=25%), methane concentrations were as high as 14%. At even higher of enrichments (O_2=30-35%), methane concentrations dropped to 10-11%.

Dixon[13] evaluated the effects of O/C ratio and injection velocity on a packed bed reactor composed of 3 mm diameter alumina pellets. Air and n-heptane were independently heated before mixing and injection into the reactor. Of all the experimental conditions evaluated, Dixon reported the highest reforming efficiency for n-heptane fuel. His reactor demonstrated reforming efficiencies as high as 82%, with a syngas consisting of 25% hydrogen and 21% carbon monoxide at velocities of 80 cm/sec and an O/C ratio of 1.26. Reactor temperatures were up to 1500°C.

In one set of experiments, inlet velocity was held constant at 60 cm/sec, while O/C ratios were varied from 0.83 to 2.24. Lower oxygen to carbon ratios were found to favor higher concentrations of hydrogen (5% to 26%) and carbon monoxide (8% to

22%). Reactor temperatures diminished from 1625°C to 1325°C with decreasing O/C ratios.

In another set of experiments, injection velocity was varied from 20 to 125 cm/sec, for a fixed O/C ratio of 1.26. Higher injection velocities fostered higher hydrogen (12% to 21%) and carbon monoxide (16% to 21%) concentrations. Reactor temperatures increased with injection velocity from 1275°C to 1575°C. Equilibrium conditions were presented for both experiments and found to be consistent with experimental data.

Soot formation was observed at all conditions including those near full combustion. At velocities of 50 cm/sec, a small amount of soot was observed on the pellets at oxygen to carbon ratios of 1.6-2.1. At O/C ratios lower than 1.6, the pellets were described as heavily covered in soot. Soot formation decreased as velocity was increased from 50 cm/sec to 75 cm/sec; however, velocities higher than 125 cm/sec also promoted soot formation.

Smith[9] evaluated Jet-A, in packed bed (alumina beads) and ceramic foams (ZTM, YZA). Serious damage was observed for all porous media. Syngas composition was discussed in terms of yields. Fuel was atomized through a nozzle and allowed to mix with heated air in a quartz mixing changer, before flowing into the porous media. The reactor was operated at O/C ratios of 1.0 and inlet temperatures of 170-200°C. Droplet size was approximately 20 microns.

Smith showed extensive damage to both the alumina pellets (53% volume reduction) and both ceramic foam (YZA and ZTM). Figure 2-5 shows the damage to the ZTM foam and an unused sample.

Figure 2-5. Damaged and undamaged ceramic foam[9]

In the first set of experiments, O/C ratios were varied between 0.59-2.95 at a fixed velocity of 40 cm/sec. The reactor demonstrated reforming efficiencies up to 61% at O/C ratio of 1.0. For the alumina pellets, peak yields (50% H_2 and 70% CO) were reported at an O/C ratio of 1.48 at 40 cm/sec. Reforming efficiency was at most ~60%. No temperature measurements were reported.

In a second set of experiments, injection velocity was varied from 25-60 cm/sec at a fixed O/C of 0.99. Peak yields (~45% H_2 and ~60% CO) occurred at inlet velocities of 30-40 cm/sec. This also corresponded to the highest reactor temperature (~1440°C).

A porous media consisting of YZA foam was evaluated over 0.99-2.96, at injection velocities of 40 cm/sec and 60 cm/sec. At injection velocities of 40 cm/sec, yields where at most ~35% hydrogen and 65% carbon monoxide, which occurred at an O/C ratio of 1.48. Reforming efficiency was around ~55%. At injection velocities of 60 cm/sec, yields where at most ~45% hydrogen and 70% carbon monoxide, which occurred at an O/C ratio of 1.29. Reforming efficiency was not stated.

The porous media employing a ZTM foam was only evaluated at 1.48-2.96 at 40 cm/sec. Reactor damage limited experimentation. Peak yields consisted of 50% hydrogen and 70% carbon monoxide.

2.1.2 Heat Exchanger Based

An alternative approach to creating super adiabatic conditions is to employ heat exchangers to preheat the incoming reactants. This approach avoids the use of stabilizing media (foams and packed beds), which enhances residence time. Higher reactor temperatures and the reducing environment make sealing the reactor a challenging issue. Material limitations impose restrictions on reactor temperature. Additionally, prolonged heating of a premixed fuel-air mixture can lead to pre-ignition.

Schoegl[100] investigated a reformer consisting of two opposed flow channels, see Figure 2-6. Both channels shared a common wall, which served to transfer heat between them. Propane was used as the feedstock. The reactor demonstrated reforming efficiencies as high as 75%, with syngas consisting of 16.7% hydrogen and 17.2% carbon monoxide. Reactor temperatures were restricted to 1300°C to prevent damage to the reactor. No damage was observed over a 150 hour period. Carbon balance indicated full detection within the margin of uncertainty of the experiment.
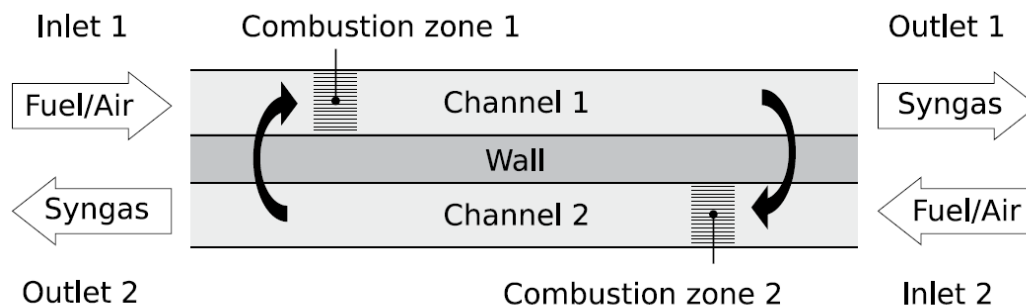
Figure 2-6. Parallel channel reactors[100]

Schoegl evaluated the influence of injection velocity and O/C ratio on reformate product distribution. Initially reactants were injected at a fixed velocity of either 125 cm/sec or 250 cm/sec, while the O/C ratio was varied between 1.15-1.5. At O/C ratios of 1.5 to 1.6, beyond normal operating conditions, flashback was observed; but no damage was noted. As O/C ratio was increased from 1.15 to 1.52, hydrogen concentrations increased from 14% to 16.7%. In addition, increasing O/C ratios from 1.15 to 1.26 caused the carbon monoxide concentrations to decay from 17% to 16%. Higher oxygen to carbon ratios fostered carbon monoxide formation, reaching a maximum of 17.2% at O/C ratio of 1.52. Significant concentrations of methane (0.5-4.5%), acetylene (0.75-2.0%), and ethylene (0.1-1.5%) were detected in the reformate, most notably at lower O/C ratios. Temperatures ranged between 1000-1300°C, with higher temperatures corresponding to higher oxygen to carbon ratios.

Shoegl also evaluated the effects of injection velocity on reformate composition. The reactor was operated at a fixed O/C ratio of 1.39, while injection velocity was varied between 37.5 cm/sec to 300 cm/sec. Initially, increasing injection velocities from 37.5 cm/sec to 125 cm/sec increased hydrogen concentrations from 9.5% to a maximum of 16.7%. However, higher injection velocities hindered

hydrogen formation. This was shown by a decay in hydrogen concentrations to 12.5%

at velocities of 300 cm/sec. The initial hydrogen increase was attributed to higher

levels of heat recirculation, while the decrease was associated with a reduction in

residence time.

Carbon monoxide concentrations decayed from 16% to 15% as inlet velocity

rose from 37.5 cm/sec to 300 cm/sec. Significant methane (0.8-1.5%), acetylene

(1.25-2.4%), and ethylene (0.25-0.5%) concentrations were detected. Similar to

hydrogen, an increase in injection velocity promoted hydrocarbon formation with the

exception of acetylene. Injection velocities greater than 80 cm/sec suppressed

acetylene formation, which was attributed to the higher reactor temperatures (1050-

1300°C).

Belmont[101] investigated n-heptane in a parallel channel counter flow heat

exchanger reformer. Reactants were operated in a premixed configuration. Prior to

the reactor, fuel was atomized through a nozzle placed within a mixing chamber. The

atomized fuel was mixed with preheated air heated (150°C) to achieve full

vaporization. The reformer demonstrated reforming efficiencies as high as ~70%,

with syngas composition consisting of 14.5% hydrogen and 17.5% carbon monoxide.

Significant hydrocarbon formation (CH_4, C_2H_2, and C_2H_4) was observed. Carbon

balance indicated that, under certain conditions, up to 11% of carbon was not detected

by GC.

O/C ratios were varied from 0.83 to 1.12; with a constant velocity of 125

cm/sec. Maximum reactor temperatures were reported up to 1250°C. Oxygen to

carbon ratios less than 1.26, caused hydrogen concentrations to decrease from 14.5%

to 10.5%. Carbon monoxide concentrations remained unaffected by the changes in O/C ratio, and remained stable at ~17%.

In a second set of experiments, O/C ratio was fixed at 1.05, while inlet velocity was varied between 50-200 cm/sec. Increasing velocity promoted higher concentrations of carbon monoxide (16.6-17.5%) and hydrogen (12.8-14.4%). Schoegl[100] observed similar results. Higher injection velocities reduced the total hydrocarbon formation from 5.5% to 4.4%. Belmont calculations indicated that this exceeded equilibrium values.

Chen[12] evaluated propane, n-heptane, and JP-8 in a six turn Swiss-roll heat exchanger based reformer. The propane air mixture was varied between O/C ratios of 1.1 to 1.28. Reformer demonstrated efficiencies up to 59.8% at an O/C ratio of 1.28. The syngas consisted of 18.22% hydrogen and 17.87% carbon monoxide. Reactor temperatures were reported as high as 1380°C.

N-heptane and JP-8 were also evaluated using this reactor at O/C ratios of 1.0 and 1.05, respectively. A heated chamber with a spray nebulizer was used to atomize the n-heptane and JP-8 fuels, while air was preheated separately from the fuel. The atomized fuel was premixed with the air in a heated chamber nebulizer prior to reactor. Significant oxygen and hydrocarbons were detected in the syngas for n-heptane (H_2=14.86%, CO=14.8%, O_2=3.69%, C_2H_4 & C_2H_2=0.14%, C_3H_8=0.04%) and JP-8 (H_2=10.22%, CO=18.45%, O_2=0.75%, C_2H_4 & C_2H_2=0.26%). This could be a sign of poor mixing, which is supported by the low hydrogen concentrations and oxygen breakthrough. The n-heptane flame was described as a steady blue flame,

while the JP-8 flame was as an intermittent yellowish flare, which is indicative of soot formation. No physical damage to the reformer was reported for either fuel.

Roth[16] evaluated diesel reformation with a focus on understanding the effects of oxygen to carbon ratios, reactor pressure, reactor temperature, and steam content on the syngas product distribution. The reformer, shown in Figure 2-7, consisted of two concentric tubes, constructed from cast refractory parts. Reactions occurring in the inner tube preheated the incoming air located within the outer tube.
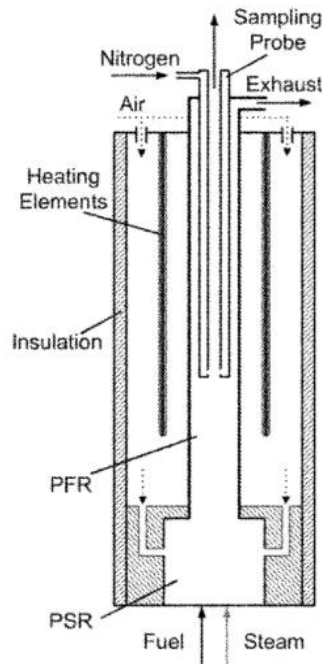
Figure 2-7. Imbedded heat exchanger[16]

Prior to injection, the fuel and steam were premixed and sprayed into a feed evaporation system, then preheated in a tube furnace. The premixed fuel and steam feed was mixed with the preheated air inside a mixer before injection into the inner tube. The premixed charge would react within the inner tube, which acted as a plug flow reactor. Wall temperatures were restricted to 1300°C to avoid damage to the

reformer. Roth determined the reactor residence time to be within 400 ms. No reforming efficiency was reported for this work.

Reactor temperatures had a strong impact on reformate quality. At low temperatures of 800° C, almost no soot was observed. However, the syngas consisted of 5% hydrogen, 5.7% carbon monoxide, and 9.4% carbon dioxide. Methane was detected up to 1.9%, but no acetylene was reported. At higher reactor temperatures, conversion increased, which resulted in a change in the syngas species distribution. Both hydrogen and carbon monoxide concentrations increased up to 15% and 10.5%, respectively. Increasing the reactor temperatures from 800 to 1000°C, caused methane concentrations to increase from 1.9% to 4.6%. Methane concentrations decreased from 4.6% to 0.7% as reactor temperatures increased from 1000°C to 1300°C. Increasing reactor temperatures reduced the formation of carbon dioxide from 9.4% at 800°C to ~5% at 1300°C. Soot formation was undetectable at temperatures of 800-900°C. Soot formation was first detected at temperatures of 1000°C at 15 mg/g_{fuel} increasing to 35 mg/g_{fuel} at temperatures of 1300°C

Reformate composition was also strongly influenced by variation in the O/C ratio. Higher oxygen to carbon ratios were associated with combustion conditions, that generated lower hydrogen concentrations (1.2%), soot (35 mg/g_{fuel}), and carbon monoxide (2%), while favoring combustion products such as carbon dioxide and water (not measured). Lower oxygen to carbon ratios of 1.0 (reduced reactor oxygen concentrations) approached ideal reforming conditions. This resulted in an increase in hydrogen (15%), carbon monoxide (14%), and soot (50 mg/g_{fuel}) formation. Carbon

dioxide concentrations decreased from 12.5% to 5% as the oxygen to carbon ratio decreased.

Roth was the only available literature studying the effects of steam addition to partial oxidation of a middle distillate fuels in a non-catalytic reactor. The reactor was operated at 1300°C, 1 bar, and at O/C ratio of 0.95. The S/C ratio was increased from 0.2 to 0.6 and had a positive impact on reformate quality. Notably, detected levels of soot formation decreased from 50 mg/g_{fuel} to 35 mg/g_{fuel}. In addition, acetylene concentrations decreased from 1,100 ppm to 290 ppm. Increasing S/C ratio fostered greater concentrations of hydrogen (13 to 15%), carbon monoxide (8.1% to 10.8%), and carbon dioxide (4.5% to 5.1%).

Reactor pressure had a strong effect on reformate product distribution. Reactor pressure was increased from 1 to 4 bar for a fixed O/C ratio of 0.95. Increasing pressure promoted soot production. As pressure increased from 1 to 4 bar, soot increased 40% from 35 mg/g_{fuel} to 49 mg/g_{fuel}. This correlated to an increase in acetylene concentrations (300 ppm to 18300 ppm). Increasing pressures fostered higher hydrogen (15.0% to 21.7%), carbon monoxide (10.8% to 13.9%), and carbon dioxide (5.4% to 10.6%) concentrations.

2.1.3 Non-Super Adiabatic Designs

A less common approach is to operate at conventional combustion temperatures without preheating the reactants. These designs do not achieve the super adiabatic conditions and thus have shown inferior performance. This presents as lower conversion and higher hydrocarbon formation. Lower reactor temperatures

promote significant hydrocarbon formation, reducing reactor stability and reforming efficiency.

Gonzalez evaluated diesel in a modified combustor[102]. Gonzalez operated at very high O/C ratios, between 1.3 and 2.86. Fuel was atomized in a heated chamber before injection into the reactor. Reformate consisted of 8% hydrogen and 8% carbon monoxide. High concentrations of carbon dioxide were reported ranging between 8-9%. Total hydrocarbon content was reported up to 12%, which is unusual for near combustion conditions. Incomplete mixing could account for the low yields of hydrogen and high hydrocarbon formation.

Al Hamamre also developed a free flame reformer using n-heptane[95]. Fuel was injected through a nozzle into a heated mixing chamber to achieve complete vaporization before injecting into the reactor. This was thought to improve the results of the reformate compared to other free flame approaches. Reformate concentrations consisted of 10.5% hydrogen and 16% carbon monoxide. Reformate quality was significantly lower than previous reformer design using porous media stabilized flame (16% hydrogen and 18% carbon monoxide). Al Hamamre also observed that the unsupported flames were less stable, as O/C ratios less than 1.26 caused the flames to extinguish. In contrast, the porous media based design was able to maintain a stable flame at O/C ratios as low as 1.12.

Hartman[103] evaluated diesel and IGO reformate at different reactor conditions, and determined that hydrogen formation was strongly dependent on reactor temperature, see Figure 2-8. At temperatures of 600-800°C, hydrogen concentrations were no more than 5-10%. At higher reactor temperatures of 900-

73

1100°C, hydrogen concentrations increased to as high as 15-18%. Reactor temperatures higher than 1100°C appeared to negatively influence hydrogen formation. Reactor temperature appeared to positively influence carbon dioxide formation, while carbon monoxide formation appeared unaffected.
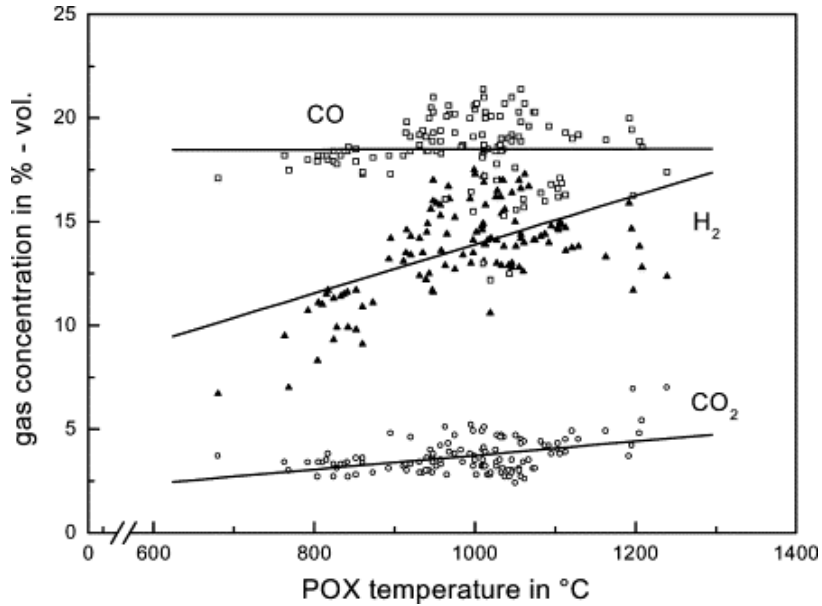
Figure 2-8. Reactor temperature effect on gas concentrations[103]

2.2 Review of HiTAC and CDC Design

HiTAC and CDC designs were reviewed to determine an approach for achieving the Distributed Reaction Regime under reforming conditions (O/C=1.0). Emphasis was given to understanding the physical characteristics of the flow field and reactor conditions necessary for achieving Distributed Reaction Regime. Reactor design and injection strategy was also considered in determining which would be most compatible for reforming conditions.

2.2.1 Flow Field

As the flame is volumetrically distributed throughout the reactor without supporting media, the flow field will have a significant impact of reactor chemistry and stability. Arghode and Gupta studied the effects of forward[104] and reverse[105] flow fields at different thermal intensities. Arghode and Gupta[104] compared a low intensity ($25kW_{th}$) and high intensity ($6.25kW_{th}$) combustor in a forward flow configuration, under premixed and non-premixed configurations. Air was injected at 128-205 m/sec, while fuel was injected at a constant at 97 m/sec.

Arghode demonstrated that injecting air at or near the centerline of the combustor allowed combustion product to recirculate along the walls of combustor and entrained into the feed. The low intensity forward flow reactor was operated under three configurations, shown in Figure 2-9.
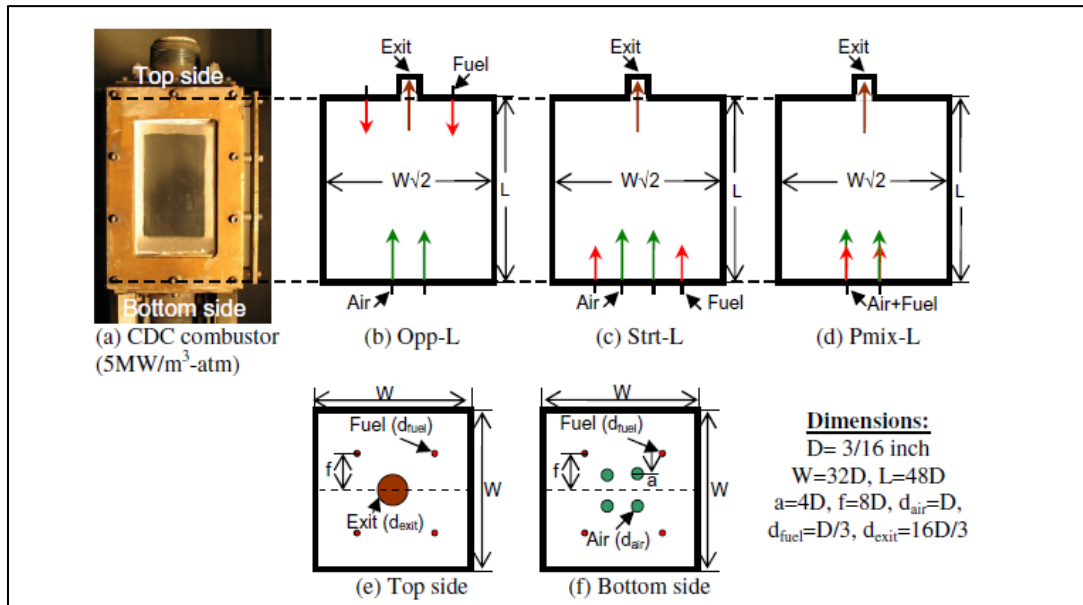
Figure 2-9. Low intensity forward flow combustor, (a) Reactor, (b) Non-premixed opposed flow configuration, (c) Non-premixed straight flow configuration, (d) Premixed, (e) Top of reactor, (f) Bottom of reactor[104]

In the non-premixed opposed flow configuration (Opp-L), air was injected through four central located points, while fuel was injected on the opposing wall adjacent to the centrally exhaust port. In the non-premixed straight flow configuration (Strt-L), air was injected through four centrally located points, while fuel was injected in between the air and the outer wall. Products were exhausted through a single central exhaust port, located on the opposing wall. In the premixed configuration (Pmix-L), a premixed fuel and air charge was injected through four centrally located injection ports, while combustion products were exhausted through a single central exhaust port located on the opposing wall.

The high intensity forward flow reactor was evaluated at three similar configurations, see Figure 2-10. In the non-premixed opposed flow configuration (Opp-H), air was injected centrally, but fuel was injected off-center on the opposing wall. Products were exhausted through a port located on the same wall as fuel injection port. In the non-premixed straight flow configuration (Strt-H), air was injected centrally. Fuel was injected on the same plane as air injection port, but off-center. Products were exhausted through a port located off-center on the opposing wall. In the premixed configuration (Pmix-H), a premixed air and fuel charge was injected from a singular central located injection port, and exhausted through an off-center port located on the opposing wall.
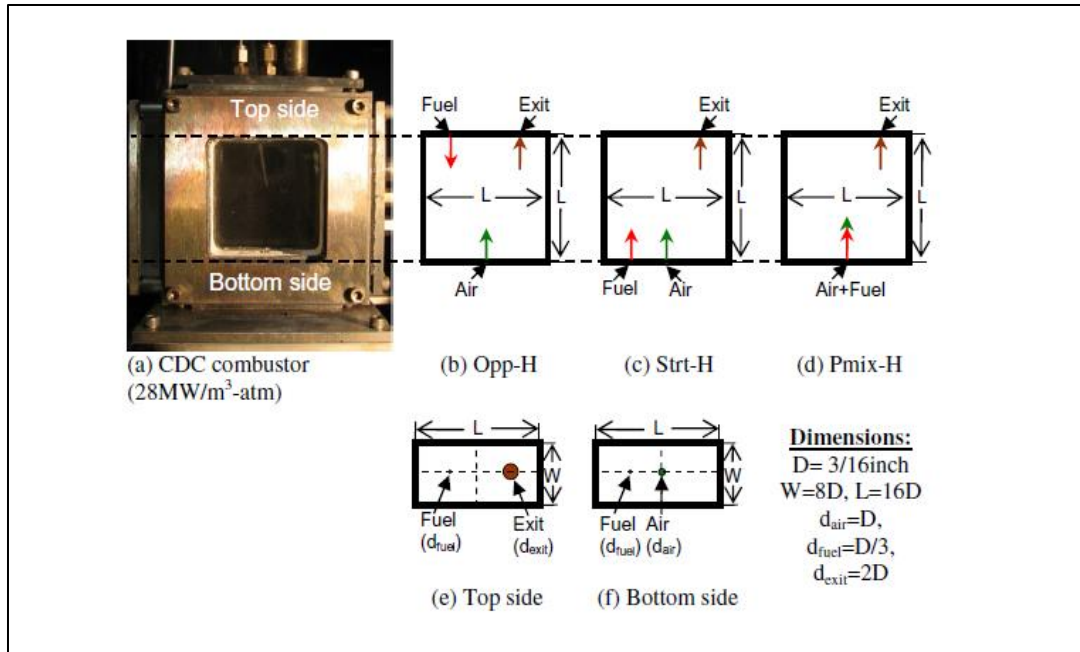
Figure 2-10. High intensity forward flow combustor, (a) Reactor, (b) Non-premixed opposed flow configuration, (c) Non-premixed straight flow configuration, (d) Premixed configuration, (e) Top of reactor, (f) Bottom of reactor[104]

For the low intensity forward flow combustor, global imaging and chemiluminescence imaging showed a significant decrease in visible emissions for the premixed configuration in comparison to the non-premixed opposed and straight flows configurations. Chemiluminescence imaging of the premixed configuration showed only faint radical emissions. In the non-premixed opposed flow configuration, moderate concentrations of hydroxyl radical concentrations occurred near the walls of the reactor. Under the non-premixed straight flow configuration, a central region of high intensity formed within the reactor.

The premixed configuration showed the lowest NO_x formation, but the highest carbon monoxide emissions. Conversely, the opposed straight flow configuration showed the highest NO_x, but the lowest carbon monoxide emissions. The low

intensity combustor had a significantly longer residence time (~90 ms vs 15 ms) than the high intensity combustor.

Visible emission for the high intensity combustor were significantly greater than observed within the low intensity combustor. As in the low intensity combustor, the high intensity combustor showed the premixed configuration to have the lowest visible emission and radical concentrations, as compared to non-premixed (opposed and straight flow configurations), see Figure 2-9 and Figure 2-10. The premixed case showed moderate concentrations of hydroxyl radicals occurring in the left corner of the reactor, but this region is smaller than what appeared in either of the non-premixed cases.

Chemiluminescence imaging of the non-premixed opposed flow configuration showed a much larger region of moderate intensity, encompassing up to 25-50% of the reactor. Similar to the premixed case, hydroxyl radicals formed in the top left portion of the reactor, away from both the exhaust and fuel injection ports. The non-premixed straight flow configuration showed very high intensity at all equivalence ratios, occurring within the center of the reactor or in the top left corner.

Emissions followed a similar trend to what was observed in the low intensity reactor. The premixed case showed the highest carbon monoxide emissions, but the lowest NO_x emissions. While the opposed flow had the highest NO_x emission, but the lowest carbon monoxide emissions.

Arghode and Gupta[105] also investigated the effects of reverse flow on the Distributed Combustion Regime within a high and low intensity combustor, see Figure 2-11 and Figure 2-12. Fuel was injected at 97 m/sec, while air was injected

between 128 to 205 m/sec. The low intensity reverse flow combustor was operated in

a non-premixed opposed flow (RO) and a premixed configuration (RP). In the non-

premixed opposed flow configuration, air was injected off center, but fuel was

injected centrally on the opposing wall. Products were exhausted through a port

located off-center on the same wall as air injection port. In the premixed

configuration (RP), the premixed air fuel mixture was injected on the same plane as

the exhaust port.
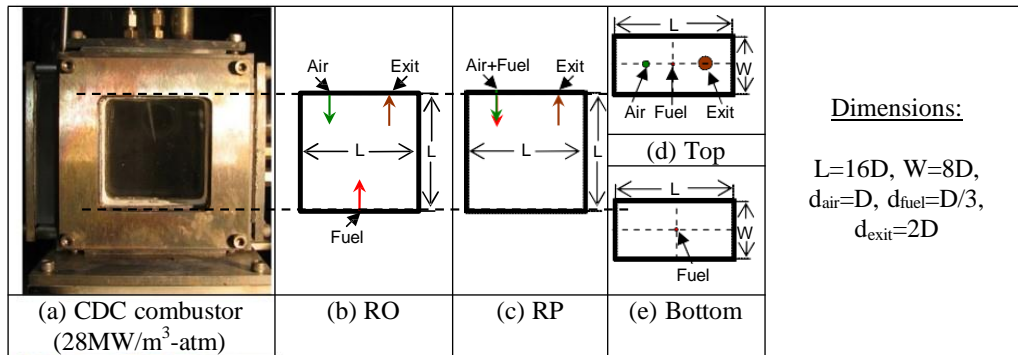
Figure 2-11. Low intensity reverse flow combustor, (a) Reactor), (b) Non-premixed opposed flow configuration, (c) Premixed flow configuration, (d) Top of reactor, (e) Bottom of reactor[105]

In the low intensity reverse flow premixed combustor (RP), chemical

luminesce showed almost no visible detection. Under the non-premixed case (RO),

low concentrations of hydroxyl were observed by the fuel injection port. Overall, the

low intensity combustors, regardless of configuration, showed the lowest

concentrations of hydroxyl in this work.

Arghode et al. [105], evaluated the high intensity reverse flow combustors

under one premixed configuration and up to five non-premixed configurations. In the

premixed configurations (RP-H), the premixed air fuel mixture was injected on the

same plane as the exhaust port, forcing the gasses to recirculate. In the non-premixed

configurations, air was injected in the same plane as the exhaust creating a reverse flow, but fuel injection point was varied. In the non-premixed opposed flow case (RO-H), fuel was injected on the wall opposite to the exhaust and air injection ports. In another set of experiments, fuel was injected from the sidewall with varying distance from the air injector port (RC1, RC2, RC3), creating a cross flow.
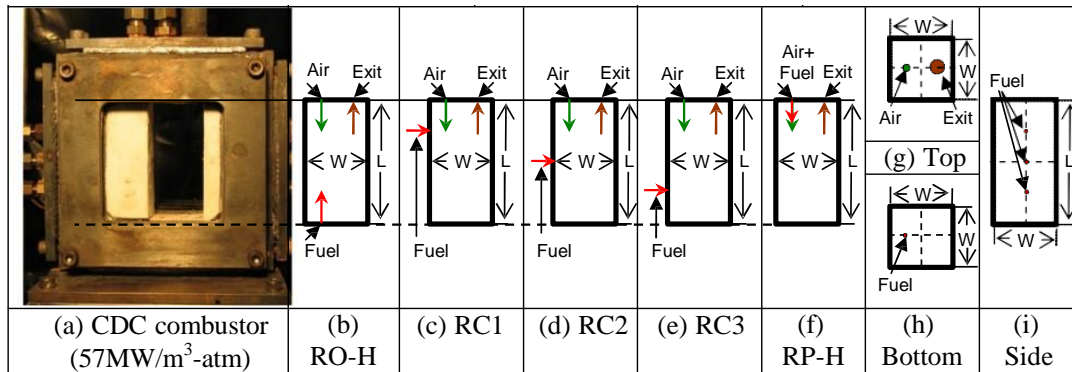
Figure 2-12. High intensity reverse flow combustor (a) Reactor, (b) Non-premixed opposed flow configuration, (c-e) Non premixed side fuel injection configurations, (f) Premixed configuration, (g) Top of reactor, (h) Bottom of reactor, (i) Side of reactor[105]

Chemiluminescence imaging showed that the high intensity reverse flow combustor, when operated premixed (RP-H) or the non-premixed opposed flow modes (RO-H), yielded very low emissions. When fuel was injected into the air jet through a cross flow, as in cases (RC1, RC2, RC3), regions of high hydroxyl concentration emerged. As the fuel injection point approached the air injector port, hydroxyl intensity decreased. Arghode attributed this to the faster mixing of the fuel and the effects of a strong cross flow of the air jet. At higher equivalence ratios of 0.8, the hydroxyl concentrations under the high intensity premixed case were much greater than the non-premixed equivalent.

In terms of emissions, both high and low intensity combustors showed reduced carbon monoxide and NO_x emissions under the premixed configuration. The non-premixed mode (RC1) was the one exception. Under this case, fuel was injected close to fuel injection port, allowing time for sufficient mixing to occur, resulting in a condition that approximates a premixed configuration. In the non-premixed configuration, emission increased as fuel injection occurred further from air injection port (RC1, RC2, RC3).

Under the reverse flow condition, hydroxyl radical intensity was greatly diminished as compared to the forward flow configuration. In addition, the low intensity combustor promoted a greater distribution of the hydroxyl radicals. For both reverse and forward flow configurations, the highest emission of hydroxyl radicals occurred near the fuel injection port or near a corner from the reactor.

Verissimo[106] evaluated the effects of air injection velocity on the Distributed Reaction Regime. The reactor consisted of a non-premixed cylindrical quartz reactor. Fuel was injected through 16 fuel nozzles located concentrically around a single central air injection jet. The nozzle associated with air was adjusted between 6-10 mm to vary the injection velocity from 113 m/sec to 311 m/sec. This experiment was repeated for equivalence ratios of 0.59, 0.66, and 0.77. At equivalence ratios lower than 0.58, the flameless combustion regime was unable to be established.

Chemiluminescence imaging showed that higher injection velocities reduced peak hydroxyl concentrations, while broadening the hydroxyl radical distribution. NO_x concentrations decreased with increasing air content. However, carbon

monoxide concentrations increased with higher injection velocities. The increase in

carbon monoxide was attributed to a reduction in residence time.

Khalil and Gupta[107] investigated the effects of swirl on the Distributed

Combustion Regime. Swirl is often used in combustion to enhance residence time

within a combustor. Exhaust and injection points were varied in order to study the

influence of the flow field on combustion conditions. Figure 2-13 shows a schematic

of swirling combustor configurations.
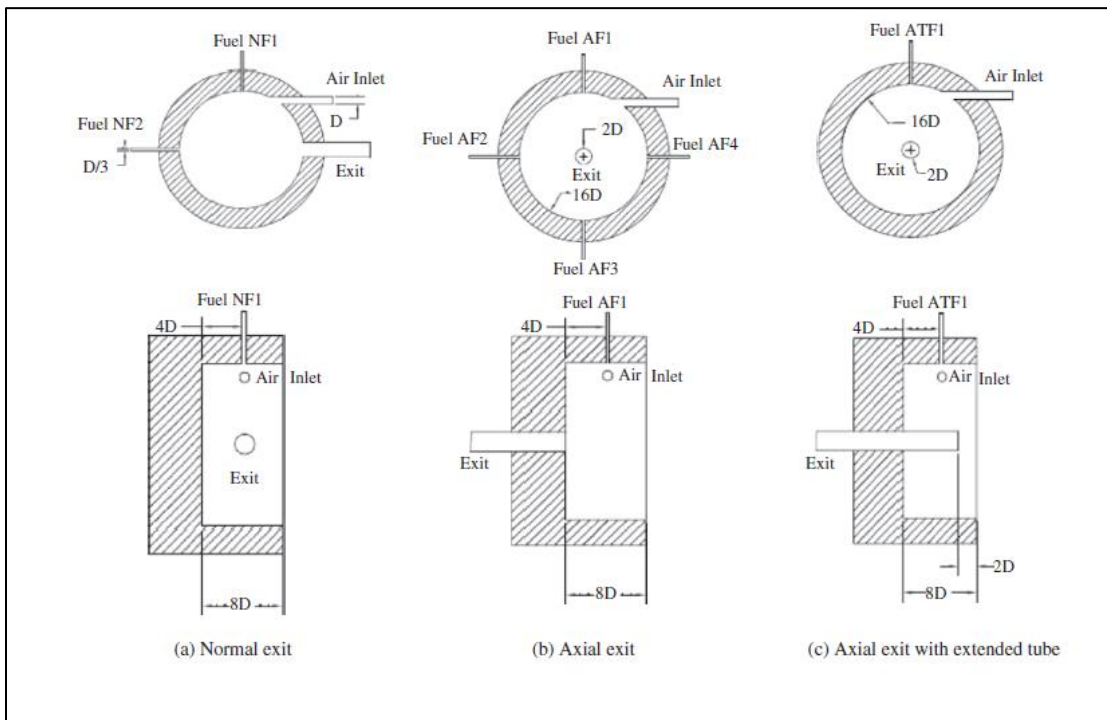
Figure 2-13. Swirl based reactor for multiple fuel injection and exhaust
configurations. (a) Normal exhaust, (b) Axial exhaust, and (c) Axial exhaust with
extended tube[107]

In the first configuration, reactants were exhausted normally to the reactor,

while the reactor was operated under one premixed (NP), and two non-premixed

(NF1, NF2) modes. In the second configuration, reactants were exhausted along the

axial axis, while the reactor was operated under one premixed (AFP), and four non-

premixed (AF1, AF2, AF3, AF4) modes. In the third configuration, reactants were exhausted through an axially extended tube that protruded into the reactor. The reactor was operated in one premixed (ATP), and one non-premixed (ATF) mode.

As found in Arghode & Gupta[104], for a fixed equivalence ratio chemiluminescence imaging of the hydroxyl radicals showed the lowest intensity for the premixed configuration, regardless of exhaust configurations.

Khalil and Gupta[107] found that the extended axial tube configuration increased recirculation and enhanced residence time. This configuration resulted in lower emissions than the normal and axial exhaust configurations. Chemiluminescence imaging showed that the axial extended tube configuration demonstrated the lowest intensity of hydroxyl radicals, followed by normal exhaust and axial exhaust configurations.

2.2.2 Reactor Conditions

Careful control of reactor conditions is required for the Distributed Reaction Regime to emerge. Dilution of the local oxygen concentrations is the critical aspect for achieving the Distributed Reaction Regime and the colorless emissions, which characterize it. Gupta[49,108] investigated the effects of oxygen concentrations on visible emission of HiTAC Combustor using a methane feedstock. Decreasing oxygen concentrations reduced the visual emissions of the combustor. At oxygen concentrations of 2-5%, the flame developed a green hue, resulting from increased C_2 radical emissions. Reactor oxygen concentrations of less than 2% generated a flame that appeared colorless. Other research shows that the colorless emissions can be achieved at higher oxygen concentrations, but require greater mixing[48,109].

The work of Mi et al.[72], indicated that a critical momentum is required to achieve the Distributed Reaction Regime. Achieving a momentum greater than this critical value did not affect the combustion characteristics. Mi noted that the premixed case (0.024 kg-m/sec^2) required 60% less momentum than the diffusion case (0.054 kg-m/sec^2) to achieve the Distributed Reaction Regime. It also was observed that reactor geometry influenced the critical moment required to achieve the Distributed Reaction Regime. It is thought that the exact value observed in this work will not be directly applicable to distributed reforming, but a critical momentum may exists.

In another set of experiments, Khalil and Gupta[73] evaluated the effects of cofiring hydrogen with methane in a swirling CDC combustor. Hydrogen and methane were injected at a $58.5\%_{vol}$ to $41.5\%_{vol}$ ratio. The reactor was operated under both a premixed and diffusion mode. Injection velocities of 96 m/sec were sufficient to prevent flash back. This study is relevant to the work, as it is expected that entrained products will contain hydrogen. Cofiring the fuel with hydrogen is thought to be comparable to conditions within this work. Khalil and Gupta noted hydrogen addition up to $40.9\%_{vol}$ caused the reaction zone to propagate upstream, but did not initiate a flash back. Higher concentrations of hydrogen did not appear to affect the reactor.

M. Derudi et al.[110] also investigated the addition of hydrogen up to $60\%_{vol}$ to mild combustion. Derudi found that, to achieve the colorless conditions, increasing the hydrogen content required higher injection velocities and recirculation. Increasing

hydrogen content from 40%$_{vol}$ to 60%$_{vol}$ further increased the minimum required

entrainment from 8 to 11. Velocities of 75 m/sec yielded a colorless reaction zone.

Duwig[111] evaluated a premixed methane air within a distributed combustor using

high-resolution planar laser which induced florescence at fuel rich conditions

comparable to reforming, shown in Figure 2-14.
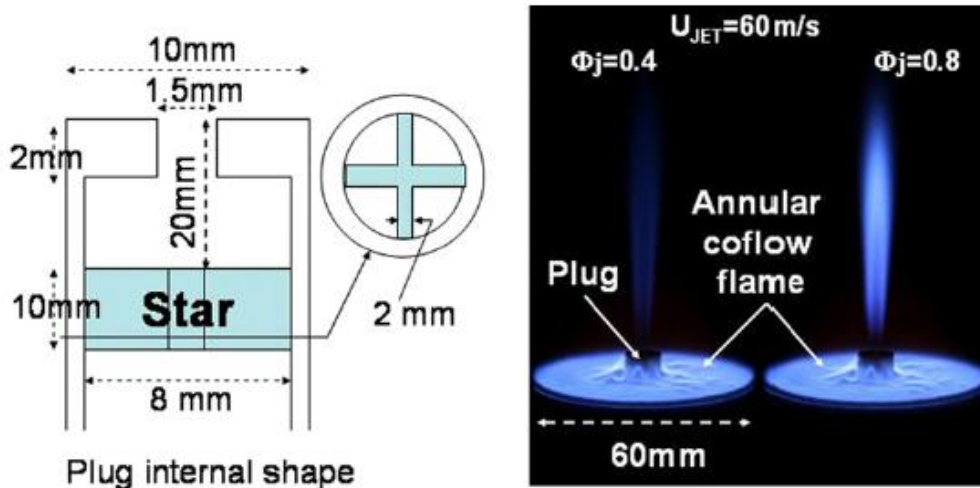
Figure 2-14. Distributed combustor schematic single injection[111]

Reactor conditions ranged from conventional combustion (Φ=0.4) to fuel rich

reforming conditions (Φ=6.0). Visible emissions were noted at all conditions

examined. The combustor consisted of a central injection point (30-60 m/sec) and

secondary injection of non-reacting mixture (50% fresh/ 50% vitiated gases) at

726.85°C. Injection velocity was noted to be lower than that used by Arghode &

Gupta[112], but no flashback was noted. Dugwig noted hydroxyl radical intensity

increased with higher equivalence ratios (lower O/C ratios), although reactions were

distributed over a larger volume. Higher intensities were attributed to the reformate interacting with coflow mixture.

Rahimi[113] investigated the concept of combining HiTAC with the catalytic reforming of methane. Experimental setup consisted of a combustor feeding exhaust gases into a reformer. The catalytic reformer employed a nickel catalyst with a $5\%_{mass}$ loading. No flame regime calculations or optical imaging were provided to prove flame regime operated within the Distributed Reaction Regime; however, both of these are poorly defined under catalytic conditions. The combustor was operated at O/C ratios of 3.0. Additional fuel was injected into the exhaust products to reduce the oxygen to carbon ratio to 1.5-2.2 within the reformer. The syngas consisted of 30-48% hydrogen and 12-22% carbon monoxide. Methane conversion ranged between 47.3-89.3%.

This approach fully oxidizes a portion of the fuel into more stable carbon steam and carbon dioxide. Fuel is then mixed with exhaust gases and reacted over a nickel catalyst. Steam and dry reforming reactions are typically slow and should not be the primary means of conversion. This is similar to older autothermal designs, which used a combustor's exhaust gasses to provide the heat for endothermic steam reforming.

In the current approach outlined within this dissertation, fuel is oxidized through partial oxidation, while minimizing steam and carbon dioxide formation. Inadvertently, some steam and carbon dioxide will be produced as a byproduct. Entraining this exhaust product back into the fresh reactant promotes both steam and dry reforming reactions in addition to the normal oxidative reactions. While this may

not be the optimum approach, it still highlights the potential of the Distributed

Reaction Regime.

Chapter 3: Distributed Reformer Design Considerations

Reformer construction and design were developed using conventional distributed combustor designs highlighted in the literature review in Section 2.2. For the Distributed Reaction Regime to emerge, the fuel-air mixture is injected through a high velocity jet, entraining exhaust products into the mixture before ignition can occur. The entrainment of exhaust products reduces local oxygen concentrations, elongating the chemical time and length scales. The high velocity jet promotes rapid mixing, which in turn reduces the turbulent time and length scales. This results in the characteristic chemical length scales exceeding the characteristic turbulent length scales, generating a volumetric distributed flame.

3.1 Calculation of Turbulent Flame Regime

Turbulent Flamelet Theory allows the approximation of the bulk turbulent flame as a compilation of multiple laminar flamelets[41]. This allows independent numerical calculation of the properties pertaining to the turbulent flow and chemistry. Turbulent premixed combustion flame regimes are classified by the ratios of the characteristic time and length scales relating to the turbulence and chemistry. The Damkohler number (Da) represents the ratio of the turbulent time scales to chemical time scales, and indicates whether the flame is limited by transport or chemistry, see Eq. 3-1. Turbulent Reynolds (Re_o) is the ratio of vicious dissipation to turbulent transport. As suggested by Glassman[114] and Law[115], Turbulent Reynolds is based on integral length scale, as shown in Eq. 3-2.

$$Da = \frac{\tau_m}{\tau_{chem}} = \left(\frac{l_o}{\delta}\right)\left(\frac{S_l}{u'}\right)$$

<div align="right">Eq. 3-1</div>

$$Re_o = \frac{u'l_o}{v} = \frac{u'l_o}{S_l\delta}$$

<div align="right">Eq. 3-2</div>

3.1.1 Characteristic Turbulent Time and Length Scales

In the Distributed Regime, complete mixing of fuel, air, and reactive exhaust products are achieved primarily through turbulent transport and not through diffusion[42]. Therefore, characteristic time and length scales pertaining to the flow and transport are based on turbulent properties. Integral length scale (l_o), kolmogorov length scale (l_k), and turbulent velocity fluctuations (u') are estimated through Eq. 3-3 to Eq. 3-8, which are a function of the volume averaged turbulent kinetic energy (k) and turbulent energy dissipation (ε)[42]. As the desire of this work is to distribute the reaction zone throughout the reactor, characteristic turbulent time scales (τ_m) are based on the characteristic lifetime of large eddies.

$$u' = \left(\frac{2}{3}k\right)^{1/2}$$

<div align="right">Eq. 3-3</div>

$$l_o = \frac{\left(\frac{2}{3}k\right)^{1.5}}{\varepsilon}$$

<div align="right">Eq. 3-4</div>

$$l_k = \left(\frac{v^3}{\varepsilon}\right)^{\frac{1}{2}}$$

<div align="right">Eq. 3-5</div>

$$\tau_m = \frac{l_o}{u'}$$

<div align="right">Eq. 3-6</div>

Turbulent time scales were estimated using a commercial computational fluid dynamics code Fluent. A k-epsilon realizable viscous model was utilized with standard wall functions. Arghode[104] found strong agreement using k-epsilon

realizable viscous model with a similar distributed combustor. Due to geometrical symmetry, a quarter of the reactor was modeled allowing mesh size to be reduced to ~500,000 elements. Results were allowed to converge until residual decreased below 10^{-5}. Arghode verified the accuracy of this approach on a comparable distributed combustor using PIV[48]. Initial turbulence intensity was approximated as 10%[116].

3.1.2 Characteristic Chemical Time and Length Scales

Characteristic chemical time and length scales are derived from the laminar flame properties. Laminar flame thickness (δ) represents the characteristic length for a reaction to occur. Laminar flame thickness was estimated using a correlation suggested by Turns[43], which relates the ratio of thermal diffusivity (α) to laminar flame speed (S_l), see Eq. 3-7. The chemical time scale (τ_{chem}) is the characteristic time for the flame to propagate through laminar flame thickness, which is defined by the ratio of flame length (δ) to laminar flame speed (S_l), see Eq. 3-8 [43,48,117].

$$\delta = \frac{2\alpha}{S_l} \qquad\qquad \text{Eq. 3-7}$$

$$\tau_{chem} = \frac{\delta}{S_l} \qquad\qquad \text{Eq. 3-8}$$

Experimental data under fuel rich conditions with dilution is unavailable in literature. Instead laminar flame speed data was calculated through numerical modeling, using Chemkin Pro[118]. A reduced kinetic mechanism composed of 121 species and 2,673 reactions was employed[119]. This model has been validated for hydrocarbon fuels ranging between hexane and hexadecane.

A JP-8 surrogate, proposed by Violi[120], was used to represent JP-8. This surrogate (cited as Violi# 3) has been previously validated for both ignition delay and flame speed. This surrogate is designed to be a good representation of the various hydrocarbon distributions in JP-8, representing the three major hydrocarbon groups: alkanes (dodecane and isooctane), cyclo-alkane (methyl-cyclohexane), and mono-aromatics (toluene and benzene). Of the surrogates evaluated in Section 4.1.3, this surrogate was designed to replicate JP-8's sooting propensity, distillation curve, flame speed, and auto ignition characteristic. It was believed this would provide the best representation of the of chemical time and length scales.

3.2 Entrainment and Recirculation

In order to elongate the characteristic chemical time and length scales, the fuel-air mixture was injected through a high velocity jet, which entrained exhaust products into the mixture, diluting the local oxygen concentrations. Without this entrainment and dilution, a conventional flame would have emerged, as reactions would have proceeded at conventional time and length scales. Figure 3-1 shows the dilution of a premixed charge as a function of recirculation. As recirculation increases, local fuel and oxygen concentrations deminish, while local concentrations of hydrogen, steam, carbon monoxide, and carbon dioxide increase. Increasing steam and carbon dioxide concentrations promote steam and dry reforming reactions, which increases reformate yield.

As the syngas contains high concentrations of hydrogen, it will promote a more rapid reaction requiring greater delution. Hydrogen was not expected to exceed 30% of reformate concentrations. Based on the work of Derudi[110] and Khalil[121],

which compared the addition of hydrogen to a methane flame under CDC conditions, a minimum entrainment/recirculation of 7-10 would be required.
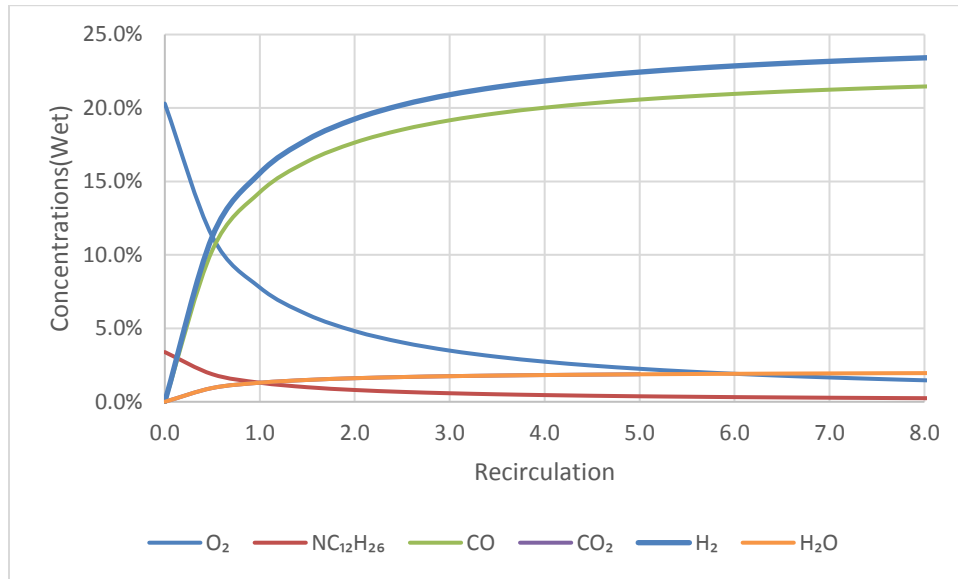
Figure 3-1. Dilution of the injected premixed charge as a function of recirculation. O/C=1.0 dodecane

The recirculation was calculated assuming free jet entrainment, using the calculation recommended by Ricou[122]. The Recirculation ratio (R) is defined as the ratio of the recirculated mass $(\dot{m}_{rec})$ to injected mass $(\dot{m}_{jet})$. Recirculation increased linearly with distance from the nozzle inlet. Smaller injection diameters (d_{jet}) promoted greater recirculation and entrainment. Larger reactor diameters (d_{Reac}) promoted greater recirculation. Decreasing the density of reactive flow (ρ_{rec}) reduced recirculation. However, decreasing the density of injected mass (ρ_{jet}) enhanced recirculation. Ce represents a coefficient of recirculation for this work; a value of 0.32 was used. Under conventional combustion conditions, Han et al.[123], found that a reactive flow will reduce entrainment by about one third. However, under conditions more comparable to this work, Yang[124] noted

recirculation was not diminished at higher temperatures and under oxygen depleted

conditions recirculation. Calculations were confirmed using the CFD approach

outlined in Section 3.1.1.

$$R(X) = \frac{\dot{m}_{rec}}{\dot{m}_{jet}} = \frac{C_e X}{d_{jet}} \left(\frac{\rho_{rec}}{\rho_{jet}}\right)^{\frac{1}{2}} - 1 \qquad \text{Eq. 3-9}$$

$$\theta = \frac{d_{jet}}{d_{Reac}} \left(\frac{\rho_{rec}}{\rho_{jet}}\right)^{\frac{1}{2}} \qquad \text{Eq. 3-10}$$

$$R_{max} = \frac{\dot{m}_{rec_{max}}}{\dot{m}_{jet}} = \frac{.455}{\theta} - \frac{1}{2} \qquad \text{Eq. 3-11}$$

$$\frac{.455 d_{reac}}{C_e} + \frac{1}{2} \frac{d_{jet}}{C_e} \left(\frac{\rho_{jet}}{\rho_{rec}}\right)^{\frac{1}{2}} = X_{Crit} \qquad \text{Eq. 3-12}$$

Recirculation increased linearly with distance from the nozzle inlet. Smaller

injection diameter promoted greater recirculation and entrainment. Increasing the

temperature of the recirculated gases reduced recirculation. The finite volume of the

reactor limits maximum recirculation, Eq. 3-11 and Eq. 3-12.

As shown in Figure 3-2, the recirculation in the CFD model compared very

well to the free jet theory. A sample calculation was preformed below. The inlet feed

consisted of 37 SLPM of air preheated to 500°C. The injection port had an inner

diameter of 4.0 mm. The reactor had a diameter of 8 cm and a length of 15 cm. There

was some discrepancy toward the rear of the reactor (12-15 cm), which was attributed

to wall effects and the recirculating effluent. CFD and theory were in strong

agreement with peak recirculation. However, CFD predicted the maximum would

occur at 13 cm, while theory predicted it as closer to 12 cm.
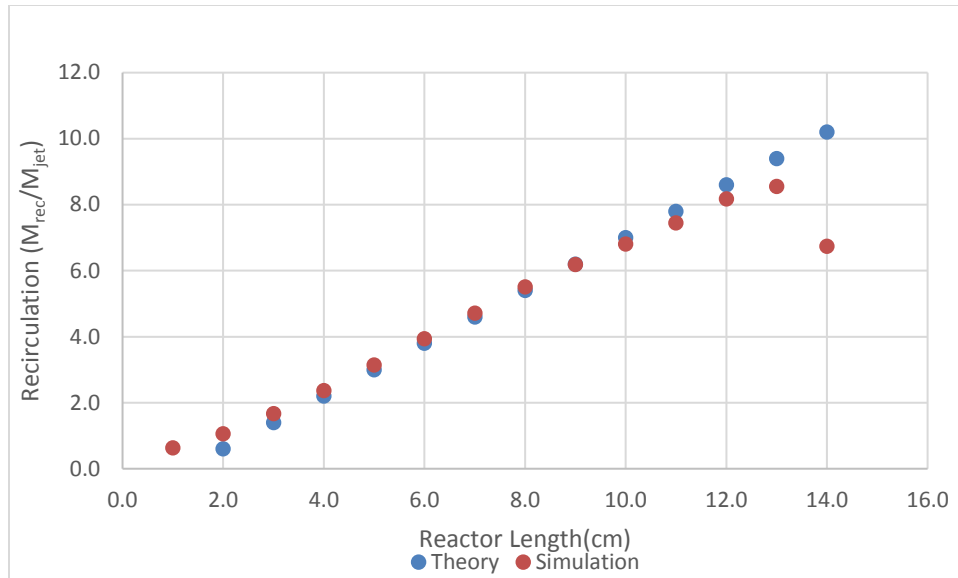
Figure 3-2. Jet theory vs jet CFD
(Inlet D=4.0 mm inlet, Reactor D=8.0 cm, Reactor L=15.0 cm)

3.3 Ignition Delay

The ignition delay must be long enough to allow for both the entrainment of exhaust products and the corresponding reduction of local oxygen concentration, before ignition occurs. If ignition transpires before achieving sufficient entrainment and dilution, a conventional flame will emerge. To achieve the Distributed Reaction Regime, the ignition delay must be significantly longer than the characteristic turbulent time scale[48]. Operating at fuel rich conditions should enhance ignition delay as compared to conventional CDC conditions. However, ignition delay must be shorter than the average resident time of the reactor in order to have sufficient time for reactions to propagate fully.

Characteristic turbulent time scales were calculated using the approach outlined in Section 3.1.1. No experimental information was available on ignition delay for fuel rich conditions and reduced oxygen concentrations for a JP-8 fuel.

94

Instead, a more conservative assumption of no dilution was employed, see Eq. 3-13.
The ignition delay was calculated using the experimental data[125] of JP-8 at an
Φ=3.0 for temperatures between 900 K to 1600 K, see Figure 3-3. A 1/P presure
correlation recommended by Jayakishan[125] was used to correct data to relavent
pressures.

$$t_{ing} = \left(5.4 \pm 0.65 \text{ x } 10^{-2}\right) \exp\left(\frac{10955}{T}\right) \quad (1000 - 1600 \text{ K}) \qquad \text{Eq. 3-13}$$
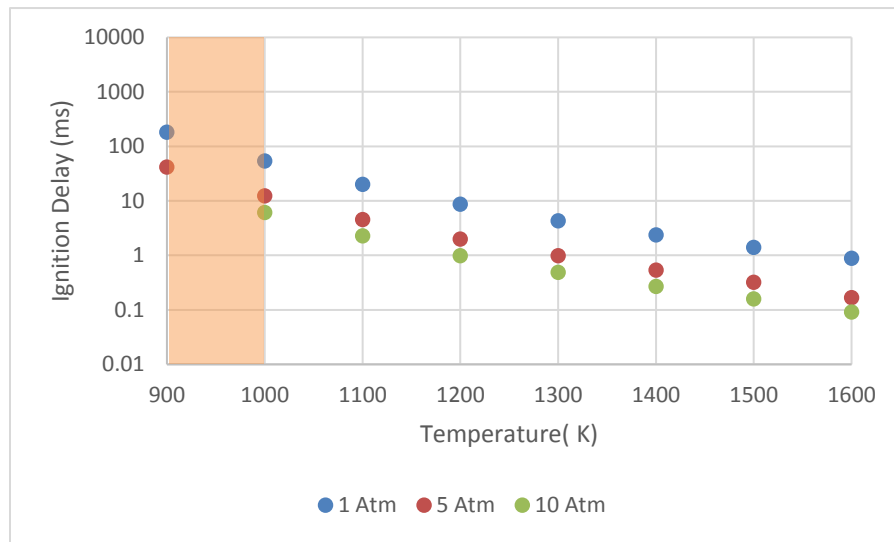
Figure 3-3. Ignition delay of Jet-A1 at O/C~1.0

Assuming a reactor temperature of 1000°C, an injection temperature of 450°C
generated an average mixture temperature of 725°C, resulting in an ignition delay of
55.5 ms. Using the higher injection temperatures of 750°C generated an average
mixture temperature of 875°C, which shortened the ignition delay to 13.2 ms.
Characteristic turbulent time scales are on the order of 1.0-1.7 ms. It was determined
under all experimental conditions there would be sufficient time for entrainment to
occur.

95

It was determined that mixture preparation had a significant impact on reformate product distribution. Al Hamamre[95] determined through careful control of residence time and ignition delays that preheats as high as 700°C could be employed without pre-ignition. The mixer and reactor were designed to avoid pre-ignition for the desired operating conditions ranging for 300-750°C.

Residence time and relevant volumes are defined from the initial contact of the separate air and fuel feeds to the injection into the reactor. The volume of the mixer was 4.4 cm^3 and was calculated by assuming the volume of the tube without the mixing elements. The combined volume (V) of the tube and nozzle was calculated to be 0.46 cm^3. The volumetric flow ($\dot{V}$) of air rate was 30.0 L/min at 300°C. This condition corresponded to the lowest flow rate (O/C=1.0, 3.0 kW$_{th}$) and was thought to be the condition with the highest chance of pre-ignition. The average residence time of the mixer and nozzle was calculated to be 8.8 ms and 0.92 ms, respectively, with a combined residence time of 9.7 ms.

$$\tau_{res} = \frac{V}{\dot{V}} \qquad\qquad \text{Eq. 3-14}$$

Using Eq. 3-13, assuming hottest injection temperatures of 750°C at an O/C ratio of 1.0, ignition delay was 42.5 ms. The combined residence time of the fuel mixer and nozzle was 9.7 ms, which was approximately 1/5th of the ignition delay (54 ms). A lower injection temperature of 600°C, would have extended the ignition delay to 267.6 ms. Both conditions would allow mixing without pre-ignition.

3.5 Difference Between Distributed Reforming and Distributed Combustors

The fundamental difference between combustor and reformer are their purposes. A combustor oxidizes all hydrocarbons to their highest oxidative states, while extracting the maximum amount of heat and minimizing residual chemical energy. Conversely, a reformer reduces all hydrocarbons to hydrogen and carbon monoxide, maximizing residual chemical energy. These differences influenced both reformer's design and material choices.

As combustors are designed to operate with excess air for a given thermal loading, a reformer will operate with one-fifth the air as a typical combustor. Lower volumetric airflow rates will reduce the injection velocity and momentum of the injected mass, which in turn limits the entrainment. A reduction in injection velocity also increases the risk of flashback.

Within a distributed combustor and reformer, the injection velocity must be significantly greater than flame speed, in order to prevent the flame from propagating into the injector. To compensate, an additive of steam can be introduced to increase volumetric flow rate, while simultaneously quenching potential reactions. A reduction of either nozzle size or number of injection points can also increase the injection velocity.

As stated previously, in combustion the objective is to oxidize hydrocarbons to their highest oxidative states, while extracting the maximum amount of heat. However, in reformation, the objective is to covert the hydrocarbons into a hydrogen and carbon monoxide rich gas, while minimizing the formation of heat. While the heat should be minimized, heat is still necessary to activate the desired chemical

97

reactions. Ideally, 80-90% of the energy should be retained within the hydrogen and carbon monoxide species, while 10-20% will be converted to heat. This results in reformers being more susceptible to heat loss.

In distributed combustion, the hot exhaust gases are relatively inert (CO_2, N_2, and H_2O). Conversely, in distributed reformation, the exhaust gases are composed of more active species (H_2, H_2O, CO, CO_2, CH_4, and C_2H_2). Variations in the entrained gas will cause a change in the chemistry between combustion and reforming conditions. It was expected that higher levels of entrainment would be required to prevent ignition in reforming, as the effluent contains more reactive species (hydrogen & carbon monoxide).

The radically different gas composition within combustors and reformers requires different insulation materials. Hydrogen and carbon monoxide, the major species in reforming, are both strong reducing agents. In reforming, the reducing environment will destroy silica-based insulation, which is commonly used in combustors[105,126]. Instead, alumina-based insulation is commonly employed in reforming as it can withstand the reducing environment. However, alumina is significantly more sensitive to thermal stress, so the design must incorporate stress relief into the design.

Chapter 4: Design of Distributed Reactor

Using the conclusions drawn from literature, a reformer was developed through one dimensional numerical simulations and computational fluid dynamics simulations. Initially, the kinetic mechanisms and surrogates were evaluated using existing non-catalytic reforming data. One-dimensional numerical calculations (Chemkin) were used to estimate the optimum O/C ratio, reactor, volume, and residence times. Cold flow simulations were then used to determine a flow field necessary to achieve those conditions.

4.1 Validation of Kinetics and Surrogate

Kinetic mechanisms and Jet-A1/JP-8 surrogates were validated against experimental data of Jet-A1 kerosene[11]. The experimental data[11] was derived from the reformation of Jet-A1 kerosene in a porous media reformer with a stationary flame. Numerical simulations were based on the work of Vourliotakis[127], who determined that this type of reactor could be modeled numerically using a reactor network consisting of a series of zero and one dimensional reactors.

4.1.1 Reactor Network

A reactor network was developed using the approach outlined by Vourliotakis[127], who successfully modeled the thermal partial oxidation of methane in a porous media. A series of zero and one dimensional reactors were used to represent the mixing cone, flame holder, and diffuser. Figure 4-1 shows a visual display of the reactor network. The spray cone that developed from the nozzle,

allowing the fuel and air to mix, was modeled as an adiabatic plug flow reactor with a variable cross-sectional area. Diameter was varied linearly from 1 mm (inlet size) to 70 mm over a distance of 100 mm. While the plug flow reactor assumed perfect mixing of the fuel and air, the addition of modeling the spay cone accounted for any chemistry that might be occurring under these conditions.
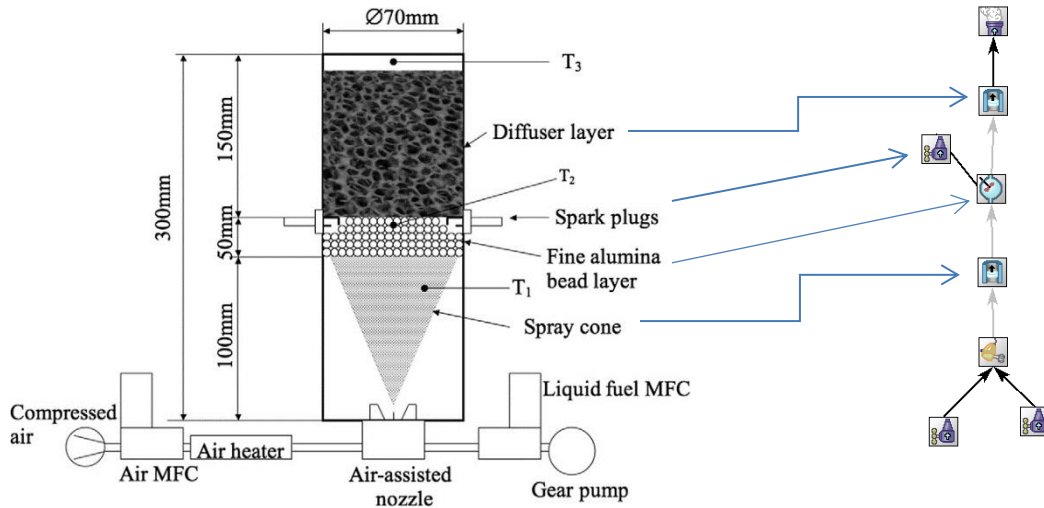
Figure 4-1. Experimental[14] and modeling setup

The fine bead layer in the reformer acted as a flame holder. Premixed reactants would enter this region and ignite. The flame holder consisted of a layer of alumina beads with a diameter in the range of 2 to 4 mm and a spark plug. The flame holder and spark plug were represented as a continuously stirred transient reactor (CSTR) with a small transient injection of super-heated air (1000°C). The air was injected at a flow rate of 1.0 g/sec for six seconds, and reduced to 0.5 g/sec for four seconds, before being reduced to 0.0 g/sec. The CSTR reached a steady state in about 10-15 seconds. The void space of the flame holder was 74.92 cm^3, and this value was used for the volume of the CSTR.

The diffuser in the rear of the reactor consisted of zirconia oxide foam from Linik[128]. The reactor dimensions were 70 mm in diameter and 150 mm long. The diffuser was represented as an adiabatic plug flow reactor (PFR), with a volume equal to the void space of the porous media. The porosity of the reactor could not specifically be determined, but after examining other suppliers, it was determined that the void fraction for this type of porous media with a porosity of 30 pores per inch (ppi) typically ranges between 90-95%[129,130]. The void fraction was modeled as 90%, and resulted in the effective reactor length being reduced to 135 mm.

4.1.2 Kinetic Mechanisms

Limited kinetic modeling has been conducted with reforming; primarily emphasis has been placed on combustion regime[91]. It was thought that a detailed kinetic combustion mechanism, which included kinetics for pyrolysis may be able to represent reforming conditions. Models must be of sufficient complexity to capture the behavior of larger more complicated hydrocarbons. Initially dodecane was chosen as a surrogate for Jet-A1/JP-8, as it previously had been used to represent kerosene and JP-8 in catalytic work[88,91]. Two models were found to meet these criteria.

The first model was developed in 2009, by Charles Westbrook, at the Lawrence Livermore National Lab (LLNL)[131]. The model contains detailed kinetic data for alkane hydrocarbons ranging from hexane to hexadecane for pyrolysis and combustion reactions. Validation occurred at equivalence ratios of 0.20 to 1.50 (O/C=2.06-15.42), pressures of 1 to 80 atm, and temperatures of 650-1600 K. The model was composed of 11,173 reactions and was acquired from the Lawrence

Livermore National Labs website https://combustion.llnl.gov/. However, this model does not contain kinetics for soot formation.

The second kinetic model was developed by E Ranzi, at the University of Milan in the Chemical Reaction Engineering Chemical Kinetics group (CRECK)[119,132]. This model was intended to model combustion, pyrolysis, and soot formation of alkane hydrocarbons ranging from methane to hexadecane. The model was validated was conducted for equivalence ratios of 0.2 to 2.0 (O/C=1.54-15.4), at pressures ranging between 0.08 to 50 atm, and temperature ranging between 550 to 2000 K. A lumping mechanism detailed in Ranzi 2001[133] was used to reduce the number of reactions to 13,532, but was found to take longer to converge than the LLNL mechanism. The kinetic information acquired from the CRECK kinetic website listed at http://creckmodeling.chem.polimi.it.

Numerical simulation were compared to experimental data of Jet-A1 kerosene generated by Pastore[11]. Pastore evaluated Jet-A1 in a porous media reformer with a stationary flame, at O/C ratio of 0.98 to 1.96. Experimental data was curve fitted with a polynomial blue line to show reformate trend. The experimental data from Pastore was polynomial curve fitted below with a blue line.

Both kinetic models were able to predict the general product distribution, but had difficulty predicting the formation of hydrocarbons. Numerical simulations of fixed gas concentrations were in strong agreement with the experimental data between O/C ratios of 1.46 to 1.96, shown in Figure 4-2 to Figure 4-4 . This was expected as both models were validated within this range.

At O/C ratios less than 1.47, the numerical simulation diverged from the experimental data. Of the fixed gases, carbon monoxide and carbon dioxide for both models showed the greatest divergence from experimental data. Divergence was the most pronounced at O/C a ratio of 1.18. Numerical simulations under predicted carbon monoxide formation and over predicted carbon dioxide formation. At lower oxygen to carbon ratios ~ near an O/C ratio of 1.0, the agreement improved. It was observed that the LLNL model showed greater divergence from the experimental data.
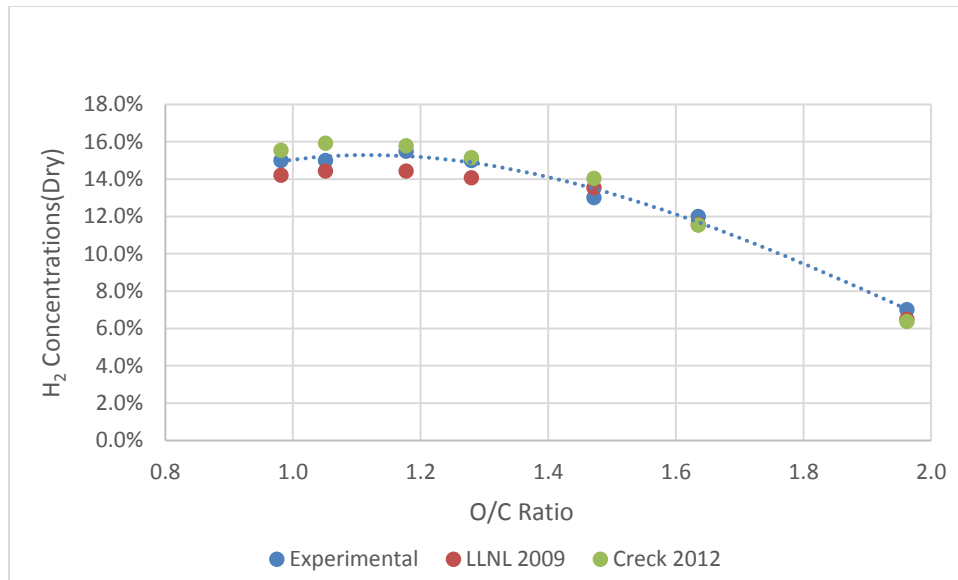
Figure 4-2. Hydrogen concentrations of experimental and numerical simulations at O/C ratios of 0.98 to 1.96
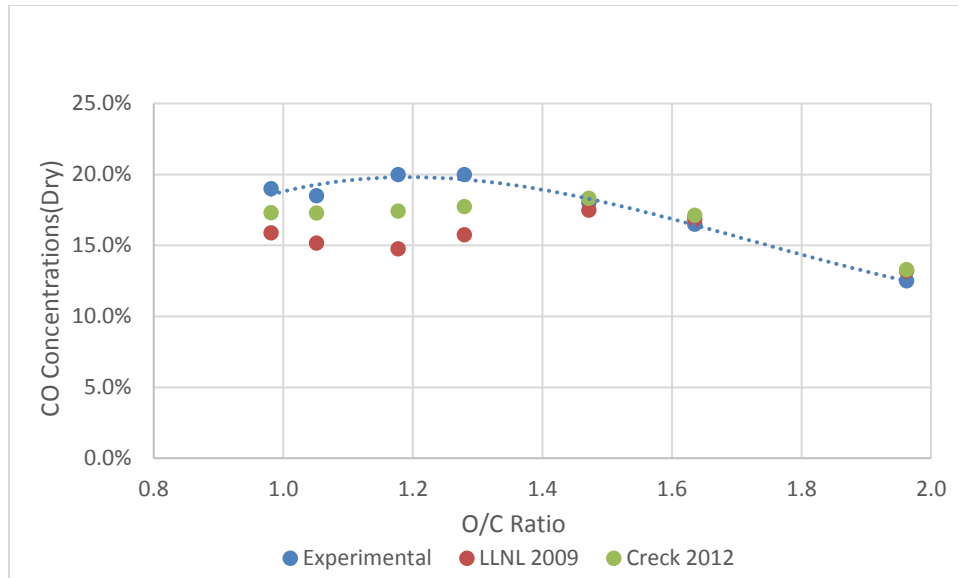
Figure 4-3. Carbon monoxide concentrations of experimental and numerical simulations at O/C ratios of 0.98 to 1.96
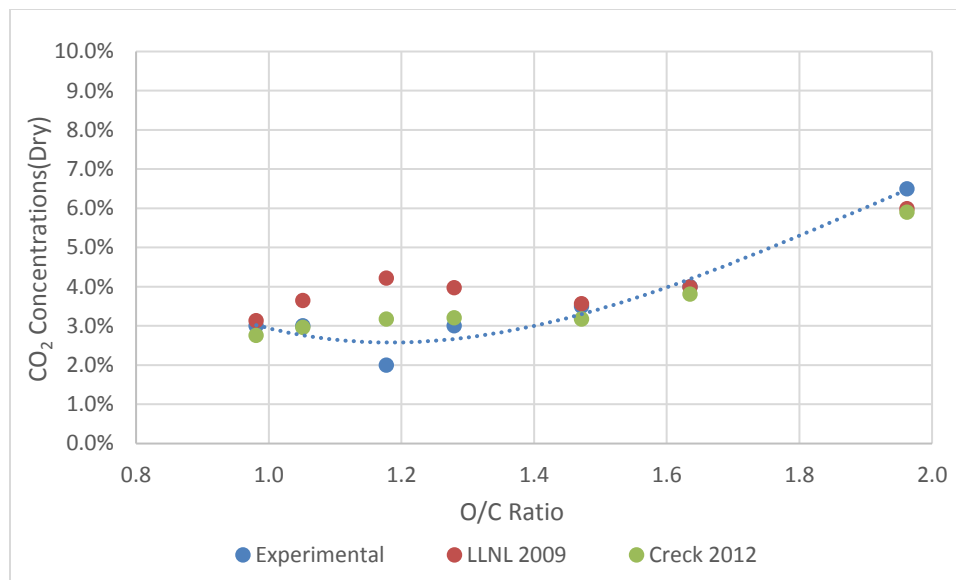
Figure 4-4. Carbon dioxide concentrations of experimental and numerical simulation at O/C ratios of 0.98 to 1.96

The divergence of numerical simulation of fixed gas from the experimental

data was attributed to a failure to accurately predict the hydrocarbon formation. The

simulated fixed gas's deviations from experimental data occurring between O/C ratios

of 0.98 to 1.47 strongly corresponded with the overly predicted acetylene formation, as shown in Figure 4-5. At O/C ratio of one, the experimental data showed acetylene to be at most 0.10%, while the LLNL and CRECK models predicted acetylene formation up to 4.43% and 1.59%, respectively.

Numeral simulations of methane and ethylene formation were generally under predicted, as shown in Figure 4-6 and Figure 4-7. Neither mechanism predicted the formation of ethane, which was consistent with experimental data. The divergence in the numerical simulation of acetylene was believed to have influenced the formation of methane and ethylene. The stronger agreement occurring at O/C ratios of 1.47-1.96 was attributed to operating closer to the validated region.

The divergence of the numerical simulations of the hydrocarbons from the experimental data can be explained by incomplete knowledge of the kinetics and the choice to represent a complex hydrocarbon with single component surrogate. The average molecular formula of Jet-A1 and JP-8 has been shown[85] to be very similar to dodecane, but this simplification ignores the contribution of the aromatic and cyclo-alkane compounds. DuBois[88] compared dodecane to a kerosene based JP-8 under catalytic autothermal reforming, and noted that dodecane produced higher concentrations of lower hydrocarbon and carbon monoxide.
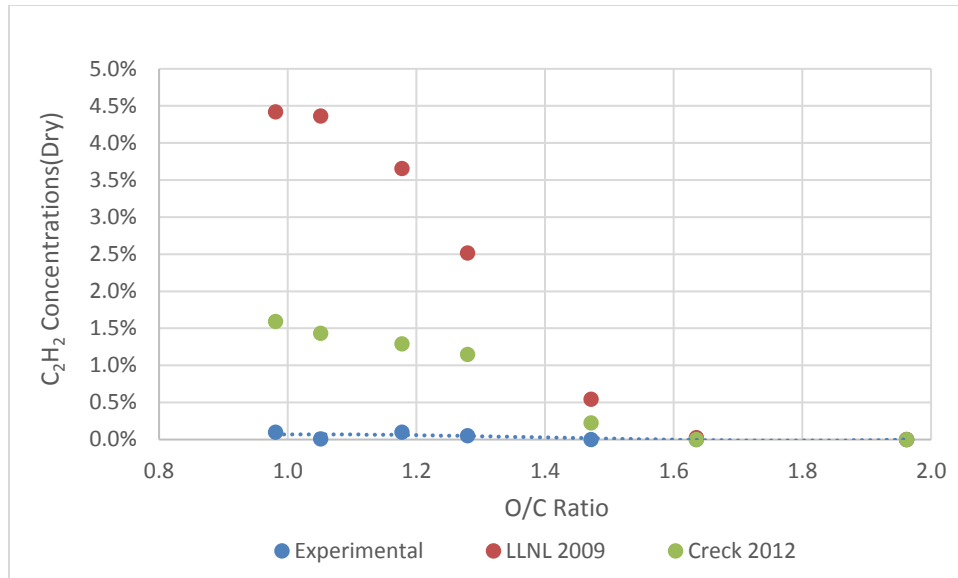
Figure 4-5. Acetylene concentrations of experimental and numerical simulations at O/C ratios 0.98 to 1.96
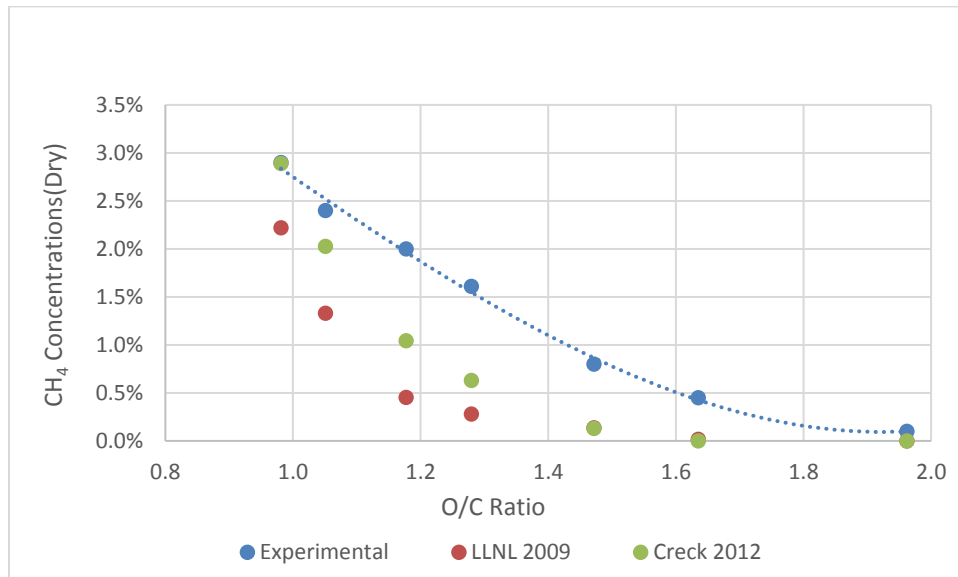
Figure 4-6. Methane concentrations of experimental and numerical simulations at O/C ratios of 0.98 to 1.96

106
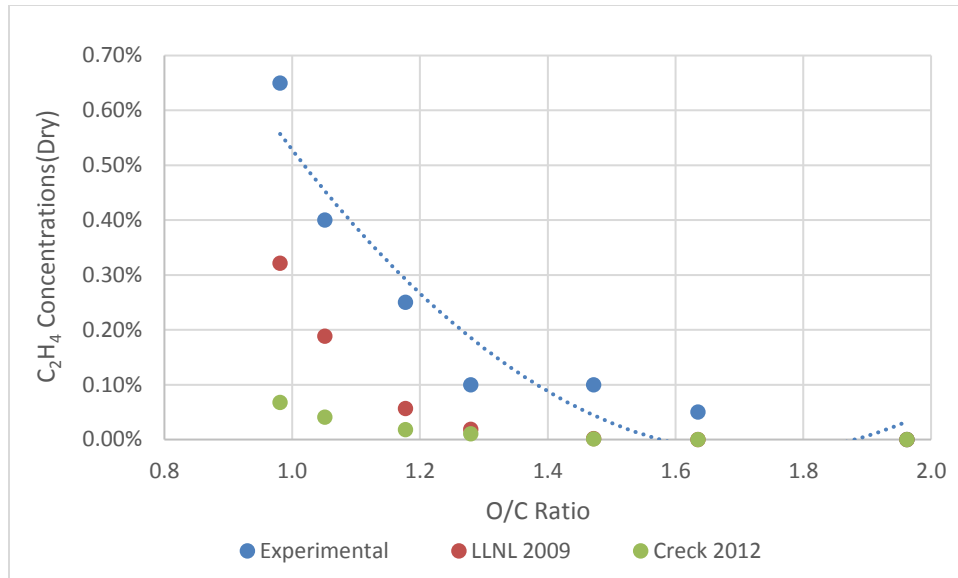
Figure 4-7. Ethylene concentrations of experimental and numerical simulations at O/C ratios 0.98 to 1.96

Due to the addition of soot formation kinetics, the CRECK mechanism showed greater accuracy in predicting the formation of hydrocarbon and fixed gas concentrations. The soot formation kinetics greatly improved the modeling of the acetylene and carbon monoxide compounds.

Initially, through reaction (R. 4-1), acetylene would form soot ($C_{20}H_{10}$) generating hydrogen radicals.

$$C_{16}H_9 + C_2H_2 => 0.50 \, C_{16}H_{10} + 0.5 \, C_{20}H_{10} + H \qquad\qquad \text{R. 4-1}$$
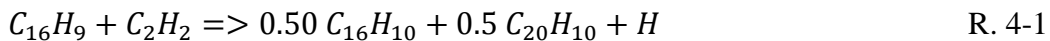
Then hydroxyl radicals would oxidize the soot, forming smaller hydrocarbons and formyl radicals through reaction (R. 4-2). The formyl radicals then decompose through third body reactions, generating additional hydrogen radicals and carbon monoxide (R. 4-3).

$$OH + C_{20}H_{10} => 0.25 \, C_{16}H_{10} + 0.75 C_{20}H_{10} + HCO \qquad\qquad \text{R. 4-2}$$

$$HCO + M = CO + H + M \qquad\qquad \text{R. 4-3}$$
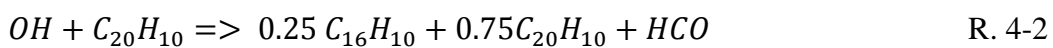
As shown in Figure 4-8, reactions R. 4-2 and R. R. 4-3 are very active in the rearward portion of the diffuser, as shown by the rate of production (ROP) of formyl radicals. The additional hydrogen radicals generated in reactions R. 4-1 & R. 4-3 react to form additional hydroxyl radicals, repeating the processes and further enhancing other reactions.
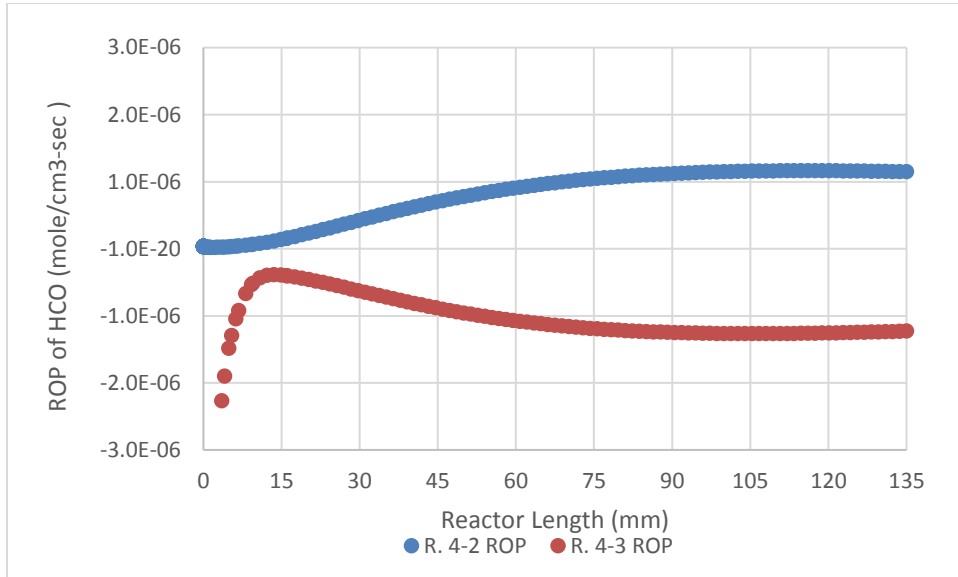
Figure 4-8. Rate of production (ROP) of formyl radicals in diffuser at O/C=1.18
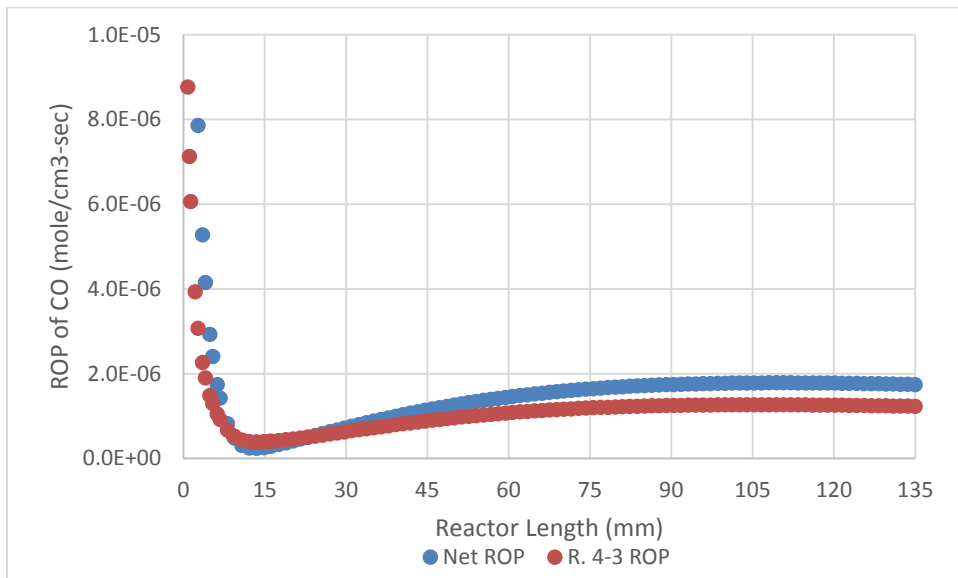
Figure 4-9. Rate of production (ROP) of carbon monoxide in diffuser at O/C=1.18

Within the CRECK, between 70-100% of carbon monoxide formation was produced through reaction R. 4-3, as shown in Figure 4-9. Reaction R. 4-3 was included in the LLNL model, but was less active as there was no means of converting acetylene to formyl radicals.

4.1.3 Comparison of JP-8 Surrogates

Using the CRECK mechanism, four surrogates were evaluated against the experimental data of Pastore using the approach outlined in Section 4.1.1. The average chemical composition of JP-8/Jet-A/Jet-A1 on a volumetric basis consists of: iso and normal alkanes (50-65%), cyclo-alkanes (10-20%), mono-aromatics (15-20%) and poly-aromatics (1-3%). Dagaut[91] reported the average molecular formula of JP-8 varies between $C_{10.9}H_{20.9}$ to $C_{12.0}H_{23.0}$, which results in an average molar hydrogen to carbon ratio (H/C) of ~1.92.

Surrogates chosen range in complexity from a single component up to six components, to represent the different hydrocarbon classes and molecular weights present in JP-8/Jet-A1.

Single component surrogates are computationally easier and represent the dominate hydrocarbons (alkane) present in JP-8/Jet-A1, but may not capture the behavior induced by aromatic and cyclo-alkane compounds. Complex surrogates are composed of the alkanes, cyclo-alkanes, and mono-aromatic hydrocarbons, which are a better representation of the fuel, but are more computationally demanding. Poly-aromatic hydrocarbons were not included for simplification of the surrogate as they only compose 1-3% of total volume. Surrogate hydrocarbon compositions are

reported in Table 4-1 as liquid volume fraction. Surrogate properties are reported in

Table 4-2.

	JP-8/Jet-A	Hydrocarbon	Single	Binary	Tertiary	Senary
Iso and Normal Alkane	50-65%	Iso-octane	0%	0%	0%	10%
		Dodecane	100%	62.6%	70%	30%
		Tetradecane	0%	0%	0%	20%
Cyclo-Alkane	10-20%	Decalin	0%	0%	10%	0%
		Methyl-cyclohexane	0%	0%	0%	20%
Mono-Aromatic	15-20%	Tetralin	0%	37.4%	0%	5%
		Toluene	0%	0%	20%	0%
		Xylene	0%	0%	0%	15%
Poly-Aromatic	1-3%	NA	0%	0%	0%	0%

Table 4-1. JP-8/Jet-A and surrogate chemical composition. Reported in liquid fraction.

	JP-8/Jet-A	Single	Binary	Tertiary	Senary
H/C ratio	~1.9	2.16	1.845	1.88	1.91
LHV(MJ/kg)	42.48-43.22	44.11	43.74	43.06	43.2
MW(g/mol)	151.98-167.31	170.33	156.05	140.4	133.12
Molecular Formula	$C_{10.9}H_{20.9}$-$C_{12}H_{23}$	$C_{12}H_{26}$	$C_{11.25}H_{20.76}$	$C_{10.1}H_{19.0}$	$C_{9.6}H_{18.3}$
H%$_{mol}$	65.72%	68.42%	64.85%	65.29%	65.59%
C%$_{mol}$	34.28%	31.58%	35.15%	34.71%	34.41%

Table 4-2. JP-8/Jet-A surrogate properties

The first surrogate was composed of pure dodecane, which represents the

primary hydrocarbon class (iso and normal alkanes) found in JP-8/Jet-A. This

surrogate is commonly used in reforming literature to represent JP-8[7,88,134].

Dodecane was chosen over decane based on the work of DuBois[88] which showed

better agreement with JP-8 in autothermal reforming. Representing a complex

hydrocarbon fuel with a single alkane neglects the effects of aromatic and cyclo-

alkane content, which are typically found in jet fuels. The average H/C ratio, lower

heating value, and molecular weight are greater than what is typically found in JP-8/Jet-A.

A binary surrogate proposed by Gould[134] was evaluated. It represents the iso and normal alkanes content with dodecane and mono-aromatic content with tetralin. This surrogate has a comparable molecular weight to JP-8, but its H/C ratio and lower heating value are below what is typically found in JP-8. This surrogate showed good agreement in the experimental work done by Goud, but has a higher aromatic content than is typically allowed in middle distillate fuels like JP-8/Jet-A.

A tertiary surrogate was proposed by DuBois[88]. This surrogate represented all three major hydrocarbon classes in JP-8/Jet-A with dodecane (iso and normal alkanes), decalin (cyclo-alkanes), and toluene (mono-aromatics). This surrogate represents 97-99% of the hydrocarbons present in JP-8/Jet-A. The tertiary surrogate's H/C ratio and lower heating value are comparable to JP-8/Jet-A; however, its molecular weight is lighter than what is typically found in JP-8/Jet-A.

A senary surrogate was proposed by Violi[120] for JP-8. It is considered a more accurate representation of the hydrocarbon product distribution within JP-8 and is thought to improve agreement with the experimental data, see Table 4-1. This surrogate was designed to replicate JP-8's sooting propensity, distillation curve, flame speed, and auto ignition characteristics. The iso and normal alkanes are represented using a blend of iso-octane, dodecane, and tetradecane. Cyclo-alkane hydrocarbons are represented by methyl-cyclohexane. Mono-aromatic hydrocarbons are represented using a blend of m-xylene and tetralin.

Like the tertiary surrogate, the senary surrogate represents the three major classes of hydrocarbons within JP-8, but with a more accurate representation of the hydrocarbon distribution. The lower heating value and H/C ratio are in strong agreement with the average properties found in JP-8, although the average molecular weight is significantly lighter than what is typically found. This surrogate has been previously shown to accurately represent JP-8 in combustion[120].

Reformate concentrations for the surrogates are compared against experimental data in Figure 4-10 and Figure 4-11. Primary region of interest in reforming occurs between O/C ratios of 0.98 to 1.47, which is considered a regime where most reformers operate. Ideal reforming conditions occur at an O/C ratio of 1.0. Fuel rich combustion conditions are typically considered at O/C ratios of 1.5-2.0.

(A)   (B)
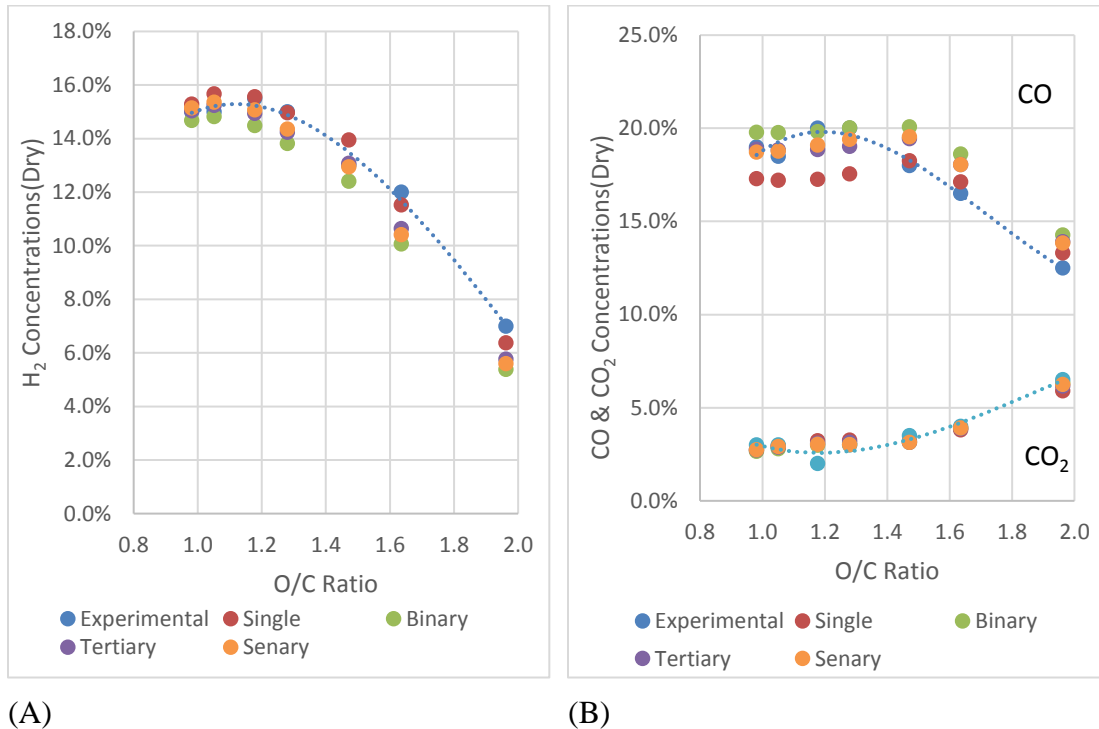
Figure 4-10. Numerical simulation of fixed gas concentration for JP-8 surrogates at O/C=1.0-2.0
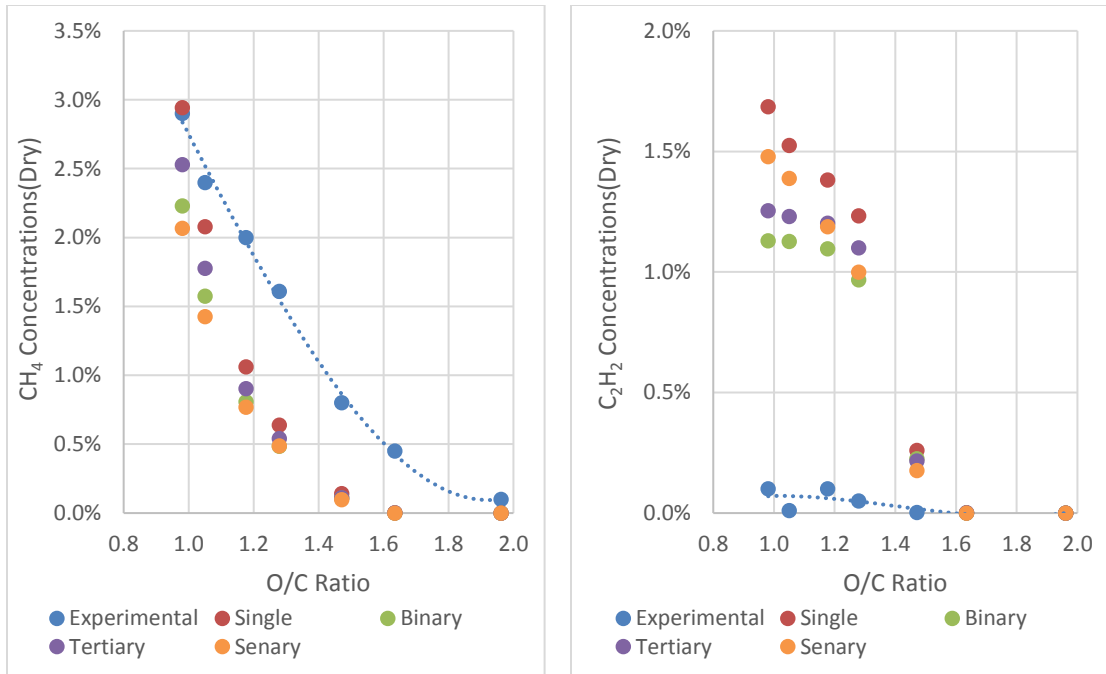
(A)

(B)
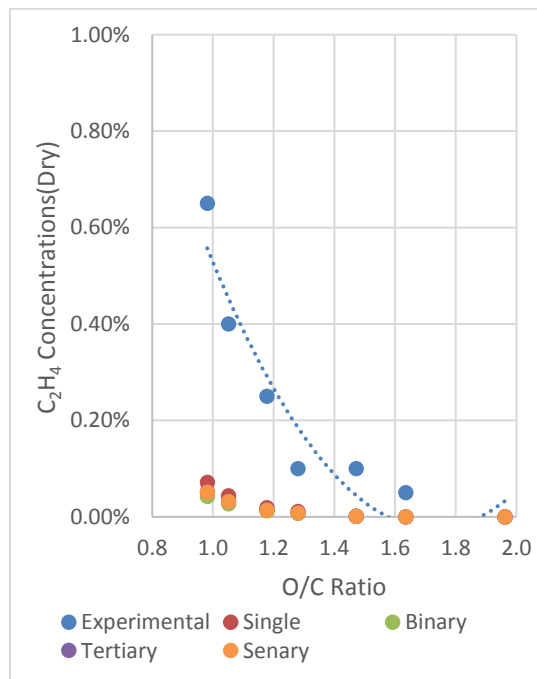
(C)

Figure 4-11. Numerical simulation of hydrocarbon concentrations for JP-8 surrogates at O/C=1.0-2.0

113

4.1.3.1 Single Component Surrogate

The single component surrogate had limited success at predicting fixed gas formation. Numerical simulations over predicted hydrogen concentrations, see Figure 4-10A. In addition, numerical simulations of carbon monoxide diverged from the experimental data between O/C ratios of 1.05 to 1.47, see Figure 4-10B. The single component surrogate exhibited difficulty in predicting hydrocarbon formation, see Figure 4-11. The numerical simulations of methane and acetylene showed poor agreement with the experimental data at O/C ratios of 1.05 to 1.64. Simulations of ethylene concentrations were in agreement with experimental data, but the divergence was comparable to the other surrogates.

The single component surrogate is only suitable for modeling reformate at an O/C ratio of 1.0 and under fuel rich combustion conditions. The large deviations in carbon monoxide concentrations between the experimental and the numerical simulations was partially attributed to dodecane's lower carbon content, which is indicated by a higher H/C ratio, see Table 4-2. In addition, this surrogate only represents the primary hydrocarbon class (iso and normal alkanes) found in JP-8. As will be shown in the following surrogates, the addition of mono-aromatic hydrocarbons greatly improved agreement with experimental data.

4.1.3.2 Binary Component Surrogate

The binary surrogate showed better agreement with the experimental data when compared to the single component surrogate. This was shown by numerical simulation of carbon monoxide, carbon dioxide, and acetylene formation showing a stronger agreement with the experimental data, see Figure 4-10B and Figure 4-11B.

114

While all surrogates had difficulty predicting acetylene formation, the binary surrogate demonstrated the lowest divergence from the experimental data, see Figure 4-11B. This was attributed to the binary surrogate having the largest mono-aromatic content of all surrogates evaluated. However, the binary surrogate significantly under predicted hydrogen formation, see Figure 4-10A. The poor agreement with hydrogen formation was attributed to the binary surrogate having a lower hydrogen content. Numerical simulations showed methane concentrations increasingly diverging from the experimental data as O/C ratios decreased, as shown in Figure 4-11A. Numerical simulations of ethylene were in general agreement with the experimental data, but the performance was similar to other surrogates, see Figure 4-11C.

While the binary surrogate's average molecular formula is comparable to JP-8, the mono-aromatic content of the binary surrogate is significantly higher than what is typically found within JP-8. The lack of cyclo-alkanes could have further contributed to the deviation from experimental data. While the numerical simulation employing the binary surrogate showed stronger agreement in terms of carbon monoxide formation, the poor agreement of hydrogen and methane formation limits the usability of this surrogate.

4.1.3.3 Tertiary Component Surrogate

The tertiary surrogate, as compared to the single and binary surrogates was in stronger agreement with the experimental data for fixed gases. In particular, numerical simulations of hydrogen, carbon monoxide, and carbon dioxide concentrations showed stronger agreement with experimental data, as shown in Figure 4-10. Numerical simulations of hydrocarbon formation were in mixed

115

agreement with the experimental data, as shown in Figure 4-11. Predicted methane formation deviated from the experimental data, but not as greatly as it did in the other multi-component surrogates. Numerical simulations over predicted acetylene formation at O/C ratios less than 1.47, but the divergence was comparable to the binary surrogate. Ethylene concentrations were in agreement with experimental data, but the results were comparable to other surrogates.

This surrogate's accuracy extends from its representation of the major classes of the hydrocarbon, and having an H/C ratio similar to that of JP-8. DuBois[88] represented each hydrocarbon class present in JP-8 with a single hydrocarbon. The addition of cyclo-alkanes improved accuracy over the binary surrogate. Moreover, this surrogate was in the strongest agreement with the experimental data as compared to any other surrogate evaluated. Accordingly, this surrogate will be used to predict reformate composition in the current investigation.

4.1.3.4 Senary Component Surrogate

The senary surrogate behaved comparably to the tertiary surrogate, by accurately predicting fixed gases, but numerical simulations of hydrocarbons were in poor agreement with the experimental data. This surrogate was originally developed to replicate JP-8's sooting propensity, distillation curve, flame speed, and auto ignition characteristics. Hydrogen, carbon dioxide, and carbon monoxide concentrations predicted by the senary surrogate were in strong agreement with both the experimental data and the tertiary surrogate, see Figure 4-10. The numerical simulation showed hydrocarbon formation to be in poor agreement with the experimental data, see Figure 4-11. Methane showed the greatest deviation from the

116

experimental data, when compared to the other surrogates. The senary surrogate over predicted acetylene formation, as did the binary and tertiary surrogate. Ethylene formation was in agreement with experimental data, but this performance was comparable to other surrogates.

While the senary surrogate was considered to have a more accurate representation of the hydrocarbon distribution, hydrocarbon formation actually demonstrated poor agreement with the experimental data. The added complexity of the senary surrogate did not enhance the agreement with experimental data accuracy. Instead, it was found to be in weaker agreement with the experimental data than the tertiary surrogate was. DuBois[88] concluded that a surrogate with accurate H/C ratio and hydrocarbon distribution alone was an insufficient representation of JP-8, as the selections of individual hydrocarbons are relevant to reformate product distribution.

Even through the tertiary surrogate showed a more accurate representation of the product distribution, it was felt that the senary surrogate would yield the best representation of the characteristic chemical properties. The senary surrogate was able to predict general composition of the syngas and was designed to replicate flame speed and auto ignition characteristics of JP-8.The tertiary surrogate was not designed to replicate the flame speed or auto ignition characteristics of JP-8.

4.2 Numerical Simulations of the Distributed Reactor

Validation indicated that the CRECK mechanism and the tertiary surrogate would yield strongest results. Previous works have described distributed combustion as a perfectly stirred reactor[48]. For an idealized condition, this is correct; however, experimentally the reactants experience a finite residence time within the reactor. As

117

a result, the reactor was modeled as adiabatic plug flow reactor with a recirculation loop. This approach accounts for the finite residence time, while creating an environment similar to perfectly stirred reactor. However, this is still an approximation as it assumes uniform recirculation. Prior to the plug flow reactor, there is a non-reacting mixer, where the recirculated effluent perfectly mixes with the incoming fuel and air mixture. In experimental conditions, there will be a finite period of time before reactants can mix with reformate, reducing oxygen concentrations. When designing the reactor the average residence time was used.
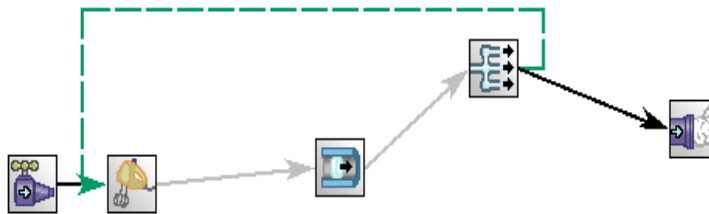
Figure 4-12. Distributed reformer Chemkin model

Simulations predicted high concentrations of hydrogen and carbon monoxide in the reformate. Inlet temperatures were evaluated between 300-600°C and O/C ratios between 0.80-1.30. The reactor was operated at flow rates of $3kW_{th}$. The reactor was 8 cm diameter and a length of 15 cm. Figure 4-13 showed that higher temperatures improved reformate quality, which is consistent with the work in Al-Hamamre[95].

At O/C ratios less than unity, there was insufficient oxygen to completely oxidize the carbon content of the fuel to carbon monoxide, but hydrogen concentrations rose with increasing temperature. Higher temperatures promoted dehydrogenation reactions, but also produced more soot. An increasing in O/C ratios

promoted the oxidization of hydrogen. As inlet temperatures increased, hydrogen

concentrations increased at lower O/C ratios (O/C<1.0).
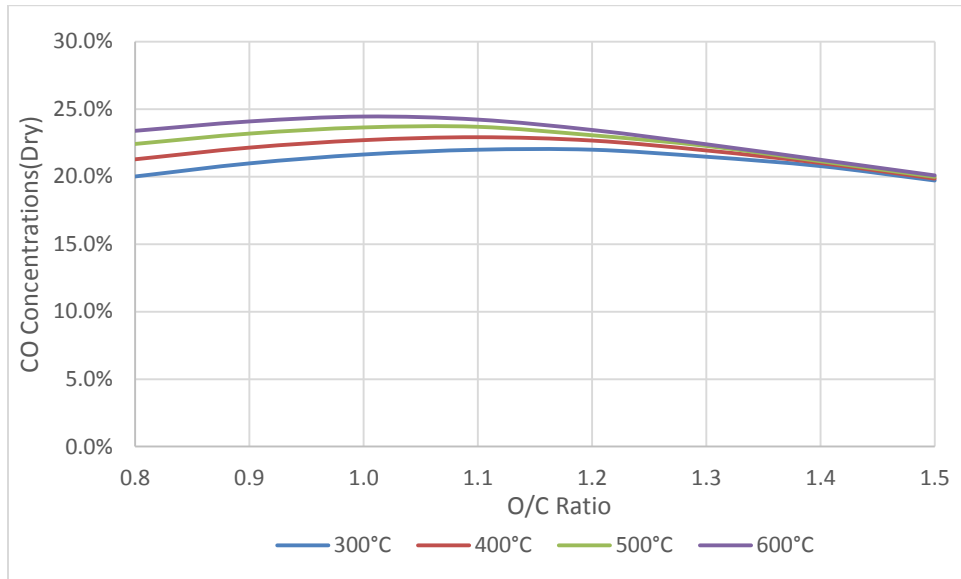
Figure 4-13. Simulated hydrogen concentrations

Figure 4-13 and Figure 4-14 show simulated hydrogen and carbon monoxide

concentrations for a distributed reactor. Hydrogen concentrations ranged between

13.5-23.4%. At 300°C, peak hydrogen concentrations occurred at an O/C ratio of one,

but as injection temperatures increased, peak hydrogen concentrations occurred at

lower O/C ratios. Increasing the O/C ratios caused a gradual increase in hydrogen

concentrations. In literature, hydrogen concentrations ranged from 10 to 24% for a for

Jet-A1 or JP-8[12,14,19].

Carbon monoxide concentrations ranged between 19.7-24.5%. At 300°C, peak

carbon monoxide (CO=22.0%) occurred at O/C ratios of 1.1 to 1.2. As injection

temperatures increased, peak carbon monoxide concentrations increased and occurred

at lower oxygen to carbon ratios. Peak carbon monoxide concentrations occurred near

the point of full conversion. In literature for Jet-A1 and JP-8, carbon monoxide concentrations ranged between 15-25%[12,14,19].
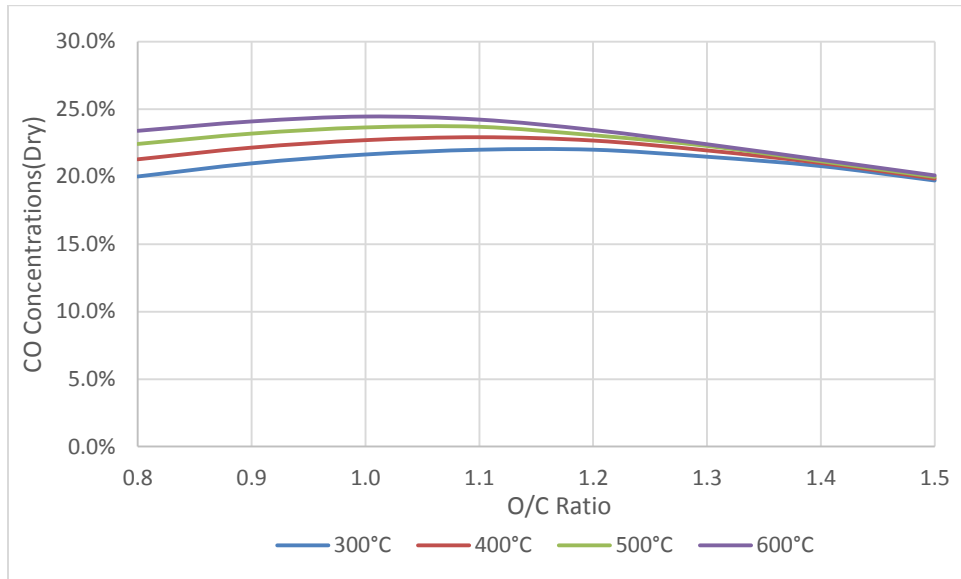
Figure 4-14. Simulated carbon monoxide concentrations

As temperature rose from 300°C to 600°C, full conversion occurred at lower O/C ratios. Full conversion occurred at O/C ratios greater than 1.2. Peak efficiency was demonstrated near or at full conversion. Experimental reforming efficiency and conversion are expected to be higher than the model predictions, as numerical models over predicted acetylene formation and under predicted carbon monoxide formation. Reforming efficiency increased with inlet temperature and occurred at lower O/C ratios. The highest efficiency ($\eta_{H_2,CO}$) predicted was 76.8%. Maximum efficiency and conversion may be higher and occur at slightly lower O/C ratios than predicted by simulation, due to the tendency to over predict acetylene and other lower hydrocarbons. Smith[9] and Pastore[11] demonstrated reforming efficiencies between 60-70%.
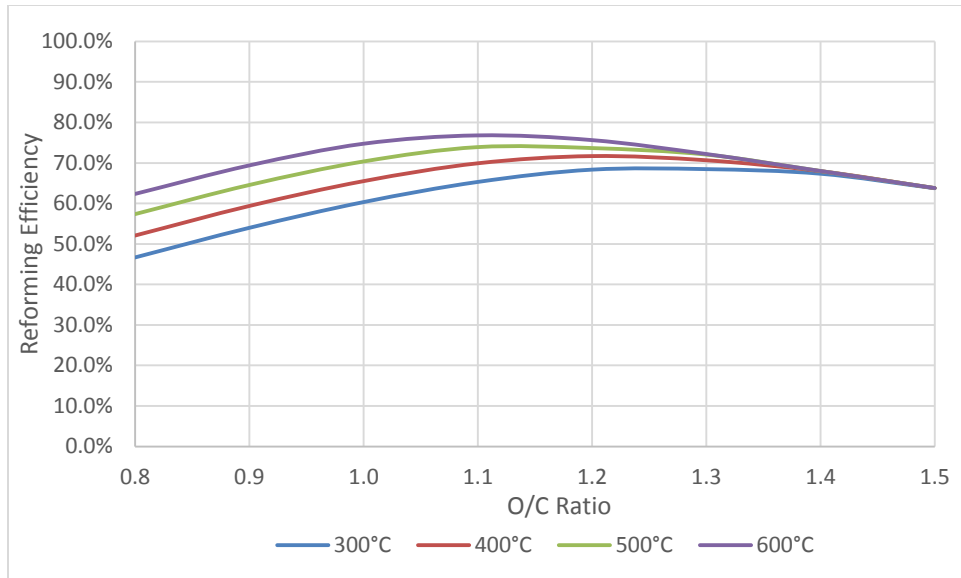
Figure 4-15. Simulated reforming efficiency in a distributed reformer
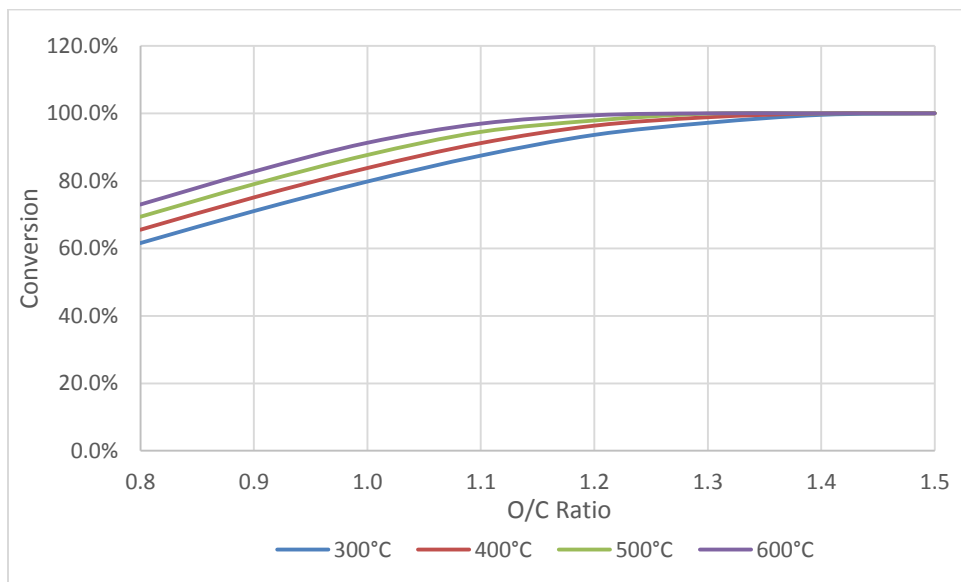
Figure 4-16. Simulated conversion in a distributed reformer

4.3 Computational Fluid Dynamics Cold Flow

Cold flow simulations were conducted using the commercial CFD code Fluent to determine the non-reacting flow fields of the reactor, residence times, and to ensure proper recirculation. The details of the approach are described in Section 3.1. A

121

similar reactor was developed by Arghode[48], and was verified using PIV. The original work was done with non-reacting flows at inlet temperatures of 500°C. This was due to the complexity of the kinetics for reforming, the limitation of computational power, and the availability of an accurate reduced mechanism. A grid independence study was done in addition, comparing 250 million elements to 500 million elements. Initial designs were based off the distributed combustor[48,135].

The impact of injector diameters on recirculation was evaluated at a fixed inlet condition of 600°C and a mass flow rate of 0.0713 g/sec. Three inlet diameters were compared (3.0 mm, 3.8 mm, and 4.5 mm), which were determined by the inner diameters of available stainless steel tubing, but were also found to be sufficient. As injector diameter increased, recirculation decreased. Peak recirculation for all nozzles appeared at 13 cm from nozzle inlet. Figure 4-17 shows that decreasing the diameter of the nozzle caused entrainment to increase, as shown by higher recirculation. For nozzle diameters of 3.8 mm & 4.5 mm, recirculation increased linearly with distance, but for nozzle 3.0 mm, the recirculation was enhanced near the back of the reactor. After reviewing the streamlines, it was determined the decay in recirculation was due to wall effects. As recirculation is strongest in the rear of the reactor, it is thought to be the most distributed region.
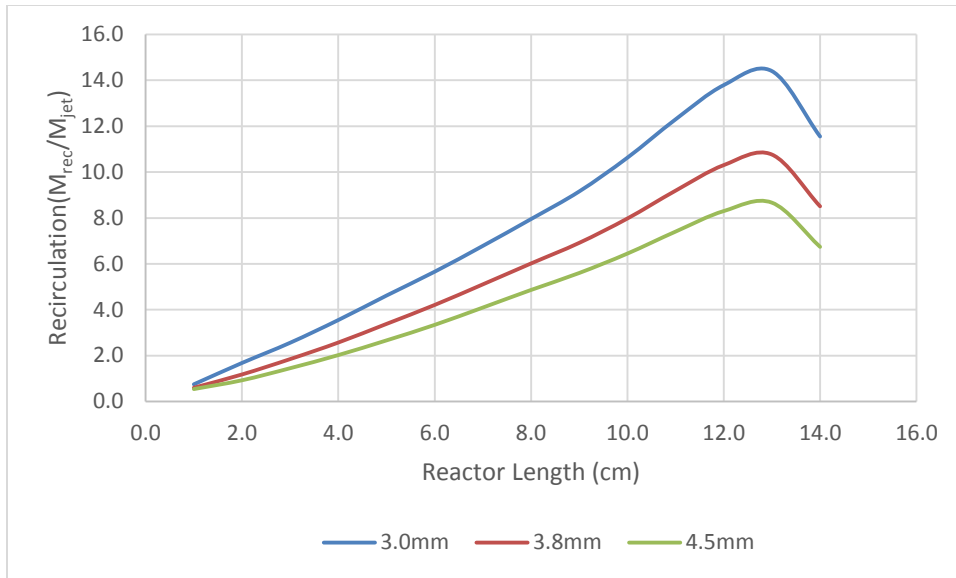
Figure 4-17. Numerical simulation of recirculation vs jet diameter

Chapter 5: Experimental Facility

5.1 Test Bed

The test bed was developed based on the work of DuBois[8]. A schematic diagram of the test bed is shown in Figure 5-1. The test bed was housed in a walk-in hood designed to handle hydrogen and carbon monoxide.
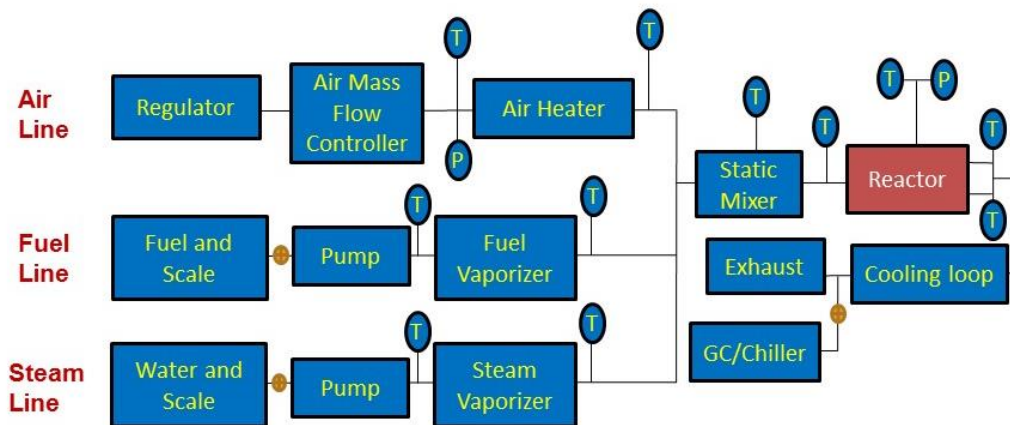
Figure 5-1. Schematic of reactor test bed

The flame regime within the reactor was controlled through the characteristic chemical time and length scales. Injection temperatures, as well as the fuel and steam feeds, were used to control chemical time and length scales. In order to minimize characteristic turbulent properties, airflow rates were fixed. As air composes ~97% of the volumetric flow rate, changes in fuel feed minimized the impact to the time and length scales associated with turbulent transport. This allows a near constant residence time to be achieved. Controlling through fuel feed allows for a finer resolution of data points.

Multiple reactors would be required to maintain a constant residence time while controlling flame regime through the characteristic turbulent properties. This

would have been both time intensive and costly, without offering significant benefit. In addition, at lower operating conditions, a lower flow rate could induce flashback into the premixed fuel-air charge. As this is a new approach to reforming, a lower risk approach was chosen

Ideal reforming conditions for reforming kerosene, Jet-A1 and JP-8[9,16] occur at equivalence ratio of 2.8-3.0, which correlates to O/C ratios between 1.0 to 1.1. At a molar oxygen to carbon ratio of one, there is exactly one oxygen atom for every carbon atom of the fuel. This is considered stoichiometric reforming conditions. However, in literature it was observed that full conversion often required higher oxygen to carbon ratios[14]. Air and fuel subsystems were designed to support an O/C ratio between 1.0-1.5.

5.1.1 Air Sub System

Air was preheated separately from the fuel and steam. Dry filtered air was obtained from a regulator with a maximum pressure of 120 psi. In the low temperature reactor, airflow was controlled through Cole Palmer mass flow controller (0-50 SCFM) with an accuracy of 0.8%AF+0.2%FS. Mass flow rate was determined by pressure drop through laminar flow element. Pressure drop across the controller was no greater than 0.6 psi. System pressure was used as an indicator of system status, and monitored with a pressure transducer.

In the high temperature reactor, a thermal capacitance mass flow controller (Serria) was employed (0-50 SCFM) and had an accuracy of 0.25% full scale. A thermal capacitance based mass flow controller was more accurate and less sensitive to back pressure generated by reactor.

The air was then heated with a modified 1.6kW$_{th}$ potted air heater (Slavonia). In order to compensate for lower flow rates, the voltage was reduced from 240V to 120V, reducing power to 0.8 kW$_{th}$. Electrical power was regulated by a silicon controlled rectifier (SCR) power controller, which allowed improved control, quicker response time, and extended heater life over conventional mechanical relay. The air heater was able to achieve temperatures up to 760°C; however, it was restricted to 750°C to preserve air heater life.

5.1.2 Fuel and Steam Subsystem

Fuel and water were stored in two tanks located on top of the 8 kg scales (Ohous Adventurer). The scales output was recorded by a data acquisition system written in Lab View. Fuel and steam was metered into the test bed with an isocratic pump (Chromtec), and fuel consumption calculated by the average change in weight over a period of 10-20 minutes (scale accuracy of ±0.1 g). The scale was calibrated against an 8000g ±50 mg standard. The isocratic pump has a maximum flow rate of 10 ml/min and a maximum pressure of 5000 psi.

The fuel and steam feeds were independently vaporized and combined after vaporization. Each vaporizer consisted of a coiled tubing (approximant volume of 0.185 L), wrapped in heat tape (430 watt) and insulation, see Figure 5-2. Both insulated units sit adjacent to each other, wrapped with an additional layer of insulation. PID controllers were used to regulate temperatures within each vaporizer. A thermocouple was positioned between the heat tape and coiled tubing. A duty cycle for the heater on the fuel vaporizer was between 46-55%.

Vaporization of JP-8 can induce cracking and carbon deposition. Altin et al.[136,137] observed that cracking and carbon formation can be avoided if temperatures are restricted to 470°C. Rawson[138] evaluated the effect of contact time and vaporization temperature of both JP-8 and Dodecane. Over a period of 10 seconds, no carbon deposition was noted for vaporization temperatures of 300-350°C. Minor carbon formation was noted at temperatures of 400°C. The final boiling point of JP-8 is 300°C. Rawson[138] also recommended short contact times to reduce carbon formation. Some studies noted carbon formation occurring over a period of 5-6 hours at lower temperatures (200-300°C)[136,137]. Within this work, JP-8 was only preheated to 300-330°C and resided in the vaporizer for 5-10 seconds. Vaporizer and mixer design allowed full vaporization and short contact times, without the formation of carbon.

Figure 5-2. Fuel and steam vaporizer

Prior to injection, the heated air, fuel, and steam flow were combined and mixed in a static mixer. The mixer was a stainless steel blade design (KoFlo), which included three mixing elements. The static mixer's dimensions are ½" by 2.5". KoFlo was consulted in mixer selection. Per manufacture, mixing efficiency was greater than 99.99% under the experimental conditions. This design favors higher velocity mixing, while minimizing residence time. Reduced residence times decreased the potential for reactions to occur. Residence time within the mixer was no more than 9.8 ms. A second mixer was used briefly, which was ½" by 4.5" and included six elements. It was determined that the larger mixer did not change reformate composition, indicating that the reactants were sufficiently well mixed. Mixer and

injection line was wrapped in a 50 watt heat tape and insulation, to prevent condensing and to maintain a constant injection temperature. Heat tape was controlled with a rheostat power controller.

Mixture preparation can strongly influence reformate composition. Poor mixing often presents as high concentrations of carbon dioxide and hydrocarbons, resulting from the uneven distributions of oxidizer throughout the reactor. Under this condition, no region of the reactor will operate under the desired O/C ratio. Instead, regions that are fuel rich will promote the formation of carbon, coke, and incomplete conversion, which can damage downstream components. Regions that are fuel lean will promote full oxidation and localized regions of high temperature, which can damage the reactor. In order to achieve full conversion, additional oxygen will be required to oxidize the fuel rich regions of the reactor. This would present as full conversion and peak efficiency occurring at higher oxygen to carbon ratios, than what will occur under well-mixed conditions. Proper mixing results in high yields of hydrogen and carbon monoxide, minimizing the formation of hydrocarbons and carbon dioxide. A lower, more even temperature distribution will occur under well-mixed conditions. Within the literature review, it was observed that the mixing of gaseous fuel (natural gas or propane) yielded better performance[10]. When reactors are converted from a gaseous to a liquid fuel, reforming efficiency often diminishes[10,12]. This is attributed gaseous fuels being easier to mix.

Within the literature review, it was observed that improved mixing correlated with better reformate quality. The approach of atomizing the fuel and mixing with preheated air yielded the lowest reforming efficiencies[10–12,17]. However,

129

independently heating and vaporization of liquid hydrocarbons and mixing with preheated air has shown superior performance over an atomization based approach[13,19,95]. Hydrogen concentrations were reported to be almost twice than what has been reported elsewhere in literature for a middle distillate fuel[19]. Al-Hamamre[139] achieved injection temperatures as high as 700°C without pre-ignition, so long as residence times of the mixer and vaporizer are controlled.

5.2 Reactors

Two reactors were developed over the course of this work. Initially, a low temperature reactor, detailed in Chapter 6, was designed for optical validation of the Distributed Reaction Regime and development of numerical modeling. The second reactor, detailed in Chapter 7, was designed to explore ideal reforming conditions. Both reactors designs and construction techniques were based on the work of Gupta, Arghode, and Khalil[112,140]. From the literature review, the following was determined.

Duwig[111] was the only literature to conduct chemiluminescence imaging under fuel rich conditions (O/C=0.5). He noted increased equivalence ratios (decreasing O/C ratios) yielded higher visible emissions, but the reaction zone was distributed over a larger volume. This condition was richer than that what occurs within reforming, but is indicative that reforming under Distributed Reaction is feasible, but may require a larger volume then colorless distributed combustors.

Informed by Arghode's work[105], this investigation concluded that the strongest results would be obtained by operating under premixed mixed conditions, with a reactor based on the reverse flow low intensity design. Optical and

chemiluminescence imaging showed the reverse flow to yield the most distributed conditions. The reverse flow configuration also enhanced residence time, which was believed to be essential in minimizing hydrocarbon presence in the reformate. Chemiluminescence imaging indicated the premixed configuration to be the most distributed, when compared to diffusion flame.

A cylindrical reactor with a central injection point was chosen, as it allows uniform entrainment throughout the reactor. From the literature, it was observed that rectangular reactors experienced reduced flow in the corners, which may promote radical or soot formation. In Arghode[105], under certain conditions high concentrations of radical emissions occurred near the rear corners of the reactor. However, Khalil[126] and Verissimo[106] both employed cylindrical based combustors, and did not observe this issue.

An alternative geometry was considered based on the use of swirl. Swirl offers a more narrow residence time distribution, with high recirculation. This shows significant promise for reforming application. However, this is a relatively new design and more data is available on distributed combustor design such as Arghode[105]. The better-understood design was chosen as it presented lower risk of failure. Future work can follow up on the development of this design.

Multiple works have addressed the importance of injection velocity for establishing the distributed conditions and preventing flashback[104,106,121]. Lower injection velocities of 30 m/sec were considered similar to Duwig[111], but from chemical luminescence imaging, the reactor appeared less distributed. Arghode[105], Verissimo[106], and Khalil[126] demonstrated a wide range of velocities

131

(60-311 m/sec) could achieve regimes with no visible emissions. Khalil and Gupta[121] found velocities of 96 m/sec to be sufficient to prevent flashback when operating under premixed methane hydrogen flame. In addition, Mi[72] indicated a critical momentum is required for the Distributed Reaction Regime to develop. The critical valued varied with reactor design, but it was concluded that premixed configuration requires less momentum to generate distributed conditions.

Due to the lower flow rates inherent in reforming, it was determined that a single injection point of 100m/s would be most compatible with reforming conditions. As reformers use a fifth of the air as traditional combustors, a multi-point injection was not feasible as used in Arghode[104]. A single premixed central injection point was chosen over multiple injection points to maximize injection velocity and momentum, similar to Verissimo[106].

In distributed reforming, syngas will entrain into the premixed fuel-air charge. Hydrogen will cause reactions to propagate faster, thus requiring additional dilution. As the hydrogen concentrations in the reformate were not expected to exceed 30%, a target recirculation of 7-10 was used. Based on the work of Derudi[110] and Khalil[121], this was believed to be sufficient.

In literature, higher reactor temperatures are cited as an ideal condition[14,100]. However, from literature the best results were obtained at 900-1100°C[103] for middle distillate fuels. Reactor temperatures greater than 1100°C appear to be detrimental to reformate quality[9,11,15,94,100,141]. Zhdanok[19] showed the highest hydrogen concentrations of any non-catalytic reformer, while operating at temperatures of 1070-1125°C.

132

Reactor temperatures below 600-800°C were found to be insufficient to fully activate the reforming reactions, resulting in poor conversion. Reactor temperatures exceeding 1100 °C enhanced hydrogen yields, but promoted the cracking of hydrocarbons and soot formation[16,17]. Some instances in literature have reported up to 40% of the molar carbon in the fuel deposited within the reactor walls[17]. This was determined through molar carbon balance conducted on the exhaust. Higher reactor temperatures appear to pose a risk to the reactor structure[17]. Reactor temperatures in excess of 1300°C repeatedly have been shown to damage alumina-based reactors[9]. Roth[16] is the only design that showed improved hydrogen yields with reactor temperatures above 1100 °C; however, an increase in soot formation was also noted. Two reactors in this work were developed to explore the low temperature regime (700-800°C) and high temperature conditions (900-1100°C).

A spark igniter, located in-line with the inlet, was used to ignite the mixture. The reformate was exhausted through two outlets on the same plane as inlet. Dual outlets reduced the chances of any catastrophic failure in case of unwanted blockage in one of the outlets.

5.2.1 Low Temperature Reactor

Figure 5-3. Low temperature reactor

Reactor vessel consisted of a cylindrical quartz tube, with an internal volume of 0.77 liters, shown in Figure 5-3 and Figure 5-4. The inner reactor had an interior diameter of 4 cm and a length of 8 cm. Outlets were located 3.135 cm away from the inlet. Each end of the quartz tube was sealed with a steel plate and gaskets. Clamps provided the compression needed to form an adequate seal. Two 0.66 cm alumina end caps were cemented to end of the quartz tube to protect the gasket at the quartz-steel interface.

An alumina insulation blanket with a thickness of 5.08 cm was wrapped around the outer perimeter of the quartz tube with a removable section that provided optical access, when desired. This approach mitigated heat losses during operation of

134

the reactor, while allowing optical access. Average residence times were determined to be between 720ms to 890ms.
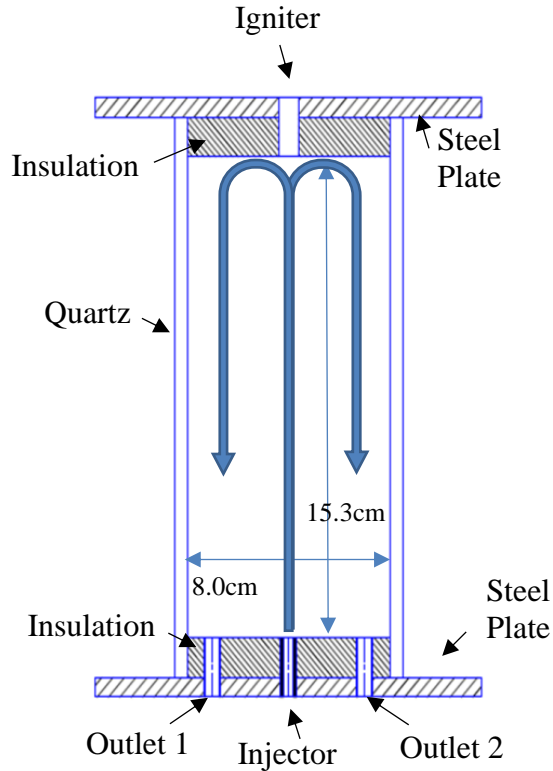
Figure 5-4. Quartz reactor schematic

Global images of the reaction zone were photographed through the quartz window at various operational conditions using a digital camera. Exposure time was automatically determined and specified below each image. After the reaction zone stabilized, the insulation was removed to photograph the reaction zone area. Observation of the reactor walls and reaction zone area showed only a faint visible emission (i.e., nearly colorless).

In the initial reactor, there were concerns of a potential for flashback and pre-ignition. In order to reduce residence time within the injection assemble, no thermocouples were included. Instead, a thermocouple was included on the outside of

the mixer. Thermocouples were placed adjacent to the exhaust. As the thermocouples are within 2.54 cm of the outlet, it is believed to be a good indication of reactor temperature.

5.2.2 High Temperature Reactor

A second reactor was developed to explore the high temperature regime and ideal reforming conditions, see Figure 5-5. Higher reactor temperatures promote higher yields of syngas and reduce the formation of hydrocarbons.
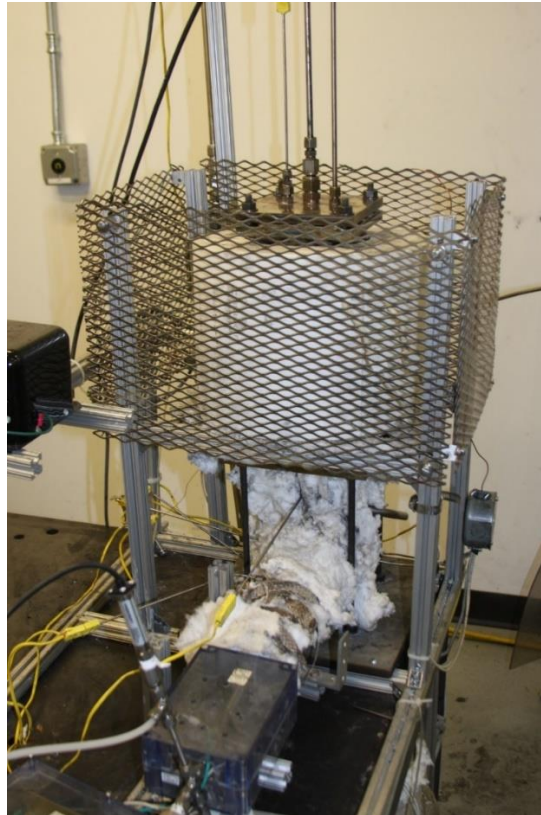
Figure 5-5. High temperature reactor test stand shown with tube furnace

The reactor was comprised of a stainless steel pressure vessel (SS304) having an internal volume of 0.926 L. High purity alumina insulation mixed with alumina binder coated the interior of the reactor. This liner was 2.54 cm thick along the inner

walls of the chamber. The insulation at the top and base of the reactor was 5.08 cm thick, Figure 5-6. A high purity alumina insulation was employed (97%$_{mass}$) as it is resistant to reduction by the syngas. Alumina is a common insulation in reformers and catalysts supports. In both applications, the alumina is considered unreactive[17,94]. The tubular potion of the insulation was divided into four segments to reduce thermal stress within the reactor, shown in Figure 5-7.
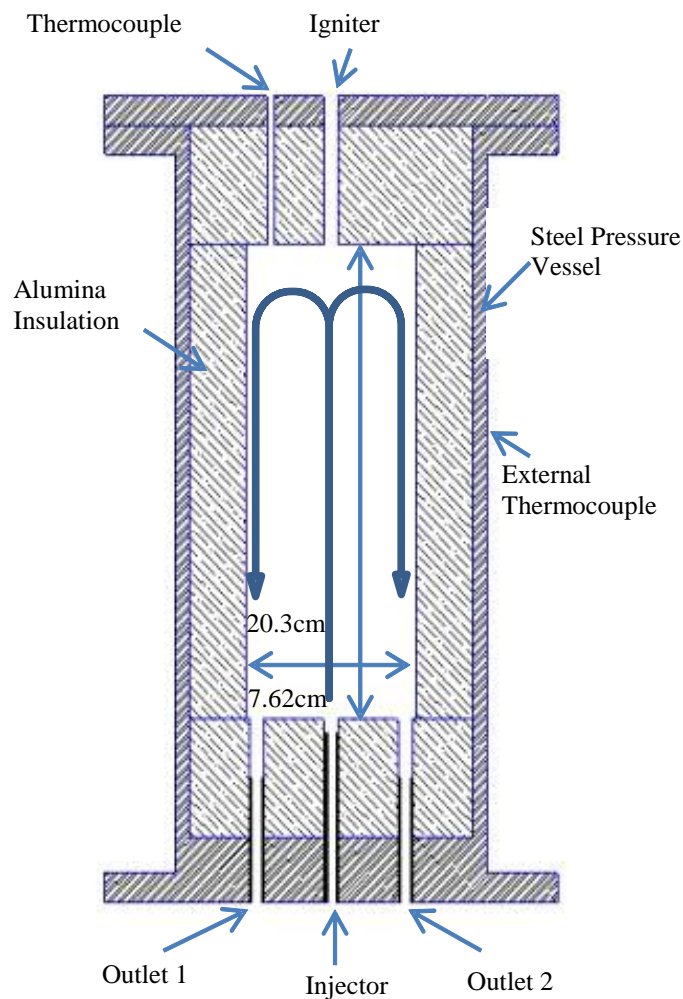
Figure 5-6. Distributed reactor schematic
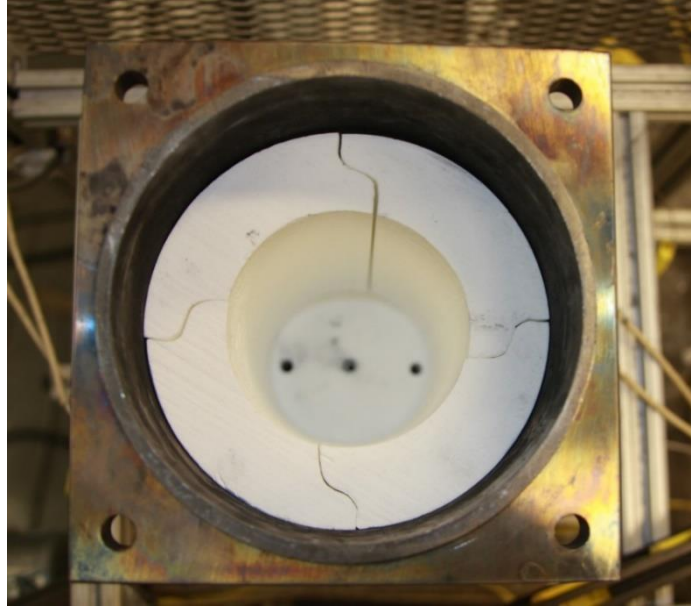
Figure 5-7. Alumina insert in high temperature reactor (shown without tube furnace)

Average residence time was on order of 660 to 900ms. The reactor vessel was surrounded by a tube furnace, which served to preheat the reactor and reduce the temperature gradient across the insulation. Reducing the temperature gradient allowed near adiabatic conditions to be achieved. A thermocouple was placed in the center of the reactor, located between the center outer steel pressure vessel and secondary insulation. This was used to monitor reactor surface temperatures.

Mean temperatures in the test bed and reactor were measured using K type thermocouples that were capable of withstanding to 1325°C. Reactor temperatures were monitored with an internal thermocouple positioned flush to the inner surface of the reactor to avoid obstruction to the flow. As reactor temperature was directly monitored, two thermocouples were placed 12.7 cm downstream of the exhaust to monitor for potential blockages. Exhaust thermocouples were not a direct indicator of reactor temperature.

A premixed fuel-air mixture was injected into the reactor through a central location, having an inner diameter of 3.86 mm. Prior to its injection, the temperature of premixed charge mixture was measured. Reformate was exhausted through two outlets on either side of the injector, located 3.02 cm apart. The outlets had an inner diameter of 5.59 mm.

5.2.3 Start Up

In the low temperature reactor, detailed in Chapter 6, on startup the reactor was operated in a fuel rich combustor mode of O/C ratio 2.0 and then transitioned to fuel rich reforming conditions. However, in the high temperature reactor this was found to damage internal thermocouples. Instead, the reactor was operated directly in the fuel rich reforming regime.

Upon ignition, the high temperature reactor did not initially operate under Distributed Reaction Regime. Distributed Reaction Regime is the result of entraining exhaust products into the fuel-air mixture. Instead, on ignition the reactor operated under a conventional flame until sufficient exhaust products can entrain and reduce the oxygen concentrations. After which, the Distributed Reaction Regime will emerge, altering reformate composition. This presents as two distinct flame regimes, which can be seen in the reformate composition and the reactor temperature profiles. The low temperature reactor was believed to achieve transition faster as combustion condition minimizes soot formation and consumes the oxygen in the reactor faster. However, the low temperature reactor did not have sufficient thermocouples to determine this. The following section shows the high reactor operating at conditions

139

of 4.1kWth, at oxygen/carbon (O/C) ratio of 1.25. The feed stream was injected at
515°C.
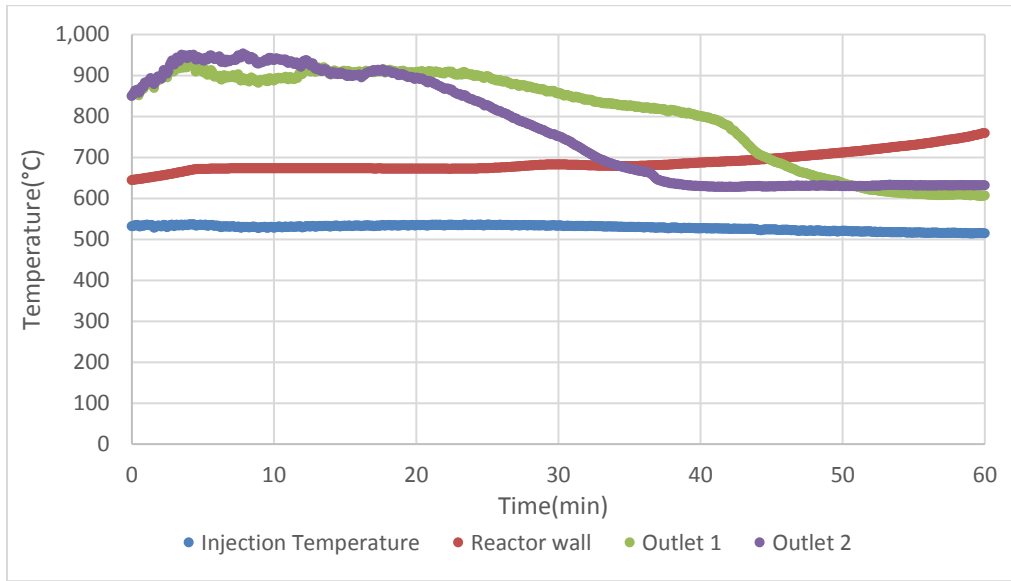
Figure 5-8. Temperature profile during startup at O/C =1.25
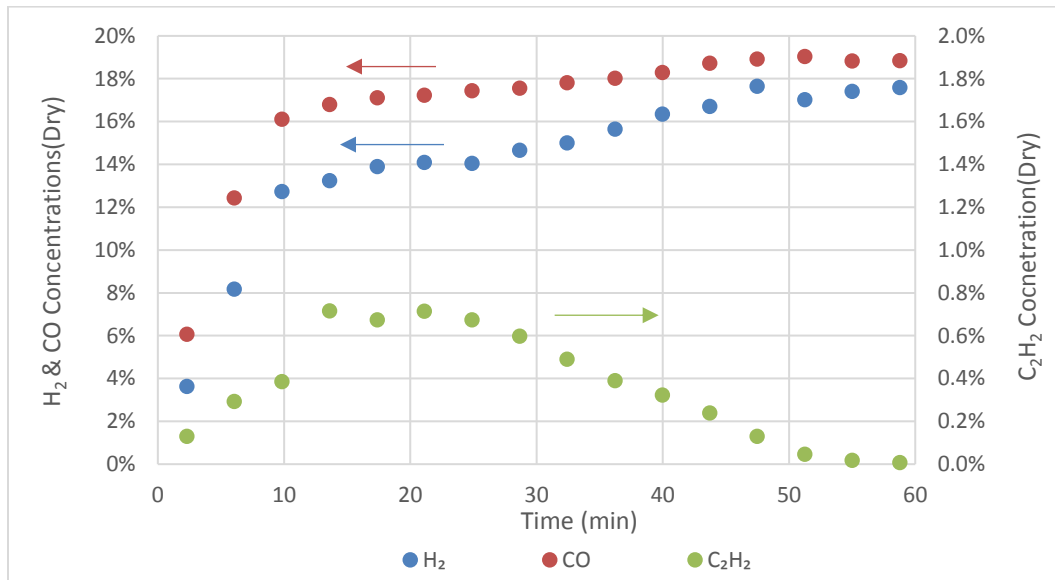
Figure 5-9. Reformate concentrations during startup

On startup, the reactor experienced a transitional mode until the reactor
stabilized, characterized by poor quality reformate. This is thought to be a more
conventional sooting flame. Initially within the reactor, there were no exhaust

140

products. Only air and fuel were present. As the dilution of the premixed air fuel charge is necessary for achieving Distributed Reaction Regime, it was conjectured that the initial entrainment of air into the premixed charge promoted an oxygen rich environment. This in turn promoted a conventional flame and higher hydrocarbon formation. During this condition, it is believed that hydrocarbons and soot deposits formed within the reactor. Deposits were observed when the reactor operated with a conventional flame, under the low temperature work detailed in Chapter 6.

Temperature profiles support this conclusion, shown in Figure 5-8. On ignition, the elevated temperatures at the front of the reactor indicated flame occurred primarily at the front of the reactor, which is indicative of a non-volumetric combustion condition. Thermocouples located at the injector and in exhaust gas stream both reported elevated temperatures, while outer wall thermocouple reported decreased temperatures relative to the second mode, see Figure 5-8. Elevated injection temperatures were conjectured to be the result of heat conducted back through the nozzle. In addition, reformate quality was considerably reduced as compared to the later mode. The results shown in Figure 5-9, show reduced hydrogen and carbon monoxide concentrations, and elevated acetylene concentrations. The high acetylene concentrations, a known soot precursor, corresponded with visible smoke emission from the exhaust.

A temperature differential occurred between the two exhausts under this mode. This was attributed to soot deposit obstructing the flow, inducing a pressure drop. These obstructions caused an initial imbalance in-between the two outlets. The visible smoke emissions support the formation of soot.

141

This transitional mode lasts until exhaust gases can form and entrain, reducing oxygen concentrations. After which, a period of time is required to remove these deposits. This can be seen as reactor temperature stabilizes before reformate composition does.

After a period of approximately 20 minutes, the reactor begins to transition into a more stable distributed mode. The reaction zone detaches from the front of the reactor and distributes throughout the reactor. This is conjectured from the decreased injection and exhaust gases temperatures, and a corresponding increase in wall temperatures, see Figure 5-8. After a period of 20 minutes, Figure 5-9 shows hydrogen and carbon monoxide concentrations increasing, with a corresponding decrease of hydrocarbons. Acetylene concentrations dropped below the detectible limits of 10 ppm. The drop in acetylene concentrations, a known soot precursor, corresponded with visible disappearance of smoke emission from the exit pipe. In 45 minutes, the blockage in the exhausts cleared as the two exhaust achieved equal temperatures. The reformate products distribution appeared to stabilize after a period of 50 minutes.

5.2.4 Reformate Stability

In order to access reformate stability, the reactor was operated for a period of 45 minutes at an O/C ratio of 1.04 and a S/C ratio of 0.05. Reformate consisted of $24.4\pm0.4\%$ hydrogen and $21.8\pm0.4\%$ carbon monoxide, see Figure 5-10. Fluctuations in syngas concentrations were no greater than $\pm0.4\%$, which is consistent with catalytic reforming[8].

142
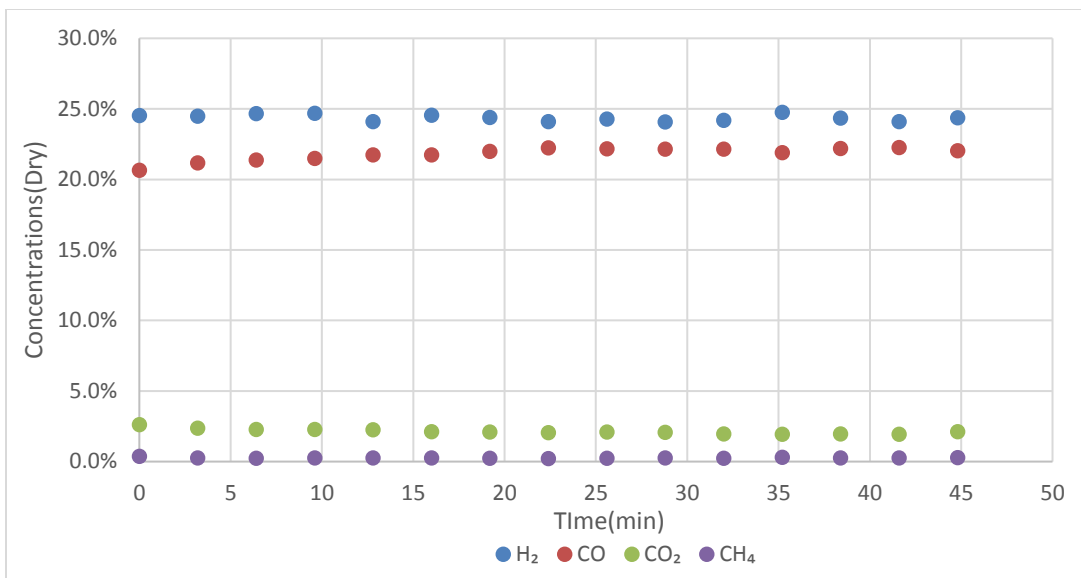
Figure 5-10. Reformate concentrations over a period of 45 minutes.
S/C=0.05 & O/C=1.04

5.3 Instrumentation

5.3.1 Gas Chromatograph

Reformate product distribution was monitored using an online gas

chromatograph (Agilent Micro GC 3000), capable of detecting fixed gases and

hydrocarbons up to hexane. Each species was calibrated using two primary standards

and an origin, generating a multipoint calibration curve. The calibration standards

consisted of a mixture of 10-14 hydrocarbons species at different concentrations. The

gas chromatograph had a relative uncertainty of 1.02% of the detected value within

the calibration limits. Calibration standards have an accuracy of 0.02% reported

value. Error bars were found to be within the data point and were not displayed to

enhance legibility. The uncertainty in gas concentrations was relatively small. For

example, a reading of 1.02% would be between 1.188-1.212%. Curve fits were

provided to show general trends of the data. Water was observed in the condensate

143

trap on the GC. This is expected, as some hydrogen will inadvertently be oxidized. However, this was not directly measured.

The gas chromatograph (GC) was equipped with four columns that each had their own individual thermal conductivity detector. The first column (A) was configured with Molecular Sieve column (10 m x 0.32 mm), and heated to 100°C with an argon carrier gas. Column (A) was configured to detect hydrogen, nitrogen, methane, and carbon monoxide. The second column (B) was configured with a Plot U column (8 m x 0.32 mm), and heated to 75°C with a helium carrier gas. Column (B) detected carbon dioxide, ethylene, ethane, and acetylene. The third column (C) was equipped with a Alumina column (10 m x 0.32 mm), and heated to 145°C with a helium carrier gas, which allowed the detections of propylene, propane, n-butane, trans-2-butene, iso-butene,1-butene, cis-2-butene, iso-pentane, n-pentane, 1,3 butadiene, trans-2-butene, 2 methyl-2-butene, 1-pentene, and cis-2-pentene. The forth column (D) was configured with an OV1 column (10 m x 0.15 mm x 2.0 m), and heated to 90°C with helium a carrier gas. This column detected iso-butane and hexane. Prior to the gas chromatograph, a filter and condenser were included to mitigate the transport of soot, particulates, or water into the GC. Additional information in GC Calibration standards and hydrocarbon peak identification is provided in Appendix B.

The term reformate quality has been used to describe overall product distribution and its compatibility with fuel cell applications. A high quality reformate consists of high concentrations of hydrogen and carbon monoxide, and low concentrations of hydrocarbons. This presents as high reforming efficiency and

conversion. Under this situation, a fuel cell can utilize a larger portion of the syngas gas, with little post processing required. Low quality reformate consists as low concentrations of hydrogen and carbon monoxide, and high concentrations of hydrocarbons. This presents as low conversion and reforming efficiency. A fuel cell would only be able to utilize a small portion of the available energy in the reformate and would still require significant conditioning.

5.3.2 Thermocouples

Mean temperatures in the test bed and reactor were measured using K type thermocouples that were capable of withstanding to 1325°C. Thermocouple locations are described within Section 5.2. Thermocouples employed had an uncertainty of ±0.75% of the reported value. Each thermocouple had a diameter of 0.125" and a response time of 0.55sec. Thermocouple leads were kept away from the heated regions.

Chapter 6: Low Temperature Reactor

A reactor was constructed using computational fluid dynamics and one-dimensional kinetic modeling. The outer casing of the reactor was constructed from an insulted quartz tube to allow direct observation of the reaction zone. The reactor was developed to assess the feasibility of the concept, and develop an initial understanding of Distributed Reaction Regime's impact on reformate product distribution. The reaction regime inside the reactor was controlled through variations in the characteristic chemical properties, while minimizing the impact on characteristic turbulent properties. Higher temperatures and oxygen content foster a more rapid chemical reaction, which shortened the chemical time and length scales. Optical imaging provided verification of flame regime.

At each transition, global images of the reaction zone were photographed through the quartz window using a digital camera. Exposure time is specified in the caption of each image. After the reaction zone stabilized, a portion of the insulation was removed to photograph the reaction zone area. Observation of the reactor walls and reaction zone area showed only a faint visible emission (i.e., nearly colorless).

Conditions within this reactor were thought to be too low to fully activate steam and dry reforming reactions. This will minimize the impact on fixed gas concentrations. However, the more distributed condition will promote greater entrainment of exhaust products. Steam and carbon dioxide are known in combustion to interfere with the soot formation kinetics[16,54–56]. More distributed condition should limit activity of dehydrogenation reaction, which should cause the more

146

distributed condition to favor reformate products with a higher H/C ratio (CH_4 and C_2H_4).

6.1 Effect of Oxygen to Carbon Ratio on Chemical Time Scales

Initially, variations in oxygen to carbon ratios were used to control the characteristic chemical time and length scales, causing a controlled transition from the Distributed Reaction Regime to the Flamelets in Eddies Regime. Higher oxygen content promotes a more rapid chemical reaction, shortening both chemical time and length scales. The reactor was evaluated over a series of oxygen to carbon ratios ranging from 1.0 to 1.5. Preheats were gradually increased (450°C, 600°C, and 750°C) so that a shift in the O/C ratios would cause a visual transition from the Distributed Reaction Regime into the Flamelets in Eddies Regime. Oxygen content was increased in increments of 0.10 from 1.0 to 1.5. Flame regime was later confirmed through numerical calculations, as described in Section 3.1.

In order to minimize the impact to the characteristic turbulent time and length scales, air was injected at a fixed flow rate of 32.5 SLPM, while fuel flow rates were adjusted to vary oxygen to carbon ratios. As air has a significantly larger volumetric flow rate than fuel, fuel flow rates could be adjusted without significant change to the bulk volumetric flow or injection velocity. Fuel was preheated to 330°C, which assured complete vaporization while avoiding coke formation. Carbon balance was conducted and found to be 95% or higher. A flow rate of 32.5 SLPM was chosen, as this was the highest flow rate that could be supported and yield a range of O/C ratio of 1.0 to 1.5. Reynolds number in the nozzle was determined to be in the range of

2870 to 4750. The JP-8 within this series of experiments had a hydrogen content of 13.6%$_{mass}$, and a heating value of 42.8MJ/kg.

6.1.1 Flame Regime

Increasing the oxygen to carbon ratio and air preheats caused the reactions to occur faster, with a shorter characteristic chemical time scales, as shown in Figure 6-1. This is represented by an increase in the Damkohler number.
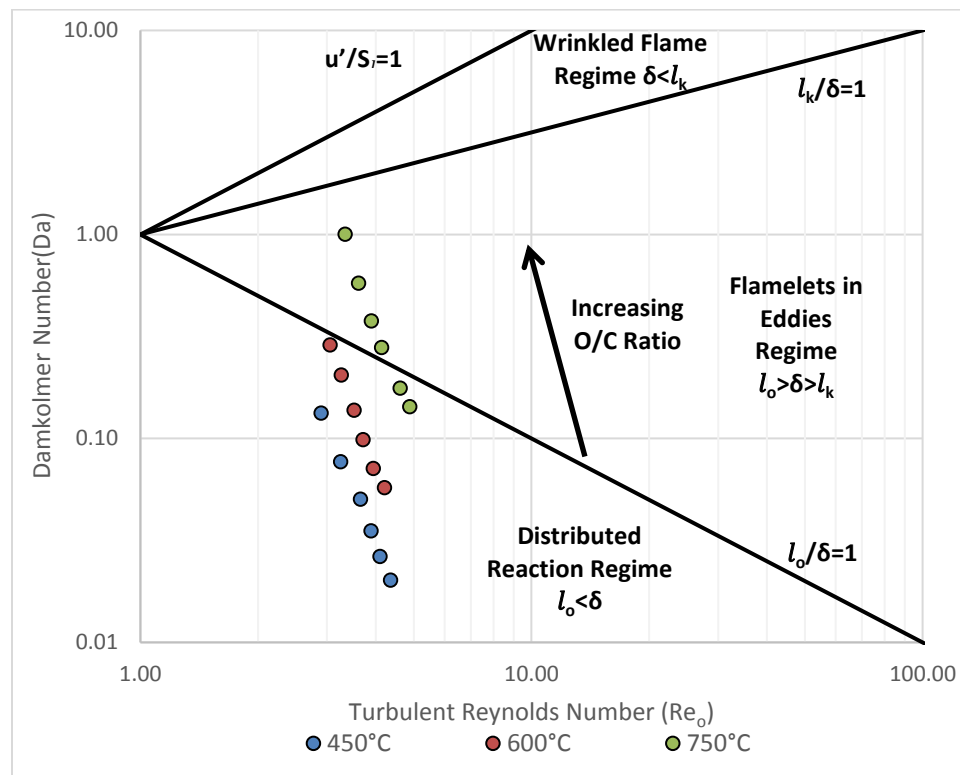
Figure 6-1. Turbulent flame regime at air preheats of 450, 600, 750°C

Air preheats between 450°C and 600°C resulted in the reactor operating within the Distributed Reaction Regime or along the Damkohler Criterion. However, at air preheats of 750°C and at O/C ratio of 1.21 to 1.29, the laminar flame thickness decreased from 1.43 to 1.19 mm, to decrease below the integral length scale (l_o=1.27

mm). This causes a transition from the Distributed Reaction Regime to the Flamelets in Eddies Regime. As a result of the decreased laminar flame thickness, the eddies are no longer able to completely reside within the reaction front, resulting in reduced mixing.

6.1.2 Global Imaging of Reaction Zone

Global reactor observations are shown in Figure 6-2 to Figure 6-4. For all oxygen to carbon ratios evaluated, at air preheats of 450°C or 600°C a transparent reaction zone was observed. This is similar to that reported for Colorless Distributed Combustion, except for a faint reddish orange hue observed throughout the entire reactor. Note, a typical reformer using a middle distillate fuel presents a bright yellowish flame, which is typically associated with soot formation. A transparent flame indicated that the reactor operated within the Distributed Reaction Regime, see Figure 6-4. No visible flame fronts were observed, which suggests that the reaction zone was distributed uniformly throughout the reactor. The observed intensity of the visible emission increased with air preheats; see Figure 6-2 to Figure 6-4. Even though the reactor operated within a soot formation regime, when the reactor demonstrated a transparent reaction zone, little to no soot was observed forming on the reactor walls, see Figure 6-2 to Figure 6-4.

(A) O/C=0.98 F 4.5, 1/60	(B) O/C=1.07 F 4.5, 1/60	(C) O/C=1.17 F 4.5, 1/60
(D) O/C=1.27 F 4.5, 1/60	(E) O/C=1.36 F 4.5, 1/80	(F) O/C=1.47 F 5.0, 1/60
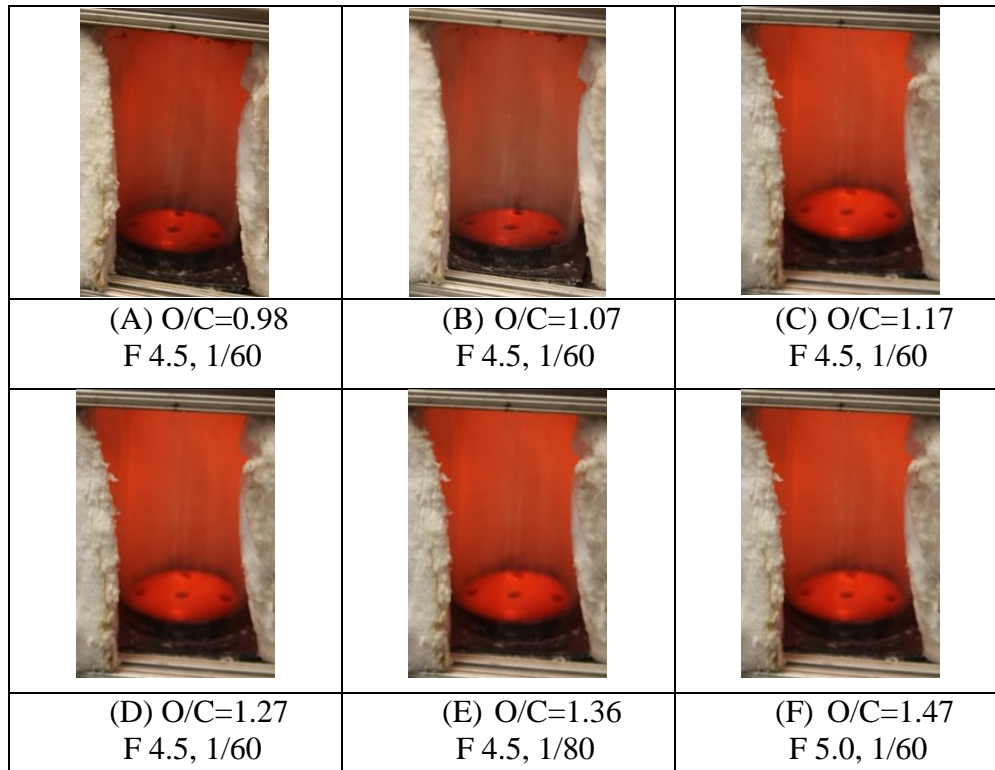
Figure 6-2. Global view of the reactor at air preheats of 450°C. The camera F-stop and exposure time (sec) for each picture is given in each picture.

(A) O/C=0.99 F5.6, 1/80	(B) O/C=1.09 F5.0, 1/60	(C) O/C=1.20 F5.6 , 1/60
(D) O/C=1.29 F5.0, 1/80	(E) O/C=1.40 F5.6, 1/60	(F) O/C=1.48 F 5.6, 1/60
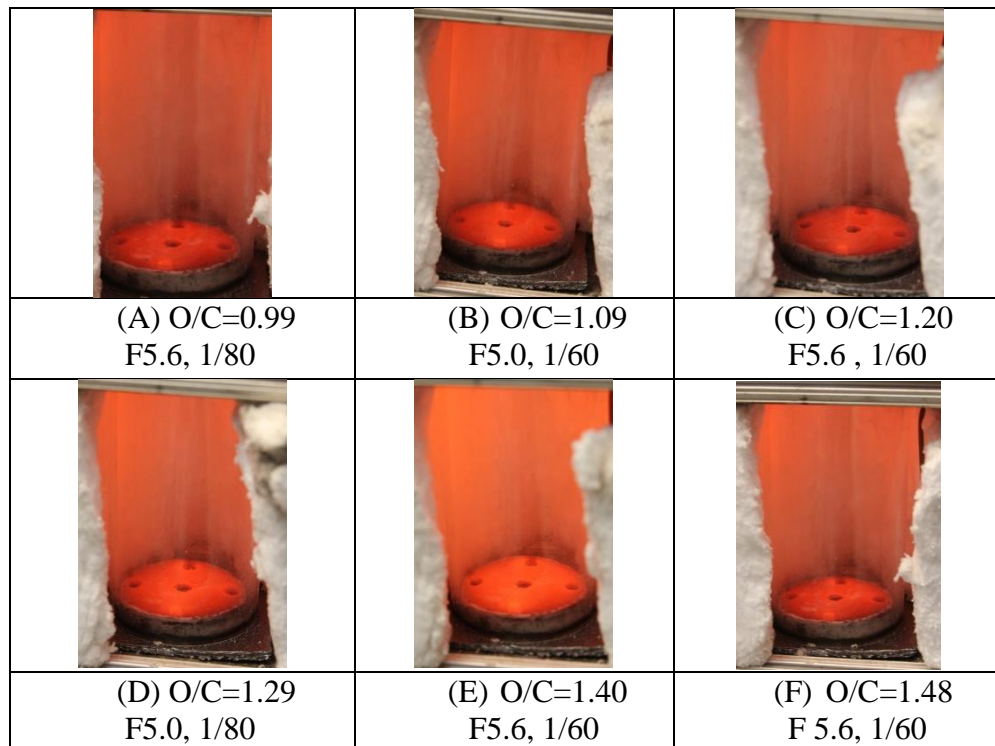
Figure 6-3. Global view of the reactor at air preheats of 600°C. The camera F-stop and exposure time (sec) for each picture is given in each picture.

At air preheats of 750°C, increasing the O/C ratio to 1.21 caused a visible transition from a transparent reaction zone to a luminous yellow visible flame, which is more typically associated with reforming, see Figure 6-4. The conventional flame was significantly less transparent with higher visible emission than with preheats of 450°C or 600°C. A yellowish visible flame represents black body radiation of soot particles. Noticeable amounts of soot are formed on quartz walls under conventional flame conditions. At O/C ratios of 1.0-1.07, minor soot formation was observed on lower portions of the reactor near to the exhaust ports. Soot formation was most pronounced at O/C ratios of 1.21 and enveloped up to ~60% of the view port, as the reactor transitioned into the Flamelets in Eddies Regime.
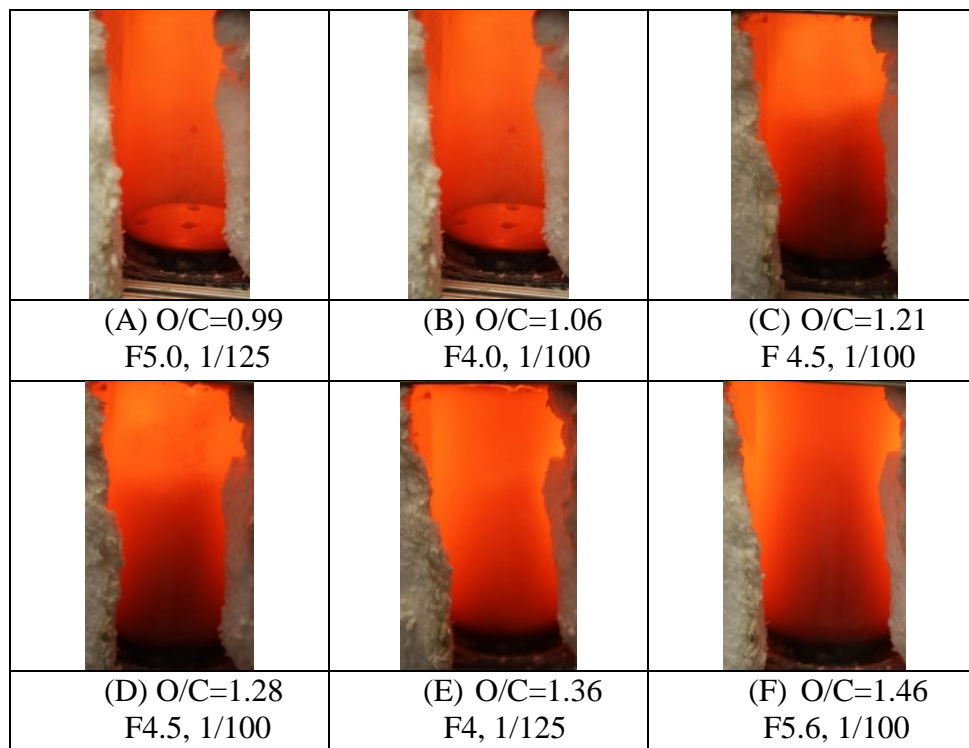
Figure 6-4. Global view of the reactor at air preheats of 750°C. The camera F-stop and exposure time (sec) for each picture is given in each picture.

At O/C ratios greater than 1.2, soot formation thickness decreased, as excess air oxidized the soot deposits. This was conjectured from the corresponding decrease in acetylene concentrations. Between O/C ratios of 1.21 to 1.46, the presence of soot blocked visual imaging of the reaction zone and alumina insulation. The visible flame was attributed to shorter ignition delay (higher injection temperature and oxygen content), which caused the fuel to ignite prior to sufficient entrainment of exhaust products. The entrained exhaust products are theorized to interfere with the soot formation kinetics.

6.1.3 Reformate Composition

A stable reaction zone was demonstrated at temperatures of $764\pm5.7°C$ to $874\pm6.6°C$, which is significantly lower than the $1000\text{-}1200°C$ exhibited by catalytic reforming, see Figure 6-5. Lowest temperatures were observed at O/C ratios of 0.98-1.0. Highest temperatures occurred at O/C 1.46-1.48, which indicates that the additional oxygen content oxidized the syngas. In the presence of Distributed Reaction Regime, reactor temperatures ranged from $764\pm5.7°C$ to $770\pm5.8°C$ (with air preheats of 450°C) and from $776\pm5.8°C$ to $817\pm6.1°C$ (with air preheats of 600°C). At air preheats of 750°C, within the Distributed Reaction Regime, increasing the O/C ratios from 1.0 to 1.07 demonstrated a small change in reactor temperature ($834\pm6.3°C$ to $835\pm6.3°C$). However, as the reactor transitioned into Flamelets in Eddies Regime, increasing the O/C ratio from 1.28 to 1.46 caused the reactor temperatures to rapidly increase from $835\pm6.3°C$ to $874\pm6.6°C$. For all cases, the low reactor temperatures were attributed to significant heat flux exiting from the reactor

152

walls (both top and bottom endcaps) and this was confirmed using thermal imaging (FLIR) diagnostics.
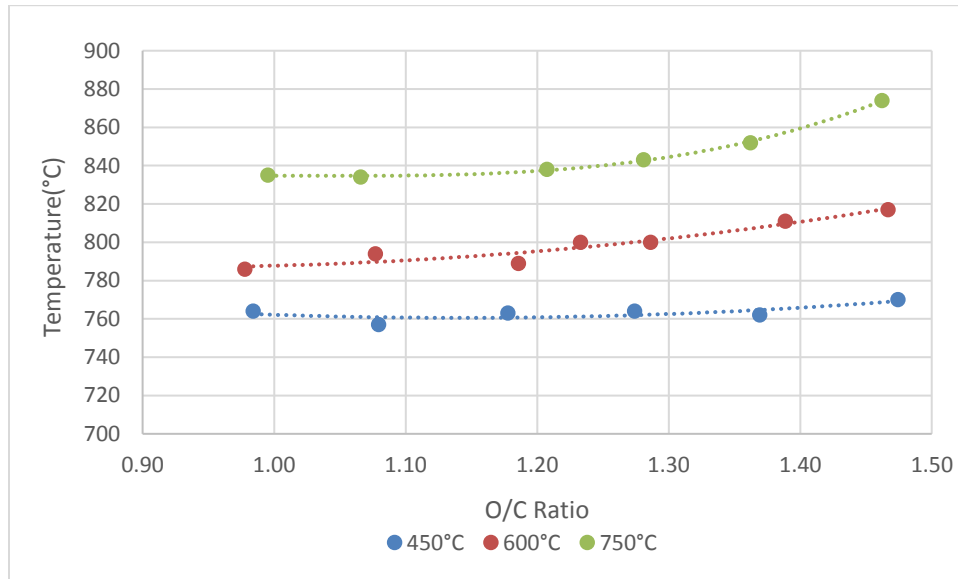
Figure 6-5. Reformate exhaust temperature at air preheats of 450, 600, 750°C

Increasing air preheats in the order of 450°C, 600°C, and 750°C, caused hydrogen concentrations to increase to 8.68±0.09%, 8.91±0.09%, and 9.92±0.10% respectively, as shown in Figure 6-6. Peak hydrogen concentrations occurred between O/C ratios of 0.98-1.08. Carbon monoxide concentrations occurred up to 18.12±0.18 and 18.58±0.19%, at O/C ratios of 0.98-1.0. Hydrogen and carbon monoxide concentrations are much higher than previously reported data under low temperature conditions. At temperatures between 700-800°C, Hartman and Roth [16,103] reported hydrogen concentrations of only 4-7.5% and carbon monoxide concentrations of 5.7-17% .

(A)

(B)

(C)
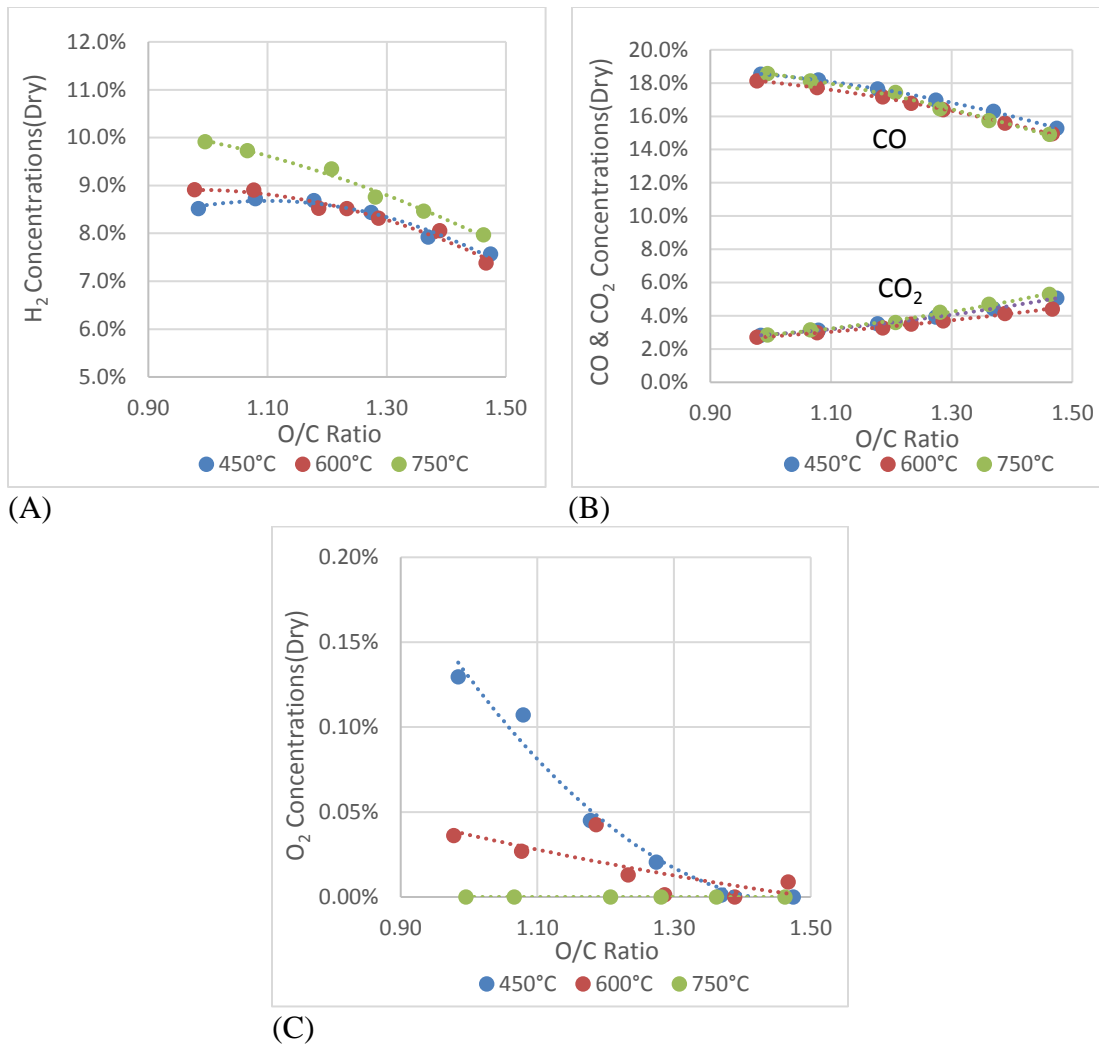
Figure 6-6. Fixed gas concentration at air preheats of 450, 600, 750°C

As described previously, contrary to combustion, high concentrations of carbon monoxide and low concentrations of carbon dioxide indicate the presence of a well-mixed condition, see Figure 6-7B. Residual oxygen and hydrocarbons were observed at lower O/C ratios, but were attributed to the low reactor temperatures, as shown in Figure 6-5. The highest concentrations of oxygen and hydrocarbons occurred at an O/C~1.0, which corresponds to the lowest reactor temperatures.

The low temperature regime promoted the formation of hydrocarbons. However, flame regime had a significant impact on product distribution and sooting

propensity. For a given O/C ratio, conditions that occurred adjacent to or exceeded the Damkohler Criterion (Flamelets in Eddies Regime) exhibited higher concentrations of acetylene and slightly higher hydrogen concentrations, see Figure 6-7A. For conditions occurring below the Damkohler Criterion (Distributed Reaction Regime), favors the formation of ethylene, see Figure 6-7B.

Conditions adjacent to or exceeding the Damkohler Criterion (Flamelet in Eddies Regime) appeared to foster dehydrogenation reactions. An increase in acetylene and hydrogen concentrations and a corresponding decrease in ethylene concentrations support this assertion. This is particularly noticeable at low oxygen to carbon ratios. Dehydrogenation reactions are associated with both acetylene and soot formation through Hydrogen Abstraction Carbon Addition (HACA) mechanism[16,54–56]. Noticeable soot formation occurred at conditions within the Flamelets in Eddies, see Figure 6-1 and Figure 6-4.

The Distributed Reaction Regime formed hydrocarbons with a lower propensity for soot formation than that under a conventional flame. Sooting propensity increases in the order of ethane, ethylene, and acetylene[142,143]. Under a Distributed Reaction Regime, acetylene concentrations were 20-23% lower, but ethylene concentrations were 10-68% higher, see Figure 6-7A and Figure 6-7B. Methane concentrations were 7-24% higher under the Distributed Reaction Regime, see Figure 6-7C. This is consistent with the theory that the more distributed conditions allow greater entrainment of exhaust products, suppressing soot formation and interfering with HACA mechanism. Higher methane concentrations are desirable as methane is resistant to sooting and can be utilized directly in a SOFC. Trace

155

amounts of ethane were detected, but not in significant quantities in either regime, see

Figure 6-7D. In addition, operation under a conventional flame is less desirable due to

the formation of blockages in the cooling loop, which were not observed under the

Distributed Reaction Regime.

(A)

(B)

(C)

(D)
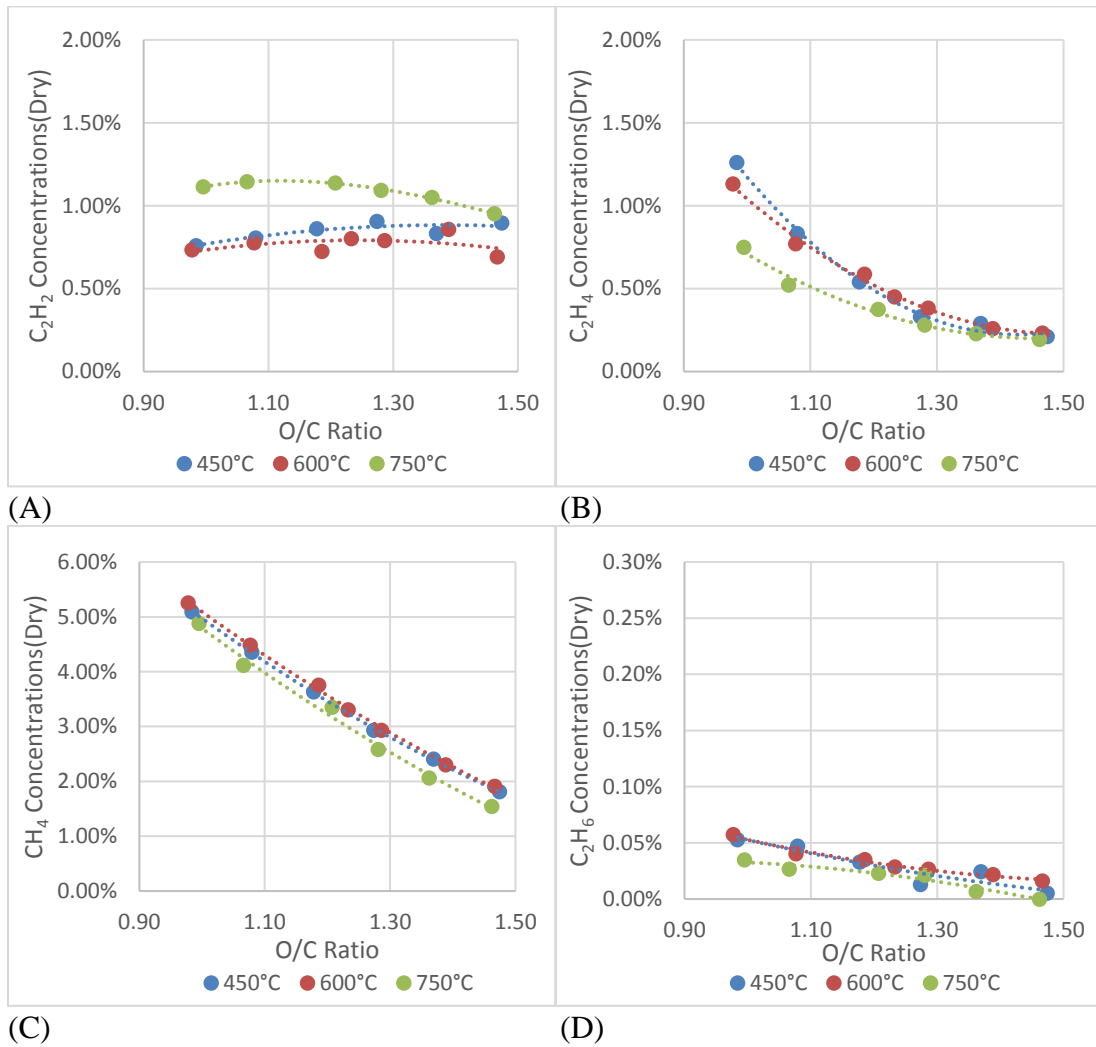
Figure 6-7. Reformate hydrocarbon (C1-C2) concentrations at air preheats of 450, 600, 750°C

Available data in the literature only reported hydrocarbons up to

ethane[11,12,102]. The gas chromatograph used in the present study detected

hydrocarbons up to C6 (hexane). In the reformate trace amounts of hydrocarbons

detected were above ethane, see Figure 6-8. Peak hydrocarbon formation occurred at O/C ratios of 0.98-1.00 and decreased with increasing oxygen content.

(A)   (B)

(C)
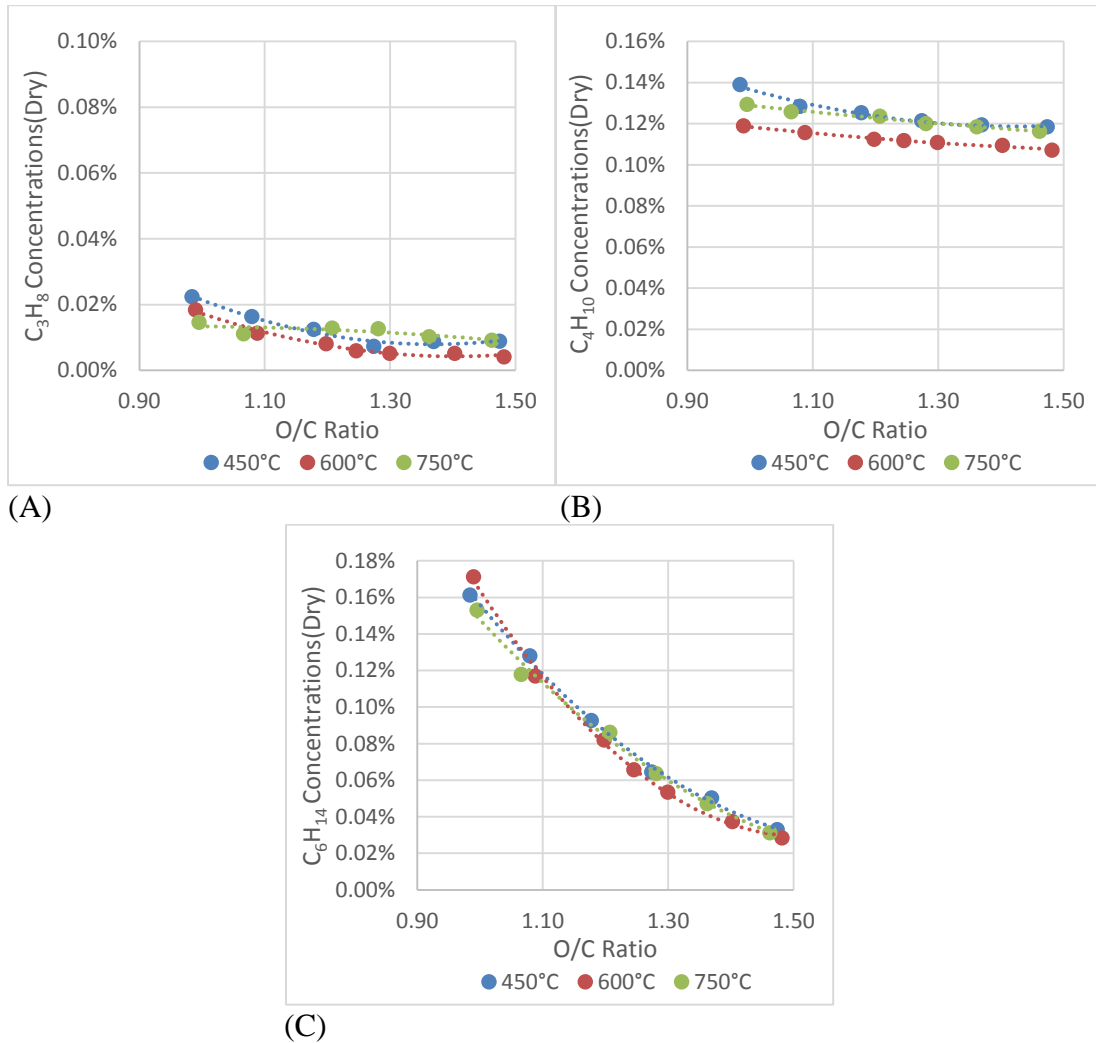
Figure 6-8. Reformate hydrocarbon (C3-C6) concentrations at air preheats of 450, 600, 750°C

Lower reactor temperatures promoted the formation of hydrocarbons in the reformate. Higher reactor temperatures are expected to reduce hydrocarbon formation. The lowest concentrations of butane and propane occurred under the Distributed Reaction conditions at preheats of 600°C, see Figure 6-8A and Figure 6-8B. Trace concentrations of propane were detected between 0.001±10 ppm to 0.02%±10 ppm, see Figure 6-8A. Butane (C_4H_{10}) was detected at concentrations

between 0.11%±11 ppm to 0.14%±14 ppm, see Figure 6-8B. No propylene or pentane hydrocarbons were detected over the range of conditions examined. Lower limit of detection is between 10-20 ppm. Hexane (C_6H_{14}) was detected at concentrations between 0.03%±10 ppm to 0.16%±16 ppm, see Figure 6-8C.

Flame regime and air preheats temperature had minimal impact on conversion, only variations in oxygen to carbon ratios showed a significant effect. The additional oxidizer caused the reaction zone to become less distributed. However, the greater oxygen concentrations enhanced the partial oxidation reactions, which increased conversion. The significant formation of lower hydrocarbon limits conversion to a maximum 81.5%. Uncertainty in the conversion term was no greater than ±2.03%. Exhaust temperatures indicate the reactor operated beneath 1000°C, which limited conversion.
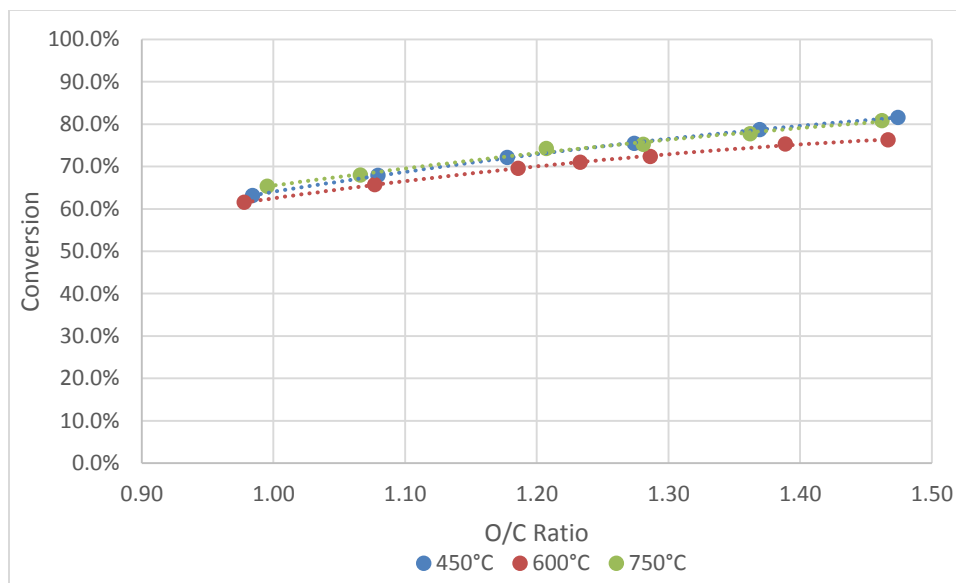
Figure 6-9. Conversion of JP-8 at air preheats of 450, 600, 750°C

Reforming efficiencies ($\eta_{H_2,CO}$ & η_{H_2,CO,CH_4}) were calculated through Eq. 1-4 and Eq. 1-5. Maximum error in reforming efficiency was found to be no more than ±1.92%. Reforming efficiency as a function of O/C ratios is presented in Figure 6-10. Reforming efficiency (η_{H_2,CO,CH_4}) for SOFC was noticeably higher than the reforming efficiency ($\eta_{H_2,CO}$) for PEMFC and occurred at lower O/C ratios. Methane constituted 19-36% in the recovered energy; therefore, peak reforming efficiency (η_{H_2,CO,CH_4}) occurred at lower O/C ratios. However, the highest reforming efficiency ($\eta_{H_2,CO}$) for PEMFC occurred only at higher O/C ratios, in regions of high conversion.

Higher reforming efficiencies at higher O/C ratios (O/C=1.2-1.47) are more desirable due to the lower concentrations of butane and hexane, see Figure 6-8B and Figure 6-8C. Hydrocarbons present in the reformate can be detrimental to the fuel cell and other downstream components in a system.

The suppressions of the dehydrogenation reactions are associated Hydrogen Abstraction Carbon Addition (HACA) in the Distributed Reaction Regime promoted formation of methane yielded higher reforming efficiency (η_{H_2,CO,CH_4}) when paired with SOFC. The Flamelets in Eddies Regime promotion of these reactions increased hydrogen concentrations, which promoted greater reforming efficiency ($\eta_{H_2,CO}$) when paired with PEMFC. The higher reforming efficiency (η_{H_2,CO,CH_4}) for the Distributed Reaction Regime indicates that low temperature reforming is best paired with a SOFC, which can handle a wider composition within the syngas.
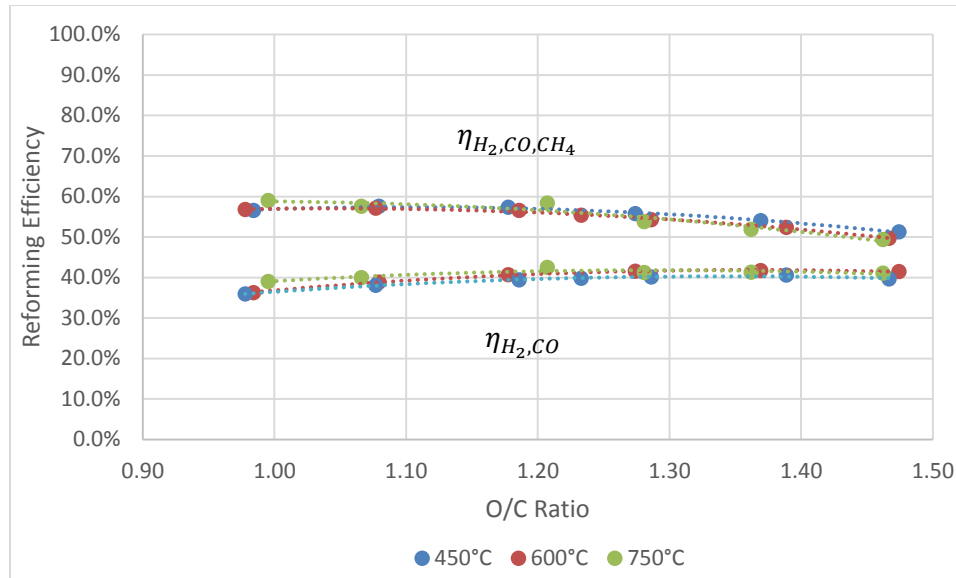
Figure 6-10. Reforming efficiency for $\eta_{H_2,CO}$ and η_{H_2,CO,CH_4} at air preheats of 450, 600, 750°C

6.1.4 Section Summary

Oxygen concentrations were observed to have a significant effect on reformate quality. At all O/C ratios evaluated with air preheats of 450°C and 600°C, a transparent reaction zone was observed in the entire reactor similar to that observed in Colorless Distributed Combustion, except for a faint reddish orange hue. A stable reaction zone was demonstrated at temperatures of 764±5.7°C to 874±6.6°C, which is significantly lower than typical catalytic reforming temperatures of 1000-1200°C. At air preheats of 750°C and O/C ratios of 1.28, the reactor transition from the Distributed Regime to Flamelets in Eddies Regime. At this transition, a conventional flame was observed. This is attributed to higher oxygen concentrations and injection temperatures shortening the ignition delay, which caused the fuel to ignite before sufficient entrainment could occur.

The reformate quality obtained herein was of a higher quality syngas

(8.68±0.09% to 9.92±0.10% hydrogen and 18.12±0.18% to 18.58±0.19% carbon

monoxide) than previously reported in literature (4.0-7.5% hydrogen and 5.7-17%

carbon monoxide) using low temperature thermal partial oxidation[16,103]. Such

increases in hydrogen concentrations are significant and beneficial. The major

hydrocarbons detected are presented in increasing order: acetylene < ethylene <

methane. Hexane (0.03%±10 ppm and 0.16%±16 ppm) and butane (0.11%±11ppm to

0.14%±14 ppm) were also detected in low concentrations; this is attributed to the low

temperature reaction zone. The Distributed Reaction Regime at preheats of 450°C

demonstrated reforming efficiency (η_{H_2,CO,CH_4}) for SOFC that was either comparable

(O/C=0.98-1.20) or superior (O/C=1.2-1.47) to a conventional reforming flame. The

Distributed Reaction Regime formed hydrocarbons with lower propensity to soot.

Acetylene concentrations in the Distributed Reaction Regime were 20-23% lower

than a conventional reforming flame. It was theorized that the greater entrainment of

exhaust products occurring within the Distributed Reaction Regime the suppressed

the activity of the HACA mechanism.

Even though the reformer operated in a soot formation regime, no visible soot

was observed on the reactor walls while operating within the Distributed Reaction

Regime. Departure from Distributed Reaction Regime resulted in the emergence of a

conventional flame and visible formation of soot. Soot enveloped up to 60% of the

reactor area, occurring strongest near the lower portion of the reactor closest to the

exhaust ports. Peak soot formation occurred at an O/C ratio of 1.21, which

corresponded to highest acetylene concentrations.

Mixture injection temperatures were used as an alternative means to control characteristic chemical time and length scales. Higher preheats foster a more rapid chemical reaction, which results in a shorter chemical time and length scales. Both global imaging and numeral calculations were used for identification of the flame regime. Similar to the work conducted by Al Hamamre[139], preheats were observed to have a significant impact on reactor temperature.

Air and fuel flow rates were fixed at an O/C ratio of 1.3, while air heater temperature was adjusted between 600°C to 750°C. Fuel was preheated to 330°C, which allowed complete vaporization of JP-8. Fuel and air were injected at 7.52 ml/min and 32.5 SLPM respectively, which resulted in oxygen to carbon ratios between 1.28-1.29. Reynolds number in the nozzle was determined to be in the range of 2870 to 3752. Using a fixed mass flow rate, while only varying the preheats minimized the changes to characteristic turbulent length and time scales. The JP-8 employed had a hydrogen content of 13.6%$_{mass}$ with a heating value of 42.8MJ/kg. Carbon balance of 95.2 to 98% was achieved, indicating complete detection of hydrocarbon species.

6.2.1 Flame Regime

Increasing the temperature of the fuel-air mixture caused the flame regime to shift from the Distributed Reaction Regime into the Flamelets in Eddies Regime. Figure 6-11 shows a Borghi diagram, which denotes individual combustion regime against Damkohler and Turbulent Reynolds number. Increasing preheats did not affect the Integral length scale as it remained constant at ~1.27 mm. Turbulent

velocity varied slightly between 1.43-1.51 m/sec. This resulted in turbulent time

scales of ~0.85-0.89 ms. Increasing the air preheats increased the laminar flame speed

from 30.3 cm/sec to 47.8 cm/sec, but decreased laminar flame thickness from 1.78

mm to 0.99 mm. This decreased the chemical time scales from 5.86 ms to 2.07 ms.

Damkohler number increases with air preheat, while the chemical time scale

decreases.
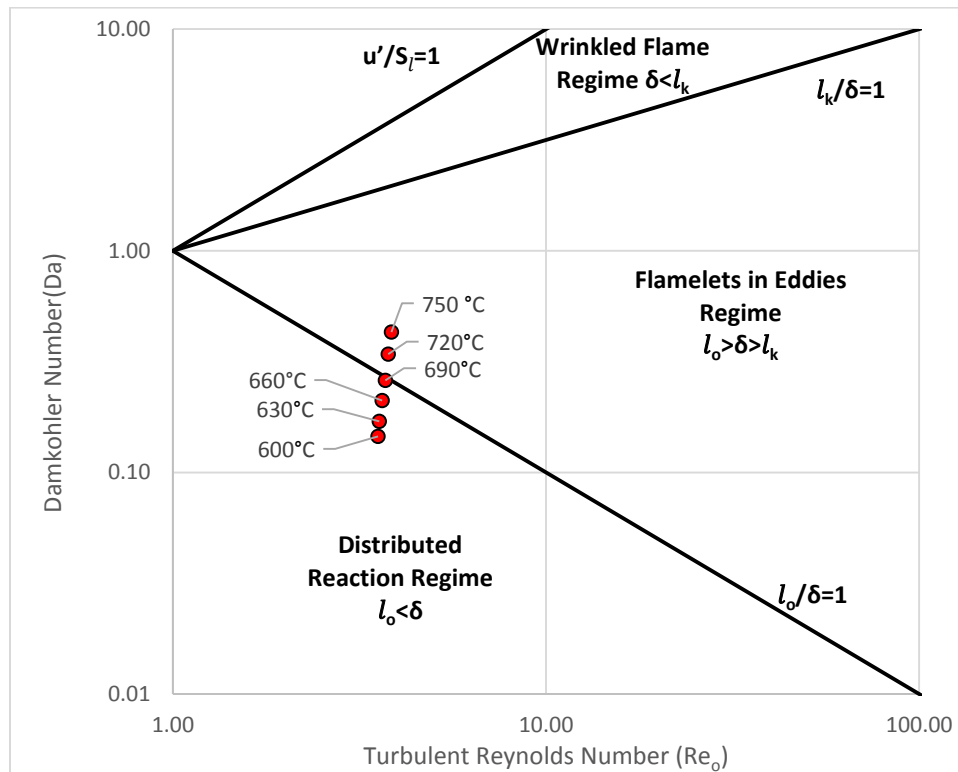
Figure 6-11. Numerical calculation of flame regime

The reactor demonstrated a Distributed Reaction Regime at air preheats of

600°C, 630°C, and 660°C. This is supported by Damkohler number occurring below

the Damkohler Criterion. Under these conditions, eddies (l_o=1.27 mm) were

sufficiently small enough to completely reside within the reaction front (δ=1.45-178

mm). This indicates that there was sufficient time for entrainment. Global imaging

supports the presence of Distributed Reaction Regime, as shown in Figure 6-12A to Figure 6-12C. An increase in air preheats, shortened the characteristic chemical time and length scales.

At air preheats of 690°C, the laminar flame thickness (δ=1.30 mm) approximately equaled integral length scale (l_o=1.27 mm), resulting in a condition occurring along Damkohler Criterion. Under these conditions, the reaction zone demonstrates a transitionary regime, having characteristics of both Distributed Reaction Regime and a conventional flame. This indicates that the reaction is only partially entraining the hot reaction species into the reforming zone. This regime correlates well with the emergence of minor soot formation, see Figure 6-12C.

At higher preheat temperatures of 720°C and 750°C, the reactor operated within the Flamelets in Eddies Regime. Higher air preheats caused the laminar flame thickness (δ=0.99-1.12 mm) to decrease below the integral length scale (l_o=1.27 mm), which causes the Damkohler numbers to exceed the Damkohler Criterion. As a result of the decreased laminar flame thickness, the eddies were no longer able to completely reside within the flame front, resulting in reduced mixing. Reactions proceeding before sufficient mixing could occur, which caused the emergence of a visible flame and visible soot formation, as shown in Figure 6-12E to Figure 6-12F.

6.2.2 Global Imaging of Reaction Zone

Global imaging of the reaction zone at preheats of 600°C to 660°C demonstrated a transparent reaction zone that was comparable to the reaction zone seen in previous work in distributed combustion[47,107,126,144]. No visible flame front or noticeable soot formation was observed on quartz walls of the reactor, even

though these conditions are considered a soot formation regime. Increase in air preheats caused an increase in visible emissions as seen from Figure 6-12A to Figure 6-12C. Visible emission appears as a light reddish orange hue distributed evenly throughout the reactor.

At preheats of 690°C, a transitional regime was observed, which demonstrates characteristics of both the Distributed Reaction Regime and a conventional reforming flame. Global imaging shown in Figure 6-12D, showed minor soot formation on the reactor wall nearest to the exhaust ports, but this did not progress beyond the initial formation. Soot formation did not cause any significant influence on the reactor performance.

The reactor did not reveal a visible reaction zone at 690°C as was demonstrated at higher preheats of 720°C to 750°C. However, the reaction zone was more luminescent than what was observed at lower air preheats temperatures, see Figure 6-12A to Figure 6-12C. In Figure 6-12D, the top of the reaction zone demonstrated a yellowish color flame, similar to that of a conventional reforming flame. While the lower portion of the reactor demonstrates a lighter reddish orange hue that more closely resembles the volumetric distributed combustion.

At preheats of 720°C to 750°C, the reactor transitioned to a defined flame front, with soot enveloping the quartz window, as shown in Figure 6-12E to Figure 6-12F. Visible emission transitioned from the lighter red/orange hue to a brighter yellow flame. The reaction zone demonstrated a flame that was more typical of that found in the work of Pastore and Chen[11,12]. A luminous yellow flame represents the black body radiation of soot particles at elevated temperatures.
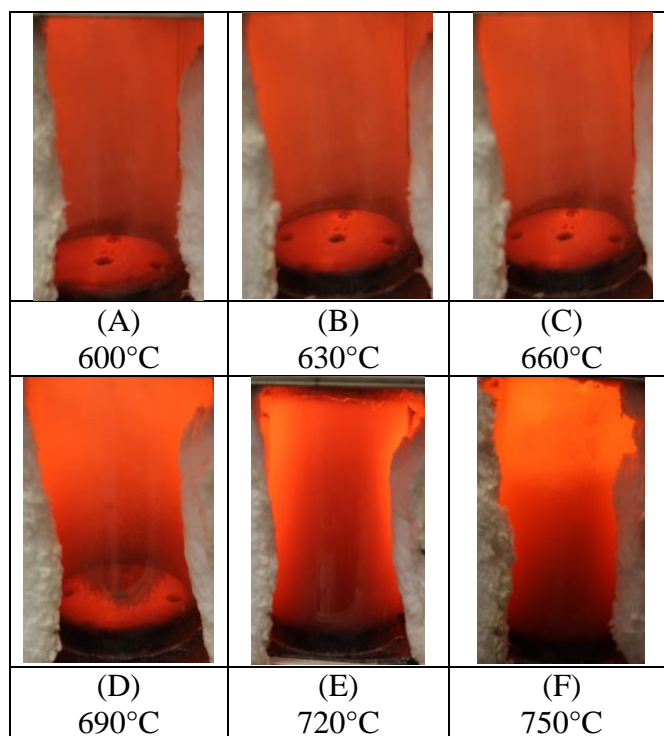
Figure 6-12. Global imaging of flame regime O/C=1.3 and preheats from 600-750°C

6.2.3 Reformate Composition

Fixed gas concentrations were found to gradually change as air preheats increased, as shown in Figure 6-13. Hydrogen concentrations increased with air preheats, while carbon monoxide concentrations decreased. No immediate changes in fixed gas concentrations were noticed upon change in flame regimes. A contributing factor to changes in fixed gas concentrations were conjectured to be from the water gas shift reaction, see R. 6-1. The water gas shift is active under these conditions.

$$CO + H_2O \rightarrow CO_2 + H_2 \hspace{4cm} \text{R. 6-1}$$

While no water was added to the reactor, some hydrogen will oxidize to form water. Water formation was confirmed at the condenser prior to the gas chromatograph upon completion of the experiment. Increased reactor temperatures, resulting from an increase in air preheats, promoted the water gas shift reaction. This

166

observation is supported by an increase in carbon dioxide concentrations. No oxygen was detected under the conditions tested.
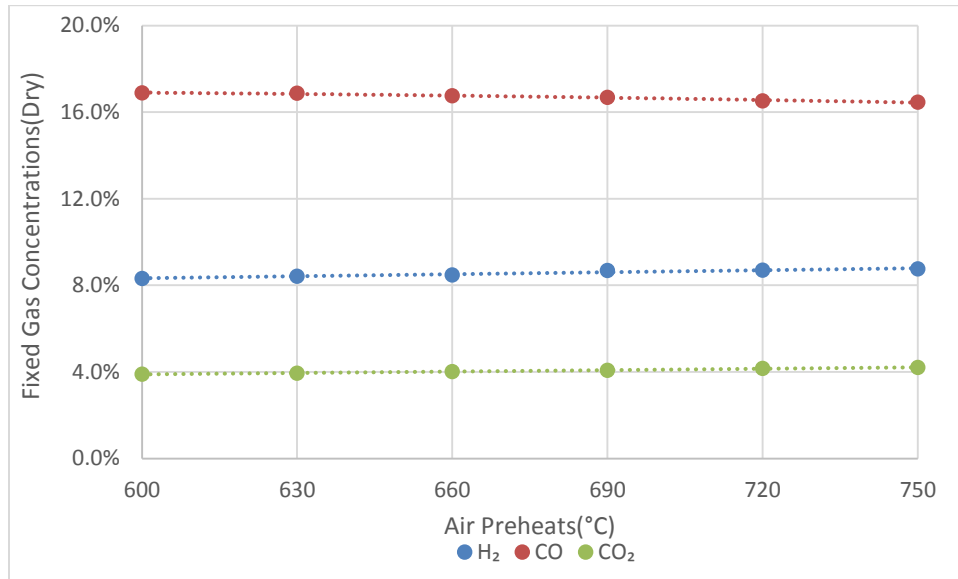
Figure 6-13.Concentration of fixed gases at preheats of 600-750°C, in increments of 30°C at O/C =1.3

Air preheats were found to effect the formation of lower hydrocarbons. As the reaction zone transitioned from the Distributed Reaction Regime to a more conventional flame, most hydrocarbons exhibited a gradual change. Methane and ethylene gradually decrease with increase in air preheats from 600°C to 750°C, see Figure 6-14. Acetylene concentrations increased slowly at air preheats of 600°C to 690°C. However, at air preheats of 720°C to 750°C, acetylene concentrations increased more rapidly.

Acetylene is a stronger soot precursor than ethylene[142,143]. Lower hydrocarbon formation under the Distributed Reaction Regime is more desirable, as methane is directly compatible with a SOFC. Higher concentrations of ethylene are more desirable, due to ethylene being a weaker soot precursor than acetylene.

The higher acetylene concentration and soot formation at air preheats of 720°C to 750°C, were attributed to the ignition occurring before sufficient entrainment could occur, as shown in Figure 6-14. Sufficient entrainment will promote steam reforming and dry reforming reactions, which suppresses acetylene formation. Without sufficient entrainment, the fuel is more prone to undergo cracking and dehydrogenation reactions, which promote acetylene formation. This is consistent with the theory that a less distributed condition minimizes the entrainment of exhaust products, allowing soot formation to propagate.

Previous work[50] indicated air preheats had a more pronounced effect on lower hydrocarbon distribution, as oxygen to carbon ratios approach unity. As oxygen to carbon ratios increased, the difference between the two regimes decreased. Added oxygen content enhanced the extent of the reforming reactions, so that the Distributed Reaction Regime's effects are less pronounced. In addition, previous work evaluated preheats with larger temperature intervals, which helped to observe the changes but may have missed any nonlinear effects.

In reforming, high concentrations of carbon monoxide and low concentrations of carbon dioxide indicate complete mixing occurred, even though hydrocarbons are detected in the exit stream. Low reactor temperatures allowed the formation of hydrocarbons.
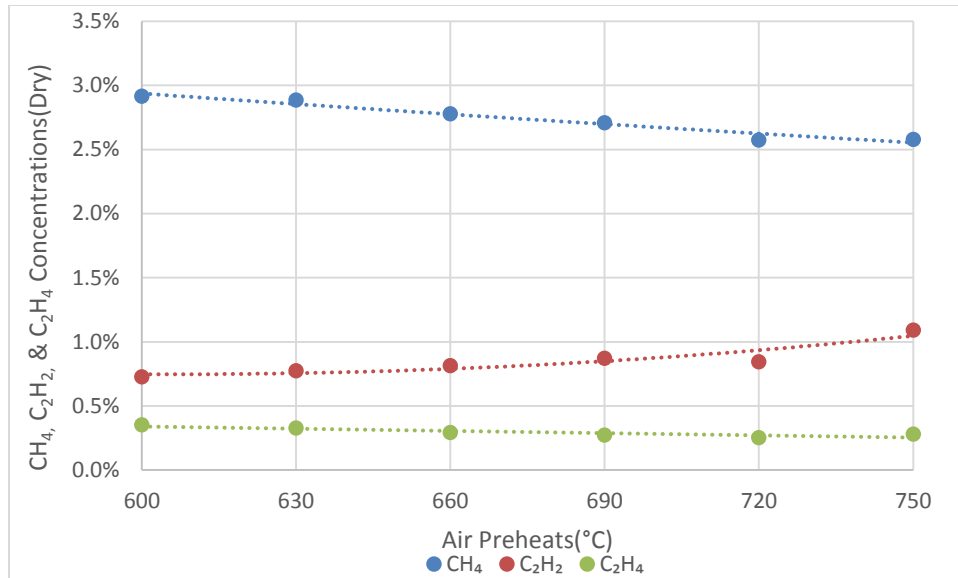
Figure 6-14. Lower hydrocarbon formation at preheats of 600-750°C, in increments of 30°C at O/C =1.3

Noticeable lower hydrocarbon were detected in the reformate. Hydrocarbon are presented in decreasing composition, butane (0.12%±12 ppm to 0.13%±13 ppm), followed by hexane (0.04%±10 ppm to 0.06%±10 ppm), and propane (0.01%±10 ppm). Oxygen concentrations had the largest impact on hydrocarbon formation, neither flame regime or injection temperature showed as strong an influence. Propane and butane showed slightly higher formation under the Flamelets in Eddies Regime. Flame regime had a much stronger influence on the C2 hydrocarbons.

A slight decrease in conversion was noted as preheats increased. Increases in hydrocarbon formation can explain this decrease shown in Figure 6-14 and Figure 6-15, but it should be noted that this was within the margin of error.
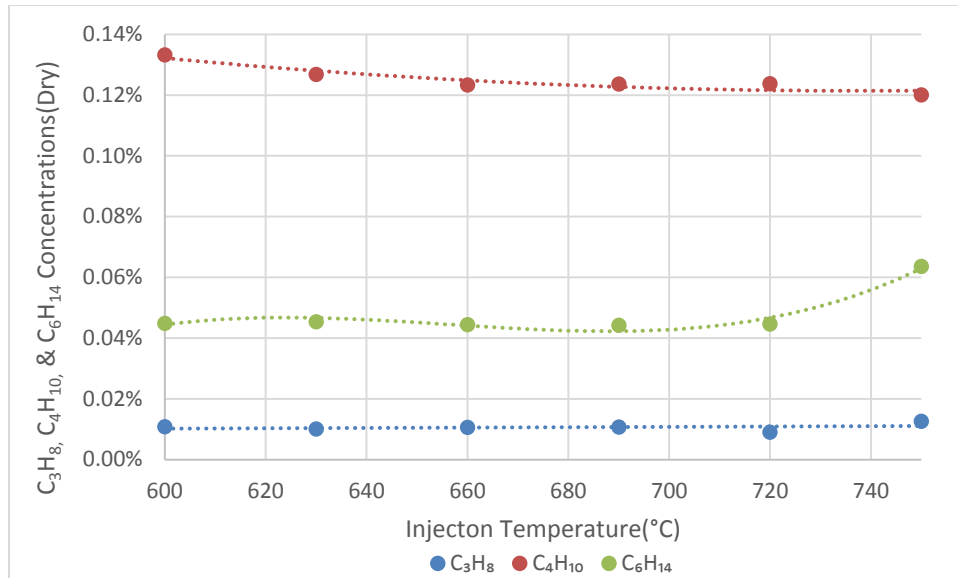
Figure 6-15. Hydrocarbon formation at preheats of 600-750°C, in increments of 30°C at O/C =1.3
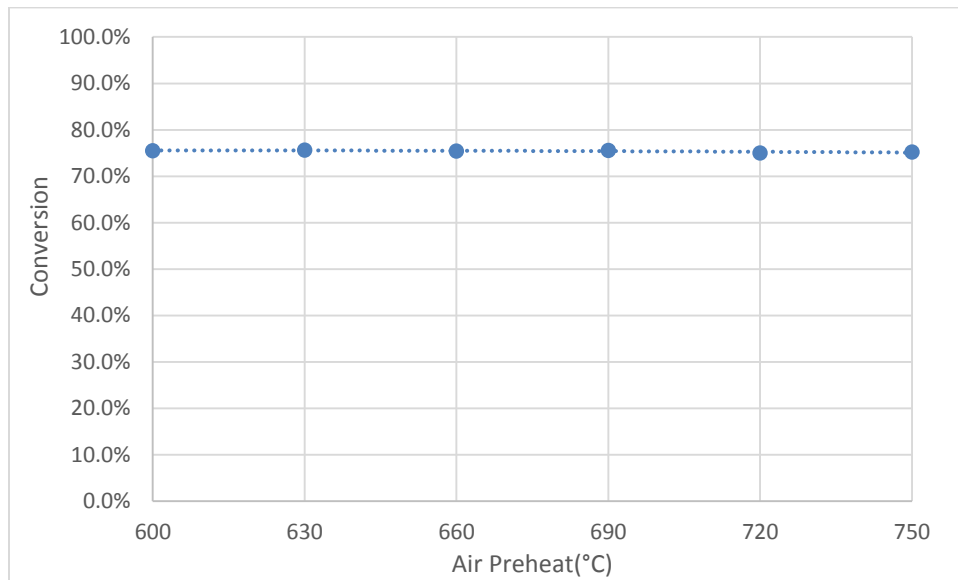
Figure 6-16. Conversion at preheats of 600-750°C, in increments of 30°C at O/C =1.3

As there was significant hydrocarbon formation, reforming efficiencies are presented for both $\eta_{H_2,CO}$ and η_{H_2,CO,CH_4}. As methane contributed 10-19% of the energy recovered, increasing air preheats reduced methane formation, which reduces reforming efficiency calculated through η_{H_2,CO,CH_4}. Reforming efficiency calculated

170

through $\eta_{H_2,CO}$ remained unaffected. Uncertainty of the conversion calculation was no greater than ±2.03%
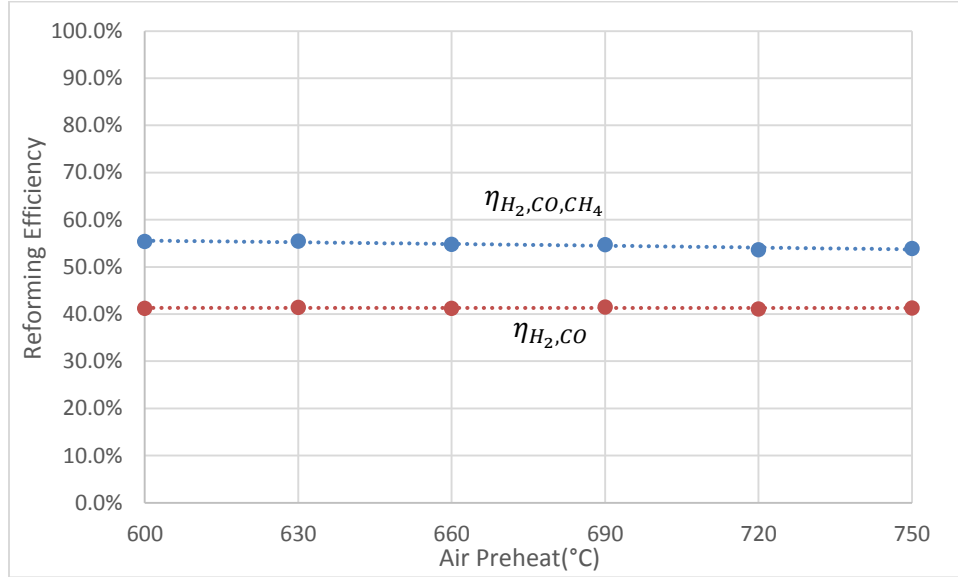
Figure 6-17. Reforming efficiency for $\eta_{H_2,CO}$ and η_{H_2,CO,CH_4} at preheats of 600-750°C, in increments of 30°C at O/C =1.3

The exhaust temperature increased with increasing air preheats, see Figure 6-19. Exhaust temperatures are curve fitted to show the increase in temperature with air preheats and consistency. Exhaust temperatures ranged from 789±5.9°C to 842±6.3°C, which is considered a low temperature regime. Typical non-catalytic reforming occurs at high temperatures with optimum results found at temperatures of 1000-1100°C. Higher reactor temperatures are expected to decrease lower hydrocarbon formation and promote addition hydrogen formation as was seen by Roth[16] and Hartmann[103] in conventional partial oxidation. Heat transfer from quartz windows and through the top of the reactor limited reactor temperatures, as determined through FLIR imaging, see Figure 6-18. The uncertainty of efficiency calculations was no greater than ±1.75%.

171
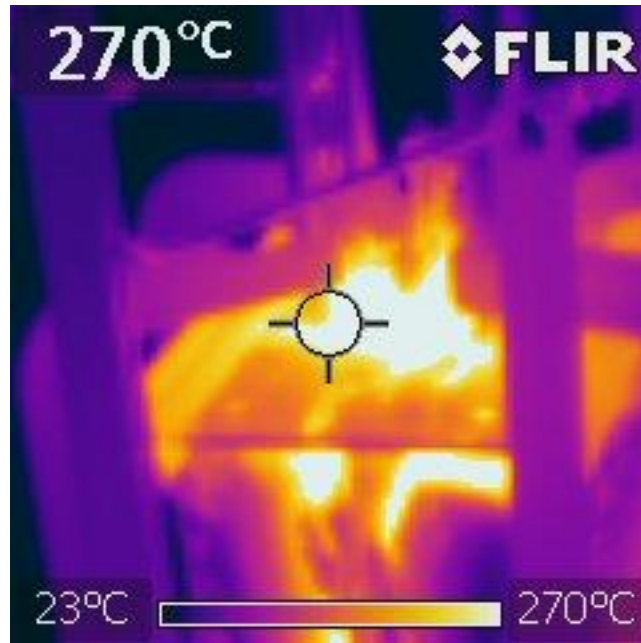
Figure 6-18. Thermal image of quartz reactor

Flame regime did not demonstrate an observable impact on the exhaust temperatures. Measurement of the temperature distributions within the reactor was not conducted due to limitations of the reactor and concerns that those thermocouples may disrupt the flow within the reactor. However, with this reactor configuration under the Distributed Reaction Regime, it is thought that the exhaust temperatures are a good indication of reactor temperature. Under a conventional flame, it is thought that a more uneven temperature distribution would emerge, with higher localized temperatures. This is anticipated due to reactions initiating before sufficient entrainment could occur, resulting in larger volumetric heat release and higher peak temperatures.
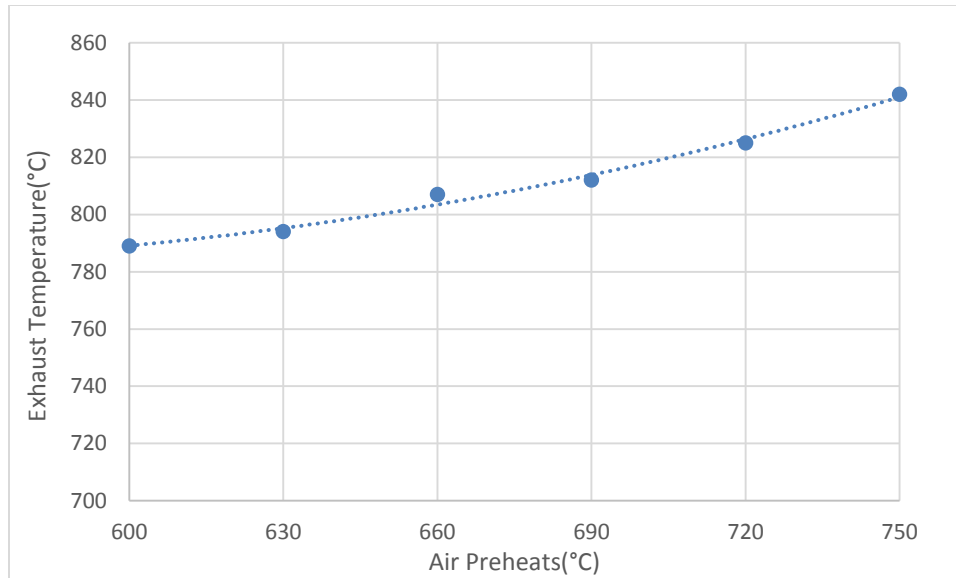
Figure 6-19. Reactor exhaust temperature at preheats of 600-750°C, increasing in
increments of 30°C at O/C =1.3

6.2.4 Section Summary

Air preheats were adjusted to control the chemical time scale. Chemical time

and length scales decreased with increasing air preheats. Air preheats of 600°C,

630°C, and 660°C were shown to develop a Distributed Reaction Regime, with

Damkohler Numbers occurring below the Damkohler Criterion. Calculations

indicated that the integral length scales were sufficiently smaller than the laminar

flame thickness. Under this condition, fuel and reformate have sufficient time to mix

before initiation of the reactions. This entrainment is attributed to suppressing the

soot formation reactions.

At temperatures of 690°C, laminar flame thickness approximately equals to

that of the integral length scale, resulting in a condition occurring along the

Damkohler Criterion. This results in the transient regime showing characteristics of

both the Distributed Reaction Regime and a more traditional reforming flame. Minor soot formation was noted on the reactor walls under this condition.

At preheat temperatures of 720°C and 750°C, the laminar flame thickness was smaller than the integral length scale. This results in conditions that exceed the Damkohler Criterion. A visible yellow flame was observed, as a result of insufficient time for the entrainment of exhaust products into the reactants and the corresponding dilution of oxygen concentrations. The flame appeared similar to that shown in the literature under non-catalytic reforming conditions using middle distillate fuels.

Reformate concentrations of fixed gases and lower molecular weight hydrocarbons gradually changed with air preheats. Transition of the reaction from the Distributed Reaction Regime to Flamelets in Eddies Regime caused a drastic change in acetylene concentrations, other hydrocarbon only exhibited a gradual changed. The results in Section 6.1 indicate a more pronounced change occurred in product distribution at lower oxygen to carbon ratios of 0.98-1.0.

Exhaust temperatures increased with increasing in air preheats. Flame regime did not demonstrate a noticeable impact on exhaust temperature. However, it is expected that flame regime will affect peak reactor temperatures. The faster chemical time scales in conventional flames are expected to result in higher volumetric heat release from the peak temperatures. The extent of distributed reformation requires quantification from the measured thermal field uniformity.

Chapter 7: High Temperature Reactor

The reactor developed in Chapter 6 was limited by heat loss, which degraded reformate quality. A high temperature reactor was developed to operate to explore more ideal reforming conditions. Accurate numerical calculations of flame regime allowed the removal of the optical window. In order to reduce heat flux, the reactor was encased in a tube furnace, which reduced the temperature gradient of the reactor and allowed near adiabatic conditions.

Higher operating temperatures were needed to promote higher quality reformate. Equilibrium calculations for dodecane at a O/C ratio of 1.0 showed, optimum temperatures to occur between 900-1100°C, which is consistent with experimental observations by Hartmann[103] and Zhdanok[19]. The reactor was designed to operate under comparable conditions. Figure 7-1 presents reformate composition at equilibrium conditions, as a function of reactor temperature. Lower operating temperatures (600-800°C) predict the formation of methane and reduced hydrogen concentrations, which was consistent with results obtained in Chapter 6. Increasing reactor temperatures up to 900°C favors the formation of carbon monoxide and hydrogen over that of steam and carbon dioxide. From the literature[16,58–63,67–71], it was determined that temperatures of 800-1000°C were sufficient to activate steam and dry reforming reactions. After the experiments conducted in Section 7.1, reactor temperature was limited to 1200°C, due to a concern that higher temperatures would damage the exhaust ports and thermocouples. The high temperature reactor produced low concentrations of methane and other hydrocarbons.

For Chapter 7, reforming efficiency was calculated using the energy content of hydrogen and carbon monoxide, relative to the energy content of the fuel, Eq. 1-4. Methane concentrations were so low that the added energy would not influence available energy, $\eta_{H_2,CO} \sim \eta_{H_2,CO,CH_4}$.
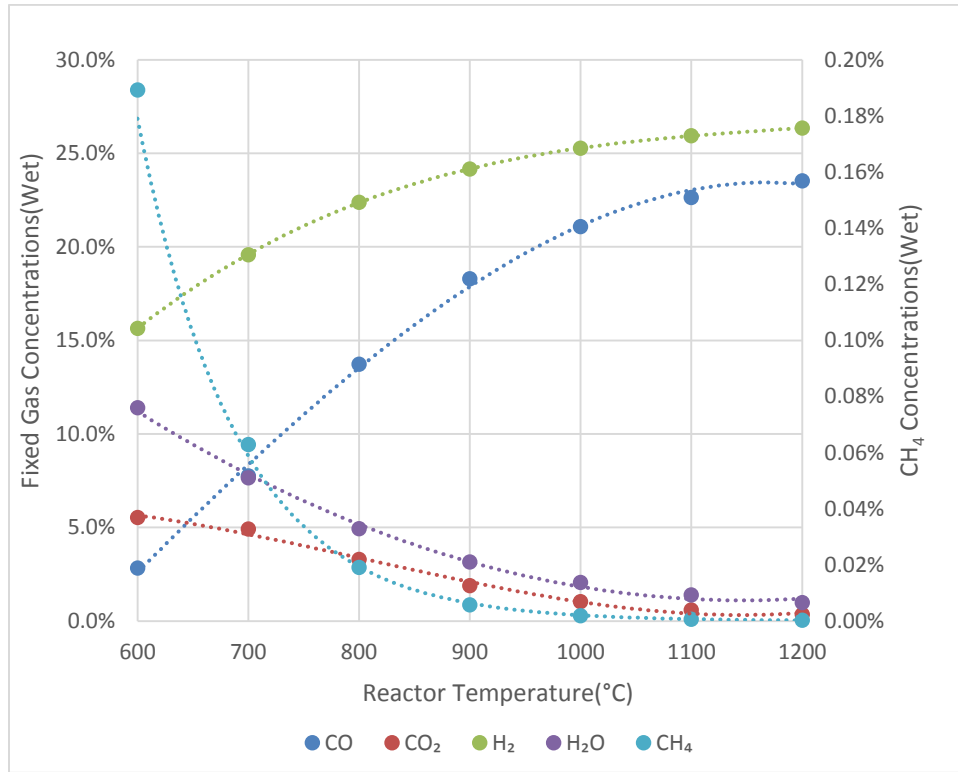
Figure 7-1. Syngas composition at equilibrium conditions at O/C=1.0

Similar to the low temperature reactor, the chemical time scales were controlled through variations in preheats, oxygen to carbon ratios, and steam addition. Characteristic turbulent properties were held near constant. Air was injected at 30 SLPM for all experiments, while fuel flow rate was adjusted. As air composes ~97% of the volumetric flow rate, changes in fuel feed rates would have minimal impact to the characteristic turbulent length and time scales. The reactor was operated solely within the Distributed Reaction Regime to enhance the reactor operational time.

7.1 Preheat Effect on Chemical Time Scales

Injection temperatures were used to control the characteristic chemical time and length scales, while minimizing the impact to characteristic turbulent properties. Enhancing injection temperatures enhanced the activity of the chemical reaction causing the reactor to become less distributed.

The reactor was operated at 5.1kWth, with a fixed oxygen to carbon ratio of unity. Air was injected at a constant flow rate of 30 SLPM (at 21°C and 1 atm), while air preheats were used to control the injection temperature. Injection temperatures, measured prior to injection into the reactor, ranged from 383°C to 556°C. Fuel was vaporized at a constant 300°C. To prevent fuel condensation after vaporizer, lower injection temperatures were limited to 383°C. Reynolds number in the nozzle was determined to be in the range of 3674 to 4190. The reactor stability was determined from the observed reactor temperatures and reformate's concentration. The JP-8 employed had a hydrogen content of 13.6%$_{mass}$, and a heating value of 42.8 MJ/kg. Molar carbon balance of 80-93% indicated high detection. Higher detection was achieved at lower injection temperatures.

During ignition, reactor temperatures exceeded thermocouple limit of 1325°C. Numerical calculations were conducted and it was determined that, under most conditions evaluated, the reactor would exceed maximum temperatures allowable for internal thermocouples.

7.1.1 Flame Regimes

The flame regime was determined through numerical calculations detailed in Section 3.1, as the reaction zone was unobservable. Previous work has shown strong

capability of predicating the emergence of Distributed Reaction Regime[145], with a comparable design. Under conditions tested, shown in Figure 7-2, reactions only occurred under the Distributed Reaction Regime. Numerical calculations indicated that increasing injection temperatures resulted in a less distributed reactor, as experimental conditions transitioned away from Distributed Reaction Regime.
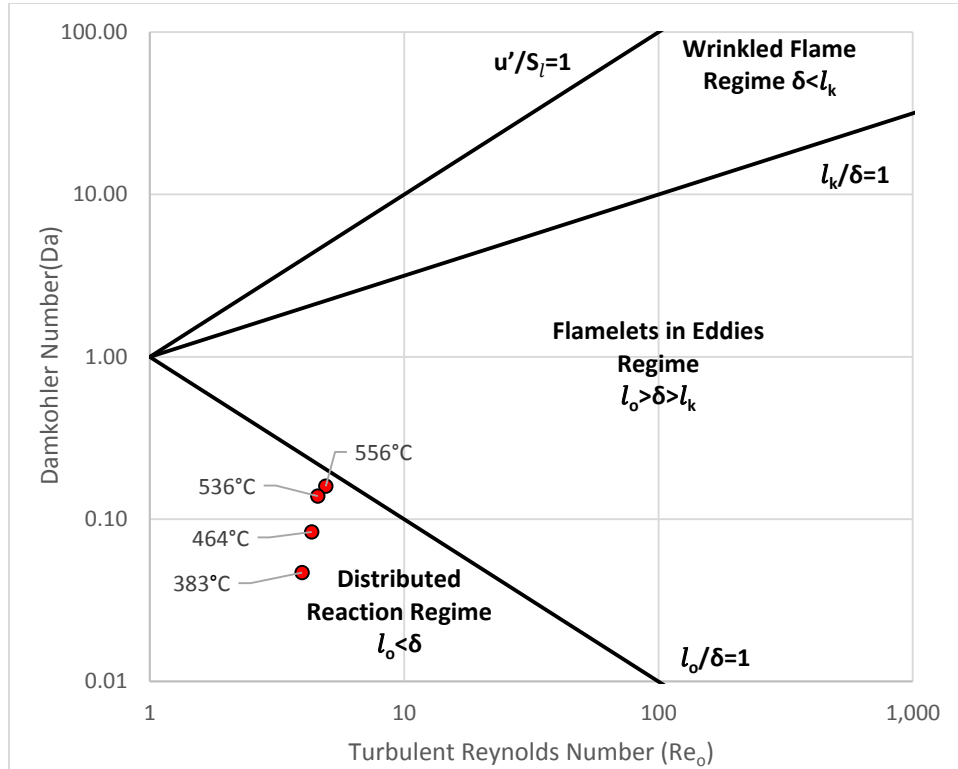
Figure 7-2. Flame regime with injection temperatures of 383 to 555°C at O/C=1.0

Higher injection temperatures fostered conditions that accelerated the laminar flame speed and shortened the laminar flame length (thickness). The integral length scales were found to range between 1.88-1.91 mm. Turbulent velocity increased from 0.91 to 1.25 m/sec with increasing injection temperature. Laminar flame speed increased from 9.9 to 22.5 cm/sec, while laminar flame thickness decreased from 4.1 mm to 2.1 mm.

7.1.2 Reformate Composition

Variations in injection temperatures produced a noticeable impact to reformate composition. As the reactor became less distributed, due to an increase in injection temperatures, hydrogen and carbon monoxide concentrations were adversely affected, see Figure 7-3. Similar to the low temperature work detailed in Chapter 6.2, the less distributed conditions promoted hydrocarbon formation, see Figure 7-4. Reformate composition changed rapidly as experimental conditions approached the Damkohler Criterion. However, carbon dioxide concentrations were not strongly influenced by either injection temperatures or reaction regime. The high concentrations of carbon monoxide and low concentrations of carbon dioxide indicated complete mixing had occurred.

Previous low temperature work detailed in Chapter 6.2 indicated that, under Distributed Reaction Regime, higher injection temperatures showed a small increase in the hydrogen content of the reformate, but adversely affected product distribution. In that work, reactor conditions occurred below optimum temperatures (less than 1000°C). As injection temperatures increased, reactor conditions occurred closer to optimum temperatures, slightly improving hydrogen yields. Increased reactor temperatures offset the negative effects of a less distributed reactor.

In the current work, the reactor conditions met or exceeded the optimum temperatures (900-1000°C). As injection temperatures rose, the negative effects of the reactor transitioning away from Distributed Reaction Regime became more apparent.

Reported syngas composition for catalytic partial oxidation of JP-8 have consisted of 24% hydrogen and 24% carbon monoxide[1]. Syngas composition

179

shown here approached that of catalytic reforming, consisting of 19.2±0.20% hydrogen and 20.8±0.21% carbon monoxide. The non-catalytic literature[14] of jet fuel shows hydrogen and carbon monoxide concentrations of 14% and 19%, respectively. Hydrogen and carbon monoxide concentrations demonstrated in this work exceeded those demonstrated in the low temperature reactor[50] detailed in Chapter 6.
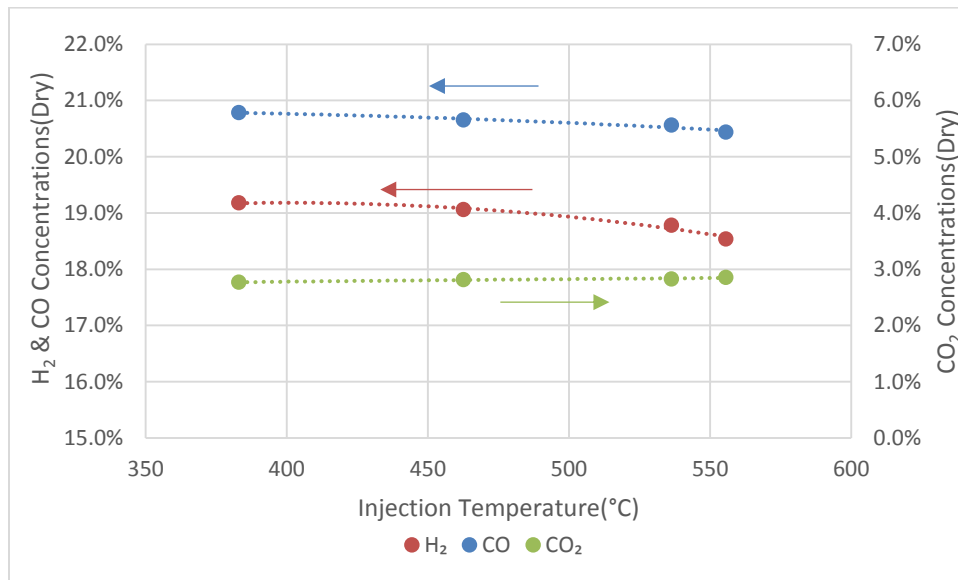
Figure 7-3. Fixed gas concentrations with injection temperatures of 383 to 555°C at O/C=1.0

Of the hydrocarbons detected, only methane was detected in considerable amount. However, methane is a desirable hydrocarbon. Solid oxide fuel cells can internally reform methane, allowing direct utilization of methane. Propane and acetylene were detected only in trace quantities (less than 15 ppm), see Figure 7-4. Propane and acetylene concentrations were detected near the lower calibration limit for the micro-GC (10 ppm lower limit). In the low temperature distributed reactor[50] ethylene, ethane, and trace amounts of higher hydrocarbons (butane and hexane) were

detected, but were not detected within the high temperature reactor work presented here. Literature shows that optimum reforming conditions occurred at higher reactor temperatures[103]. Higher temperatures are associated with the dissociation, steam reforming, and dry reforming of methane and other simple hydrocarbons.
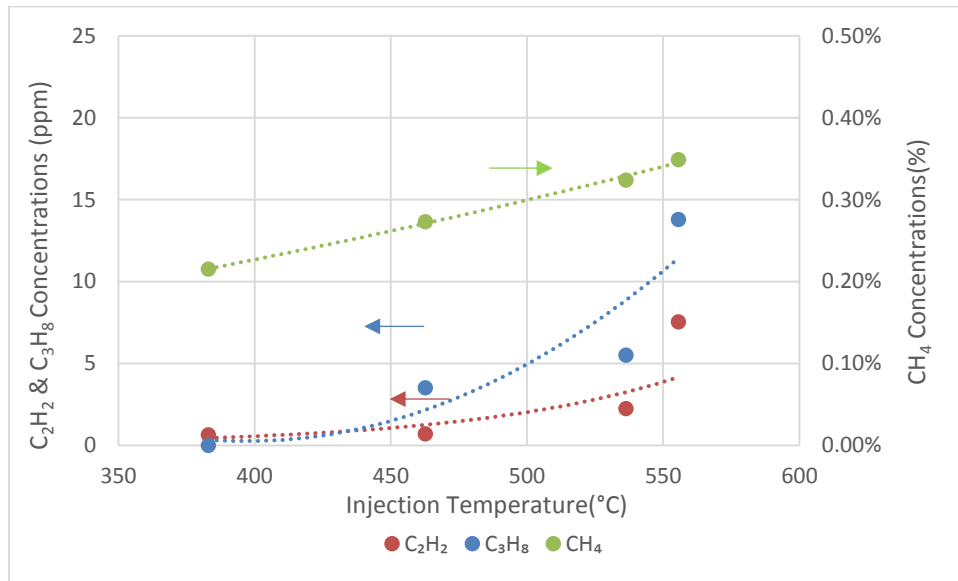
Figure 7-4. Hydrocarbon formation with injection temperatures of 383 to 555°C at O/C=1.0

Lower injection temperatures promoted increased conversion. This is attributed to the reactor becoming more distributed. Enhanced conversion will also increase reforming efficiency as more fuel is converted. Conversion was significantly higher than the lower temperature reactor reported in Chapter 6.
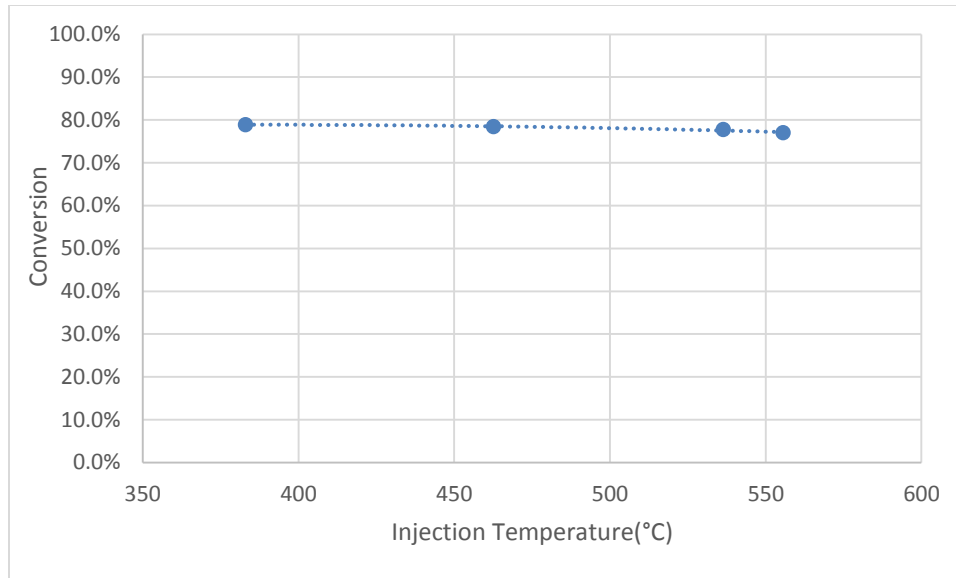
Figure 7-5. Conversion with injection temperatures of 383 to 555°C at O/C=1.0

Reforming efficiency ($\eta_{H_2,CO}$) was calculated through Eq. 1-4. Increased injection temperatures caused the reactor to become less distributed, which decreased reformate quality and reformer efficiency. The low yield of hydrocarbons resulted in comparable efficiency between the two reforming efficiencies calculated for $\eta_{H_2,CO}$ and η_{H_2,CO,CH_4}. Uncertainty in the conversion and efficiency calculations was no greater than ±1.7% and ±1.67%, respectively.

Previous work on Distributed Reaction Regime at low temperature conditions, detailed in Chapter 6, showed reforming efficiency to be between 35.6-40.7±1.35% ($\eta_{H_2,CO}$) and 56-57±1.87% (η_{H_2,CO,CH_4}) at comparable conditions. In this work, reforming efficiency ranged from 56.4-58.6±1.67% ($\eta_{H_2,CO}$). Methane constituted 19-36% of the recovered energy, while reforming at low temperature conditions. Methane only accounted for 1-2% of the recovered energy in high temperature conditions. The higher reactor temperatures promoted the dissociation, steam reforming, and dry reforming of methane, which in turn generated higher

182

concentrations of both hydrogen and carbon monoxide. Notably, the reformate concentrations presented here are significantly better than that reported in previous non-catalytic reforming studies[9,12,50]. Reforming efficiency for catalytic partial oxidation ranged from 75-85%[1], but are susceptible to sulfur poisoning.
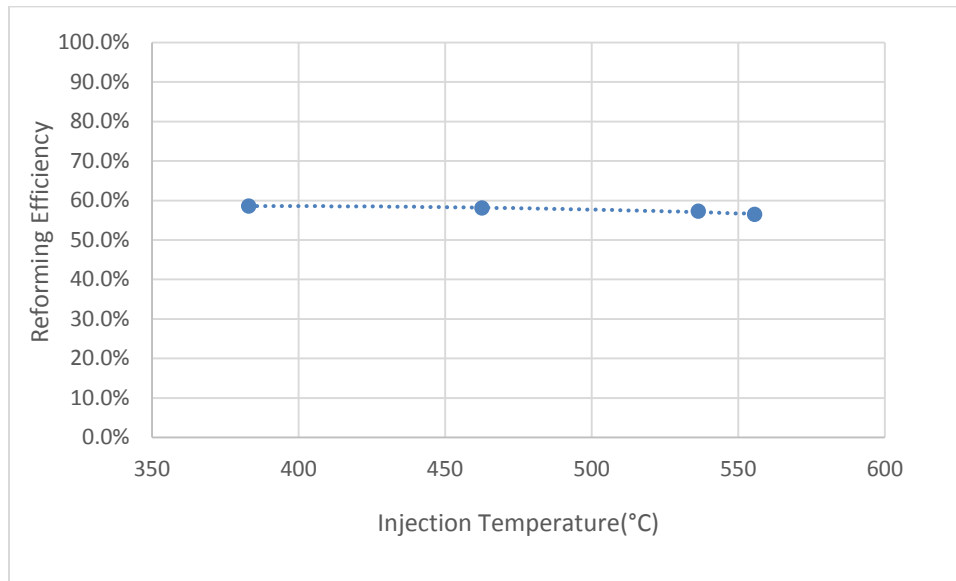
Figure 7-6. Reforming efficiency with injection temperatures of 383 to 555°C at O/C=1.0

7.1.3 Section Summary

Air preheats were used to control the characteristic chemical properties, while minimizing the effect on the characteristic turbulent properties. Higher preheats foster a more rapid chemical reaction, which results in a shorter chemical time and length scales. This increases the Damkohler number and results in less distributed conditions.

The syngas obtained was of better quality in terms of product distribution, which approached that of catalytic reforming. Here, syngas consisted of 19.2±0.20% hydrogen and 20.8±0.21% carbon monoxide. Literature has shown catalytic reformate

is typically composed of 24% hydrogen and 24% carbon monoxide[1]. A majority of non-catalytic approaches only yielded syngas that were at most 14% hydrogen and 19% carbon monoxide[14].

The interaction of reformate product distribution to injection temperature was of significant importance. Lower injection temperatures promoted conditions that favored the formation of higher quality reformate. Numerical diagnostics indicated that the reaction regime became less distributed with higher injection temperatures, negatively influencing the reformate quality. The lower quality reformate negatively impacted reforming efficiency. Reformate quality changed more rapidly as reaction regime approached the Damkohler Criterion.

7.2 Effect of Oxygen on Chemical Time Scales

Reactor oxygen concentrations had a significant influence on reactor chemistry and characteristic chemical properties. As the reactions were limited by the availability of oxygen, additional oxygen promoted higher conversion. However, increasing reactor oxygen concentrations also fostered a more rapid chemical reaction, which shortened the chemical time and length scales to result in a less distributed condition. While a less distributed reactor typically results in lower quality reformate (reduction of steam and dry reforming reactions), increasing the limiting reactant (oxygen) fostered greater conversion through partial oxidation. In this particular case, the less distributed conditions generated lower yields of steam and carbon dioxide in the exhaust products, minimizing the potential for steam and dry reforming reactions. Reactor oxygen concentrations were varied to reveal the impact

184

on the thermochemical behavior and reformate product distribution. Flame regime was calculated using the numerical approach outlined in Section 3.1.

As determined in Chapter 6.2, oxygen to carbon ratio (O/C) had a significant impact on reformer performance and reaction regime. O/C ratios were used to control the chemical time and length scales, while injection temperature was maintained at 375°C. As air composed ~97% of the volumetric flow rate, changes in fuel feed rates had minimal impact on the characteristic turbulent time and length scales. This resulted in the reactor operating at a thermal load of 4.4 to 5.1 kW$_{th}$.

Air and fuel feeds were independently heated then mixed prior to injection. Fuel was vaporized at 300°C, which was high enough to allow complete vaporization but low enough to prevent carbon formation[138]. Air was injected at a constant flow rate of 30 SLPM (at 21°C and 1 atm), while air preheats were used to maintain a constant injection temperature of 375°C. Reynolds numbers ranged from 3989 to 4075. The reactor was operated under near design conditions to minimize wear on the reactor. The JP-8 employed had a hydrogen content of 14.4%, with a heating value of 43.6MJ/kg. Carbon balance indicated 83-98% detection. Lower carbon balance corresponded with lower oxygen to carbon ratios, which resulted in soot forming in exhaust line.

Running without steam induced greater wear on the reactor and some deposits were noted downstream of the reactor. While the Distributed Reaction Regime reduced wear on the reactor, ignition and shutdown occurred under a conventional flame. Preferred operation of the reactor occurred with the smallest oxygen to carbon ratio.

185

7.2.1 Flame Regime

Numerical calculations, as detailed in Section 3.1, were used to calculate flame regime. Under all conditions evaluated (preheats of 375°C and O/C=1.04-1.20), the reactor operated within the Distributed Reaction Regime. An increase in oxygen content fostered a more rapid chemical reaction, which increased the laminar flame speed (9.99 cm/sec to 13.12 cm/sec) and decreased laminar flame thickness (0.41 cm to 0.35 cm). Integral length scale and turbulent velocity remained unaffected by an increase in O/C ratio, both remaining constant at 1.88 mm and 1.28 m/sec, respectively. An increase in O/C ratio and the resulting change in characteristic chemical properties, caused an increase in Damkohler number and a minor decrease in Turbulent Reynolds number. Figure 7-7 shows that an increase in oxygen content caused the flame regime to shift away from the Distributed Reaction Regime toward the Flamelets in Eddies Regime.
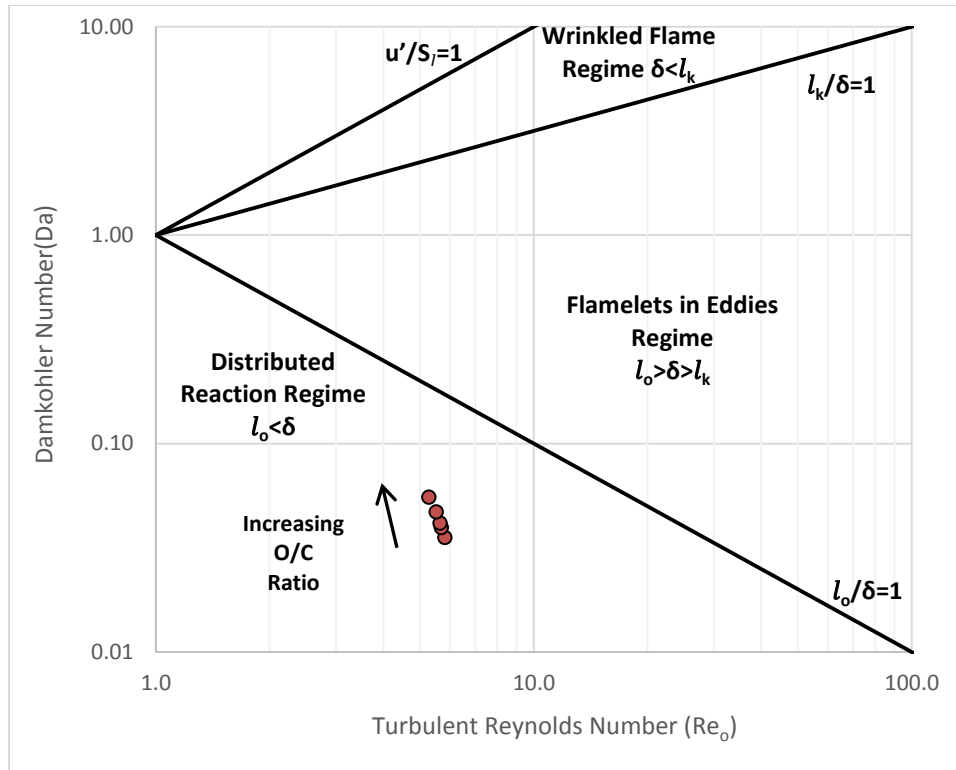
Figure 7-7. Flame regime under dry partial oxidation conditions at molar O/C ratio of 1.04 to 1.20

7.2.2 Reformate Composition

Reformate chemical composition was strongly influenced by the availability of oxygen, and to a lesser extent, the flame regime. Syngas composition consisted of $20.7\pm0.21\%$ to $22.3\pm0.23\%$ hydrogen and $20.2\pm0.21\%$ to $21.5\pm0.22\%$ carbon monoxide, see Figure 7-8 and Figure 7-9. Carbon dioxide was detected at concentrations of $2.35\pm0.02\%$ to $2.85\pm0.03\%$, see Figure 7-9.

Up to an O/C ratio of 1.10, an increase in oxygen content promoted higher concentrations of hydrogen. Under regimes of low conversion, the reactor generated low yields of syngas. Under this condition, an increase in oxygen content was more likely to oxidize the unconverted hydrocarbons than the limited syngas produced. At O/C ratios greater than 1.10, a reduction in hydrogen concentrations was noted. In

regimes of high conversion, the reactor generated higher yields of syngas and lower

yields of unconverted hydrocarbons. Under regimes of high conversion, the added

oxygen content became more likely to oxidize the more abundant syngas than the

remaining hydrocarbons. This is supported by a small increase in reactor

temperatures, as shown in Figure 7-13.

In the low temperature reactor detailed in Section 6.1, air preheats of 450°C

resulted in peak hydrogen formation occurring at a similar O/C ratio (O/C=1.10).

However, hydrogen concentrations in the high temperature reactor were almost twice

as much as what was reported at lower operating temperatures. Higher reactor

temperatures, steam reforming, and dry reforming of hydrocarbons, which enhanced

conversion.
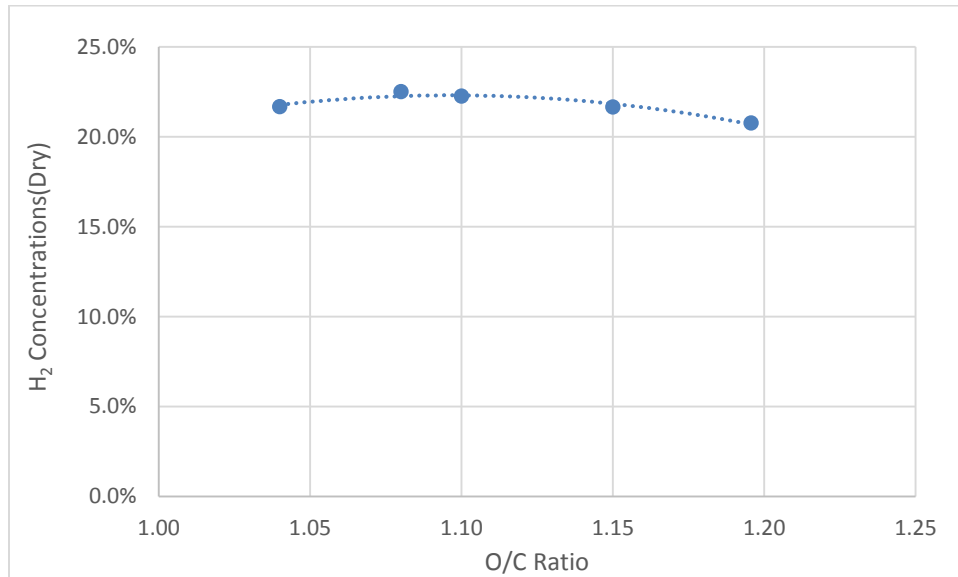
Figure 7-8. Hydrogen concentrations at O/C=1.04 to 1.20

Additional oxygen content promoted the formation of carbon monoxide, while

carbon dioxide remained unaffected, see Figure 7-9. It was expected that after peak

conversion, additional oxidant content would promote the oxidation of carbon

monoxide. There was concern that operating without steam may produce an adverse condition, limiting the reactor operational behavior and longevity.
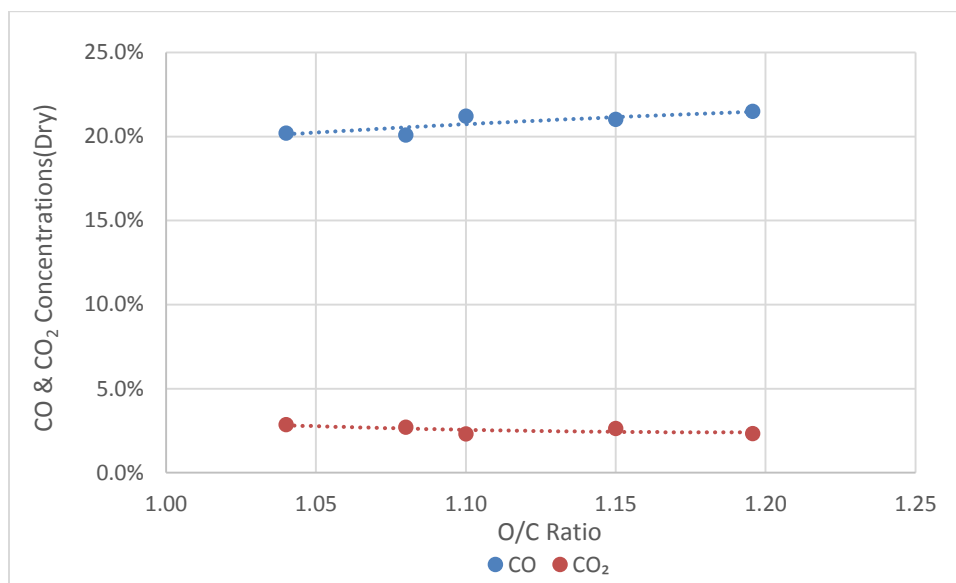
Figure 7-9. Carbon monoxide and carbon dioxide concentrations at O/C=1.04 to 1.20

The gas chromatograph detected low concentrations of methane and ethylene in the reformate. Figure 7-10 shows methane concentrations ranging from 0.12%±12 ppm to 0.28%±29 ppm. The highest methane concentrations correspond to the lowest O/C ratios. Trace amounts of ethylene (0.01%±10 ppm) were detected only at an O/C ratio of 1.08. This may be the result of instrumental error. The gas chromatograph detected no other hydrocarbon present in the reformate.

In comparison, when operating at lower reactor temperatures (700-800°C), as detailed in Section 6.1, preheats of 450°C generated a wide range of hydrocarbons, ranging from 5.09±0.05% methane to 0.18%±18 ppm hexane. The lower reactor temperatures suppressed the steam reforming, and dry reforming of hydrocarbons. This in turn caused the excess oxygen to oxidize the syngas (carbon monoxide and hydrogen), resulting in higher water and carbon dioxide yields. Operating at higher

reactor temperatures (900-1100°C) promoted the dry reforming, and steam reforming reactions, which enhanced syngas yields and conversion, see Figure 7-11 and Figure 7-12.
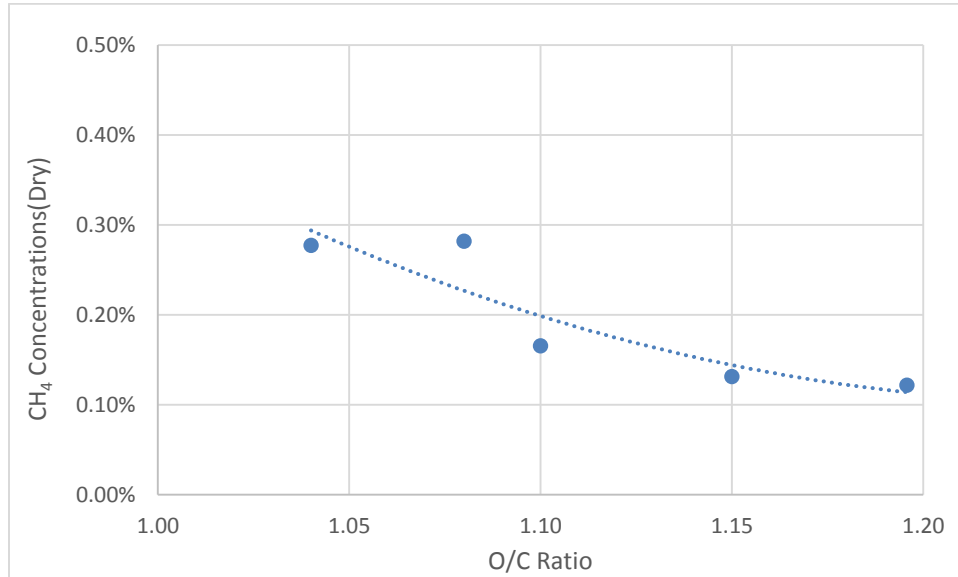
Figure 7-10. Methane concentrations at O/C=1.04 to 1.20

Increasing oxygen to carbon ratios enhanced conversion. As conversion increased, more hydrogen and carbon monoxide were released, which enhanced reforming efficiency. Reforming efficiency $(\eta_{H_2,CO})$ is presented only for PMFC, as lower hydrocarbon formation was relatively low and did not affect the reformate quality. Uncertainty in the conversion and efficiency calculations was no greater than ±2.10% and ±2.20%, respectively.

The availability of oxygen limited the extent of the reforming reactions. Increasing oxygen content fostered a more rapid chemical reaction, which shortened chemical time and length scales, resulting in less distributed conditions. In previous works[63,146], this would have resulted in poorer reformate quality, as it would have minimized the potential of steam and dry reforming reactions. However, the negative

190

effects of the reactor becoming less distributed were offset by the increased

availability of the oxygen. As the reactions were limited by the availability of oxygen,

the addition of oxygen enhanced the extent of reforming reactions, promoting

increased conversion and reforming efficiency. In addition, the more distributed

condition (lower O/C ratios) produced less combustion products, minimizing the

reactions caused by the entrained products.
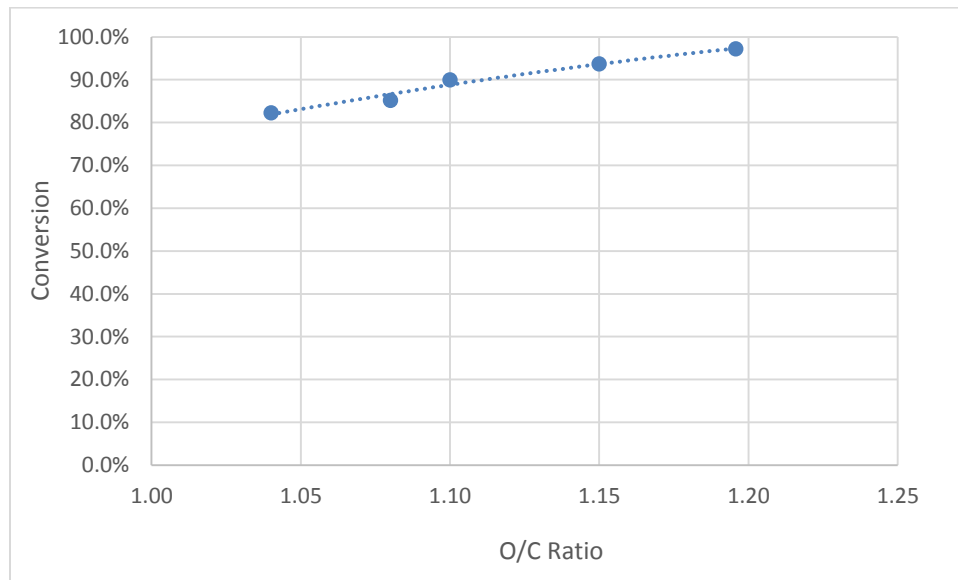
Figure 7-11. Conversion at O/C=1.04 to 1.20

As discussed previously, under regimes of low conversion, an increase in

oxygen content caused a strong improvement to conversion. This results from oxygen

being more likely to oxidize the more abundant unconverted hydrocarbons than the

less abundant syngas. In regimes of high conversion, the addition of oxygen was less

beneficial, as the reactor generated higher yields of syngas and lower yields of

unconverted hydrocarbons. The additional oxygen content was more likely to oxidize

the more abundant syngas than the remaining hydrocarbons.
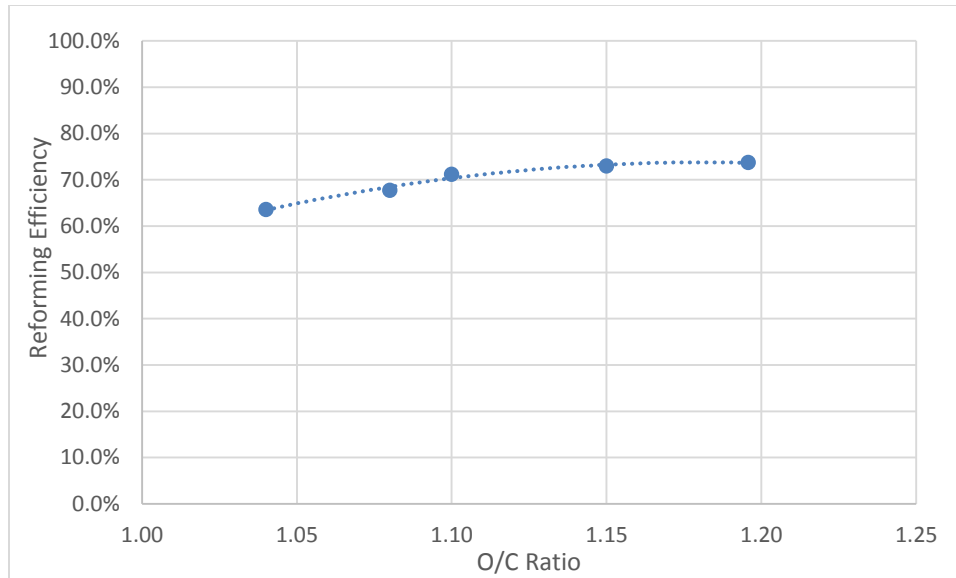
Figure 7-12. Reforming efficiency at O/C=1.04 to 1.20

Reactor oxygen concentrations had a strong impact on reactor temperature, as shown in Figure 7-13. An increase in the O/C ratios (reducing fuel feed) from 1.04 to 1.10 lowered the thermal loading on the reactor from 5.12 kWt$_h$ to 4.8 kWt$_h$, which resulted in a decrease to the reactor temperatures. At an O/C ratio of 1.10, the reactor was at its coolest, which also corresponded to the highest hydrogen concentrations. At O/C ratios greater than 1.10, the reactor temperature increased, which was attributed to the increased oxidation of the syngas. Figure 7-8 and Figure 7-13 show that hydrogen concentrations diminished as reactor temperature increased.

An increase in oxygen content resulted in a small change in the overall reactor temperature. The entrainment of reactants necessary for achieving the Distributed Reaction Regime spreads heat over a larger volume, developing a uniform temperature field. An increase in oxygen content promoted the partial oxidation reactions; however, the heat generated was less apparent due to the uniform thermal field.
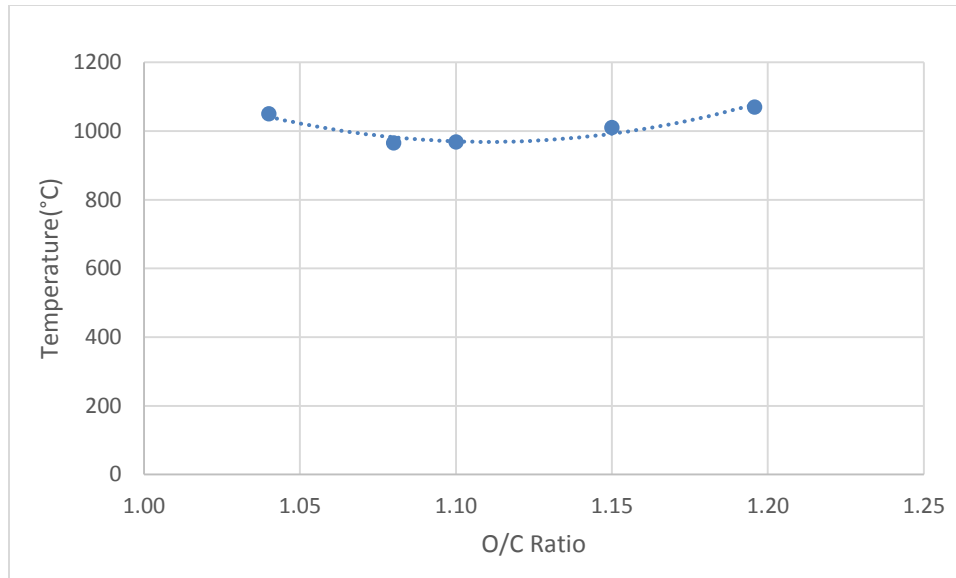
Figure 7-13. Reactor temperature at O/C=1.04 to 1.20

7.2.3 Section Summary

Oxygen content has a pronounced effect on the Distributed Reaction Regime and reformate yields. Increasing reactor oxygen concentrations allowed greater conversion through partial oxidation reactions, directly improving reforming efficiency. A similar trend was observed when operating at low temperatures, detailed in Section 6.1.

Reformate composition was most strongly influenced by the availability of the limiting reactant (oxygen) and to a lesser extent, flame regime. An increase in O/C ratios fostered a more rapid chemical reaction, which shortened the chemical time and length scales, resulting in a less distributed reactor. In previous works[63,146], this would have resulted in poorer reformate quality, as it limited the potential for added steam and dry reforming reactions caused through the entrainment of exhaust products. However, the negative effects of the reactor becoming less distributed were offset by the increased availability of oxygen. As the reactions were limited by the

availability of oxygen, the addition of oxygen enhanced the extent of reforming reactions, promoting both increased conversion and reforming efficiency. In addition, the more distributed condition (lower O/C ratios) produced less combustion products, minimizing the reactions caused by the entrained products.

Lower reactor oxygen concentrations reduced the activity of partial oxidation reactions, which lengthened the characteristic chemical time and length scales. This resulted in a more distributed condition within the reactor. However, the reduced activity of the partial oxidation reactions reduced the conversion and reforming efficiency.

Syngas composition consisted of 20.7±0.21% to 22.3±0.23% hydrogen and 20.2±0.21% to 21.5±0.22% carbon monoxide. Low concentrations of methane were observed from 0.12%±12 ppm to 0.28%±28 ppm. Ethane was detected up to 0.01%±10 ppm, only at an O/C ratio of 1.08. The reformer demonstrated reforming efficiency of 63.6±1.8% to 73.8±2.2% and conversion of 82.3±1.8% to 97.2±2.1%. At lower oxygen-to-carbon ratios (O/C=1.04-1.10), an increase in the O/C ratios resulted in a significant increase to both conversion and hydrogen concentrations. However, at higher O/C ratios (O/C=1.10 to 1.15), an increase in oxygen content was not as effective in improving conversion. The added oxygen content was believed to have promoted the oxidation of the syngas. This is supported by increased reactor temperatures and decreased hydrogen concentrations.

Reactor temperatures were found to depend on reactor oxygen concentrations. Initially, increasing the O/C ratio to 1.10 reduced the reactor temperature, as a result of reduced thermal loading. At O/C of 1.10, peak hydrogen concentrations were

observed, which corresponded to the coolest reactor conditions. However, at oxygen-to-carbon ratios greater than 1.10, reactor temperature increased as the added oxygen promoted the oxidation of the syngas

7.3 Wet Partial Oxidation Effect on Chemical Time Scales

The addition of steam to partial oxidation, also known as wet partial oxidation, was used as an alternative means to control characteristic chemical length and time scales. The addition of steam increases turbulent velocity, while reducing laminar flame speed, to promote a more distributed condition. The addition of steam delays ignition, thus allowing more time for the reactants to mix before ignition occurs.

The addition of steam to partial oxidation promoted both steam reforming and water gas shift reactions, which enhanced the hydrogen concentrations in the syngas. Steam has commonly been employed in the catalytic reforming process as either a primary or secondary oxidizer[8]. Steam enhanced syngas yields, reduced soot formation, and protected the catalysts. Limited information was available in the literature on non-catalytic reactors employing steam[16].

However, only a limited amount of steam should be added to avoid detrimental effects to the reforming process. Prior data reveals that optimum results should occur between steam to carbon ratios of 0.0 to 0.60[16]. The endothermic nature of the steam reforming reactions reduces the reactor temperature, which limits the chemical kinetics. To a lesser extent, steam can act as a thermal diluent, further reducing the reactor temperature. The addition of steam to the premixed fuel-air

mixture enhances volumetric flow rates, which reduces the average residence time of reactants in the reactor. From the literature, it was determined active steam reforming reactions require temperatures of at least 800-1000°C[16,58–63].

Reformate chemical composition was a result of the balance between the faster, highly exothermic partial oxidation reaction (R. 7-1), the slower endothermic steam reforming (R. 7-2), and the water gas shift (R. 7-3) reactions. The heat of reaction (ΔH_r) for reactions R. 7-1 to R. 7-3 was calculated assuming dodecane feedstock. Steam reforming generates higher yields of hydrogen, but it is limited by its endothermic nature. Partial oxidation is an exothermic reaction, but it produces lower yields of hydrogen. The water gas shift reaction can shift the composition of the reformate to favor higher concentrations of hydrogen, but only occurs after partial oxidation and steam reforming reactions. The faster oxidative reactions are conjectured to occur before the slower steam reforming and water gas shift reactions.

$$C_xH_y + \left(\frac{x}{2}\right)O_2 \rightarrow \left(\frac{y}{2}\right)H_2 + xCO \quad ; \quad \Delta H_r = -1319\frac{kJ}{mol} \qquad \text{R. 7-1}$$

$$C_xH_y + xH_2O \rightarrow \left(x + \frac{y}{2}\right)H_2 + xCO \; ; \quad \Delta H_r = 1583\frac{kJ}{mol} \qquad \text{R. 7-2}$$

$$CO + H_2O \rightarrow H_2 + CO_2 \qquad ; \quad \Delta H_r = -41\frac{kJ}{mol} \qquad \text{R. 7-3}$$
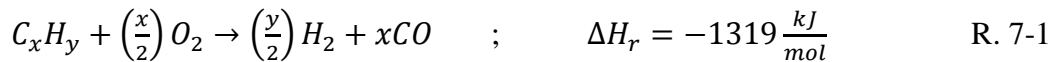
Under ideal conditions, only a limited amount of fuel will be oxidized to generate the heat necessary for the onset of endothermic steam reforming reactions. However, the reactor temperature must be maintained, to avoid hindering the chemical kinetics. Excess oxygen will promote the partial oxidation of the fuel and reduce the amount of fuel available to undergo steam reforming. Excess oxygen also has the potential to oxidize the reformate. Insufficient oxygen reduces both reactor

196

temperature and activity of steam reforming reactions, resulting in reduced conversion.

Under wet partial oxidation, reformate composition is a function of the equilibrium steam reforming and partial oxidation reactions. Therefore in order to understand the related effects both molar steam to carbon (S/C) and oxygen to carbon (O/C) ratios were varied over the range of S/C=0.0-0.25 and O/C=1.04 -1.15, respectively. Oxygen to carbon ratios below 1.04 were restricted due to low conversion. As steam is the more desirable oxidizer, it was evaluated over a wider range than oxygen. In this work, the steam to carbon ratio was increased until reformate quality degraded. The reactor was operated at 4.6-5.1kWth. The airflow rate was fixed at 30 SLPM (1atm. and 21°C), while fuel and steam flow rates were varied to adjust the molar ratios of oxygen to carbon and steam to carbon. Reynolds numbers ranged from 4012 to 4560. The JP-8 employed had a hydrogen content of 14.4%$_{mass}$, with a heating value of 43.6 MJ/kg. A polynomial curve fit of the data was provided to show the trends and to enhance legibility of the data. As the effects of the exothermic partial oxidation reactions and endothermic steam reforming reactions are interrelated the data will be presented first, followed by an explanation of the trends. A carbon balance of 95-100% was achieved, indicating complete detection within the margin of error.

7.3.1 Flame Regime

Turbulent flame regime was determined through numerical calculation conducted in manner outlined in Section 3.1. Figure 7-14 presents the relevant flame regimes for the various experimental conditions. Increasing steam content caused the

reactor to become more distributed, as it shifted away from the Flamelets in Eddies
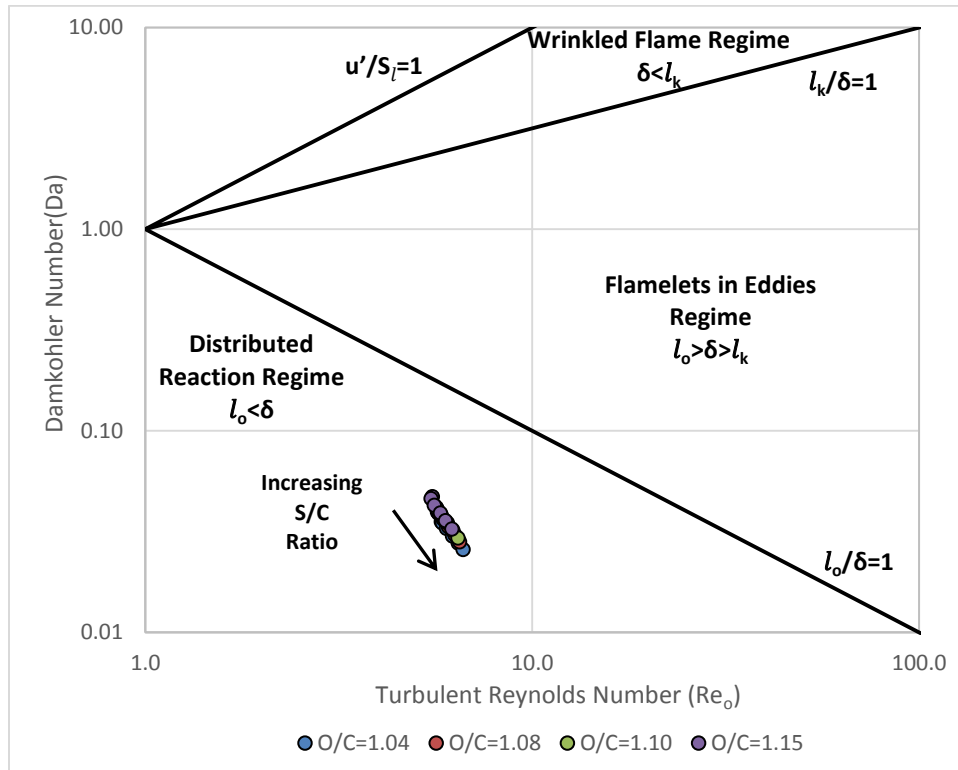
Regime.

Figure 7-14. Flame regime determined through numerical calculations at S/C=0.0-
0.25 and O/C=1.04 -1.15

For a fixed oxygen to carbon ratio, the addition of steam promoted a more

Distributed Reaction condition. Increasing the S/C ratios from 0.0 to 0.23 reduced the

laminar flame speed from 11.83 to 8.68 ms and elongated the laminar flame length

from 0.37 cm to 0.45 cm. The characteristic turbulent properties were affected to a

lesser extent. Turbulent velocity increased from 1.28 to 1.39 m/sec, while integral

length scale was determined to be consistently between 1.88-1.89 mm. Steam also

tended to delay ignition, which resulted in enhanced time for mixing. This presents as

a decrease in the Damkohler number, but an increase in the Turbulent Reynolds

number.

However, increasing the O/C ratio, while maintaining a constant S/C ratio, promoted a less distributed condition as Damkohler number decreased. Higher oxygen content fostered a more rapid chemical reaction, which shortened the characteristic chemical time and length scales. For example, under dry partial oxidation conditions, as O/C ratio increased from 1.04 to 1.15, the laminar flame length decreased from 0.41 cm to 0.37 cm; while laminar flame speed increased from 9.99 cm/sec to 11.83 cm/sec. Characteristic turbulent properties remained near constant. As air composes ~97% of the volumetric flow rate, changes in fuel feed rates would have minimal impact to the characteristic turbulent time and length scales.

While adding oxygen results in a less distributed reactor, a certain amount of oxygen is required for the reaction to propagate and provide the necessary heat for endothermic steam reforming reactions. However, this amount must be limited, in order to maintain high reforming efficiency.

7.3.2 Reformate Composition

Reformate product distribution was affected by the flame regime and availability of oxidants. The addition of steam, even in trace amounts (S/C~0.01), drastically altered reactor temperature and reformate composition, which also promoted a more distributed reactor, see Figure 7-15 to Figure 7-18. The syngas composition consisted of high concentrations of both hydrogen ($21.7\pm0.22\%$ to $24.8\pm0.25\%$) and carbon monoxide ($20.1\pm0.21\%$ to $23.3\pm0.24\%$). Only small amounts of methane ($0.13\%\pm13$ ppm to $1.04\%\pm106$ ppm) and trace amounts of acetylene ($0.0\%\pm10$ ppm to $0.06\%\pm10$ ppm) and ethylene ($0.0\%\pm10$ ppm to

0.08%±10 ppm) were detected. Additional oxygen content negatively influenced

hydrogen formation, as observed in Figure 7-16A. For a constant S/C ratio of 0.11,

increasing O/C ratios from 1.04 to 1.15 decreased hydrogen concentrations from

24.5±0.25% to 23.0±0.23%. Previous work detailed in Section 6.1 showed that small

changes in the O/C ratio had a more limited effect on syngas composition[50].
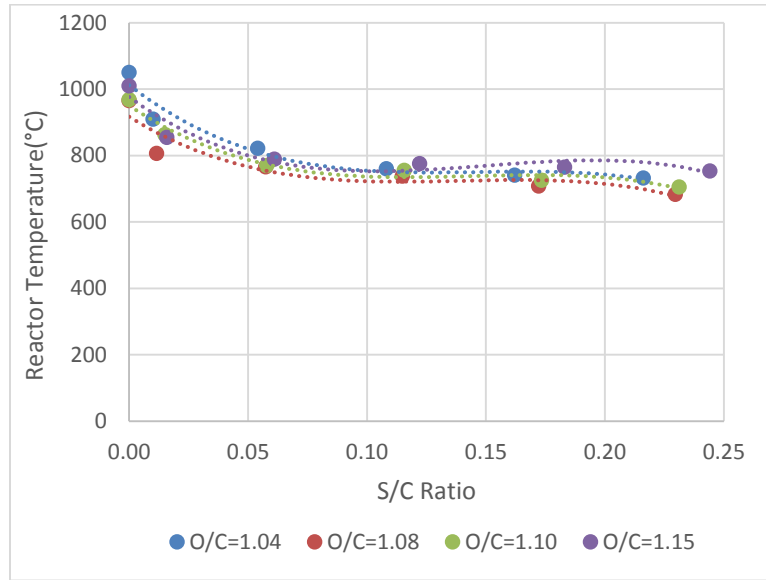
Figure 7-15. Reactor temperature
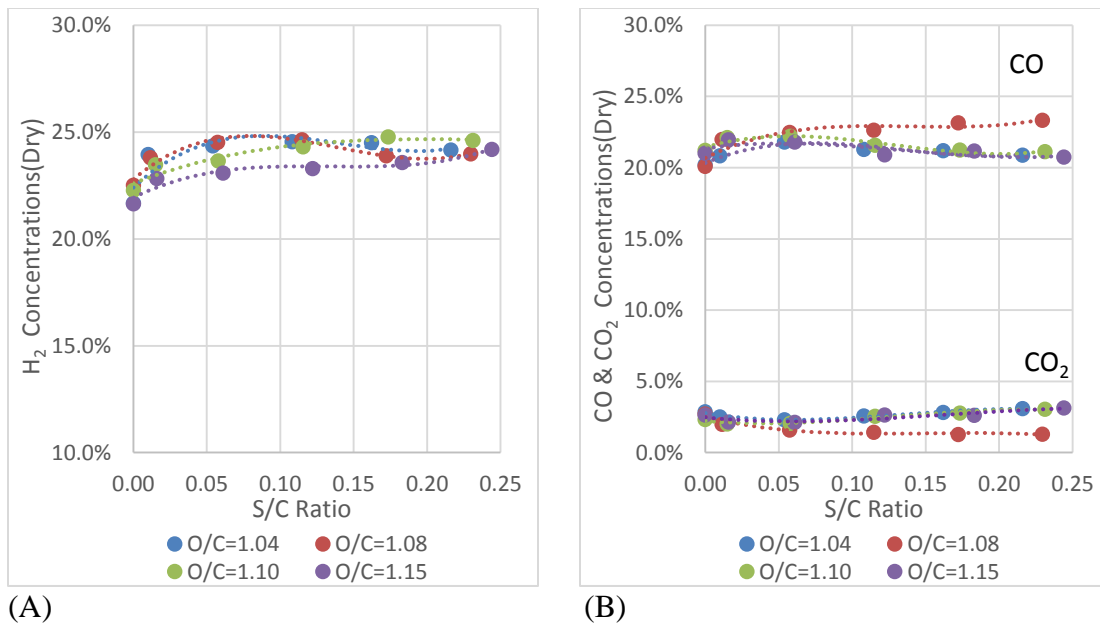
(A)

(B)

Figure 7-16. Fixed gas concentration: (A) Hydrogen, (B) Carbon monoxide and
Carbon dioxide

(A)

(B)

(C)
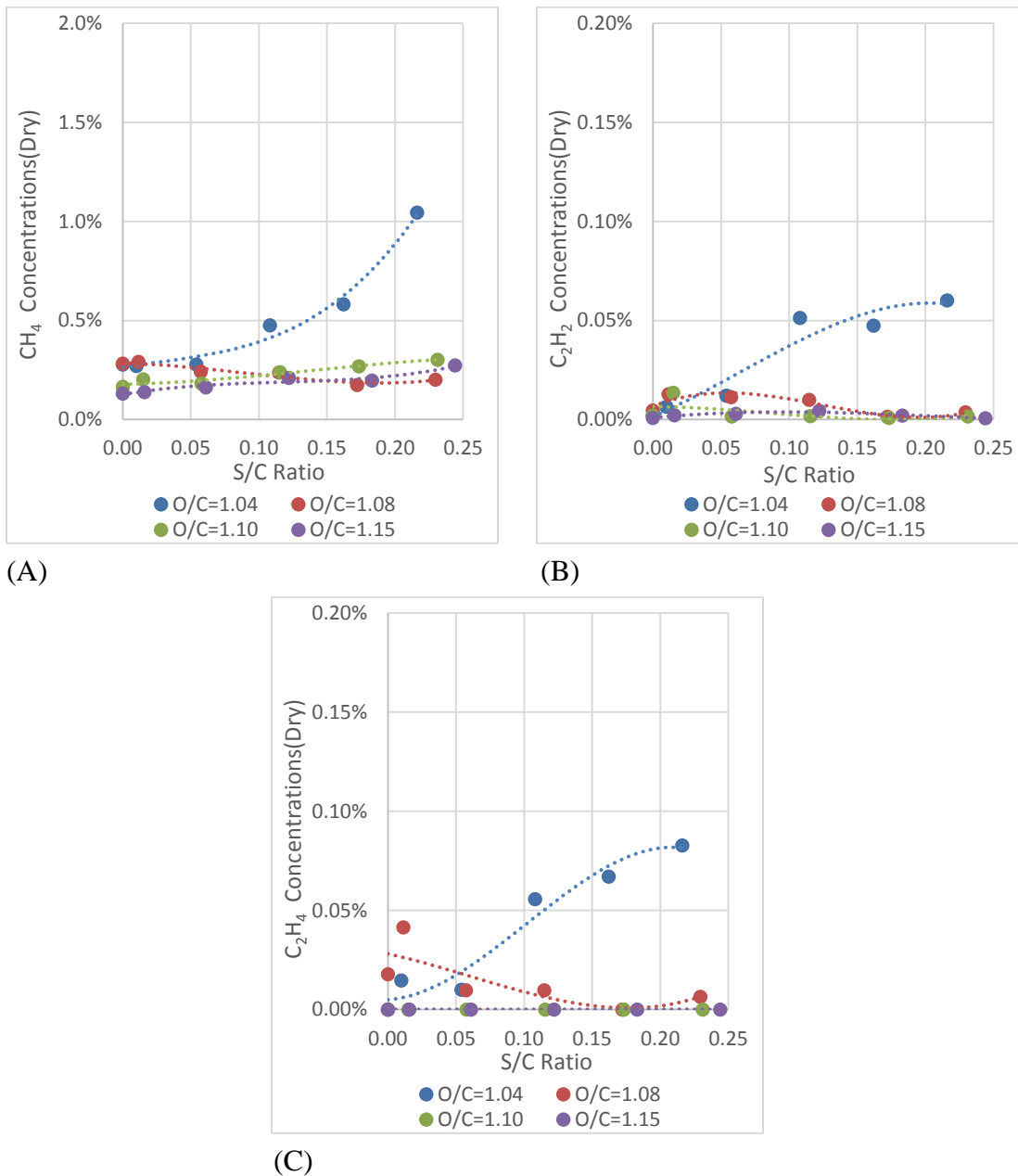
Figure 7-17. Hydrocarbon concentrations: (A) Methane concentrations, (B) Acetylene concentrations, (C) Ethylene concentrations

The reformer demonstrated high reforming efficiencies $(\eta_{H_2,CO})$ ranging from 63.3±1.8% to 80.1±2.3%, as calculated by Eq. 1-4. Reforming efficiency is defined as the ratio of the lower heating value (LHV) of the syngas to the lower heating value of the fuel. Hydrocarbon conversion was between 82.2±1.7% to 99.9±2.06%, as

calculated by Eq. 1-6. Conversion (η_{conv}) is a measure of fuel oxidation, defined as the ratio of combined sum of molar flow rates of the carbon monoxide and carbon dioxide to the molar flow rate of the carbon present in the fuel. Conversion and efficiency are presented in Figure 7-18. Uncertainty in the reforming efficiency calculation was found to be no more than ±2.3% of reported value. Uncertainty in the conversion calculation was found to be no more than ±2.08% of the reported value.

(A)   (B)
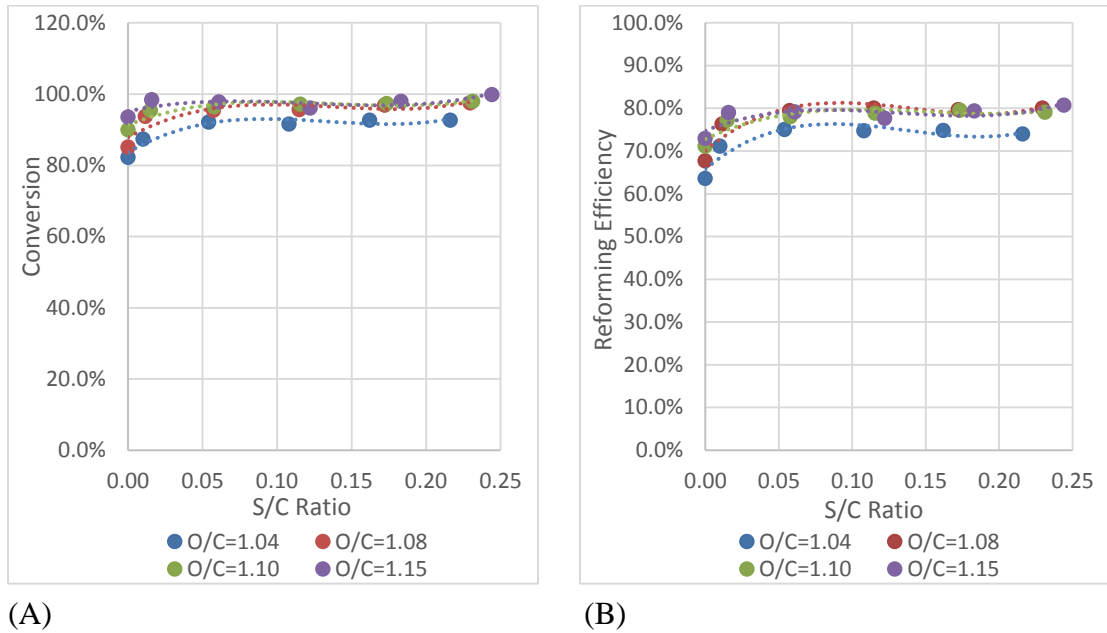
Figure 7-18. Reformate quality: (A) Conversion, (B) Reforming efficiency

7.3.3 Effect of Steam on Wet Partial Oxidation

Reactor temperature is primarily a function of the equilibrium between the partial oxidation and the endothermic steam reactions and to a lesser extent, thermal dilution, demonstrated in Figure 7-15 to Figure 7-18. Increasing S/C ratios altered this equilibrium, by enhancing the activity of the steam reforming reactions. Steam reforming reactions absorb ~20% more energy than that which is released through

partial oxidation, which results in steam having a stronger influence on reactor temperature.

The dry partial oxidation case (S/C=0.0) resulted in the hottest reactor temperature, as expected. The reactor temperature ranged from 965±7.2°C to 1050±7.9°C, as shown in Figure 7-15. Under the dry partial oxidation conditions, reformate conversion was at its lowest, with no condition achieving conversion greater than 93.7±1.9%, as shown in Figure 7-18A.

At all evaluated O/C ratios, inclusion of trace amounts of steam (at S/C=0.01-0.05) activated the steam reforming reactions. This was demonstrated by a 4.8±3.98% to 9.89±3.61% increase in conversion and 6.2±4.1% to 11.8±4.3% increase in reforming efficiency, as shown Figure 7-18. This also corresponded to a 212±13.4°C decrease in reactor temperature, as shown in Figure 7-15.

However, the increase in conversion exceeded what could be accounted for by steam reforming alone, which was most notable at a S/C ratio of 0.01. From the dry partial oxidation case (O/C=1.08), the addition of trace amount of steam (S/C=0.01) improved conversion by 8.63±3.76%. However, the small amount of added steam could only improve conversion by at most 1.59±0.03%, assuming the added steam promoted steam reforming reactions. This additional increase in conversion was attributed to the reactor becoming more distributed.

At higher S/C ratios of 0.10 to 0.20, reforming conversion and reforming efficiency reached a maximum value. Reactor temperatures remained stable at 750±5.6°C, declining only slightly, as observed in Figure 7-15. In this regime, it was conjectured that the additional steam did not significantly enhance the endothermic

steam reforming reactions, as there was no significant increase in conversion or decrease in temperature. The small degradation in the reactor temperature was attributed to thermal dilution, caused by the presence of additional steam. Reformate composition changed slightly and this is attributed to the influence of water gas shift reaction. Reactor temperatures became too low to sustain steam reforming reactions. Literature indicated that steam reforming reactions require reactor temperatures of at least 800-1000°C[16,58–63].

Peak conversion occurred at lower S/C ratios, as O/C ratios increased, as shown in Figure 7-18A. As partial oxidation reactions are considered to occur before steam reforming reactions, an increase in oxygen content enhances the activity of the partial oxidation reactions and reduces the amounts of fuel available to undergo steam reforming. This resulted in enhanced conversion at lower steam to carbon ratios. Under dry conditions, at an O/C ratio of 1.04, only 82.2±1.7% of the fuel was converted through partial oxidation; but at a higher O/C ratio of 1.15, conversion was as high as 93.7±1.92%.

With the exception of O/C ratio of 1.04, increasing steam to carbon ratio suppressed ethylene and acetylene formation. Figure 7-17B and Figure 7-17C show no ethylene and acetylene formation at S/C ratio in excess of 0.15. However, at an O/C ratio of 1.04, S/C ratios greater than 0.15 caused an increase in hydrocarbon formation.

As S/C ratios approach 0.25, the addition of steam became detrimental to the reforming process. This was most noticeable at lower O/C ratios. Figure 7-15 and Figure 7-16A show a decrease in hydrogen concentrations and a slight decrease in the

204

reactor temperature. Although reformate quality degraded, the reactor was still stable under these conditions. This degradation is within the margin of error.

With the exception of O/C ratio of 1.08, the addition of steam beyond a S/C ratio of 0.01, appeared to activate the water gas shift reaction. At O/C ratios of 1.1 to 1.15, increase in S/C ratio from 0.01 to 0.23, resulted in a decrease in carbon monoxide concentrations (-1.0±0.44%) and an increase in both hydrogen (1.2±0.49%), and carbon dioxide (0.97±0.05%) concentrations, presented in Figure 7-16.

7.3.4 Effect of Oxygen on Wet Partial Oxidation

Oxygen content had a pronounced effect on the conversion, as the O/C ratio increased from 1.04 to 1.15, conversion increased from 82.2±1.7% to 96.7±1.9%. Partial oxidation provides the heat necessary for steam reforming to occur. Therefore, the availability of oxygen, steam, and fuel will govern the product distribution. Oxygen was adjusted until there was a noticeable change in reformate, while operating the reactor near peak efficiency.

Variations in O/C ratios had little observable impact on reactor temperature, as observed in Figure 7-15. Oxygen content was evaluated over a more limited range, which limited the change in overall reactor temperature. The entrainment necessary to initiate the Distributed Reaction Regime will spread heat evenly throughout the reactor, which reduces any increase in reactor temperature. A greater impact would be expected if oxygen content were evaluated over a larger range.

At an O/C ratio of 1.04, there was insufficient oxidizer to achieve full conversion, as demonstrated in Figure 7-18A. Under these conditions, the addition of

steam to partial oxidation was only beneficial between S/C ratios of 0.01 to 0.10.

Increasing steam content, only improved conversion up to S/C ratio of 0.05, reaching

a maximum value of 92.7±1.9%. At S/C ratios in excess of 0.10, the excess steam

promoted the formation of lower molecular weight hydrocarbons (such as methane,

acetylene, and ethylene), while reducing hydrogen concentrations, as shown in Figure

7-16 and Figure 7-17.

The availability of excess steam activated the water gas shift reaction at an

O/C ratio of 1.04. As expected at the onset of water gas shift reaction, an increase in

S/C ratios from 0.05 to 0.22 showed a small increase in carbon dioxide (0.79±0.05%)

concentrations, along with a small corresponding decrease in carbon monoxide

(-0.90±0.44%) concentrations, as shown in Figure 7-16.

Increasing the O/C ratio to 1.08 increased reforming efficiency up to

80.1±2.3%, with hydrogen concentrations up to 24.6±0.25%, as shown in Figure

7-16A and Figure 7-18B. These concentrations and performance are very similar to

those of catalytic reformers and demonstrate the feasibility of employing a non-

catalytic reforming approach as a replacement for catalytic reformers for their direct

application in solid oxide fuel cell systems.

Higher O/C ratios enhanced the activity of partial oxidation reactions,

releasing more heat. This in turn promoted endothermic steam reforming reactions. It

was conjectured that at an O/C ratio of 1.08, there was sufficient steam, air, and heat

to convert fuel through steam reforming and partial oxidation reactions, but the

amount of steam was insufficient to activate the water gas shift reaction. Increasing

S/C ratios from 0.0 to 0.23, increased carbon monoxide concentrations by 3.2±0.4%,

but caused a 1.4±0.04% decrease in carbon dioxide concentrations, which indicated that the water gas shift reaction was not active. However, increasing the S/C ratios from 0.0 to 0.23 increased conversion by 12.4±3.86% and reduced reactor temperature by 282±12.4°C, indicating that the additional steam enhanced the activity of the steam reforming reactions. Peak conversion (97.6±2.08%) was achieved at an S/C ratio of 0.23. At O/C ratios of 1.08 and higher, there was sufficient heat available that increasing S/C ratios did not promote the formation of hydrocarbons, as seen at an O/C ratio of 1.04.

Generally, catalytic reactors use greater amounts of steam (S/C=1.0-2.0) than what was used in the present study (S/C=0.0-0.25), which is sufficient to activate both steam reforming and water gas shift reactions[8].

At higher oxygen to carbon ratios (O/C>1.08), the activity of oxidative reactions increased, thus reducing the amount of fuel available to undergo steam reforming. This resulted in increased conversion occurring at lower O/C ratios, but reduced hydrogen concentrations. For a fixed S/C ratio of 0.02, increasing the O/C ratio from 1.10 to 1.15 increased conversion from 95.5±2.0% to 98.5±2.0%. As steam reforming reactions became less active, excess steam became available to support the water-gas shift reaction. After peak conversion, an increase in S/C ratios caused a drop in carbon monoxide concentrations (-1.0±0.44%) and an increase in both hydrogen (1.2±0.49%), and carbon dioxide (0.97±0.05%) concentrations, as presented in Figs. 3-4. This supports the assertion that the water gas shift was active.

The addition of oxygen had a stronger impact on the formation of hydrogen than the formation of carbon monoxide. Figure 7-16A shows that increasing the O/C

ratios negatively affected hydrogen concentrations. For example, at a constant S/C ratio of 0.11, increasing the O/C ratio from 1.04 to 1.15 decreased hydrogen concentrations from 24.5±0.25% to 23.0±0.23%. Since the distributed reactor entrains exhaust products into the fuel-air charge, hydrogen is more readily oxidized than other gases, such as CO, CH_4, and C_2H_2, which causes a more pronounced effect on hydrogen concentrations.

7.3.5 Section Summary

Wet partial oxidation has been shown to enhance reformate yields over that of the dry partial oxidation case. Steam was found to foster a more distributed reaction environment, which promoted a higher quality reformate. The addition of steam to the premixed fuel-air mixture resulted in decreased Damkohler numbers and increased Turbulent Reynolds numbers. Steam delayed ignition, allowing more time for exhaust products to entrain into the premixed jet. Steam, even in trace amounts, was found to improve the reformate quality.

JP-8 fuel reforming under wet partial oxidation conditions demonstrated a substantial increase in the reformate quality. The reactor achieved high reforming efficiencies up to 80.1±2.3%, which is comparable to the results reported using catalytic reforming. Syngas was composed of high concentrations of hydrogen (21.7±0.22% to 24.8±0.25%) and carbon monoxide (20.1±0.21% to 23.3±0.24%). Only small amounts of methane (0.13%±13 ppm to 1.04%±106 ppm) and trace amounts of acetylene (0.0%±10 ppm to 0.06%±10 ppm) and ethylene (0.0%±10 ppm to 0.08%±10 ppm) were detected. These results demonstrate the viability of non-catalytic approach too efficiently reform JP-8.

Under the dry partial oxidation case, the reactor ranged between $965\pm7.2°C$ to $1050\pm7.9°C$, and this was the highest temperature observed. With the addition of trace amounts of steam, reactor temperature drastically decreased due to endothermic steam reforming reactions. At S/C ratios of 0.10 to 0.20, the reactor temperature stabilized. Under these conditions, the reformer achieved near full conversion. As S/C ratios approached 0.25, reactor temperature and reformate quality began to degrade from the thermal dilution of the steam.

Variations in oxygen content had little impact on observed reactor temperatures. The role of oxygen content in the feed stream was evaluated over a limited range, which limited the overall change in reactor temperature. In addition, the entrainment/thermal dilution necessary to foster the Distributed Reaction Regime spreads heat evenly throughout the reactor, minimizing the change in reactor temperature. Steam was found to have a stronger influence than oxygen on reactor temperature. This was a result of steam reforming reactions absorbing ~20% more energy than was released from partial oxidation reactions, which suggests that steam has the greatest impact on reactor temperature.

Insufficient oxygen (O/C=1.04) reduced conversion and reformer efficiency. At peak performance (O/C=1.08), it was conjectured that there was sufficient steam, air, and heat to convert all the fuel through steam reforming and partial oxidation reactions, but insufficient steam to activate the water gas shift reaction. Excess oxygen (O/C>1.10) enhanced oxidative reactions, reducing fuel available to undergo steam reforming reactions and subsequently limited the performance.

Chapter 8: Conclusion and Recommendations for Future Work

8.1 Conclusion

This work determined it was both possible and beneficial to achieve the Colorless Distributed Conditions within fuel rich reforming regime. Under certain conditions, reformate quality was comparable to that produced by catalytic reformers. The Distributed Reaction Regime activated chemical reactions not present under normal reforming conditions. Two reactors were developed within this work to evaluate the low and high temperature conditions within the Distributed Reaction Regime. Flame regime was controlled through variations in the chemical properties, while minimizing changes to the turbulent properties (turbulent mixing). It was determined that flame regime, reactor temperature, and the availability of the oxidizer had a discernable impact to reformate product distribution and reforming efficiency.

Through the course of the investigation, it was observed that conditions that promoted a more distributed reactor yielded higher quality reformate. In the low temperature reactor, more distributed conditions shifted the hydrocarbon carbon distribution to favor ethylene and methane over acetylene. In the higher temperature reactor, this resulted in higher hydrogen and carbon monoxide yields. It was theorized that the benefits from the Distributed Reaction Regime are derived from entrainment of the hot exhaust products into the fuel-air mixture. The more distributed conditions reduce the activity in the partial oxidation reactions and allowing greater entrainment. The entrained exhaust products influence the reaction in two ways.

The entrainment of exhaust products, in particular steam and carbon dioxide, have been shown in combustion literature to suppress soot formation[16,54–56]. Soot

210

abatement is induced through dilution and chemical interactions of the carbon dioxide and steam. Steam and carbon dioxide promote hydroxyl radical formation, which interferes with the acetylene formation and the hydrogen abstraction carbon addition (HACA) soot formation mechanism[16,54–56]. Conditions occurring within the Flamelet in Eddies Regime caused the partial oxidation reactions to propagate faster, limiting entrainment. Little to no carbon deposits were observed within the reactor, while operating under the Distributed Reaction Regime for either reactor. Some carbon was observed within the insulation expansion joints, but this was expected. As this region is outside of the bulk flow, the reactions are thought not to be distributed. Any fuel entering this region would undergo cracking and promote soot deposition.

At higher reactor temperatures of 800-1100°C, the entrained exhaust products (steam and carbon dioxide) promote the potential for steam reforming and to a lesser extent dry reforming reactions, enhancing reformate yields. As mentioned previously, the more distributed condition promoted greater entrainment; and this corresponded to increased potential for steam and dry reforming reactions. Adding additional steam (wet partial oxidation) will only increase this effect. It is thought that the Distributed Reaction Regime will be influenced primarily by steam reforming reactions, as the Distributed Reaction Regime promotes a well-mixed condition (minimizing carbon dioxide formation) and steam reforming reactions are considered up to three times faster[57]. Dry reforming reactions are still thought to occur, but are not as active. This is supported by minimal changes to carbon dioxide. In conventional partial oxidation, steam reforming reactions only occur toward the rear of the reactor, where in distributed reforming they occur throughout the reactor.

8.1.1 Low Temperature Reactor

The low temperature reactor allowed direct visual observation of the flame regime. The Distributed Reaction Regime's impact to the reformate product distribution became more discernable at lower temperatures, as there was a wider product distribution within the reformate to observe. Optical access allowed direct observation of the reaction zone and direct visualization of soot formation. Flame regime was controlled through chemical time and length scales, which were adjusted through the O/C ratios and mixture preheats. Two approaches allowed verification of the Distributed Reaction Regime's effects. Reactor temperatures ranged between $764\pm5.7°C$ to $874\pm6.5°C$. Also, operating at temperatures below ideal conditions generated low yields of hydrogen and significant hydrocarbon formation.

Operating at temperatures ($764\pm5.7°C$ to $874\pm6.5°C$) below ideal conditions ($1000°C$) generated low yields of hydrogen and significant hydrocarbon formation. The reformate consisted of $8.68\pm0.09\%$ to $9.92\pm0.10\%$ hydrogen and $18.12\pm0.18\%$ to $18.58\pm0.19\%$ carbon monoxide. Reactor temperature was low enough that oxygen was detected in the exhaust. A wide range of hydrocarbons was detected, ranging from $5.09\pm0.05\%$ methane to $0.18\%\pm18$ ppm hexane. However, hydrogen concentrations were greater than that was reported in conventional reforming literature for comparable conditions[16,103].

Lower reactor temperatures ($764\pm5.7°C$ to $874\pm6.5°C$) limited the activity of reactions associated conventional reforming reactions (partial oxidation and pyrolysis) and those promoted by the Distributed Reaction Regime (steam and dry reforming). Changes in inlet conditions showed little change in the hydrogen and

carbon monoxide concentrations as reactor became more distributed. This supports the limited activity of the steam and dry reforming reactions.

Although reactor temperatures were not sufficient to fully activate steam and dry reforming reactions, the entrainment of exhaust products (steam and carbon dioxide) influenced the hydrocarbon product distribution and the activity of the HACA soot formation reactions. More distributed condition suppressed dehydrogenation reaction associated with acetylene formation and soot formation, which yields hydrocarbons with a higher H/C ratio. In Section 6.1 and Section 6.2, it was observed that for a given O/C ratio, conditions that occurred within the Flamelets in Eddies Regime exhibited higher concentrations of hydrogen, acetylene, and soot, indicating the activity of the HACA mechanism. For conditions that occurred within Distributed Reaction Regime, product distribution was shifted to favor higher concentrations of ethylene and methane, without observable soot formation, indicating a reduction in the HACA mechanism's activity. This in turn influenced reforming efficiency. As the Distributed Reaction Regime favored greater formation of methane, this yielded higher reforming efficiency (η_{H_2,CO,CH_4}) when paired with a SOFC. However, the Flamelet in Eddies Regime promoted additional hydrogen formation through the HACA mechanism, generating higher reforming efficiency ($\eta_{H_2,CO}$) for PEMFC applications.

Visual observations revealed that the Distributed Reaction Regime visual emissions were similar to that of Distributed Colorless Combustion, but with a faint reddish orange hue. In contrast, the flame within a distributed combustor emits as either colorless or with a faint green hue (resulting from C_2 radicals). When reactor

was operated within the Flamelets in Eddies Regime, global imaging revealed a brighter yellow flame, more typical of a conventional reforming flame. A luminous yellow flame represents black body radiation of soot particles at elevated temperatures.

Heat losses profoundly affected reformate quality, as seen by the difference in reformate quality between the high and low temperature reactor. Unlike a combustor, a reformer's goal is to minimize the energy converted to sensible heat and to maximize the chemical potential of hydrogen and carbon monoxide. However, reforming reactions are positively affected by hotter reactor conditions. The reactor must be operated at higher oxygen to carbon ratios to compensate for heat loss, reducing reforming efficiency.

A significant amount of energy is retained in the lower weight molecular hydrocarbons, which can only be directly utilized by a SOFC. Operating with a PMFC would require significant syngas conditioning, which would reduce system level efficiency.

The low temperature reactor allowed the development of a numerical approach to predict the emergence of the Distributed Reaction Regime. Numerical calculations accurately predicted the emergence of the Distributed Reaction Regime and its transition to Flamelets in Eddies Regime at multiple conditions. Visual imagining of the reaction zone confirmed flame regime and transitions. Accurate numerical calculations allowed for development of a well-insulated reactor without the need for optical access.

The Distributed Reaction Regime allowed a stable reaction zone to be established at low O/C ratios, without the need of a flame holder or porous media. Previous work[95] cited instabilities in the flame front at O/C ratios less than 1.26.

8.1.2 High Temperature Reactor

The high temperature reactor was developed based on the geometry of the low temperature reactor, but was operated at optimum reforming conditions. Flame regimes were controlled through variations in the chemical time and length scales, which were adjusted through the O/C ratios, mixture temperature, and steam addition. Reformate quality was notably better than previous low temperature work. The results presented in this work demonstrated the feasibility of using a non-catalytic reformer to achieve a hydrogen rich reformate using a middle distillate fuel. A well-insulated reactor is capable of demonstrating reformate suitable for a SOFC or high temperature PEMFC. Reformate quality was comparable to catalytic reforming and occurred at comparable efficiencies.

Reformate quality was noticeably higher than the low temperature conditions, detailed in Chapter 6. Mitigation of thermal losses from the insulated reactor allowed higher reactor temperatures that were not possible in the prior low temperature reactor studies[145]. Lower heat loss required less fuel to undergo partial oxidation to sustain reactor temperatures.

Within the high temperature reactor (800-1100°C), conditions were sufficient to fully activate the steam and dry reforming reactions, generating higher hydrogen yields. The more distributed conditions reduce the activity in the partial oxidation reaction, allowing greater entrainment and higher activity in the steam and dry

215

reactions. This presents as the more distributed cases yielding higher concentrations of hydrogen and carbon monoxide.

Within Section 7.1, reducing the air preheats promoted a more distributed reactor, which correlated with an increase in conversion and efficiency. Decreasing air preheats increased hydrogen and carbon monoxide concentrations. Under wet partial oxidation conditions shown in Section 7.3, the addition of trace amounts of steam (S/C=0.01) resulted in a more distributed condition and a corresponding increase in conversion up to 8.63±3.76%. However, assuming that all added steam promoted steam reforming reactions; the small amount of added steam could have only improved conversion by at most 1.59±0.03%. This discrepancy in conversion was attributed to the steam reforming induced by the entrained exhaust products.

In Section 7.2, the effects of Distributed Reaction Regime were less discernable, as there were two competing effects. Increasing oxygen content resulted in a less distributed condition, but showed improved reformate quality. However, as the reactions are limited by the availability of oxygen, the addition of oxygen enhanced the extent of reforming reactions. This promoted increased conversion, which offset the negative effects caused by the reactor becoming less distributed. Typically, the more distributed conditions promoted greater entrainment, enhancing steam and reforming reactions. Under this case, the more distributed condition (lower oxygen content) also promoted less steam formation, minimizing the steam and dry reforming reactions that were initiated through entrainment.

It was observed that the more distributed cases generally yielded higher quality reformate and hydrogen concentrations. This improvement was attributed to

the activation of the steam reactions and to a lesser extent dry reforming reactions. From the literature, it was determined that reactor temperatures of at least 800-1000°C[16,58–63,67–71] are required to activate steam and dry reforming reactions. Under all reforming conditions, some steam and carbon dioxide will form in the exhaust products. The entrainment of exhaust products (steam and carbon dioxide) and heat into the fuel-air mixture promoted the potential for steam reforming reactions and to a lesser extent dry reforming reactions. Adding additional steam (wet partial oxidation) will only increase this effect. Less distributed conditions result in a shorter ignition delay, which causes the fuel to ignite before sufficient entrainment can occur, minimizing the steam and dry reforming reactions.

For the dry partial oxidation case, ideal reactor temperatures appeared to be 900-1000°C. However, with the addition of steam, lower reactor temperatures of 700-900°C became viable. This was attributed to the activation of additional kinetic pathways (steam reforming reactions), enhancing conversion.

Reactor temperatures were found to be dependent on oxidizer concentrations and preheat. Even trace amounts of steam were found to reduce reactor temperatures due to the promotion of the endothermic steam reforming reactions. However, at conditions near full conversion, the addition of steam no longer promoted additional steam reforming and appeared to have a diminished effect. Reactor temperatures also dropped below conditions which literature indicated active steam reforming reactions would typically have occurred. Oxygen concentrations had a unique effect on reactor oxygen concentrations. Initially increasing oxygen to carbon ratios to 1.10 reduced reactor temperature, resulting from reduced thermal loading. At oxygen to carbon

217

ratios of 1.10 peak hydrogen concentrations formed, which corresponded to the coolest reactor conditions. However, at oxygen to carbon ratios greater than 1.10, reactor temperature increased as the added oxygen promoted the oxidation of the syngas. Elevating preheats quickly elevated reactor temperatures, which damaged the internal thermocouple within the reactor. This was not repeated as simulations indicated that reactor temperatures would be sufficient to damage thermocouples.

Under regimes of low conversion, an increase in oxidizers (oxygen and steam) caused a strong improvement to conversion. This resulted from oxidizers being more likely to oxidize the more abundant unconverted hydrocarbons than the less abundant syngas. In regimes of high conversion, the addition of oxidizer was less effective, as the reactor generated higher yields of syngas and lower yields of unconverted hydrocarbons. In the case of oxygen, the additional oxygen content was more likely to oxidize the more abundant syngas, than the remaining hydrocarbons.

Operating under wet partial oxidation yielded superior reformate quality than under dry partial oxidation. Under dry partial oxidation, the syngas was composed of $20.7\pm0.21\%$ to $22.3\pm0.22\%$ hydrogen and $20.2\pm0.21\%$ to $21.5\pm0.22\%$ carbon monoxide. Wet partial oxidation yielded a syngas consisting of $21.7\pm0.22\%$ to $24.8\pm0.25\%$ hydrogen and $20.1\pm0.21\%$ to $23.3\pm0.24\%$ carbon monoxide. Even low S/C ratios of 0.05 were found to have a strong impact on reformate concentrations. Steam was found to reduce reactor wear and promote better reformer operations. The additional steam also prevented soot formation from occurring downstream of the reactor.

218

At low steam to carbon ratios (S/C=0.05), a small increase in acetylene and ethylene concentrations over the dry partial oxidation case (S/C=0.0) occurred. This was attributed to instabilities in the pulp causing fluctuations in steam concentrations. At higher steam to carbon ratios of 0.10-0.25, no acetylene and ethylene were detected. Steam can only be added in limited amounts as it increases the potential for quenching.

Out of the three approaches employed to foster the distributed conditions, steam was the strongest approach. An increase in steam fostered a more distributed condition within the reactor, while simultaneously promoting steam reforming reactions, which in turn increased conversion. Increasing the oxygen to carbon ratios improved conversion, but resulted in less distributed conditions. Decreasing preheats was found to enhance reforming conversion and efficiency, but it did not provide the same level of performance as wet partial oxidation.

The higher operating temperatures maximize syngas yields and reduce hydrocarbon formation. This enhances the compatibility with fuel cell systems as the reformer can operate with either high temperature PEMFC or SOFC. Higher temperatures promoted higher reforming efficiencies, making it competitive with diesel generator technology.

8.2 Recommendations

Primary emphasis of this work was to develop a fundamental understanding of reforming within the Distributed Reaction Regime. Recommendations for future research focus on maturating the technology and broadening the scope of this research.

8.2.1 Catalytic Distributed Reforming

The addition of catalysts to the Distributed Reaction Regime yields superior results over non-catalytic distributed reformation. The Distributed Reaction Regime's uniform thermal field and suppression of soot formation should enhance the durability of a catalyst. The well-mixed nature of the distributed reactor will suppress hot spots, preventing catalyst sintering.

Catalysts should be selected to promote steam reforming reactions. The Distributed Reaction Regime was able to support a stable flame at low temperatures (700-800°C); however, the reactor was limited to low steam to carbon ratios. Non-catalytic steam reforming was only observed at temperatures greater then 800-1000°C. Catalyst could promote steam reforming reactions at lower temperatures of 700-800°C. Nickel is employed most commonly in reforming due to its high activity and low cost. However, it has a tendency to promote soot formation reactions. As demonstrated by this work, the Distributed Reaction Regime may suppress this.

8.2.2 Alternative Fuels

JP-8's high sulfur content and tendency to form carbon make it a challenging fuel to reform. However, this technique can be used with other challenging fuels that are prone to contamination and tendency to form carbon. Potential candidates are fuel oils, waste oils, and diesels. The non-catalytic distributed reforming process has the potential to reform a wide range of fuels with little potential for damage. Slurries of biomass could also be compatible with this approach. The higher temperatures may also help mitigate tar formation, which can occur under gasification conditions.

Diesel is expected to produce syngas with a comparable product distribution. Its higher poly-aromatic content may require higher temperatures.

8.2.3 Kinetic Mechanism

The primary purpose of this investigation was to characterize the thermochemical behavior of reforming under Distributed Reaction Regime. Within this work, a kinetic mechanism designed for combustion was used to provide an initial understanding of reactor development. However, this kinetic mechanism was a poor predictor of hydrocarbon formation under fuel rich conditions. Current mechanisms are as large as 15,742 reactions with as many as 417 species. The size and complexity of this mechanism prevents direct numerical simulations using CFD, which would aid in reformer design. Development of a reduced kinetic mechanism designed specifically for reforming would offer an enhanced understanding of the relationship between turbulent transport and chemistry. Kinetics should be included for partial oxidation, steam reforming, pyrolysis, soot formation, and potentially steam reforming.

While the proposed mechanism would focus on homogeneous reforming reactions, this could be employed in conjunction with a heterogeneous catalytic mechanism. Typically, modeling of heterogeneous catalytic reforming ignores the homogeneous phase or uses global mechanism to approximate homogenous phase reactions. However, detrimental olefin formation is thought to occur in the homogeneous phase[147]. A reduced mechanism would allow for a better understanding of catalytic reactors and the true reactants reaching the catalyst's surface.

By applying the Distributed Reaction Regime to reforming, this work established a new form of reforming that yields results comparable to non-catalytic reforming. Future work should focus on refining and developing this approach.

Chapter 9: Appendices

Appendix A: Publications

A.1 Journal Publications

- Scenna, Richard, and Ashwani K. Gupta. 2015. "Partial Oxidation of JP8 in a Distributed Reactor." Fuel Processing Technology 134: 205-213.

- Scenna, R., and Gupta, A., 2016, "Preheats Effect on Distributed Reaction Fuel Reforming," J. Energy Resour. Technol., 138, 1–7.

- Scenna, Richard, and Ashwani K. Gupta. 2016. "Partial Oxidation of JP8 in a Well-Insulated Distributed Reactor." Fuel Processing Technology 142: 174-181.

- Scenna, Richard, and Ashwani K. Gupta. 2017, "Dry and Wet Partial Oxidation in a Distributed Reactor," Int. J. Hydrogen Energy. 42(7), 4102–4110.

A.2 Conference Publications

- Scenna, Richard, and Ashwani K. Gupta. "Soot Formation Reaction Effect in Modeling Thermal Partial Oxidation of Jet," Proceeding of ASME Power Energy Conference 2014. Baltimore, MD, 2015

- Scenna, Richard, Terry DuBois, and Ashwani K. Gupta, "Chemical Modeling of Thermal Partial Oxidation of a JP8/Jet A Surrogate," Proceeding of 46th Army Power Sources, Orlando, FL, 2014

- Scenna, Richard, Ashwani K. Gupta, "Preheats Effect on Distributed

Reaction Fuel Reforming," Proceeding of ASME Power Energy Conference 2015, San Diego, Ca, 2015

- Scenna, Richard, Terry DuBois, and Ashwani K. Gupta, "Effect of Oxygen and Steam on JP8 Fuel Reforming in a Distributed Reactor," Proceeding of 47th Army Power Sources, Orlando, FL, 2016

- Scenna, Richard, Ashwani K. Gupta, "Wet Partial Oxidation of JP8 in a Well-Insulated Reactor," Proceeding of ASME Power Energy Conference 2016, Charlotte, NC, 2016

- Scenna, Richard, Ashwani K. Gupta, "Effect of Oxygen to Carbon Ratios on the Distributed Flame Regime," Proceeding of ASME Power Energy Conference 2017, Charlotte, NC, 2017

- Scenna, Richard, Ashwani K. Gupta, "Influence of Distributed Reaction Regime on Fuel," Proceedings of the ASME 2017 International Design Engineering Technical Conferences & Computers and Information in Engineering Conference 2017, Cleveland, OH, 2017

B.1 Calibration Standard

	Channel	Species	Standard 1	Standard 2
1	A	Hydrogen	49.354%	24.5271%
2	A	Nitrogen	20.762%	49.154%
3	A	Methane	4.993%	0.2965%
4	A	CO	2.066%	23.7396%
5	B	CO2	18.219%	0.9911%
6	B	Ethylene	3.052%	0.0991%
7	B	Ethane	1.522%	0.0792%
8	B	Acetylene	10 ppm	570 ppm
9	C	Propane	30 ppm	987 ppm
10	C	Propylene	21 ppm	798 ppm
11	C	n-butane	20 ppm	775 ppm
12	C	t-2 butene	13 ppm	594 ppm
13	C	isobutylene	30 ppm	898 ppm
14	C	1-butene	21 ppm	695 ppm
15	C	c-2-butene	8 ppm	495 ppm
16	C	isopentane	31 ppm	999 ppm
17	C	n-pentane	20 ppm	801 ppm
18	C	pentenes	ppm	ppm
19	C	Cis-2-pentene	9 ppm	273 ppm
20	C	1-pentene	31 ppm	997 ppm
21	C	trans-2-pentene	22 ppm	720 ppm
22	C	2,3 dimethylpentane	10 ppm	97 ppm
19	D	isobutane	30 ppm	994 ppm
20	D	hexane plus	%	%
21	D	n-hexane	10 ppm	397 ppm
22	D	2-methyl-2-butene	0 ppm	8 ppm
23	D	2-methyl-1-butene	0 ppm	4 ppm
24	D	3-methylpentane	0 ppm	13 ppm
25	D	methylcyclopentane	0 ppm	17 ppm
26	D	2,2, dimethylpropane	0 ppm	3 ppm

Table 9-1 Calibration Standards

B.2 Gas Chromatograph Peak Identification
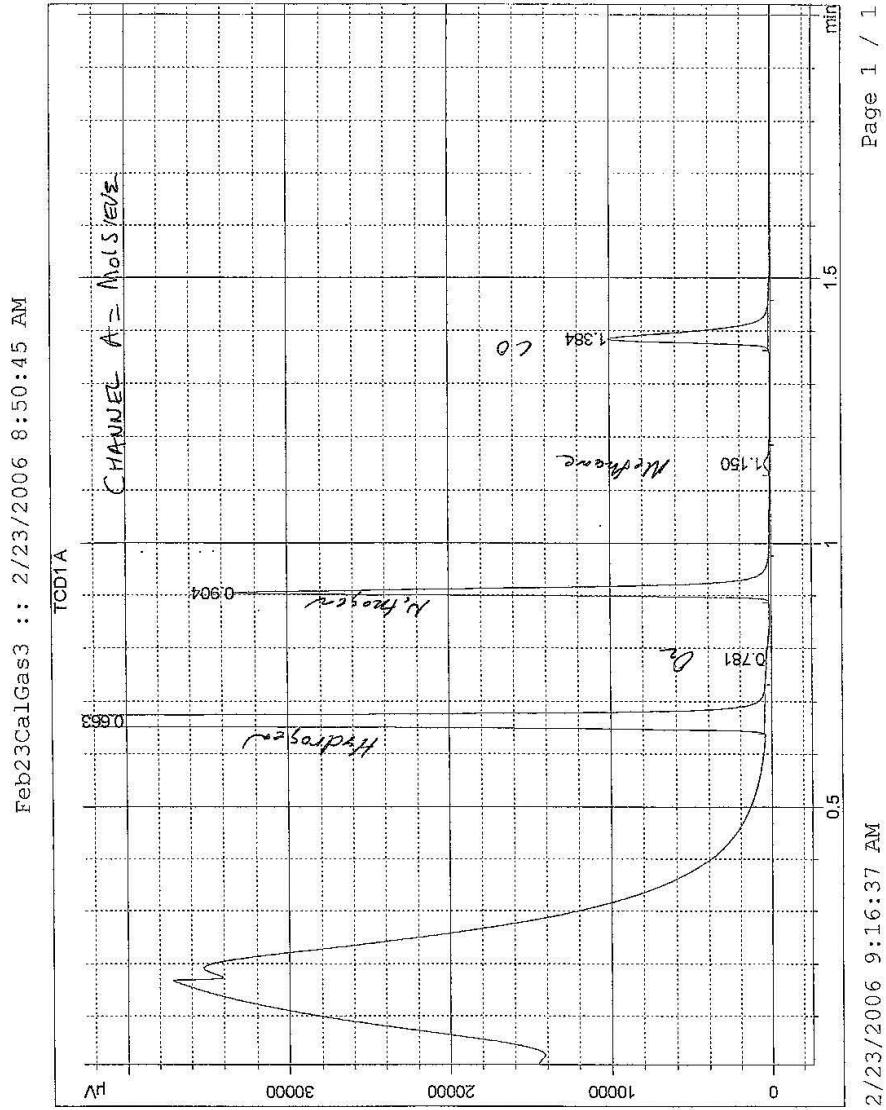
Figure 9-1 Column (A), Molecular Sieve column: hydrogen, nitrogen, methane, and carbon monoxide.
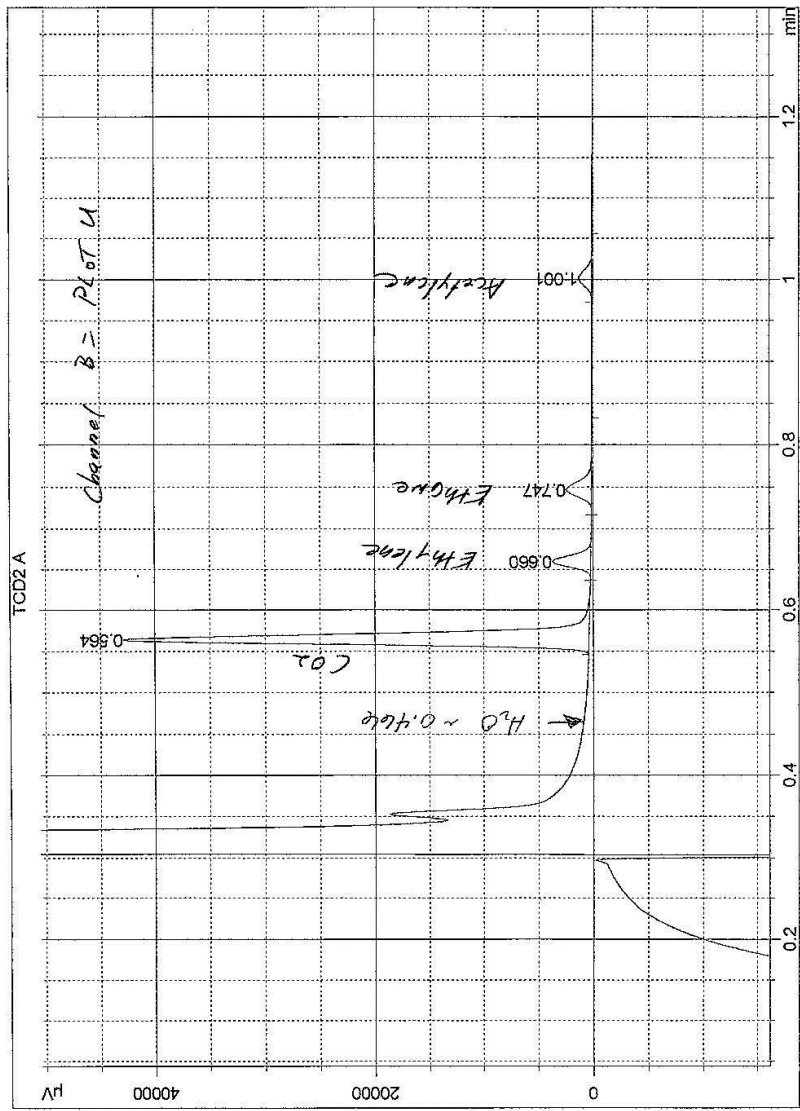
Figure 9-2 Column (B), Plot U column: Carbon dioxide, ethylene, ethane, and acetylene.
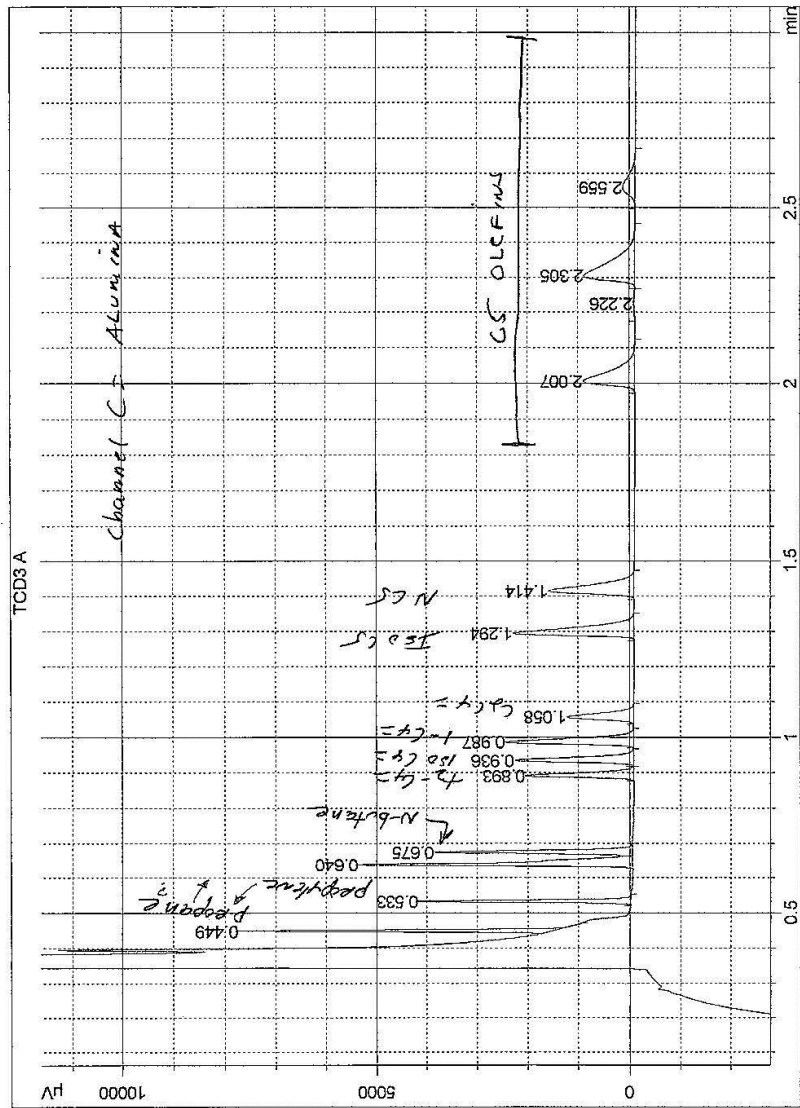
Figure 9-3 Column (C), Alumina column: propylene, propane, n-butane, trans-2-butene, iso-butene,1-butene, cis-2-butene, iso-pentane, n-pentane, 1,3 butadiene, trans-2-butene, 2 methyl-2-butene, 1-pentene, and cis-2-pentene.

228
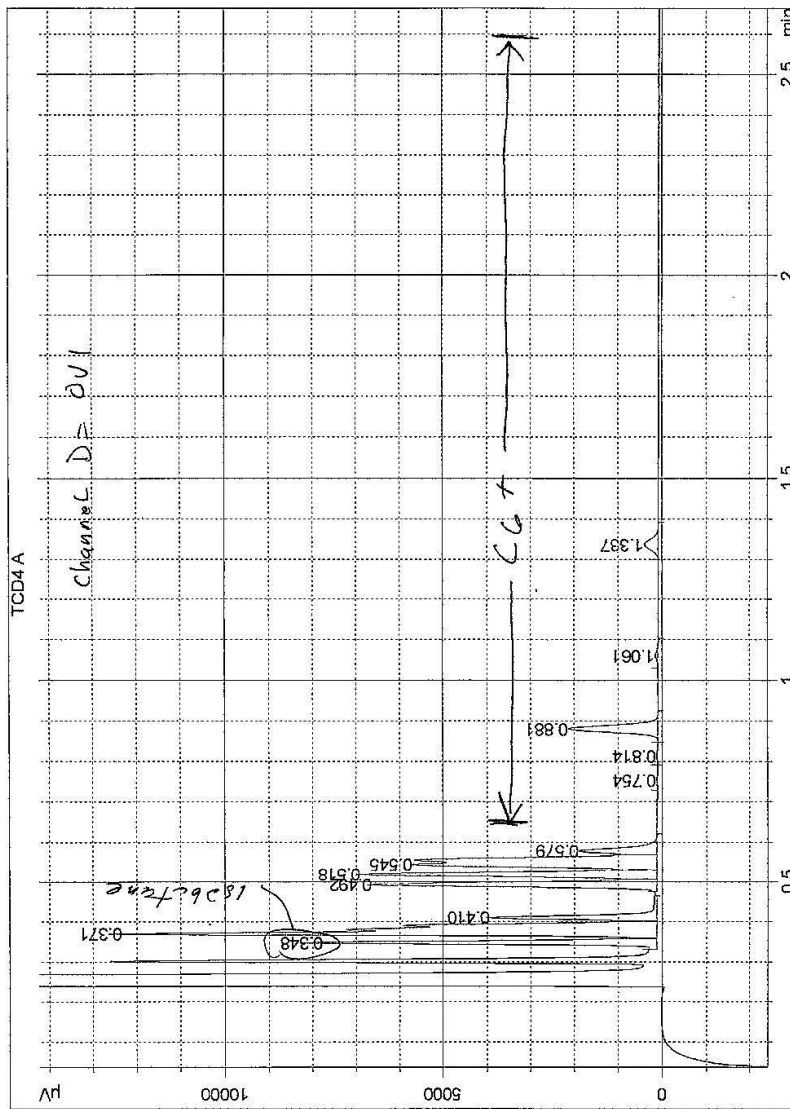
Figure 9-4 Column (D), OV1 column: iso-butane and hexane

Error was calculate using a Taylor series expansion of the terms.

      C.1 Terms

$N_{Ref}^{\cdot}$	Molar flow rate of reformate
$SLPM_{Air}$	Volumetric flow rate of air
ρ_{air}	Density of air @ 21C
MW_{air}	Molecular weight of air
$X_{N2\ in\ air}$	Mole fraction of nitrogen in air (20.95%)
X_{N2}	Mole fraction of nitrogen in reformate
$\dot{N}_{N2}$	Mole flow rate of nitrogen
$N_{Ref}^{\cdot}$	Mole flow rate of reformate
LHV_{JP8}	Lower heating value of JP-8
LHV_{CO}	Lower heating value of carbon monoxide
LHV_{H_2}	Lower heating value of hydrogen
LHV_{H_2}	Lower heating value of hydrogen
LHV_{CH_4}	Lower heating value of methane
X	Mole Fraction
X_{H_2}	Mole fraction of hydrogen in reformate
X_{co}	Mole fraction of carbon monoxide in reformate

C.2 Uncertainty in Reforming Efficiency for PEMFC

$$\eta_{H_2,CO} = \frac{\dot{N}_{Ref}\left(X_{H_2} * LHV_{H_2} + X_{co} * LHV_{CO}\right)}{LHV_{JP8} * \dot{M}_{JP8}}$$

$$\eta_{H_2,CO} = \left(\frac{X_{N_2\,in\,air}\rho_{air}}{LHV_{JP8} * MW_{air}}\right)\left[\left(\frac{SLPM_{Air}}{X_{N_2}}\right)\left(\frac{\left(X_{H_2} * LHV_{H_2} + X_{co} * LHV_{CO}\right)}{\dot{M}_{JP8}}\right)\right]$$

$$\Delta\eta_{H_2,CO} = \left|\frac{\partial\eta_{H_2,CO}}{\partial\dot{M}_{air}}\right|\Delta\dot{M}_{air} + \left|\frac{\partial\eta}{\partial\dot{N}_{N_2}}\right|\Delta\dot{N}_{N2} + \left|\frac{\partial\eta}{\partial X_{H_2}}\right|\Delta X_{H_2} + \left|\frac{\partial\eta}{\partial X_{co}}\right|\Delta X_{co} + \left|\frac{\partial\eta}{\partial\dot{M}_{JP8}}\right|\Delta\dot{M}_{JP8}$$

- $\left|\frac{\partial\eta_{H_2,CO}}{\partial SLPM_{Air}}\right|\Delta M_{air} = \left|\left(\frac{X_{N_2\,in\,air}\rho_{air}}{LHV_{JP8}*MW_{air}}\right)\left(\frac{1}{X_{N_2}}\right)\left(\frac{\left(X_{H_2}*LHV_{H_2}+X_{co}*LHV_{CO}\right)}{\dot{M}_{JP8}}\right)\right|\Delta SLPM_{Air}$

- $\left|\frac{\partial\eta_{H_2,CO}\eta}{\partial X_{N_2}}\right|\Delta X_{N_2} = \left|\left(\frac{X_{N_2\,in\,air}\rho_{air}}{LHV_{JP8}*MW_{air}}\right)\left(\frac{SLP\dot{M}_{Air}}{X_{N_2}^2}\right)\left(\frac{\left(X_{H_2}*LHV_{H_2}+X_{co}*LHV_{CO}\right)}{\dot{M}_{JP8}}\right)\right|\Delta X_{N_2}$

- $\left|\frac{\partial\eta_{H_2,CO}}{\partial X_{H_2}}\right|\Delta X_{H_2} = \left|\left(\frac{X_{N_2\,in\,air}*\rho_{air}}{LHV_{JP8}*MW_{air}}\right)\left(\frac{SLPM_{Air}}{X_{N_2}}\right)\left(\frac{\left(1*LHV_{H_2}\right)}{\dot{M}_{JP8}}\right)\right|\Delta X_{H_2}$

- $\left|\frac{\partial\eta_{H_2,CO}}{\partial X_{CO}}\right|\Delta X_{CO} = \left|\left(\frac{X_{N_2\,in\,air}*\rho_{air}}{LHV_{JP8}*MW_{air}}\right)\left(\frac{SLPM_{Air}}{X_{N_2}}\right)\left(\frac{\left(1*LHV_{CO}\right)}{\dot{M}_{JP8}}\right)\right|\Delta X_{CO}$

- $\left|\frac{\partial\eta_{H_2,CO}}{\partial\dot{M}_{JP8}}\right|\Delta\dot{M}_{JP8} = \left|\left(\frac{X_{N_2\,in\,air}\rho_{air}}{LHV_{JP8}*MW_{air}}\right)\left(\frac{SLPM_{Air}}{X_{N_2}}\right)\left(\frac{\left(X_{H_2}*LHV_{H_2}+X_{co}*LHV_{CO}\right)}{\dot{M}_{JP8}^2}\right)\right|\Delta\dot{M}_{JP8}$

C.3 Uncertainty in Reforming Efficiency for SOFC

$$\eta_{H_2,CO,CH_4} = \frac{\dot{N}_{Ref}\left(X_{H_2} * LHV_{H_2} + X_{co} * LHV_{CO} + X_{CH_4} * LHV_{CH_4}\right)}{LHV_{JP8} * \dot{M}_{JP8}}$$

$$\eta_{H_2,CO,CH_4} = \left(\frac{X_{N_2\,in\,air}\rho_{air}}{LHV_{JP8} * MW_{air}}\right)\left[\left(\frac{SLPM_{Air}}{X_{N_2}}\right)\left(\frac{\left(X_{H_2} * LHV_{H_2} + X_{co} * LHV_{CO} + X_{CH_4} * LHV_{CH_4}\right)}{\dot{M}_{JP8}}\right)\right]$$

$$\Delta\eta_{H_2,CO,CH_4} = \left|\frac{\partial\eta_{H_2,CO,CH_4}}{\partial SLPM_{Air}}\right|\Delta\dot{M}_{air} + \left|\frac{\partial\eta_{H_2,CO,CH_4}}{\partial\dot{N}_{N_2}}\right|\Delta\dot{N}_{N2} + \left|\frac{\partial\eta_{H_2,CO,CH_4}}{\partial X_{H_2}}\right|\Delta X_{H_2} + \left|\frac{\partial\eta_{H_2,CO,CH_4}}{\partial X_{co}}\right|\Delta X_{co} +$$

$$+ \left|\frac{\partial\eta}{\partial X_{CH_4}}\right|\Delta X_{co} + \left|\frac{\partial\eta}{\partial\dot{M}_{JP8}}\right|\Delta\dot{M}_{JP8}$$

- $\left|\frac{\partial\eta_{H_2,CO,CH_4}}{\partial M_{air}}\right|\Delta M_{air} = \left|\left(\frac{X_{N_2\,in\,air}\rho_{air}}{LHV_{JP8}*MW_{air}}\right)\left(\frac{1}{X_{N_2}}\right)\left(\frac{\left(X_{H_2}*LHV_{H_2}+X_{co}*LHV_{CO}+X_{CH_4}*LHV_{CH_4}\right)}{\dot{M}_{JP8}}\right)\right|\Delta SLPM_{Air}$

- $\left|\frac{\partial\eta_{H_2,CO,CH_4}}{\partial X_{N_2}}\right|\Delta X_{N_2} = \left|\left(\frac{X_{N_2\,in\,air}\rho_{air}}{LHV_{JP8}*MW_{air}}\right)\left(\frac{SLPM_{Air}}{X_{N_2}^2}\right)\left(\frac{\left(X_{H_2}*LHV_{H_2}+X_{co}*LHV_{CO}+X_{CH_4}*LHV_{CH_4}\right)}{\dot{M}_{JP8}}\right)\right|\Delta X_{N_2}$

- $\left|\frac{\partial\eta_{H_2,CO,CH_4}}{\partial X_{H_2}}\right|\Delta X_{H_2} = \left|\left(\frac{X_{N_2\,in\,air}*\rho_{air}}{LHV_{JP8}*MW_{air}}\right)\left(\frac{SLPM_{Air}}{X_{N_2}}\right)\left(\frac{\left(1*LHV_{H_2}\right)}{\dot{M}_{JP8}}\right)\right|\Delta X_{H_2}$

- $\left|\dfrac{\partial \eta_{H_2,CO,CH_4}}{\partial X_{CO}}\right|\Delta X_{CO} = \left|\left(\dfrac{X_{N_2\,in\,air}*\rho_{air}}{LHV_{JP8}*MW_{air}}\right)\left(\dfrac{M_{air}S\dot{L}PM_{Air}}{X_{N_2}}\right)\left(\dfrac{(1*LHV_{CO})}{\dot{M}_{JP8}}\right)\right|\Delta X_{CO}$

- $\left|\dfrac{\partial \eta_{H_2,CO,CH_4}}{\partial X_{CH_4}}\right|\Delta X_{CH_4} = \left|\left(\dfrac{X_{N_2\,in\,air}*\rho_{air}}{LHV_{JP8}*MW_{air}}\right)\left(\dfrac{SLPM_{Air}}{X_{N_2}}\right)\left(\dfrac{(1*LHV_{CH_4})}{\dot{M}_{JP8}}\right)\right|\Delta X_{CH_4}$

- $\left|\dfrac{\partial \eta_{H_2,CO,CH_4}}{\partial \dot{M}_{JP8}}\right|\Delta \dot{M}_{JP8} = \left|\left(\dfrac{X_{N_2\,in\,air}\rho_{air}}{LHV_{JP8}*MW_{air}}\right)\left(\dfrac{SLPM_{Air}}{X_{N_2}}\right)\left(\dfrac{(X_{H_2}*LHV_{H_2}+X_{co}*LHV_{CO}+X_{CH_4}*LHV_{CH_4})}{\dot{M}_{JP8}^2}\right)\right|\Delta \dot{M}_{JP8}$

C.4 Uncertainty in Conversion

$$\eta_{conv} = \frac{\left(\dfrac{SLPM_{Air}*\dfrac{\dot{\rho_{air}}}{MW_{air}}\left(X_{N_2\,in\,air}\right)}{X_{N_2}}\right)\left(X_{co}+X_{co_2}\right)}{X_{carbon}*\dot{M}_{JP8}}$$

$$\Delta \eta_{conv} = \left|\dfrac{\partial \eta_{conv}}{\partial SLPM_{Air}}\right|\Delta SLPM_{Air} + \left|\dfrac{\partial \eta_{conv}}{\partial \dot{N}_{N_2}}\right|\Delta \dot{N}_{N_2} + \left|\dfrac{\partial \eta_{conv}}{\partial X_{co}}\right|\Delta X_{co} + \left|\dfrac{\partial \eta_{conv}}{\partial X_{CO_2}}\right|\Delta X_{CO_2} + \left|\dfrac{\partial \eta_{conv}}{\partial \dot{M}_{JP8}}\right|\Delta \dot{M}_{JP8}$$

- $\left|\dfrac{\partial \eta_{conv}}{\partial SLPM_{Air}}\right|\Delta \dot{M}_{air} = \left|\left(\dfrac{X_{N_2\,in\,air}*\rho_{air}}{MW_{air}*X_{carbon}}\right)\dfrac{\left(\dfrac{1}{X_{N_2}}\right)}{\dot{M}_{JP8}}\left(X_{co}+X_{co_2}\right)\right|\Delta SLPM_{Air}$

- $\left|\dfrac{\partial \eta_{conv}}{\partial X_{N_2}}\right|\Delta X_{N_2} = \left|\left(\dfrac{X_{N_2\,in\,air}*\rho_{air}}{MW_{air}*X_{carbon}}\right)\dfrac{\left(\dfrac{SLPM_{Air}}{X_{N_2}^2}\right)}{\dot{M}_{JP8}}\left(X_{co}+X_{co_2}\right)\right|\Delta X_{N_2}$

- $\left|\dfrac{\partial \eta_{conv}}{\partial X_{co}}\right|\Delta X_{co} = \left|\left(\dfrac{X_{N_2\,in\,air}*\rho_{air}}{MW_{air}*X_{carbon}}\right)\dfrac{\left(\dfrac{SLPM_{Air}}{X_{N_2}}\right)}{\dot{M}_{JP8}}(1+0)\right|\Delta X_{co}$

- $\left|\dfrac{\partial \eta_{conv}}{\partial X_{co_2}}\right|\Delta X_{co_2} = \left|\left(\dfrac{X_{N_2\,in\,air}*\rho_{air}}{MW_{air}*X_{carbon}}\right)\dfrac{\left(\dfrac{SLPM_{Air}}{X_{N_2}}\right)}{\dot{M}_{JP8}}(0+1)\right|\Delta X_{co_2}$

- $\left|\dfrac{\partial \eta_{conv}}{\partial \dot{M}_{JP8}}\right|\Delta \dot{M}_{JP8} = \left|\left(\dfrac{X_{N_2\,in\,air}*\rho_{air}}{MW_{air}*X_{carbon}}\right)\dfrac{\left(\dfrac{SLPM_{Air}}{X_{N_2}}\right)}{\dot{M}_{JP8}^2}\left(X_{co}+X_{co_2}\right)\right|\Delta \dot{M}_{JP8}$

C.5 Uncertainty in Reformate Concentrations

The gas chromatograph had an uncertainty of 1.0% of measured values. Calibration gases had a 0.02% uncertainty.

$$\Delta X_{species} = \pm 1.02\% * X_{species}$$

C.6 Uncertainty in Temperature Measurements

Uncertainty was calculated using manufactory recommendations.

$$\Delta T = \pm 0.75\% * T$$

Appendix D: Grid Independence

As the academic version of Fluent was employed, the program was limited to 512,000 elements and notes. A grid independence study was conducted to verify the CFD simulation and remove the influence of the mesh. The reactor was modeled with 250,000 nodes and 500,000 elements. The flow fields of the two meshes appeared comparable, both depicting a void region near the rear of the reactor. Velocity profiles appeared comparable. The higher mesh was used in course of study for kinetic studies that were anticipated latter.
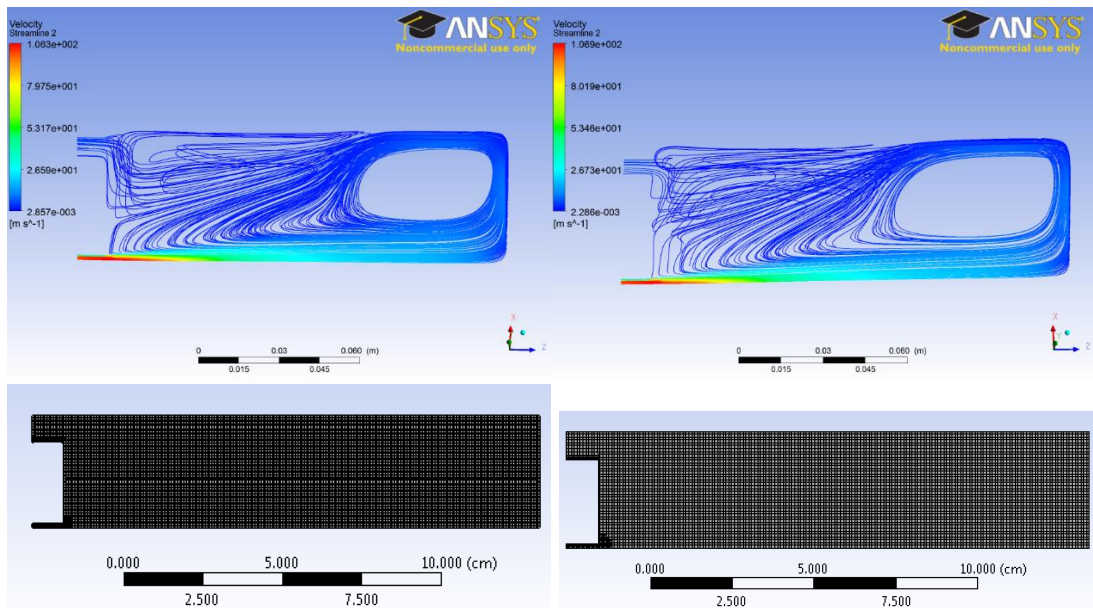

Figure 9-5. Grid Independence

Chapter 10: References

[1]   Howell, T. G., 2007, "Catalytic Partial Oxidation Refoming of JP8 and S8,"
        Air Force Institute of Technology. www.dtic.mil

[2]   Avici, A., Berry, D., Dagle, D., Fridman, A., Gallagher, M., Gangwal, S., Gao,
        J., Hasen, J., Haynes, D., Hou, Z., Karim, A., King, D., Li, G., Lous, H.,
        Mastanduno, R., Rostrup-Nieslsen, J., Onsan, Z., Roychoudhury, S.,
        Shekhawat, D., Smith, M., Speight, J., Spivey, J., Su, Y., Williams, M., and
        Zheng, X., 2011, Fuel cells: Technolgies For Fuel Processing, Elsevier,
        Amsterdam.

[3]   Brightling, J., 2014, "A Long History in Steam Reforming at Billingham,"
        Nitrogen+Syngas, **327**(January-Febuary), pp. 46–50.

[4]   Lipman, T., 2011, An Overview of Hydogen Produciton and Storage Systems
        with Renewable Hydrogen Case Studies. www.cesa.org

[5]   Alatiqi, I. M., and Meziou, A.M. Gasmelseed, G. A., 1989, "Static and
        Dynamic Simulation of Steam Methane Reformers," Sudies Surf. Sci. Catal.,
        53, pp. 535–550.

[6]   U.S. Energy Information Admin, 2016, "U.S, Price of Natural Gas Sold to
        Consumerical Consumers," (February), pp. 2–3 [Online]. Available:
        https://www.eia.gov/dnav/ng/hist/n3020us3m.htm. [Accessed: 01-Jan-2016].

[7]   Lee, I. C., and Chu, D., 2003, Literature Review of Fuel Processing.
        www.dtic.mil

[8]   DuBois, T., 2011, "Oxygen-Enriched Fuel Reforming of Heavy Liquid
        Hydrocarbon Fuels for Fuel Cells," Catholic University of America.

cuislandora.wrlc.org

[9]   Smith, C. H., Zak, C. D., Pineda, D. I., and Ellzey, J. L., 2011, "Conversion of
        Jet A to Syngas by Filtration Combustion," 7th US National Technical Meeting
        of Combustion Insitute, Alanta, pp. 1–15.

[10]   Pedersen-Mjaanes, H., Chan, L., and Mastorakos, E., 2005, "Hydrogen
        Production From Rich Combustion in Porous Media," Int. J. Hydrogen Energy,
        30(6), pp. 579–592.

[11]   Pastore, A., 2010, "Syngas Production from Heavy Liquid Fuel Reforming in
        Inert Porous Media," Cambridge. www.repository.cam.uk

[12]   Chen, C., Sur, S., Thayer, J., Pearlman, H., and Ronney, P., 2013, "A Non-
        Catalytic Fuel-Flexible Reformer," 8th U.S. National Combustion Meeting
        Western State Section, Salt Lake City, pp. 1–7.

[13]   Dixon, M., Schoegl, I., Hull, C., and Ellzey, J., 2008, "Experimental and
        Numerical Conversion of Liquid Heptane to Syngas Through Combustion in
        Porous Media," Combust. Flame, **154**(1–2), pp. 217–231.

[14]   Pastore, A., and Mastorakos, E., 2011, "Syngas Production From Liquid Fuels
        in a Non-Catalytic Porous Burner," Fuel, **90**(1), pp. 64–76.

[15]   Smith, C., 2012, "Studies of Rich and Ultra-Rich Combustion for Syngas
        Production," University of Texas at Austin. http://repositories.lib.utexas.edu

[16]   Roth, K., and Wirtz, S., 2007, "Investigation of Soot Formation During Partial
        Oxidation of Diesel Fuel," Chem. Eng. Technol, **30**(6), pp. 782–789.

[17]   Smith, C. H., Pineda, D. I., Zak, C. D., and Ellzey, J. L., 2012, "Conversion of
        Jet Fuel and Butanol to Syngas by Filtration Combustion," Int. J. Hydrogen

Energy, **38**(2), pp. 879–889.

[18] Boon, J., and Dijk, E., 2008, Adiabatic Diesel Pre-reforming Literature Survey.

[19] Zhdanok, S. a, and Brovki, P., 2003, "Porous Media Combustion Based Hydrogen production," InProc. Eur. Combust. Meet., **1**(1), pp. 1–13.

[20] Reed, N. J., 2008, "A Comparative Study of Adsorption Desulfurization of Liquid Transportation Fuels Over Different Sorbents for Fuel Cell Applications," Pennsylvania State University. etda.libraries.psu.edu

[21] Velu, S., Ma, X., Song, C., Namazian, M., Sethuraman, S., and Venkataraman, G., 2005, "Desulfurization of JP-8 Jet Fuel by Selective Adsorption Over a Ni-based Adsorbent for Micro Solid Oxide Fuel Cells," Energy and Fuels, **19**(3), pp. 1116–1125.

[22] Eow, J. S., 2002, "Recovery of Sulfur from Sour Acid Gas : A Review of the Technology," Environ. Progess, **21**(3), pp. 143–162.

[23] Sassi, M., and Gupta, A. K., 2008, "Sulfur Recovery from Acid Gas Using the Claus Process and High Temperature Air Combustion (HiTAC) Technology," Am. J. Enviromentl Sci., **4**(5), pp. 502–511.

[24] Services, P. E., AP-42 SECTION 5.18: Sulfur Recovery, Research Triangle Park, NC 27711. www.epa.gov

[25] Momeni, M., and Riahi, S., 2015, "An Investigation Into the Relationship Between Molecular Structure and Rich / Lean Loading of Linear Amine-Based CO_2 Absorbents," Int. J. Greenh. Gas Control, **42**, pp. 157–164.

[26] Lee, I. C., and Ubanyionwu, H. C., 2008, "Determination of Sulfur Contaminants in Military Jet Fuels," Fuel, **87**, pp. 312–318.

[27] Hu, L., Nie, H., Qu, L., Xia, G., Shi, Y., and Li, D., Sulfur-Resistant Bimetallic Noble Metal Catalyst for Aromatic Hydrogenation of Diesel Fuel. https://web.anl.gov

[28] Kaltschmitt, T., and Deutschmann, O., 2012, "Fuel Processing for Fuel Cells," Fuel Cell Eng., **41**, pp. 1–64.

[29] Bartholomew, C. H., 2001, "Mechanisms of Catalyst Deactivation," Appl. Catal. A Gen., **212**(1–2), pp. 17–60.

[30] Chen, Z., Yan, Y., and Elnashaie, S. S. E. H., 2004, "Catalyst Deactivation and Engineering Control for Steam Reforming of Higher Hydrocarbons in a Novel Membrane Reformer," Chem. Eng. Sci., **59**, pp. 1965–1978.

[31] Ito, T., Fujita, K., Matsuzaki, Y., Ueda, M., and Maruyama, T., 2014, "Investigation of Carbon Deposition Behavior on Ferritic Alloys in Low S C Ratio Using Direct Heating Method," Ceram. Eng. Sci. Proc., **35**(3), pp. 33–40.

[32] Chen, T., Wang, W. G., Miao, H., Li, T., and Xu, C., 2011, "Evaluation of Carbon Deposition Behavior on the Nickel / Yttrium-Stabilized zirconia Anode-Supported Fuel Cell Fueled with Simulated Syngas," J. Power Sources, **196**(5), pp. 2461–2468.

[33] Wu, H., Parola, V. La, Pantaleo, G., Puleo, F., Venezia, A. M., and Liotta, L. F., 2013, "Ni-Based Catalysts for Low Temperature Methane Steam Reforming: Recent Results on Ni-Au and Comparison with Other Bi-Metallic Systems," pp. 563–583.

[34] Nikolla, E., Schwank, J., and Linic, S., 2007, "Promotion of the Long-Term Stability of Reforming Ni Catalysts by Surface Alloying," J. Catal., **250**(1), pp.

85–93.

[35] Nikolla, E., Holewinski, A., Schwank, J., and Linic, S., 2006, "Controlling Carbon Surface Chemistry by Alloying: Carbon Tolerant Reforming Catalyst," J. Am. Chem. Soc., **128**(35), pp. 11354–11355.

[36] Xu, Y., Fan, C., Zhu, Y. A., Li, P., Zhou, X. G., Chen, D., and Yuan, W. K., 2012, "Effect of Ag on the Control of Ni-Catalyzed Carbon Formation: A Density Functional Theory Study," Catal. Today, **186**(1), pp. 54–62.

[37] Parizotto, N. V., Rocha, K. O., Damyanova, S., Passos, F. B., Zanchet, D., Marques, C. M. P., and Bueno, J. M. C., 2007, "Alumina-Supported Ni Catalysts Modified with Silver for the Steam Reforming of Methane: Effect of Ag on the Control of Coke Formation," Appl. Catal. A Gen., **330**(1–2), pp. 12–22.

[38] Jeong, H., and Kang, M., 2010, "Hydrogen Production From Butane Steam Reforming Over Ni/Ag Loaded MgAl2O4 Catalyst," Appl. Catal. B Environ., **95**(3–4), pp. 446–455.

[39] Deutschmann, O., 2012, "Catalytic Reforming of Logistic Fuels at High-Temperatures," Catalysis, **24**, pp. 48–82.

[40] Hamling, P., 2002, "Effects of Hydrogen Gas at 1450°C on Select Fibrous Alumina Insulation Products" [Online]. Available: http://www.zircarceramics.com/products.htm. [Accessed: 08-Jan-2013].

[41] Benim, A. C., and Syed, K. J., 1998, "Laminar Flamelet Modelling of Turbulent Premixed Combustion," Appl. Math. Model., **22**(1–2), pp. 113–136.

[42] Muguerza, R. R., Caldeira, A. B., and Fachini, F. F., 2011, "Analysis of Scales

For Flameless Combustion," IV Fast workshop on applied and computational mathamtics, Uberlândia, p. 17.

[43]   Turns, S. R., 2012, An Introduction to Combustion : Concepts and Applications, McGraw-Hill, New York.

[44]   Colorado, a F., Herrera, B. a, and Amell, a a, 2010, "Performance of a Flameless Combustion Furnace using Biogas and Natural Gas.," Bioresour. Technol., **101**(7), pp. 2443–9.

[45]   Duwig, C., Stankovic, D., Fuchs, L., Li, G., and Gutmark, E., 2007, "Experimental and Numerical Study of Flameless Combustion in a Model Gas Turbine Combustor," Combust. Sci. Technol., **180**(2), pp. 279–295.

[46]   Lee, D., and Huh, K. Y., 2012, "Validation of Analytical Expressions for Turbulent Burning Belocity in Stagnating and Freely Propagating Turbulent Premixed Flames," Combust. Flame, **159**(4), pp. 1576–1591.

[47]   Tsuji, H., Gupta, A. K., Hasegawa, T., Katsuki, M., Kishimoto, K., and Morita:, M., 2003, High Temperature Air Combustion: From Energy Conservation to Pollution Reduction, CRC Press, Boca Roton, London, New York, Washington DC.

[48]   Arghode, V. K., 2011, "Development of Colorless Distributed Combustion For Gas Turbine Applications," University of Maryland. drum.lib.umd.edu

[49]   Gupta, A. K., 2004, "Thermal Characteristics of Gaseous Fuel Flames Using High Temperature Air," J. Eng. Gas Turbines Power, **126**(1), p. 9.

[50]   Scenna, R., and Gupta, A. K., 2015, "Partial Oxidation of JP8 in a Distributed Reactor," J. Fuel Process., **134**, pp. 205–213.

[51] Tang, C., Huang, Z., He, J., Jin, C., Wang, X., and Miao, H., 2009, "Effects of N2 Dilution on Laminar Burning Characteristics of Propane - Air Premixed Flames," Energy & Fuels, **23**(1), pp. 151–156.

[52] Xu, F., Sunderland, P. B., and Faeth, G. M., 1997, "Soot Formation in Laminar Premixed Ethylene / Air Flames at Atmospheric Pressure," Combust. Flame, **108**, pp. 471–493.

[53] Hiblot, H., Ziegler-Devin, I., Fournet, R., and Glaude, P. A., 2016, "Steam Reforming of Methane in a Synthesis Gas from Biomass Gasification," Int. J. Hydrogen Energy, **41**(41), pp. 18329–18338.

[54] Al-Quarashi, 2007, "The Impact of Carbon Dioxide and Exhaust Gas Recirculation on the Oxidative Reactivity of Soot from Etheylene Flames and Diesel Engines," Pennsylvania State University. http://etda.libraries.psu.edu

[55] Liu, F., Consalvi, J. L., and Fuentes, A., 2014, "Effects of Water Vapor Addition to the Air Stream on Soot Formation and Flame Properties in a Laminar Coflow Ethylene/Air Diffusion Flame," Combust. Flame, **161**(7), pp. 1724–1734.

[56] Barua, A., 2012, "Soot Formation in Diffusion Flames of Alternative Turbine Fuels at Elevated Pressures," University of Toronto. tspace.libary.utoronto.ca

[57] Burnham, A., 1979, "Reaction Kinetics Between Steam and Oil-Shale Residual Carbon," Fuel, **58**(10), pp. 719–723.

[58] Woodruff, R. B., 2012, "Investigation of High Temperature Steam Gasification of Biomass Char," University of Colorado, Boulder. scholar.colorado.edu

[59] Molintas, H., 2015, "Gasification and Combustion of Large Char Particles and

Tar," University of Maryland. drum.lib.umd.edu

[60] Sharma, M., and Schoegl, I., 2013, "A Comparative Assessment of Homogeneous Propane Peforming at Intermediate Temperatures," Int. J. Hydrogen Energy, **38**(30), pp. 13272–13281.

[61] Bartekova, E., and Bajus, M., 1997, "Pyrolysis Of Hexadecane," Czech. Chem. Commun, **62**, pp. 1057–1069.

[62] Parmar, R., 2013, "A Combined Gas-Phase and Surface Reaction Mechanisitic Model of Diesel Surrogate Reforming For SOFC Application," Queen's University Kingston. qspace.libary.queensu.ca

[63] Scenna, R., and Gupta, A. K., 2017, "Dry and Wet Partial Oxidation in a Distributed Reactor," Int. J. Hydrogen Energy, **42**(7), pp. 4102–4110.

[64] Brandmair, M., 2005, "Autothermal Reforming of n-Hexane over Supported Metal Catalysts," Technische Universitat Munchen. mediatum.ub.tum.de

[65] Chen, X., Dahlberg, K. A., Gould, B. D., and Schwank, J. W., 2015, "Ni-Based Monolith N - Dodecane Reforming Catalysts : Optimization of O/C and Effect of Ni Interaction with Cordierite," Ind. Eng. Chem. Res., **54**, pp. 4136–4147.

[66] Molintas, H. J., and Gupta, A. K., 2009, "Thermal Decomposition of Cardboard Wastes using Steam Gasification," International Thermal Treatment Technologies Conference, Cincinnati, OH.

[67] Zhang, W., Zhan, Y., Zhang, M., Tian, C., and Zhao, W., 2009, "The Characteristic of CH4-CO2 Reforming Catalyzed by Carbonaceous Catalyst," ICE Gasification Conference Puplication.

[68] Lin, L., and Strand, M., 2013, "Investigation of the Intrinsic CO2 Gasification

Kinetics of Biomass Char at Medium to High Temperatures," Appl. Energy, **109**, pp. 220–228.

[69] Mani, T., and Mahinpey, N., 2013, "Flax Straw Char-CO2 Gasification Kinetics and its Inhibition Studies with CO," Can. J. Chem. Eng., **91**(5), pp. 882–888.

[70] Ahmed, I. I., and Gupta, A. K., 2011, "Kinetics of Woodchips Char Gasification with Steam and Carbon Dioxide," Appl. Energy, **88**(5), pp. 1613–1619.

[71] Barkia, H., Belkbir, L., and Jayaweera, S. A. A., 2004, "Non-Isothermal Kinetics of Gasification by CO2 of Residual Carbon from Timahdit and Tarfaya Oil Shale Kerogens," J. Therm. Anal. Calorim., **76**(2), pp. 623–632.

[72] Mi, J., Li, P., Dally, B. B., and Craig, R. A., 2009, "Importance of Initial Momentum Rate and Air-Fuel Premixing on Moderate or Intense Low Oxygen Dilution (MILD) Combustion in a Recuperative Furnace," Energy and Fuels, **23**(11), pp. 5349–5356.

[73] Arghode, V. K., and Gupta, A. K., 2011, "Hydrogen Addition Effects on Methane–Air Colorless Distributed Combustion Flames," Int. J. Hydrogen Energy, **36**(10), pp. 6292–6302.

[74] EG&G Technical Services, I., 2004, "Fuel Cell Handbook," Fuel Cell, **7 Edition**(November), pp. 1–352.

[75] Stambouli, A. B., and Traversa, E., 2002, "Solid Oxide Fuel Cells (SOFCs): A Review of an Environmentally Clean and Efficient Source of Energy," Renew. Sustain. Energy Rev., **6**, pp. 433–455.

[76] Nomnqa, M., Ikhu-omoregbe, D., and Rabiu, A., 2016, "Parametric Analysis of a High Temperature PEM Fuel Cell Based Microcogeneration System," Int. J. Chem. Eng., **2016**.

[77] Luengnaruemitchai, A., Osuwan, S., and Gulari, E., 2003, "Comparative Studies of Low-Temperature Water-Gas Shift Reaction Over Pt/CeO2, Au/CeO2, and Au/Fe2O3 Catalysts," Catal. Commun., **4**(5), pp. 215–221.

[78] Products, P. gas, "Micro Channel Palladium Hydrogen Puriffers" [Online]. Available: wwww.puregasproucts.com.

[79] Al-Mufachi, N. A., Rees, N. V., and Steinberger-Wilkens, R., 2015, "Hydrogen Selective Membranes: A Review of Palladium-Based Dense Metal Membranes," Renew. Sustain. Energy Rev., **47**, pp. 540–551.

[80] Reijers, R., and Haije, W., 2008, Literature Review on High Temperature Proton Conducting Materials Electrolyte for Fuel Cell or Mixed Conducting Membrane for H2 Separation. www.ecn.nl

[81] Knapton, B. A. G., 1977, "Palladium Alloys for Hydrogen Diffusion Membranes," Platin. Met. Rev, **21**(2), pp. 44–50.

[82] Basile, A., Iulianelli, A., Longo, T., Liguori, S., and Falco, M. De, 2011, Membrane Reactors for Hydrogen Production Processes, Springer-Verlag, Longdon.

[83] Xu, X., Li, P., and Shen, Y., 2013, "Small-Scale Reforming of Diesel and Jet Fuels to Make Hydrogen and Syngas for Fuel Cells: A Review," Appl. Energy, **108**, pp. 202–217.

[84] DOD, 1988, "DOD Directive 4140.3 'Single Fuel on The Battlefield

Initiative.'" www.dtic.mil

[85]   LePera, M., 1999, Jet A1 vs JP-8 Differences and Effects on Long Term Use. www.dtic.mil

[86]   Department of Defense, U. S. of A., 2013, MIl-DTL-83133J. www.dtic.mil

[87]   Dietzel, K., 2006, "Analytical Characterization of Jet Propellant 8(JP8) Using Chromatography/Mass Spectrometry (GC/MS)," University of Georgia. athenaeum.libs.uga.edu

[88]   DuBois, T. G., and Nieh, S., 2011, "Selection and Performance Comparison of Jet Fuel Surrogates for Autothermal Reforming," Fuel, **90**(4), pp. 1439–1448.

[89]   Canada, C. E., Science, E., and Division, T., 1999, "Jet A / Jet A-1." http://www.etc-cte.ec.gc.ca/databases/Oilproperties/pdf/WEB_Jet_A-Jet_A-1.pdf

[90]   Farrell, J. T., Cernansky, N. P., Dryer, F. L., Friend, D. G., Hergart, C. A., Law, C. K., McDavid, R. M., Mueller, C. J., Patel, A. K., and Pitsch, H., 2007, "Development of an Experimental Database and Kinetic Models for Surrogate Diesel Fuels," SAE Pap., pp. 01–0201.

[91]   Dagaut, P., and Cathonnet, M., 2006, "The Ignition, Oxidation, and Combustion of Kerosene: A Review of Experimental and Kinetic Modeling," Prog. Energy Combust. Sci., **32**(1), pp. 48–92.

[92]   Anastas, P., and Crabtree, R., 2014, Handbook of Green Chemistry, Green Catalysis, Heterogenous Catalysis.

[93]   Mujeebu, M. A., Abdullah, M. Z., Bakar, M. Z. A., Mohamad, A. a., and Abdullah, M. K., 2009, "Applications of Porous Media Combustion Technology – A Review," Appl. Energy, **86**(9), pp. 1365–1375.

[94]   Fay, M., Dhamrat, R., and Ellzey, J. L., 2005, "Effect of Porous Reactor Design on Conversion of Methane to Hydrogen," Combust. Sci. Technol., **117**(11), pp. 37–41.

[95]   Al-Hamamre, Z., Deizinger, S., Mach, A., Issendorff, F., and Trimis, D., 2006, "Thermal Partial Oxidation of Diesel in Porous Reactor for Synthesis Gas Production," Clean Air, **7**(4), pp. 391–408.

[96]   Dhamrat, R. S., and Ellzey, J. L., 2006, "Numerical and Experimental Study of the Conversion of Methane to Hydrogen in a Porous Media Reactor," Combust. Flame, **144**(4), pp. 698–709.

[97]   Drayton, M. K., Saveliev, A. V, Kennedy, L. A., Fridman, A. A., and Li, Y. D., 1998, "Syngas Production Using Superadiabatic Combustion of Ultra- Rich Methane-Air Mixtures," 27th Symposium on Combustion/The Combustion institute, pp. 1361–1367.

[98]   Kennedy, L. A., Saveliev, A. V., Bingue, J. P., and Barcellos, W., "Energy System Laboratory" [Online]. Available: http://miedept.mie.uic.edu/lab/kennedy/Filtration_changed_2.htm. [Accessed: 02-Aug-2013].

[99]   Bingue, J., 2004, "Optimization of Hydrogen Production by Filtration Combustion of Methane by Oxygen Enrichment and Depletion," Int. J. Hydrogen Energy, **29**(13), pp. 1365–1370.

[100] Schoegl, I., Newcomb, S. R., and Ellzey, J. L., 2009, "Ultra-Rich Combustion in Parallel Channels to Produce Hydrogen Rich Syngas from Propane," Int. J. Hydrogen Energy, **34**(12), pp. 5152–5163.

[101] Belmont, E. L., Solomon, S. M., and Ellzey, J. L., 2012, "Syngas Production From Heptane in a Non-Catalytic Counter-Flow Reactor," Combust. Flame, **159**(12), pp. 3624–3631.

[102] Hernandez-Gonzalez, S., 2008, "Non-Catalytic Production of Hydrogen via Reforming of Diesel, Hexadecane and Bio-Diesel for Nitrogen Oxides Remediation," Ohio State. https://etd.ohiolink.edu

[103] Hartmann, L., Lucka, K., and Köhne, H., 2003, "Mixture Preparation By Cool Flames for Diesel-Reforming Technologies," J. Power Sources, **118**(1–2), pp. 286–297.

[104] Arghode, V. K., and Gupta, A. K., 2011, "Investigation of Forward Flow Distributed Combustion For Gas Turbine Application," Appl. Energy, **88**(1), pp. 29–40.

[105] Arghode, V. K., and Gupta, A. K., 2011, "Investigation of Reverse Flow Distributed Combustion For Gas Turbine Application," Appl. Energy, **88**(4), pp. 1096–1104.

[106] Veríssimo, A. S., Rocha, A. M. a., and Costa, M., 2013, "Importance of the Inlet Air Velocity on the Establishment of Flameless Combustion in a Laboratory Combustor," Exp. Therm. Fluid Sci., **44**, pp. 75–81.

[107] Khalil, A. E. E., and Gupta, A. K., 2011, "Swirling Distributed Combustion for Clean Energy Conversion in Gas Turbine Applications," Appl. Energy, **88**(11), pp. 3685–3693.

[108] Gupta, A. K., Bolz, S., and Hasegawa, T., 2016, "Effect of Air Preheat Temperature and Oxygen Concentration on Flame Structure and Emission,"

121(September 1999), pp. 209–216.

[109]   Khalil, A. E. E., 2013, "Colorless Distributed Combustion (CDC) with Swirl
for Gas Turbine Application," University of Maryland. drum.lib.umd.edu

[110]   Derudi, M., Villani, A., and Rota, R., 2007, "Sustainability of Mild
Combustion of Hydrogen-Containing Hybrid Fuels," Proc. Combust. Inst., **31
II**, pp. 3393–3400.

[111]   Duwig, C., Li, B., Li, Z. S., and Aldén, M., 2012, "High Resolution Imaging of
Flameless and Distributed Turbulent Combustion," Combust. Flame, **159**(1),
pp. 306–316.

[112]   Arghode, V. K., and Gupta, A. K., 2010, "Effect of Flow Field For Colorless
Distributed Combustion (CDC) For Gas Turbine Combustion," Appl. Energy,
87(5), pp. 1631–1640.

[113]   Rahimi, M., Amiri, A., and Shabanian, S. R., 2013, "Experimental Study on
using HiTAC Technique For Synthesis Gas Production," Chem. Eng.
Commun., **200**(7), pp. 907–918.

[114]   Glassman, I., and Yetter, R. A., 2008, Combustion, Academic Press,
Burlington, MA.

[115]   Law, C., 2010, Combustion Physics, Cambride University Press, Cambride,
New York.

[116]   Kumar, P., and Ganesan, R., 2012, "A CFD Study of Turbulent Convective
Heat Transfer Enhancement in Circular Pipeflow," Eng. Technol., **6**(8), pp.
695–702.

[117]   Doosje, E., 2010, "Limits of Mixture Dilution in Engines," Eindhoven

University of Technology Library. repository.tue.nl

[118] "Chemkin." Chemkin-Pro 15131, Reaction design: San Diego, 2013

[119] Ranzi, E., Frassoldati, A., Grana, R., Cuoci, A., Faravelli, T., Kelley, A. P., and Law, C. K., 2012, "Hierarchical and Comparative Kinetic Modeling of Laminar Flame Speeds of Hydrocarbon and Oxygenated Fuels," Prog. Energy …, **38**(4), pp. 468–501.

[120] Violi, A., Yan, S., and Eddings, E., 2002, "Experimental Formulation and Kinetic Model for JP-8 Surrogate Mixtures," Combust. Sci. …, **174**(May), pp. 399–418.

[121] Khalil, A. E. E., and Gupta, A. K., 2013, "Hydrogen Addition Effects on High Intensity Distributed Combustion," Appl. Energy, **104**, pp. 71–78.

[122] Ricou, F. P., and Spalding, D. B., 2006, "Measurements of Entrainment by Axisymmetrical Turbulent Jets," J. Fluid Mech., **11**(1), p. 21.

[123] Han, D., and Mungal, M. G., 2001, "Direct Measurement of Entrainment in Reacting/Nonreacting Turbulent Jets," Combust. Flame, **124**(3), pp. 370–386.

[124] Yang, W., and Blasiak, W., 2005, "Flame Entrainments Induced by a Turbulent Reacting Jet Using High-Temperature and Oxygen-Deficient Oxidizers," Energy and Fuels, **19**(4), pp. 1473–1483.

[125] Jayakishan, B., 2011, "Invesitgation of Ignition Delay Times of Conventional (JP-8) and Synthetic (S-8) Jet Fuels: A Shock Tube Study," Dayton. https://etd.ohiolink.edu

[126] Khalil, A. E. E., Gupta, A. K., Bryden, K. M., and Lee, S. C., 2012, "Mixture Preparation Effects on Distributed Combustion for Gas Turbine Applications,"

J. Energy Resour. Technol., **134**(3), p. 32201.

[127] Vourliotakis, G., Skevis, G., Founti, M., Alhamamre, Z., and Trimis, D., 2008,
"Detailed Kinetic Modelling of the T-POX Reforming Process Using a Reactor
Network Approach," Int. J. Hydrogen Energy, **33**(11), pp. 2816–2825.

[128] "Lanik" [Online]. Available: http://www.lanik.eu/en/ceramic-foam-filters.

[129] "MNR Filters" [Online]. Available: http://www.mnrfilters.com/ceramic.html.

[130] "American Elements" [Online]. Available:
http://www.americanelements.com/zrfoam.html.

[131] Westbrook, C. K., Pitz, W. J., Herbinet, O., Curran, H. J., and Silke, E. J.,
2009, "A Comprehensive Detailed Chemical Kinetic Reaction Mechanism for
Combustion of N-Alkane Hydrocarbons From N-Octane to N-Hexadecane,"
Combust. Flame, **156**(1), pp. 181–199.

[132] Ranzi, E., Frassoldati, A., Granata, S., and Faravelli, T., 2005, "Wide-Range
Kinetic Modeling Study of the Pyrolysis, Partial Oxidation, and Combustion of
Heavy N-Alkanes," Ind. Eng. …, **44**, pp. 5170–5183.

[133] Ranzi, E., Dente, M., Goldaniga, A., Bozzano, G., and Faravelli, T., 2001,
"Lumping Procedures in Detailed Kinetic Modeling of Gasification, Pyrolysis,
Partial Oxidation and Combustion of Hydrocarbon Mixtures," Prog. Energy
Combust. Sci., **27**(1), pp. 99–139.

[134] Gould, B. D., Tadd, A. R., and Schwank, J. W., 2007, "Nickel-Catalyzed
Autothermal Reforming of Jet Fuel Surrogates: N-Dodecane, Tetralin, and
Their Mixture," J. Power Sources, **164**(1), pp. 344–350.

[135] Veríssimo, A., Rocha, A., and Costa, M., 2011, "Operational, Combustion, and

Emission Characteristics of a Small-Scale Combustor," Energy & Fuels, (25), pp. 2469–2480.

[136] Altin, O., and Eser, S., 2000, "Characterization of Carbon Deposits from Jet Fuel on Inconel 600 and Inconel X Surfaces," Ind. Eng. Chem. Res., **39**, pp. 642–645.

[137] Altin, O., and Eser, S., 2004, "Carbon Deposit Formation From Themal Stressing of Petroleum Fuels," American Chemical Society: Fuel Chemistry, pp. 764–766.

[138] Rawson, P., 2004, Evaluation of a Jet Fuel Thermal Stability Rig, Victoria.

[139] Al-Hamamre, Z., and Trimis, D., 2009, "Investigation of The Intermediate Oxidation Regime of Diesel Fuel," Combust. Flame, **156**(9), pp. 1791–1798.

[140] Khalil, A. E. E., Arghode, V. K., and Gupta, A. K., 2013, "Novel Mixing for Ultra-High Thermal Intensity Distributed Combustion," Appl. Energy, **105**(x), pp. 327–334.

[141] Raimondi, A., Loukou, A., Voss, S., Fino, D., and Trimis, D., "Innovative Regeneration Strategy for a Soot Trap Coupled to a TPOX Reformer," combustioninstitute.it, pp. 1–6.

[142] Ruiz, M. P., Callejas, A., Millera, A., Alzueta, M. U., and Bilbao, R., 2007, "Soot Formation From C2H2 and C2H4 Pyrolysis at Different Temperatures," J. Anal. Appl. Pyrolysis, **79**(1–2), pp. 244–251.

[143] Li, L., and Sunderland, P. B., 2012, "An Improved Method of Smoke Point Normalization," Combust. Sci. Technol., **184**(6), pp. 829–841.

[144] Arghode, V. K., Gupta, A. K., and Bryden, K. M., 2012, "High Intensity

Colorless Distributed Combustion For Ultra Low Emissions and Enhanced Performance," Appl. Energy, **92**, pp. 822–830.

[145] Scenna, R., and Gupta, A. K., 2015, "Preheats Effect on Distributed Reaction Fuel Reforming," Power and Energy 2015, ASME, San Diego, pp. 1–7.

[146] Scenna, R., and Gupta, A. K., 2016, "Partial Oxidation of JP8 in a Well-Insulated Distributed Reactor," Fuel Process. Technol., **142**, pp. 174–181.

[147] Yoon, S., Kang, I., and Bae, J., 2008, "Effects of Ethylene on Carbon Formation in Diesel Autothermal Reforming," Int. J. Hydrogen Energy, **33**(18), pp. 4780–4788.